

藉由可調控氫鍵作用力控制嵌段式共聚高分子 摻合系統之自組裝行為與相行為之探討

學生:陳世堅

指導教授:張豐志

國立交通大學應用化學研究所 博士班

摘要



在聚合物材料研究領域中，高分子混摻一直是一個被廣泛研究的課題，由於高分子混摻時，整個系統會產生很低的熵(entropy)值，使得絕大部分的高分子混摻系統都呈現著很差的相容性。透過引入高分子間特殊作用力，使得高分子混摻系統相容性顯著的提升，其中，又以氫鍵作用力被應用的最為廣泛。

在具有氫鍵作用力的高分子摻合系統中，有各種理論去描述系統中的作用力行為及相容性相圖，其中，以 Painter-Coleman association model (PCAM)最能準確的闡述高分子氫鍵摻合系統的行為。因此，在本研究中，我們利用陰離子活性聚合法合成一系列的 poly(vinylphenol-*b*-2-(dimethylamino)ethyl methacrylate) (PVPh-*b*-PDMAEMA)，並製備一系列 PVPh/PDMAEMA 混摻比例，探討在嵌段式共聚高分子及聚摻高分子在具有同樣氫鍵作用力時的行為。在比較後可發現，嵌段式共聚高分子會展現出緊密作用的高分子鏈行為導致分子間複雜體(complexation)產生，反之，在聚摻高分子系統中僅僅展現出高分子相容的行為。

近年來，由於奈米級階層性自組裝之材料被廣為應用在許多領域之中，使得嵌段式共聚高分子(diblock copolymer)在固態與液態下的自組裝行為之研究亦備受許多矚目與

探討。一般軟段—軟段嵌段式共聚高分子的自組裝行為大部分藉由一短程吸引力 (short-range attraction, covalent bond) 以及一長程排斥力 (long-range repulsion, block incompatible) 之間平衡所導致，並形成各式各樣的奈米結構，而創造出多樣性的超分子材料 (supramolecular material)。而藉由加入一均聚高分子 (homopolymer) 來控制嵌段式共聚高分子之微相分離 (microphase-separation) 行為在近年也廣為研究。

在研究中，我們將系統性的研究 A-b-B/C 嵌段式共聚高分子/均聚高分子在具有不同強度氫鍵作用力時之聚摻之相行為變化。我們利用陰離子活性聚合方式合成 poly(vinylphenol-*b*-styrene) (PVPh-*b*-PS) 嵌段式共聚高分子、poly(4-vinylpyridine) (P4VP)、poly(methyl methacrylate) (PMMA)、poly(vinylphenol) (PVPh) 均聚高分子，由於 PVPh-*b*-PS 中的 PVPh 鏈段會和 P4VP 產生強氫鍵作用力，相對地，和 PMMA 產生弱氫鍵作用力，故在 PVPh-*b*-PS/P4VP 的混摻系統會跟 PVPh-*b*-PS/PMMA 混摻系統產生截然不同的相行為。PVPh-*b*-PS/P4VP 系統會隨著 P4VP 量在系統中的增加而展現出一系列相變化，由原先的層狀結構 (lamella) 依序變成雙連續相結構 (gyroid)、六角圓柱 (hexagonal packed cylinder)、最後變成體心立方排列球結構 (body-central cubic sphere)；而 PVPh-*b*-PS/PMMA 系統並不會隨著 PMMA 量在系統中的增加而產生任何相變化。並也以 PVPh-*b*-PS/PVPh 混摻系統作為比較，發現此系統亦無任何相變化產生。最後，提出一新的參數 (K_A/K_B) 來預測是否有像變化產生之可能；如果此參數大於一相變化變化產生，反之，便無相變化。

此外，我們研究一嵌段式高分子混摻一小分子 (poly(4-vinylpyridine-*b*-styrene)/octyl-gallate 系統在不同共同溶劑下之液態自組裝行為。在不同的共同溶劑之下，由於生成不同的氫鍵作用力強度的氫鍵導致會有不同的自組裝聚集行為產生，而調控的液態下的聚集結構。

Studies on Modulating the Phase Behavior of Polymer Blends via Mediated Hydrogen Bonding

Student : Shih-Chien Chen

Advisor : Dr. Feng-Chih Chang

Institute of Applied Chemistry
National Chiao Tung University



ABSTRACT

The miscibility and interaction in polymer blends have been a topic and intense interest in polymer science. The miscibility of an immiscible blend was promoted by introducing one component which can form hydrogen bonded with another component. It is the one of the major achievements during last twenty years in polymer blend. This type of interaction has been widely described in terms of Painter & Coleman association model due to exactly prediction in most systems.

We have used anionic polymerization to prepare a series of poly[vinyl phenol-*b*-2-(dimethylamino)ethyl methacrylate] (PVPh-*b*-PDMAEMA) block copolymers. These block copolymers are miscible, with strong specific interactions occurring between the OH groups of the PVPh segments and the tertiary ammonium groups of the PDMAEMA segments. These PVPh-*b*-PDMAEMA diblock copolymers exhibit higher glass transition temperatures than do the corresponding PVPh/partially protonated PDMAEMA blends obtained from DMSO solution, which we suspect exist in the form of separate coils. The

blocks of the PVPh-*b*-PDMAEMA diblock copolymers interact strongly, resulting in polymer complex aggregation similar to the behavior of PVPh/partially protonated PDMAEMA blend complexes obtained in methanol. In addition, these PVPh-*b*-PDMAEMA diblock copolymers exhibit a novel type of pH-sensitivity: at low pH, compact spherical micelles are formed possessing PDMAEMA coronas and PVPh cores; at medium pH, vesicles are observed, consisting of partially protonated hydrophilic PDMAEMA shells and hydrophobic PVPh cores; at high pH, the spherical micelles that formed comprised ionized PVPh coronas and deprotonated hydrated-PDMAEMA cores, i.e., phase inversion of the micelles formed at pH 2.

The self-assembly of block copolymers in solution and solid state is attracting intense current attention as a route to nanostructured and hierarchical materials with variety of potential applications. Block copolymers display interesting self-assembly phenomena and allow the creation of hybrid supramolecular material. Furthermore, it is also interesting to control the morphology of microphase separated block copolymers by adding a homopolymer or other block copolymer.

In this thesis, we have investigated the phase behavior of poly(4-vinylphenol-*b*-styrene) (PVPh-*b*-PS) when respectively blended with poly(4-vinylpyridine) (P4VP), poly(methyl methacrylate) (PMMA), and PVPh homopolymers, of systematically decreased hydrogen-bonding strengths with the PVPh block of the copolymer. The PVPh-*b*-PS/P4VP blend has a much higher fraction (f_H) of hydrogen bonded PVPh blocks for a significantly higher miscibility, compared to the blends with PMMA and PVPh homopolymers. Consequently, the PVPh-*b*-PS/P4VP blend, behaving as a neat diblock copolymer, exhibited a series of order-order phase transitions from the lamellar, gyroid, hexagonally packed cylinder, to body-centered cubic structures. In contrast, both the PVPh-*b*-PS/PMMA and PVPh-*b*-PS/PVPh blends maintained essentially the lamellar structure; the lamellar structure, depending on the hydrogen bonding strength. The ratio of inter-association equilibrium

constant (K_A) over self-association equilibrium constant (K_B), K_A/K_B , is introduced as a convenient guide in estimating the phase behavior of similar polymer blends, featuring hydrogen bonding interactions between the homopolymer additive and copolymer: with a K_A/K_B ratio much larger than unity, the blend system tends to behave as a neat copolymer; with a K_A/K_B ratio significantly smaller than unity, phase separation instead of order-order phase transitions can be expected for the blend above certain volume fraction of homopolymer additive.

In addition, we have investigated the complexation-induced phase behavior of the mixtures of poly(styrene-*b*-4-vinylpyridine) (PS-*b*-P4VP) and octyl gallate (OG) due to hydrogen bonding in different solvents. For PS-*b*-P4VP/OG mixture in chloroform, the morphological transitions were induced from the unimer configuration to swollen aggregate and complex-micelles by adding OG. Interestingly, the complex-micelles can lead the formation of the honeycomb structure from chloroform solution. The PS-*b*-P4VP/OG mixture in THF, behaving an amphiphilic diblock copolymer in solution state, exhibited a series of morphological transitions by increasing the OG content. In contrast, the PS-*b*-P4VP/OG mixture in DMF maintained the unimer configuration upon adding OG. Therefore, the complexation-induced morphology of the mixtures of PS-*b*-P4VP and OG can be mediated by adopting different common solvents to affect the self-assembly behavior.

誌謝

又到了鳳凰花開、離情依依的季節，時光的飛逝讓我覺得自己仍如初次踏入校門的懵懂少年，如今即將畢業卸下學生的身分，雖然有種如釋重負的感覺，卻也有種要離開熟悉環境的不捨。五年的研究生涯在轉眼間變消逝而去，但在人生上的收穫卻遠遠超越以往所得，不論是在做學問的態度亦或是在人與人的相處以及相互合作方式皆有大相當大的成長與進步。在這段求學路上我碰到了許許多多願意指導我及幫助我的人，因為你們我才能順利的拿到博士學位，對於你們我永遠銘感於心。

在五年的研究生活中，最首要感謝張豐志老師提供良好的研究環境讓我能研究上全力以赴，並培養了我具備邏輯獨立思考能力與自動自發的研究精神，也感謝老師讓我知道除了研究外，更重要的是人與人之間的溝通與相互合作的做人處事的道理。對於老師諄諄教誨我會謹記在心。

感謝口試委員：馬振基教授、韋光華教授、邱文英教授、陳文章教授、邱顯堂教授、郭炳林教授在學生的論文上提供了寶貴的意見與指導，使學生論文更臻完整。

感謝實驗室畢業學姐董寶翔引領我進入高分子自組裝的領域，並在高分子合成技巧以及研究所需儀器使用上傾囊相授與經驗傳承，建立了我在研究上良好的基礎；沒有你，我可能也無法確定自己論文的方向而至今還裹足不前。也要感謝已畢業的廖春雄學長，願意在寶寶學姐畢業後不吝嗇地給予我研究上的建議與教導跟我討論，讓我能夠在不順利的實驗過程中得到了鼓勵。感謝這幾年來彼此勉勵互相消遣並時常提醒健忘的我許多事的好友承鈞，能夠跟你一同打拼聊八卦，使我的博士生涯充滿歡笑。也謝謝這段時間陪伴我的學長姐與學弟妹：didi、婉君、懷廣、志豪、永健、曜竹、倩婷、宜弘、文騰、筱雯、幸儀、仁志、小朱、業昇、狗弟、徐婕、佳佑、耀正、嘉蔚、昶禎、郁娟與雅萍…等等，讓我的博士生涯更添許多色彩。感謝實驗室學長郭紹偉博士給予我論文探討與實驗上給予許多幫助。也感謝在工研院 L500 組的各位，能夠在我研究之於學習到其他事務，並在我實驗忙碌時給予我各種包容。在儀器研究方面，感謝中興大學趙珮琪小姐在電子顯微鏡上的協助；小角度 X 光散射方面感謝同步輻射中心鄭有舜博士的指導與在實驗上的幫助。

還要感謝從大學時期陪我走過七個多年頭的女友珊慧，雖然在大學畢業後就分隔兩地，但妳總能在我開心時陪著我一起歡笑，而在我失落、難過、絕望時陪伴在我身邊給予我最大安慰與精神上最大的鼓勵，容忍我無時無刻的臭臉，讓我心中總是充滿了溫暖與希望，希望在未來的人生旅途中我們能夠繼續相互扶持做為對方支柱。最後，感謝的是我親愛的父母、哥哥、妹妹及叔叔在我背後默默的支持我，做我為我最強力的後盾，在你們全心全意的支持讓我在求學的路上能無後顧之憂

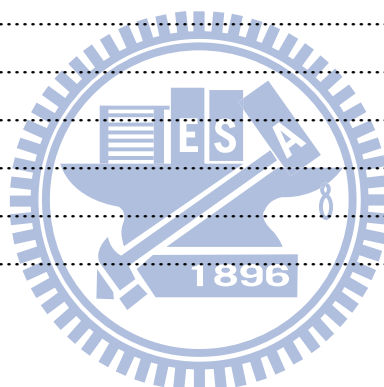
謹以此論文，獻給在我求學路上關心我與照顧我的各位。

Outline of Contents

	Pages
ABSTRACT (in Chinese)	I
ABSTRACT (in English)	III
Acknowledgment	VI
Outline of Contents	VII
List of Tables	X
List of Scheme	XI
List of Figures	XII
Chapter 1 Introduction to Hydrogen Bond in Polymer Blends	1
1-1 The Definition of the Hydrogen Bond.....	1
1-2 Hydrogen Bond in Polymer Blends.....	3
1-3 Introduction to Painter-Coleman Association Model.....	4
1-4 Influence Factors of Hydrogen Bonds.....	7
1-4.1 Acidity of the Proton Donor and Basicity of the Proton Acceptor.....	7
1-4.2 Intramolecular Screening Effect on Hydrogen Bond.....	8
1-4.3 Functional Group Accessibility Effect on Hydrogen Bond.....	11
1-4.4 Temperature Effect on Hydrogen Bond.....	13
1-4.5 Solvent Effect on Hydrogen Bond.....	14
1-5 Experimental Characterization of Hydrogen Bonds.....	15
References.....	18
Chapter 2 Introduction to Self-Assembly of Block Copolymer	20
2-1 The Definition of the Self-Assembly Behavior.....	20
2-2 Self-Assembly Behavior of Block Copolymer.....	22
2-3 Self-Assembly Behavior of Block Copolymer in Bulk State.....	23
2-4 Self-Assembly Behavior of Block Copolymer/Homopolymer Blends in Bulk State.....	27
2-5 Self-Assembly Behavior of Block Copolymer in Solution State.....	33
2-5.1 Theories of Self-Assembly Behavior of Block Copolymer in Solution State.....	34
2-5.2 Block Copolymer Micelle Free Energies.....	35
2-5.3 Estimation of Micelle Free Energy of Different Morphologies.....	37
2-5.4 Geometrical Theories of Self-Assembly Behavior of Block Copolymer in Solution State.....	39
2-6 Self-Assembly Behavior of Polymer Blends in Solution State.....	42
References.....	44
Chapter 3 Syntheses, Specific Interactions, and pH-Sensitive Micellization Behavior of Poly[vinyl phenol-<i>b</i>-2-(dimethylamino)ethyl methacrylate] Diblock Copolymers	48
Abstract.....	48

3-1 Introduction	49
3-2 Experimental Section	52
3-2.1 Materials.....	52
3-2.2 Poly[vinyl phenol- <i>b</i> -2-(dimethylamino)ethyl methacrylate] Diblock Copolymer	52
3-2.3 Blend Preparation.....	53
3-2.4 Characterization	53
3-3 Results and Discussion.....	56
3-3.1 Syntheses of Poly[vinyl phenol- <i>block</i> -2-(dimethylamino)ethyl methacrylate] Diblock Copolymers.....	56
3-3.2 FTIR Spectroscopic Analyses	57
3-3.3 2D-IR Correlation Analyses	60
3-3.4 Thermal Analyses.....	63
3-3.5 Solid State NMR Spectroscopic Analyses	65
3-3.6 pH-Induced Micellization of PVPh- <i>block</i> -PDMAEMA Copolymers.....	69
3-4 Conclusions	72
References	73
Chapter 4 On Modulating the Phase Behavior of Block Copolymer/Homopolymer Blends via Hydrogen Bonding.....	94
Abstract.....	94
4-1 Introduction	95
4-2 Experimental Section	97
4-2.1 Block Copolymer and Homopolymer Syntheses	97
4-2.2 Sample Preparation	97
4-2.3 Characterization Methodology.....	98
4-2.4 IR Data Analysis	98
4-2.5 SAXS Data Analysis	99
4-3 Results and Discussion.....	101
4-3.1 FTIR Result.....	101
4-3.2 Thermal Properties	102
4-3.3 Order-Order Structural Transitions for the HS/V Blends.....	103
4-3.4 Order-Disorder Structural Transitions for the HS/M and HS/H Blends	104
4-3.5 Correlation between the Hydrogen Strength and Phase Transition	106
4-3.6 Distribution/Chain Conformation of the Additive Homopolymers in the Blends	107
4-3.7 Interfacial Zone of the Polymer Blends	109
4-4 Conclusions	111
References	112

Chapter 5	On Modulating the Self-Assembly Behaviors of Poly(styrene-<i>b</i>-4-vinylpyridine)/Octyl Gallate Blends in Solution State via Hydrogen Bonding from Different Common Solvents	134
	Abstract	134
	5-1 Introduction	135
	5-2 Experimental Section	137
	5-2.1 Material and Synthesis of Block Copolymer	137
	5-2.2 Preparation of the PS- <i>b</i> -P4VP Aggregates by Adding OG	137
	5-2.3 Characterization Methodology	138
	5-3 Results and Discussion	139
	5-3.1 Synthesis of Poly(styrene- <i>block</i> -4-vinyl pyridine) Diblock Copolymer	139
	5-3.2 FTIR Analyses	139
	5-3.3 Characterization of the PS- <i>b</i> -P4VP / OG Aggregates in Chloroform	140
	5-3.4 Characterization of the PS- <i>b</i> -P4VP / OG Aggregates in THF and DMF	144
	5-4 Conclusions	147
	References:	148
Chapter 6		162
Conclusions		162
List of Publications		164
Introduction to the Author		166



List of Tables

		Pages
Table 1-1	Dimensionless Self- and Inter-Association Equilibrium Constants Values Determined from Miscible Polymer Blends Scaled to a Common Reference Volume (100 cm ³ /mol)	6
Table 3-1	Molecular Characterization of Poly[vinylphenol- <i>b</i> -2-(dimethylamino)ethyl methacrylate] Diblock Copolymers Prepared Using Anionic Polymerization	76
Table 3-2	Fraction of Hydrogen Bonding Groups of PVPh- <i>b</i> -PDMAEMA	77
Table 3-3	Values of T_g Obtained From PVPh/Partially Protonated PDMAEMA Blends and PVPh/Partially Protonated PDMAEMA Blend Complex Systems	77
Table 3-4	Relaxation Times, for Blends, Blend Complexes, and Diblock Copolymers at Magnetization Intensities of 45 and 115 ppm	78
Table 4-1	Molecular weights of PVPh- <i>b</i> -PS, PVPh, PMMA, and P4VP used in preparing the polymer blends. The volume fractions of PVPh and PS blocks in the neat block copolymer are respectively 37.6 and 62.4%	116
Table 4-2	Curve Fitting of the Fraction of Hydrogen-Bonded Carbonyl Groups of PVPh- <i>b</i> -PS/ PMMA Blend System	116
Table 4-3	Curve Fitting of the Fraction of Hydrogen-Bonded Pyridine Groups of PVPh- <i>b</i> -PS/P4VP Blend System	117
Table 4-4	Thicknesses of the PS (D_{PS}) and PVPh-homopolymer layers (D_{mix}) determined from 1-D correlation function	117
Table 4-5	The relative changes (with respect to the neat copolymer) in D , ρ_j , and a_j for the HS/H, HS/M, and HS/V blends; the interdomian spacing for the HS/V blends 71/29 (HPC), 48/52 (BCC spheres), and 29/71 (BCC spheres), are 45.6, 37.4, and 35.7 nm, respectively	118
Table 5-1	Summary of the Structural Parameters and Corresponding θ_w and θ_{ws} of Aggregates Formed by PS- <i>b</i> -P4VP/OG Mixtures in Chloroform	152

List of Scheme

	Pages
Scheme 3-1 Synthesis of Poly[vinylphenol- <i>b</i> -2-(dimethylamino)ethyl methacrylate] Diblock Copolymers Using Anionic Polymerization	79
Scheme 3-2 Schematic Representation of the Types of Interactions that Exist Between PVPh- <i>b</i> -PDMAEMA Diblock Copolymer Units	80
Scheme 4-1 Schematic Representation of the Types of Hydrogen Bonding Interactions Existing in the (a) PVPh- <i>b</i> -PS/P4VP and (b) PVPh- <i>b</i> -PS/PMMA Blend Systems.	119
Scheme 5-1 Schematic Representation of the Interaction that Exist Between P4VP Blocks and Octyl Gallate.	152



List of Figures

		Pages
Figure 1-1	The schematic structures of the double strand DNA molecule and hydrogen bonds formed between pyrimidine and purine residues.	2
Figure 1-2	Relationship between experimental data and theoretical prediction by PCAM of hydrogen bonded fraction of carbonyl group within various PCL blend systems: (■) henolic/PCL, (●) PVPh/PCL, (▲) phenoxy/PCL.	7
Figure 1-3	Equilibrium constant values for the PVPh-PVAc blend system (FGA: functional group accessibility)	9
Figure 1-4	Theoretical spinodal phase diagrams for PVPh/EVA blends.	10
Figure 1-5	Calculated fraction of hydrogen bonded acetoxy carbonyl groups for the PVPh-PVAc blend system at 25°C.	12
Figure 1-6	The FTIR spectra of the PCLTDP40 blend in the hydroxyl vibration region (a) and the carbonyl vibration region (b) recorded at different temperatures. From top to bottom, the temperatures are 26, 35, 45, 65, 90, 120 and 160°C.	14
Figure 2-1	Hierarchical self-assembly of collgan.	20
Figure 2-2	Examples of static self-assembly. (a) Crystal structure of a ribosome. (b) Self-assembled peptideamphiphile nanofibers. (c) An array of millimeter sized polymeric plates assembled at a water/perfluorodecalin interface by capillary interactions. (d) Thin film of a nematic liquid crystal on an isotropic substrate. (e) Micrometersized metallic polyhedra folded from planar substrates. (f) A three-dimensional aggregate of micrometer plates assembled by capillary forces.	21
Figure 2-3	Examples of dynamic self-assembly. (a) An optical micrograph of a cell with fluorescently labeled cytoskeleton and nucleus; microtubules ~ 24 nm in diameter) are colored red. (b) Reaction-diffusion waves in a Belousov-Zabatinski reaction in a 3.5-inch Petri dish. (c) A simple aggregate of three millimeter-sized, rotating, magnetized disks interacting with one another via vortex-vortex interactions. (d) A school of fish. (e) Concentric rings formed by charged metallic beads 1 mm in diameter rolling in circular paths on a dielectric support. (f) Convection cells formed above a micropatterned metallic support. The distance between the centers of the cells is ~ 2 mm.	22

Figure 2-4	Self-organization structures of block copolymers and surfactants: spherical micelles, cylindrical micelles, vesicles, fcc- and bcc-packed spheres (FCC, BCC), hexagonally packed cylinders (HEX), various minimal surfaces (gyroid, F surface, P surface), simple lamellae (LAM), as well as modulated and perforated lamellae (MLAM, PLAM).	23
Figure 2-5	(a) Schematic illustration of the self-assembly and self ordering behavior of BCPs at which the scale of microphase separation is about tens of nanometer. (b) Schematic phase diagram showing the various “classical” BCP morphologies adopted by non-crystalline linear diblock copolymer.	25
Figure 2-6	Experimental phase diagram for polystyrene- <i>b</i> -polyisoprene diblock copolymers.	26
Figure 2-7	Theoretical phase diagram for a diblock copolymer near the ODT.	26
Figure 2-8	(a) Schematic illustration of the location of the HS within the HS/PS-PI blend. TEM images of the HS/PS-PI blends with different HS/SI ratio: (b) 0/100; (c) 20/80; (d) 50/50; (e) 65/35; (f) 80/20. The dark and white regions represent the PI and PS microdomains due to the OsO ₄ staining. (g) Corresponding SAXS profiles for the samples (b)-(f).	28
Figure 2-9	Schematic illustration of the dry brush systems formed in HS/PS-PI blends with (a) small amounts of HS and (b) large amounts of HS. TEM images of HS/PS-PI blends with different HS/SI ratio: (c) 0/100; (d) 60/40; (d) 70/30; (e) 80/20. The dark and white regions represent the PI and PS microdomains due to the OsO ₄ staining.	29
Figure 2-10	Schematic of the cross-linked lamellar structure of blends of novolac and P2VP- <i>b</i> -PI. The hydrogen bonding between novolac and P2VP is also indicated. TEM images of the HMTA cured lamellar structure is also shown.	31
Figure 2-11	TEM micrographs showing different structures arose from mixing block copolymer SP 73 with homopolymers P and H.	31
Figure 2-12	Schematic illustration of (I) a star and (II) a crew-cut micelle.	34
Figure 2-13	Free energy changes with acetonitrile content for various morphologies in the PS- <i>b</i> -PEO copolymer-DMF/acetonitrile system.	38
Figure 2-14	Description of amphiphile shape in terms of the surfactant parameter (v/a_0l_c) and its relation to the interfacial mean curvature (H) and Gaussian curvature (K).	39
Figure 2-15	Dependence of final micelle structure on intrinsic molecular parameters: volume v of the hydrophobic group, and area a_0 and length l_c of the hydrophobic block.	40

Figure 2-16	Different aggregate morphologies predicted by the packing parameter (p).	41
Figure 2-17	TEM images (a, b) and optical micrograph (c) of different shapes of aggregates structures for a series of PB-PEO block copolymers ranging from spherical micelles (PB ₂₀₂ -PEO ₃₆₀) via cylindrical micelles (PB ₁₂₅ -PEO ₁₅₅) to vesicles (PB ₃₇ -PEO ₄₀). This figure illustrated the influence of the packing parameter on the self-assembly structure.	42
Figure 2-18	Models of micelle formation through mediated by hydrogen-bonding interaction of diblock copolymers mixtures and TEM images in THF (a) and DMF (b).	43
Figure 3-1	¹ H NMR spectra: (a) before hydrolysis, PtBOS- <i>b</i> -PDMAEMA; (b) after hydrolysis, PVPh- <i>b</i> -PDMAEMA.	81
Figure 3-2	¹³ C NMR spectra: (a) before hydrolysis, PtBOS- <i>b</i> -PDMAEMA; (b) after hydrolysis, PVPh- <i>b</i> -PDMAEMA.	81
Figure 3-3	FTIR spectra (room temperature, 400–4000 cm ⁻¹) of (a) pure PVPh, (b) PtBOS- <i>b</i> -PDMAEMA, (c) PVPh- <i>b</i> -PDMAEMA, and (d) pure PDMAEMA.	82
Figure 3-4	FTIR spectra (room temperature, OH stretching region) of PVPh- <i>b</i> -PDMAEMA diblock copolymers cast from DMSO solutions.	83
Figure 3-5	FTIR spectra (room temperature, OH stretching region) of a PVPh/fully protonated PDMAEMA blend cast from DMSO solution.	83
Figure 3-6	FTIR spectra (room temperature, OH stretching region) of PVPh/partially protonated PDMAEMA blends cast from DMSO solutions.	84
Figure 3-7	FTIR spectra of (a) PVPh- <i>b</i> -PDMAEMA diblock copolymers and (b) PVPh/partially protonated PDMAEMA blends cast from DMSO solutions.	84
Figure 3-8	Synchronous 2-D correlation map (1490–1780 cm ⁻¹) for (a) PVPh- <i>b</i> -PDMAEMA diblock copolymers and (b) PVPh/partially protonated PDMAEMA blends.	85
Figure 3-9	Asynchronous 2-D correlation map (1490–1780 cm ⁻¹) for (a) PVPh- <i>b</i> -PDMAEMA diblock copolymers and (b) PVPh/partially protonated PDMAEMA blends.	85
Figure 3-10	DSC curves of (a) PVPh/partially protonated PDMAEMA blends and (b) PVPh- <i>b</i> -PDMAEMA diblock copolymers.	86
Figure 3-11	Plots of T_g with respect to composition, based on the Kwei equation, for blends and diblock copolymers.	86
Figure 3-12	¹³ C CP/MAS NMR spectra of PVPh- <i>b</i> -PDMAEMA diblock copolymers.	87

Figure 3-13	Logarithmic plots of the intensities of the signals at (a) 45 and (b) 115 ppm with respect to the delay time from the ^{13}C CP/MAS NMR spectra of PVPh- <i>b</i> -PDMAEMA diblock copolymers.	88
Figure 3-14	(a) FTIR and (b) ^{13}C solid state NMR spectra of the diblock copolymer, blend complex, and blend having a PVPh:PDMAEMA ratio of 55:45.	89
Figure 3-15	(a) Synchronous and (b) asynchronous 2-D correlation maps ($2700\text{--}3800\text{ cm}^{-1}$) for PVPh- <i>b</i> -PDMAEMA diblock copolymer.	90
Figure 3-16	^1H NMR spectra of the PVPh ₃₂ - <i>b</i> -PDMAEMA ₆₈ diblock copolymer in (a) DMSO- <i>d</i> ₆ , (b) D ₂ O at pH 2, (c) D ₂ O at pH 7, and (d) D ₂ O at pH 13.	91
Figure 3-17	TEM images of the morphologies of the PVPh ₃₂ - <i>b</i> -PDMAEMA ₆₈ diblock copolymer prepared in aqueous media at (a) pH 2, (b) pH 7, and (c) pH 13.	91
Figure 3-18	(a) The Zimm plot analysis and (b) the hydrodynamic radius distribution of the PVPh ₃₂ - <i>b</i> -PDMAEMA ₆₈ block copolymer in aqueous media at pH 7.	92
Figure 3-19	Proposed pH-dependent microstructural transformations of the PVPh ₃₂ - <i>b</i> -PDMAEMA ₆₈ diblock copolymer.	93
Figure 4-1	One-dimensional correlation functions of the (a) HS/H, (b) HS/M, and (c) HS/V blend systems. The thickness of the lamellar long period was calculated from the position of the first peak; the average thickness of the thinner phase is determined from the intersection of the tangent line and baseline, as illustrated in (d) for an ideal two-phase lamellar structure.	120
Figure 4-2	FTIR spectra, recorded at 120 °C, of the OH stretching region of the (a) HS/V and (b) HS/M blend systems cast from DMF solutions.	121
Figure 4-3	FTIR spectra recorded at 120 °C in (a) the pyridine absorption region for the HS/V blends and (b) the C=O absorption region for the HS/M blends. The compositions are indicated above the respective profiles. (c) The corresponding f_b values for the fraction of hydrogen-bonded groups. Lines drawn over the data points are only for eye-guiding. The decrease of f_b (i.e. reduction of hydrogen bonding efficiency) with increase of the homopolymer volume fraction reveals a systematically decreased miscibility in both blends.	122
Figure 4-4	DSC traces of the (a) HS/V, (b) HS/M, and (c) HS/H blends, with the respective compositions indicated. Arrows indicate the respective T_g values.	123
Figure 4-5	From left to right are the DSC, FTIR, and XRD results for the PVPh- <i>b</i> -PS copolymer and the PVPh homopolymer.	124

- Figure 4-6 TEM images for the HS/V blends, after staining with I₂ for 24 h (the dark regions correspond to the PVPh-P4VP phase): (a) pure HS, (b) HS/V = 94/6, (c) HS/V = 90/10, (d) HS/V = 87/13, (e) HS/V = 85/15, (f) HS/V = 78/22, (g) HS/V = 71/29, and (h) HS/V = 29/71. Shown in the insets are the corresponding structures proposed. 125
- Figure 4-7 SAXS data for the pure HS and the blends HS/V = 94/6, HS/V = 90/10, HS/V = 87/13, and HS/V = 85/15 in (a), and HS/V = 78/22, HS/V = 76/24, HS/V = 71/29, HS/V = 48/52, and HS/V = 29/71 in (b). The peak ratios (relative to the first peak position marked as q*) or reflections planes for the corresponding ordered structures are indicated by arrows. 126
- Figure 4-8 TEM images of the solution-cast films of the HS/M blends (dark regions correspond to the PS domains): (a) HS/M = 94/6, (b) HS/M = 90/10, (c) HS/M = 79/21, (d) HS/M = 62/38, and (e) HS/M = 30/70. Cartoons in the insets present the corresponding structures proposed. 127
- Figure 4-9 TEM images of the solution-cast films of the blends (dark regions correspond to the PS domains): (a) HS/H = 94/6, (b) HS/H = 90/10, (c) HS/H = 80/20, (d) HS/H = 63/37, and (e) HS/H = 31/69. Proposed 3-D structures are shown in the insets. Cartoons in (d) and (e) illustrate concentric tubes and hollow tubes (of a single-bilayer wall) rolled from the distorted lamellar slabs. 128
- Figure 4-10 SAXS intensity profiles measured for the (a) HS/M and (b) HS/H blends, with the respective compositions indicated. The lamellar reflections are marked by the thin arrows, whereas the scattering humps from the form factor of slabs are marked with circled numbers in (b). The thick arrows nearby the first lamellar peaks indicate the coexisting of two types of lamellae. In (a) and (b) the two dotted lines across all the SAXS profiles for the HS/V and HS/M blends illustrate the opposite shifting directions of the first peak position. 129
- Figure 4-11 Correlation between the fraction of hydrogen bonded groups f_b deduced from FTIR and the phase behavior observed via TEM and SAXS, for the PS-*b*-PVPh-based, A-*b*-B/C type of polymer blends. 130
- Figure 4-12 Schematic representation of an A-*b*-B/C blend system featuring in hydrogen bonding interactions. Note that the molar weight of the homopolymer should be comparable or smaller than that of the hydrogen-bonding associated block of the copolymer. 131

Figure 4-13	Relative changes in (a) the lamellar long period D/D_0 and (b) the average distance of the chemical junctions along the interface a_1/aJ_0 , for the HS/H, HS/M, and HS/V blends, upon addition of the homopolymer. The lines over the data points are only for eye-guiding.	132
Figure 4-14	Representative relative electron density profiles of (a) the neat PVPh- <i>b</i> -PS and (b) the three blends of (b) HS/H=94/6, HS/M=94/6, and HS/V=94/6. (c) The transition zone thickness D_{tr} extracted for all the blends with a lamellar phase at lower volume fractions of homopolymers. In (a), the D_0 and D_{PS} values thus defined are consistent with the values obtained from the 1-D correlation function. The D_{tr} is defined by the zone where the electron density grows from 10% to 90% of the peak value, as illustrated.	133
Figure 5-1	(a) ^1H and (b) ^{13}C NMR spectra of PS- <i>b</i> -P4VP.	153
Figure 5-2	FTIR spectra of the pyridine band of the pure PS- <i>b</i> -P4VP and mixtures of OG and PS- <i>b</i> -P4VP in the range 1550-1650 cm^{-1} in (a) chloroform and (b) THF and in the range 990-1020 cm^{-1} in (c) chloroform and (d) THF with the different molar ratios, respectively.	154
Figure 5-3	The hydrodynamic diameter distribution of the mixtures of OG and PS- <i>b</i> -P4VP with the different molar ratios in chloroform.	155
Figure 5-4	The intensity of the scattering of the mixtures of OG and PS- <i>b</i> -P4VP with the different molar ratios in chloroform.	155
Figure 5-5	^1H NMR spectra of the (a) pure PS- <i>b</i> -P4VP and the mixtures of OG and PS- <i>b</i> -P4VP (b) at $R = 1/20$ and (c) $R = 1$ in CDCl_3 .	156
Figure 5-6	TEM images of the morphologies of the mixtures of OG and PS- <i>b</i> -P4VP (a) at $R = 1/50$, (b) at $R = 1/10$, (c) at $R = 1/3$, and (f) at $R = 1$.	156
Figure 5-7	SEM images of the morphologies of the (a) pure PS- <i>b</i> -P4VP and the mixtures of OG and PS- <i>b</i> -P4VP (b) at $R = 1/100$, (c) at $R = 1/50$, (d) at $R = 1/10$, (e) at $R = 1/3$, and (f) at $R = 1$.	157
Figure 5-8	^1H NMR spectra of the (a) pure PS- <i>b</i> -P4VP and the mixtures of OG and PS- <i>b</i> -P4VP (b) at $R = 1/20$ and (c) $R = 1$ in THF- <i>d</i> .	158
Figure 5-9	TEM images of the morphologies of the (a) pure PS- <i>b</i> -P4VP and the mixtures of OG and PS- <i>b</i> -P4VP (b) at $R = 1/50$, (c) at $R = 1/20$, (d) at $R = 1/10$, (e) at $R = 1/5$, and (f) at $R = 1$.	159
Figure 5-10	The hydrodynamic diameter distribution and intensities of the mixtures of OG and PS- <i>b</i> -P4VP with the different molar ratios in DMF.	160
Figure 5-11	Proposed the aggregate behaviors of the mixtures of OG and PS- <i>b</i> -P4VP with the different molar ratios from the different common solvents.	161

Chapter 1

Introduction to Hydrogen Bond in Polymer Blends

1-1 The Definition of the Hydrogen Bond

The hydrogen bonding has such ubiquitous influence in gaseous, liquid, and solid-state chemistry that its consequences were observed long before it was identified and given a name. Most chemists, biochemist, and even some physicists have at least a passing notion of nature of hydrogen bonding and its effect on the structure, biological and physical properties of various materials.¹⁻⁶ Classic example is water, it is now recognized that the anomalous properties of this ubiquitous material are a result of the arrangement of the molecules in a dynamic three-dimensional network, made possible by the ability of each molecule to hydrogen bond to up to four different neighbors. Another example of system where the elucidation of the role of hydrogen bonding led to an understanding of structure and functional are found in molecular biology, where Pauling et al.⁷⁻⁸ identified the α -helix and β -sheet structures of polypeptides and, of course, Watson and Crick⁹ proposed that the double stranded DNA molecules is determined by the complementary nature of the hydrogen bonds formed between pyrimidine and purine residues.(Figure 1-1) In general, if a material hydrogen bonds there is often a profound effect on various physical properties, including melting temperature, the glass transition temperature, dielectric constant, choice of crystal structure, the central concern of this study, its solubility or ability to form miscible blend with another material.

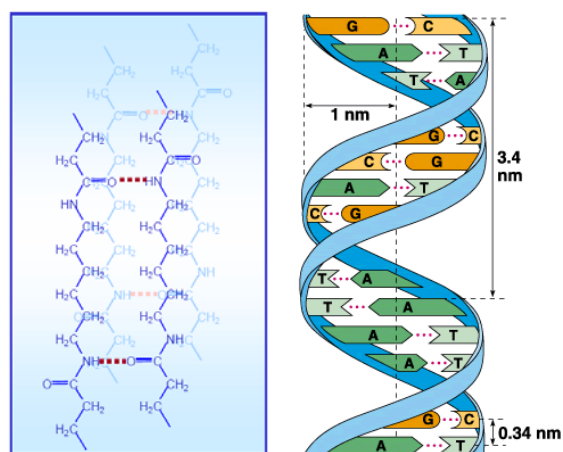


Figure 1-1. The schematic structures of the double strand DNA molecule and hydrogen bonds formed between pyrimidine and purine residues.

The general definition of a hydrogen bond was made by Pimental and McCellan¹⁰, as follows: “A hydrogen bond exist between the functional group, B-H, and an atom or a group of atoms, A, in the same or different molecules when (a) there is evidence of bond formation (association or chelation), (b) there is evidence that this new bond linking B-H and A specifically involves a hydrogen atom already bonded to B”. According to this definition, hydrogen bonding is a donor-acceptor interaction specifically involving hydrogen atoms, A and B are used for the hydrogen bond acceptor and donor respectively because of the analogy with the Brönsted-Lewis acid and base respectively; in other words, A is a proton acceptor and B is a proton donor. The proton usually lies on a line joining the A, B atoms, i.e., the hydrogen bond is linear; A-H...B, and the distance between the nuclei of the A and B atom is considerably less than the sum of the van der Waals radii of A and B and the diameter of the proton, i.e. the formation of the hydrogen bond leads to a contraction of the A-H...B system. The atom A and B are usually only the most electronegative, i.e. F, O, and N. Chlorine is as electronegative as nitrogen, but because of its larger size only form weak hydrogen bonds. Hydrogen bonds involving S, some C-H groups and the π electrons on aromatic rings have also been invoked. Different from general covalent bond, ionic bonds and van der Waals forces, hydrogen bond applies to a wider range of interaction: very strong hydrogen bonds

resemble covalent bonds, and very weak hydrogen bonds are close to van der Waals force. The majority of hydrogen bonds are distributed between two extremes. Covalent bonds have strengths of the order 50 kcal/mole; van der Waals attractions may be of the order of 0.2 kcal/mole, while hydrogen bonds most often lie in the range 1-10 kcal/mole. Furthermore, the hydrogen bonds can exist intermolecular or intramolecular and this range of energies is like in liquid at room temperature there is a dynamic situation, with hydrogen bonds constantly breaking and reforming at the urgings of thermal motion. For example, the water has been estimated that the mean lifetime of a hydrogen bond is of the order of 10^{-11} seconds.¹¹

1-2 Hydrogen Bond in Polymer Blends

Hydrogen bonding plays an important role in the polymer blend research because of their potential application in industry or in biomedical engineering. It can affect the physical properties of polymer such as glassy transition temperature¹²⁻¹³, surface free energy¹⁴⁻¹⁵, the miscibility of the polymer¹⁶⁻¹⁷, the dynamic of the polymer segment¹⁸⁻¹⁹, and so on. Moreover, for blends of nonpolar polymers²⁰⁻²¹, the mixing process is thermodynamic unfavorable because of decreasing the combination entropy of mixing as blending two or more polymers. But the miscibility can be enhanced by introducing specific interaction, especially hydrogen bonding, to decrease the van Laar type energy of interaction characterized by a Flory-Huggins interaction parameter.

Theoretically, it has become clear that the miscibility of polymer blends is mainly determined by the chemical structure, composition and molecular weight of each component. In some cases, the prepared condition of the blends is also a decisive factor. Experimentally, various techniques have been used to characterize the miscibility of the polymer blends, such as optical transparency, Fourier transfer infrared spectroscopy (FTIR), electron microscopy, differential scanning calorimetry, dynamic mechanic thermal analysis, dielectric relation, and high resolution solid state ¹³C NMR spectroscopy. Traditionally, DSC has been used to

determine the phase diagram of polymer blends, a single glass transition temperature denoting a single-phase blend. So, in the following, it will be focused on the miscibility and the glass transition temperature of polymer blend.

1-3 Introduction to Painter-Coleman Association Model

Homogeneous miscibility in polymer blends requires a negative free energy of mixing, that is $\Delta G_{\text{mix}} < 0$. According to Flory–Huggins equation:

$$\frac{\Delta G_{\text{mix}}}{RT} = \frac{\Phi_1}{N_1} \ln \Phi_1 + \frac{\Phi_2}{N_2} \ln \Phi_2 + \chi_{12} \Phi_1 \Phi_2 \quad (1-1)$$

where ΔG_{mix} is the change of free energy on mixing two polymers, R is the gas constant, T is the temperature, Φ_1 and Φ_2 are the volume fractions and N_1 and N_2 are the segment numbers of the two blend components, respectively, and χ_{12} is the Flory interaction parameter. When two high molecular weight polymers are blended, the gain in entropy, $\Phi_1 \ln(\Phi_1)/N_1 + \Phi_2 \ln(\Phi_2)/N_2$, is quite small, and the free energy of mixing, ΔG_{mix} , can be negative only if the heat of mixing is near zero or negative. The third term of Eq. 1-1 contains the ubiquitous Flory interaction parameter χ , and expresses a generally unfavorable contribution (except in rare cases when $\chi = 0$) to the free energy of mixing emanating from so-called “physical” forces. Values of χ for polymer mixtures appear to be estimated fairly accurately from Eq.1-2,

$$\chi = \frac{V_B}{RT} (\delta_A - \delta_B)^2 \quad (1-2)$$

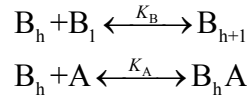
using solubility parameters (denoted δ_A , δ_B for (co)polymer A and B, respectively) calculated from group molar attraction and molar volume constants that were derived from a set of model compounds that do not self-associate to any measurable extent (i.e. molecules in which the interaction forces are dispersive or only weakly polar in nature).

Painter and Coleman used association model to describe hydrogen bonding interactions and simply added this contribution to the Flory-Huggins equation for the free energy of

mixing:

$$\frac{\Delta G_{mix}}{RT} = N_B \ln \Phi_B + N_A \ln \Phi_A + n_B \Phi_A \chi + \frac{\Delta G_H}{RT} \quad (1-3)$$

where N_B , N_A are the number of polymer molecules present and n_B is the total number of B segments. In essence, this is the classic Flory-Huggins equation plus an additional term, $\Delta G_H/RT$, that accounts for the (generally favorable) free energy contribution that arises from “chemical” forces. The free energy contribution from $\Delta G_H/RT$ was originally derived using a simple association model. For the uncomplicated equilibrium scheme depicted below:



where the distribution of hydrogen bonded species in the polymer blend may be adequately described by two equilibrium constants, one that describes “chain-like” self-association, K_B , and the other that describes inter-association, K_A , $\Delta G_H/RT$ was expressed as:

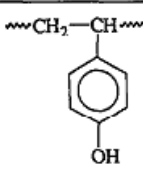
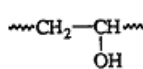
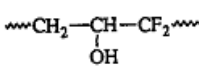
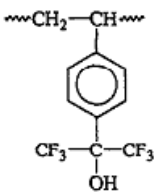
$$\begin{aligned} \frac{\Delta G_H}{RT} = & \sum n_{B_h} \ln \left(\frac{\Phi_{B_h}}{h} \right) + \sum n_{B_h A} \ln \left(\frac{\Phi_{B_h A}}{h+r} \right) + n_{A_1} \ln \left(\frac{\Phi_{A_1}}{r} \right) + n_{BB}^h + n_{AB}^h + \\ & (\text{terms in } z \text{ and } \sigma) - [n_B \ln \Phi_B + n_A \ln \Phi_A] - n_{BB}^h \ln K_B - n_{AB}^h \ln K_A \end{aligned} \quad (1-4)$$

The association model (from Flory) were used to describes the mixing of small molecules, or in effect, describes the mixing of disconnected polymer segments and therefore contains an excess combinatorial entropy of mixing (ΔS_{excess}), which must be subtracted. The excess entropy term is contained in the square bracket of Eq. 1-4. With the “physical” force deduced from solubility parameters, ΔG_H may be determined from the equilibrium constants and enthalpies of hydrogen bond formation. As the combinatorial entropy is very small, the free energy of mixing, and thus the miscibility, are dominated by the balance of the “physical” force and enthalpy of hydrogen bond formation.

The inter-association equilibrium constant K_A , often given for a particular temperature, e.g. 25 °C, provides a measure of the tendency of the inter-associated hydrogen-bonding interaction. They can be utilized to evaluate the effect of structure or other factor on

hydrogen bond formation. In fact, Coleman and co-workers reported²² that the relative strength of inter-association compared to self-association, a measure of which can be determined from the ratio of K_A/K_B (see Table 1-1), is an indicator of the relative efficiency that a particular hydroxyl group has in rendering a polymer blend system miscible. In other words, if inter-association is strong favored over self-association, as it is in the case of polymer blends involving hexafluoro-s-phenyl-2-propanol and acetoxy group ($K_A/K_B \doteq 10$), this is advantageous and something we look for in designing miscible polymer blend systems. Conversely, if self-association is strongly favored over inter-association, as it is in the case of polymer blends involving secondary aliphatic hydroxyl and acetoxy group ($K_A/K_B \doteq 0.1$), this is not an interaction of choice if polymer miscibility is our goal.

Table 1-1. Dimensionless Self- and Inter-Association Equilibrium Constants Values Determined from Miscible Polymer Blends Scaled to a Common Reference Volume (100 cm³/mol)

Polymer structure	Self-association		Inter-association	
	Dimer formation K_2	Multimer formation K_B	Methacrylate carbonyl K_A	Acetoxy carbonyl K_A
	21.0	66.8	37.8 $\left[\frac{K_A}{K_B} \approx 0.6\right]$	58 $\left[\frac{K_A}{K_B} \approx 1\right]$
	26.7	44.1	–	4.0 $\left[\frac{K_A}{K_B} \approx 0.1\right]$
	7.5	27.3	61.1 $\left[\frac{K_A}{K_B} \approx 2\right]$	–
	4.3	5.8	21.8 $\left[\frac{K_A}{K_B} \approx 4\right]$	58.7 $\left[\frac{K_A}{K_B} \approx 10\right]$

1-4 Influence Factors of Hydrogen Bonds

1-4.1 Acidity of the Proton Donor and Basicity of the Proton Acceptor

In our previous studies, the role of the chemical structure of proton donating polymers on the strength of hydrogen bonds in binary blends with poly(ϵ -caprolactone) (PCL) has been addressed. They investigated the hydrogen bonds formed between the C=O group of PCL and the hydroxyl group of the phenolic formaldehyde-phenol copolymer, poly(4-vinylphenol) (PVPh), and the phenoxy bisphenol A-epichlorohydrin copolymer through the DSC and FTIR analyses. Clearly, the fraction of hydrogen bond formation with PCL occurs in the order phenolic/PCL > PVPh/PCL > phenoxy/ PCL blends as shown in Figure 1-2.²³ Furthermore, the K_A and relative ratio of K_A/K_B calculated from Painter-Coleman association model are in the same order. Thus, the strength of hydrogen bonds decreased in the order of phenolic/PCL > PVPh/PCL > phenoxy/ PCL, which is the order of the acidity of the proton donors.

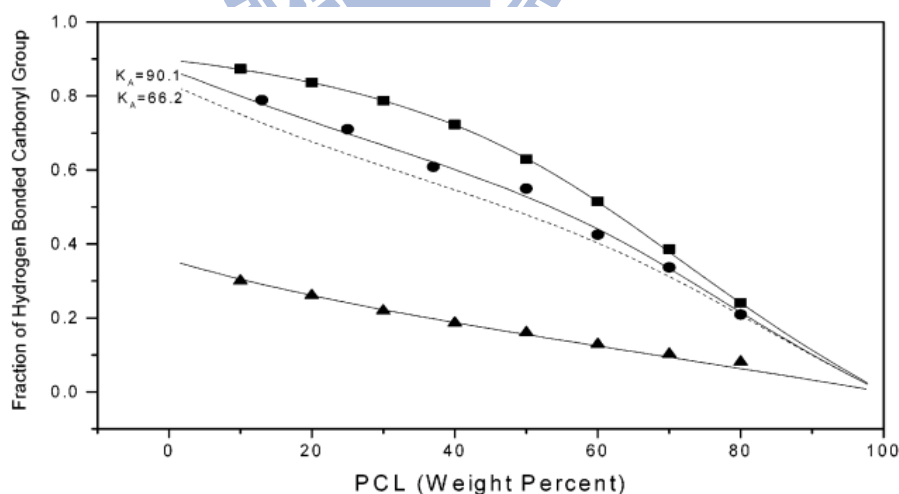
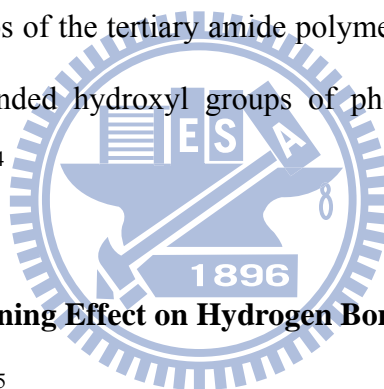


Figure 1-2. Relationship between experimental data and theoretical prediction by PCAM of hydrogen bonded fraction of carbonyl group within various PCL blend systems: (■) phenolic/PCL, (●) PVPh/PCL, (▲) phenoxy/PCL.

The impact of the chemical structure of proton-accepting polymers on the strength of hydrogen bonds has been studied. Goh et al. investigated binary blends of the phenoxy with three isomeric tertiary amide polymers: poly(*N*-methyl-*N*-vinylacetamide) (PMVAc), poly(*N,N*-dimethyl acrylamide) (PDMA), and poly(2-ethyl-2-oxazoline) (PEOx).²⁴ Phenoxy forms interpolymer complex with PMVAc and PDMA in tetrahydrofuran (THF). However, phenoxy does not form interpolymer complex with PEOx in THF, implying that a weaker inter-association of the phenoxy/PEOx blend than those of both phenoxy/PMVAc and phenoxy/PDMA blends. When using *N,N*-dimethylformamide as solvent, only miscible blends were formed between phenoxy and all three tertiary amide polymers. The FTIR analyses provided evidence that the hydrogen bonds were formed between the hydroxyl groups of phenoxy and the C=O groups of the tertiary amide polymers. Furthermore, the IR frequency shifts for the hydrogen bonded hydroxyl groups of phenoxy decreased in the order of PMVAc > PDMA > PEOx.²⁴



1-4.2 Intramolecular Screening Effect on Hydrogen Bond

In a recent publication²⁵ Coleman et al. suggested that equilibrium constants determined from appropriate low molar mass mixtures could be used to calculate the hydrogen bonding contribution to the free energy of mixing of analogous polymer blends, after due account is taken of factors attributed to chain connectivity. Two of the more important chain connectivity effects, intramolecular screening and functional group accessibility, have been previously proposed.

We commence to discuss these effects with a well-established miscible polymer blend system composed of two amorphous homopolymers, poly(4-vinylphenol) (PVPh) and poly(vinyl acetate) (PVAc). Dimensionless standard equilibrium constant values (based on a common reference molar volume $V_B^3 = 100 \text{ cm}^3/\text{mol}$) have previously been determined from

appropriate low molecular mass analogues [4-ethylphenol (EPh) and ethyl isobutyrate (EIB)].¹² These standard equilibrium constants ($K_2^{\text{Std}} = 21.0$; $K_B^{\text{Std}} = 66.8$ (self-association) and $K_A^{\text{Std}} = 170$ (interassociation)) describe the fraction of the various hydrogen bonded species present in a solution of EPh/EIB as a function of composition at 25 °C. This represents the case where there are no effects due to chain connectivity and all the values remain constant regardless of blend composition (depicted at the top of Figure 1-3; $\gamma = 0$).

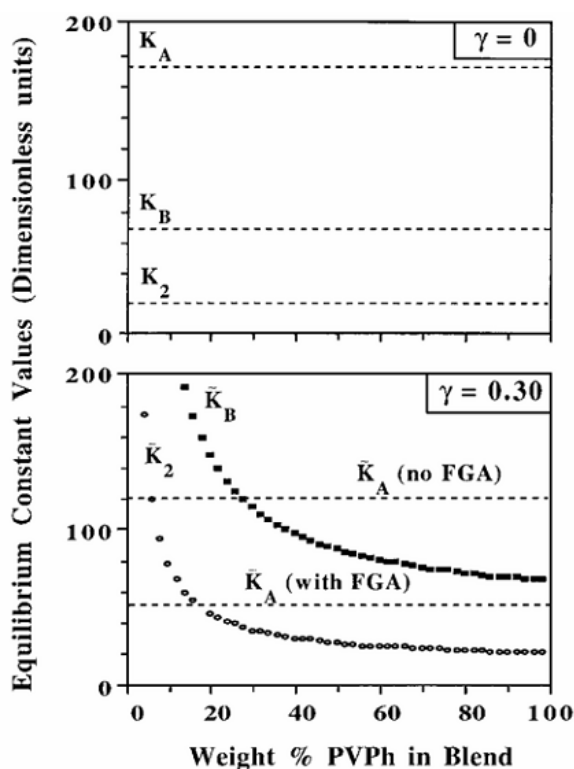


Figure 1-3. Equilibrium constant values for the PVPh-PVAc blend system (FGA: functional group accessibility).

Chain connectivity effects modify equilibrium constant values. Intramolecular screening is accounted for through the parameter γ , which is defined as the fraction of same chain contacts that originate from the polymer chain bending back upon itself, primarily through local, but also through long range effects.²⁶ It is probably sufficient to simply state

that new self-association equilibrium constants K_B (and K_2) are calculated that are now a function of blend composition (Φ_B). For example:

$$\tilde{K}_B = K_B \left[\frac{\gamma + (1-\gamma)\Phi_B}{\Phi_B} \right] \quad (1-5)$$

Typical results are depicted at the bottom of Figure 1-3 using an appropriate γ value for high molecular weight polymer blends of 0.30.²⁶ On the other hand, the new interassociation equilibrium constant, K_A , is not a function of blend composition and is given by:

$$\tilde{K}_A = K_A \left[\frac{\gamma + (1-\gamma)\Phi_B}{\Phi_A} \right] = K_A(1-\gamma) \quad (1-6)$$

This invariance is also depicted at the bottom of Figure 1-4, labeled K_A , and has a value of $170 \times 0.70 = 119$ (dimensionless units).

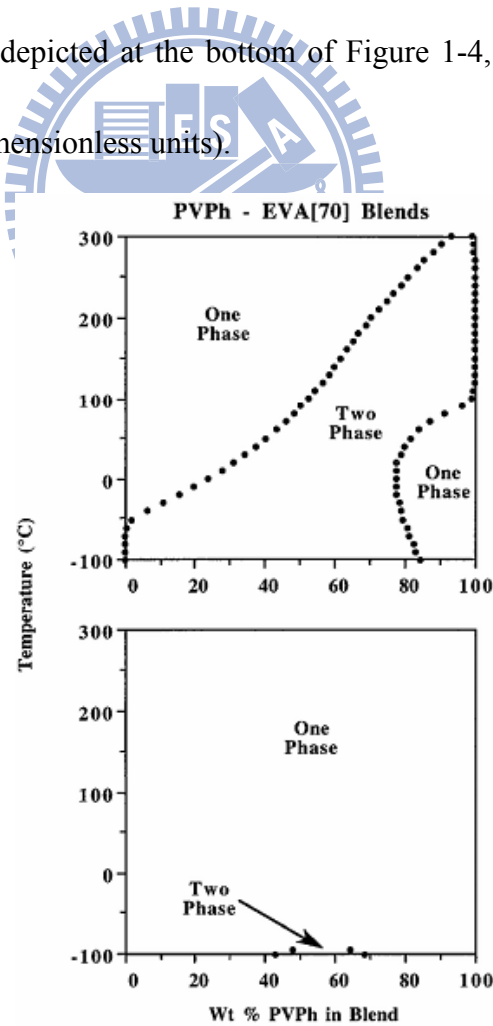


Figure 1-4. Theoretical spinodal phase diagrams for PVPh/EVA blends.

1-4.3 Functional Group Accessibility Effect on Hydrogen Bond

Functional group accessibility (FGA) is a generic term that Coleman et al. have introduced to describe the reduction in the number of intermolecular hydrogen bonds formed between complementary functional groups (e. g., phenolic hydroxyls and acetoxy carbonyls) in (co)polymer blends that arises from the close proximity of either or both functional groups in their respective (co)polymer chains.²⁷⁻²⁸ Naturally, this effect is most acute in a blend of two homopolymers like PVPh and PVAc, but becomes less important as they consider blends of copolymers where the functional groups are spaced well apart. Elsewhere Painter and Coleman have described an empirical equation determined from experimental infrared studies that describes this effect for independent copolymers containing phenolic hydroxyls and acetoxy carbonyls. This equation has the form:

$$\tilde{K}_A = 112.4 - \left[\frac{1630}{70 + R_A} + \frac{4100}{100 + R_B} \right] \quad (1-7)$$

where R_A and R_B are the average molar volumes between VAc and VPh groups, respectively, in the specific repeat of the respective copolymers. For PVPh-PVAc blends the value of K_A is calculated to be 55 dimensionless units. This is also depicted in Figure 1-3.

It is now a relatively straightforward task to employ the relevant stoichiometric equations using the different sets of equilibrium constant values discussed above and calculate the theoretical equilibrium fraction of hydrogen bonded acetoxy groups present in a single phase mixture of PVPh and PVAc as a function of blend composition at 25 °C.²²⁻²⁹

The results are displayed in Figure 1-5. The top curve denotes the fraction of hydrogen bonded carbonyl groups for the $\gamma = 0$ case (calculated using compositionally invariant values of $K_2^{\text{Std}} = 21.0$; $K_B^{\text{Std}} = 66.8$ and $K_A^{\text{Std}} = 170$ dimensionless units). If we now “switch on” intramolecular screening by introducing a c value of 0.30 (now the self-association

equilibrium constants, K_2 and K_B , are compositionally dependent, but the inter-association equilibrium constant is not and has a constant value of $K_A = 119$ (dimensionless units), we obtain the middle curve.

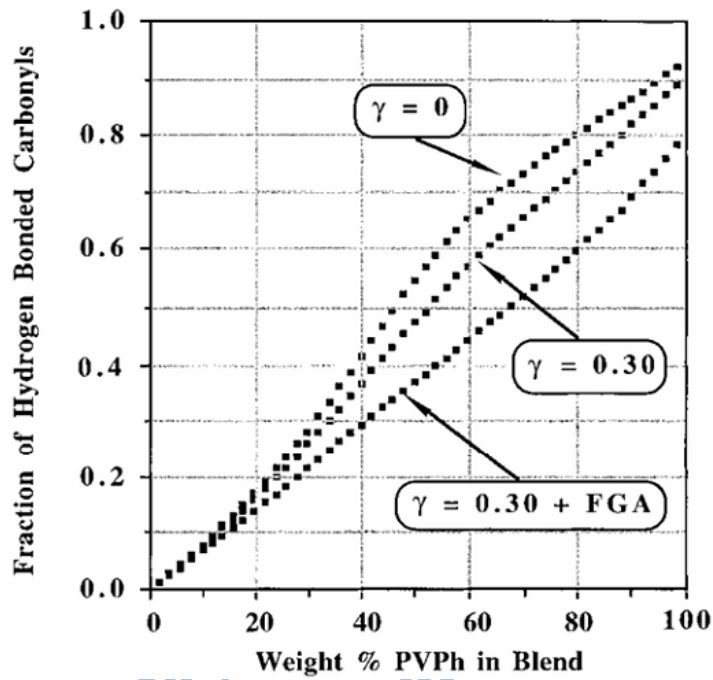


Figure 1-5. Calculated fraction of hydrogen bonded acetoxy carbonyl groups for the PVPh-PVAc blend system at 25°C.

Note that the fraction of hydrogen bonded carbonyl groups has decreased significantly over that calculated in the absence of intramolecular screening, especially for blends that are compositionally rich in PVPh. There are further substantial decreases when FGA effects are taken into account through Eq. 1-7, and this is depicted in the lower curve (here K_2 and K_B are still compositionally dependent and K_A now has a constant value of 55 dimensionless units). If we compare, for example, the theoretical fraction of hydrogen bonded carbonyl groups present in a single phase 60:40 wt.% PVPh-PVAc blend for the

three different cases, we obtain values of approximately 0.67 ($\gamma = 0$), 0.58 ($\gamma = 0.30$) and 0.45 ($\gamma = 0.30 + \text{FGA}$). These are large differences that have profound repercussions on the amount of favorable free energy that is available from the changing pattern of the hydrogen bonds formed in the mixture relative to the pure components. Clearly, intramolecular screening and functional group accessibility (spacing) effects cannot be ignored if we are to successfully predict phase behavior of polymer blends.

1-4.4 Temperature Effect on Hydrogen Bond

In general, K_A and the number of the hydrogen bonds for a given system decrease with increasing temperature because the enthalpy of the hydrogen bond formation is negative. FTIR spectra as a function of temperature were summarized in Figure 1-6 for PCL/TDP = 60/40 blend in the hydroxyl and the carbonyl vibration region.³⁰ The absorbance of the hydroxyl became weak and shifted to high wavenumber upon increasing temperature. In the carbonyl vibration region, the intensity of the peak corresponding to the hydrogen-bonded carbonyl decreases with increasing temperature. The inter-association hydrogen bonds become weak and the number of hydrogen bond decreases with increasing temperature above mentioned.

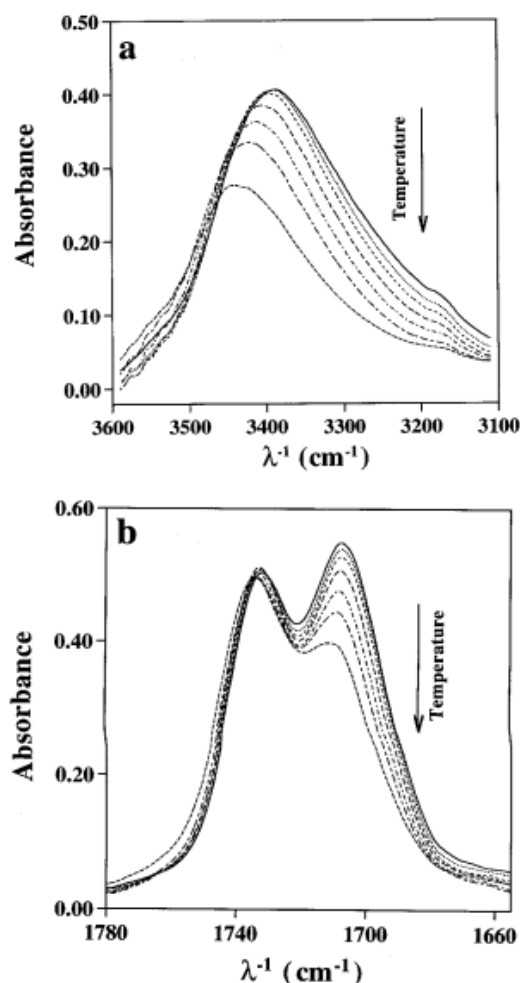


Figure 1-6. The FTIR spectra of the PCLTDP40 blend in the hydroxyl vibration region (a) and the carbonyl vibration region (b) recorded at different temperatures. From top to bottom, the temperatures are 26, 35, 45, 65, 90, 120 and 160°C.

1-4.5 Solvent Effect on Hydrogen Bond

The nature of the solvent plays an important role affecting the formation of the hydrogen bond because the solvent molecules can also participate in hydrogen bonding interactions. Taft et al. has reported that the solvatochromic comparison method to construct a β -scale of solvent hydrogen-bond acceptor ability ($\beta \sim$ HBA basicity) and a α -scale of solvent hydrogen-bond donor ability ($\alpha \sim$ HBA acidity).³¹⁻³² Through UV/Vis spectrum analysis of *N,N*-diethyl-4-nitroaniline, a nonprotonic indicator in non-HBA solvent,

shifted bathochromically with increasing solvent dipolarity, the relative hydrogen-bond donor ability or the relative hydrogen bond acceptor ability of different solvents can be obtained. DMF is a polar aprotic solvent with higher hydrogen-bond acceptor ability basicity than that of methanol, and dichloromethane is just a polar aprotic solvent with very low hydrogen-bond acceptor ability.

If the solvent molecule can play a role as a hydrogen-bond donor or hydrogen-bond acceptor, some properties of the polymer blend may be changed, especially miscibility. It is also possible to change an ordinary, miscible blend into a complex blend by merely strengthening intermolecular hydrogen-bonding interactions.³³⁻³⁴ For example, PVPh/poly(*N,N*-dimethylacrylamide) (PDMA) blends form a complex precipitate in dioxane, but do not precipitate from DMF. Because solvent molecules can also participate in hydrogen bonding interactions, they compete with PDMA for coordination to the OH groups of PVPh. Consequently, when the polymer–polymer interactions are sufficiently strong to overcome the polymer–solvent interactions, the two polymer chains can co-precipitate in the form of highly associated materials (complexes). If the solvent interacts so strongly with the polymers that it prevents precipitation, the resulting materials obtained upon evaporation of the solvent are considered to be merely blends.

1-5 Experimental Characterization of Hydrogen Bonds

Hydrogen bonds are not easily characterized. In highly crystalline solid, the positions of the hydrogen atom or, more precisely, pattern of electron density, can theoretically be determined by X-ray diffraction, but the size of the proton and the amplitude of thermal vibration make this an extraordinary demanding task. In certain materials, neutron diffraction has been used to locate the position of the proton. Even if these methods were easily applied to the whole range of crystalline solid with the hydrogen bonds, however, this would still leave a yawning gap. Many materials of interest are either liquid or amorphous

solid at ambient temperature. In principle, two types of experimental studies that could be applied to the characterization of polymers; one is thermodynamic, and the other one is spectroscopic.³⁵

Thermodynamic measurements depend upon changes in a system as a whole and can be related to molecular properties through the methods of statistical mechanism, but the results are often model dependent and sensitive to the various assumptions that have to be made. Furthermore, direct measurements of quantities such as the heat of mixing cannot be performed on polymer directly, and studies are often confined to low molecular weight analogues. Accordingly, this leaves the art of spectroscopy as the most powerful probe of the nature of hydrogen bonding. The most widely used method are:

1. Infrared (IR) and Raman technique:

Infrared and Raman spectra reveal the characteristic frequencies of molecular vibration. Such frequencies are fixed by the masses of the vibrating atoms, the molecular geometry, and the restraining forces (force constant) are simply related to chemical bond orders, vibrational spectra have been a powerful source of information concerning chemical bonding and molecular structure. Consequently, it is fortunate to reveal the vibrational spectra significantly disturbed by hydrogen bond formation.

2. Magnetic resonance spectroscopy (NMR):

Since 1950 there has been a rapid development of the use of nuclear magnetic resonance (NMR) for investigation of a variety of problems of chemical interest. The accumulating proton magnetic resonance studies of organic molecules give promise that the method will match IR spectroscopy as a diagnostic tool and a probe of molecular structure. This technique can be used to study the effect of hydrogen bond formation on the chemical shift of A-H proton.

3. Electronic absorption and fluorescence spectroscopy:

The UV/Vis spectrum of a molecule may be altered by the formation of a hydrogen

bond if the chromophoric portion of the molecule is perturbed by the hydrogen bond. Such is indeed the case: hydrogen bond formation often is accompanied by readily measurable spectral changes which contain interesting and useful information. In this spectrum, it can show the effect of hydrogen bond formation on the electronic levels of the participating molecules.

Of these, by far the most sensitive is the infrared spectroscopy. Recently, solid state NMR spectroscopy also can provide a tool to clarify the phase behavior and morphology of polymer blends involving the hydrogen bond formation. The ^{13}C chemical shift and line shape in cross polarization and magic angle spinning (CP/MAS) spectra can identify chemical environments of carbon in the blends, since the chemical shift and the line shape are highly sensitive to the local electron density. If a specific interaction affects the local electron density, a change in chemical shift can be observed. This approach has been widely offered as evidence of the interaction between the blend components. The scale of miscibility of a polymer blend can be estimated from proton spin-lattice relaxation times in the rotating frame ($T_{1\rho}^{\text{H}}$), measured by solid state NMR. However, we will show later, the vibrational spectroscopy not only allow a measure of the strength or enthalpy of hydrogen bond interactions, but also more crucially allows a determination of the number of free and hydrogen bonded groups. The determination of the hydrogen bond formation then allows a calculation of the vibration of these parameters with temperature.

References

- [1] Errera, J.; Mollet, P. *Nature* **1936**, *138*, 882.
- [2] Schwager, F.; Marand, E.; Davis, R. M. *J. Phys. Chem.* **1996**, *100*, 19268.
- [3] Van Ness, H. C.; Winkle, J. V.; Richtol, H. H.; Hollinger, H. B. *J. Phys. Chem.* **1967**, *71*, 1483.
- [4] Johari, G. P.; Dannhauser, W. *J. Phys. Chem.* **1968**, *72*, 3273.
- [5] Dannhauser, W. *J. Chem. Phys.* **1968**, *48*, 1991.
- [6] Musa, R. S.; Eisner, M. *J. Chem. Phys.* **1959**, *30*, 227.
- [7] Pauling, L.; Corey, R. B.; Branson, H. R. *Proc. Nat. Acad. Sci.* **1951**, *37*, 205.
- [8] Pauling, L.; Corey, R. B. *Proc. Nat. Acad. Sci.* **1951**, *37*, 729.
- [9] Watson, J. P.; Crick, F. H. *Nature* **1953**, *171*, 737.
- [10] Pimental, G. C.; McClellan, A. L. “*The Hydrogen Bond*”, W. H. Freeman and Company, San Francisco, **1960**.
- [11] Londe, O.; Teixeira, J. *J. Phys.* **1983**, *44*, 525.
- [12] Coleman, M. M.; Xu, Y.; Painter, P. C. *Macromolecules* **1994**, *27*, 127.
- [13] Kuo, S. W.; Kao, H. C.; Chang, F. C. *Polymer* **2003**, *44*, 6873
- [14] Chen, J. K.; Kuo, S. W.; Kao, H. C.; Chang, F. C. *Polymer* **2005**, *46*, 2354.
- [15] Liu, S.; Chan, C. M.; Weng, . T.; Jiang, M. *J. Polym. Sci. Part B: Polym. Phys.* **2005**, *43*, 1924.
- [16] Kuo, S. W.; Liu, W. P.; Chang, F. C. *Macromol. Chem.* **2005**, *206*, 2307
- [17] Neelakandan, C.; Kyu, T. *Polymer* **2009**, *50*, 2885.
- [18] Zhang, S. H.; Jin, X.; Painter, P. C.; Runt, J. *Polymer* **2004**, *45*, 3933.
- [19] Yang, Z.; Han, C. D. *Macromolecules* **2008**, *41*, 2104.
- [20] Painter, P. C.; Park, Y.; Coleman, M. M. *Macromolecules* **1988**, *21*, 66.
- [21] Lee, J. Y.; Painter, P. C.; Coleman, M. M. *Macromolecules* **1988**, *21*, 954.
- [22] Coleman, M. M.; Painter, P. C. *Prog. Polym. Sci.* **1995**, *20*, 1.

- [23] Kuo, S. W.; Chan, S. C.; Chang, F. C. *Macromolecules* **2003**, *36*, 6653.
- [24] Dai, J.; Goh, S. H.; Lee, S. Y.; Siow, K. S. *Polymer* **1996**, *37*, 3259.
- [25] Coleman, M. M.; Painter, P. C. *Macromol. Chem. Phys.* **1998**, *199*, 1307.
- [26] Painter, P. C.; Veytsman, B.; Kumar, S.; Shenoy, S.; Graf, J. F.; Xu, Y.; Coleman, M. M. *Macromolecules* **1997**, *30*, 932.
- [27] Coleman, M. M.; Pehlert, G. J.; Painter, P. C. *Macromolecules* **1996**, *29*, 6820.
- [28] Pehlert, G. J.; Painter, P. C.; Veytsman, B.; Coleman, M. M. *Macromolecules* **1997**, *30*, 3671.
- [29] Coleman, M. M.; Graf, J. F.; Painter, P. C. *Specific Interactions and the Miscibility of Polymer Blends*; Technomic Publishing, Inc.; Lancaster, PA, **1991**.
- [30] He, Y.; Asakawa, N.; Inoue, Y. *Macromol. Chem. Phys.* **2001**, *202*, 1035.
- [31] Kamlet, M. J.; Taft, R. W. *J. Am. Chem. Soc.* **1976**, *98*, 377.
- [32] Kamlet, M. J.; Abboud, J. L. M.; Abraham, M. H.; Taft, R. W. *J. Org. Chem.* **1983**, *48*, 2877.
- [33] Qiu, X.; Jiang, M. *Polymer* **1994**, *35*, 5084.
- [34] Jiang, M.; Qiu, X.; Qin, W.; Fei, L. *Macromolecules* **1995**, *28*, 730.
- [35] Jeffery, G. A. "An Introduction to Hydrogen Bonding" Oxford University Press: New York, **1997**, Ch.6.

Chapter 2

Introduction to Self-Assembly of Block Copolymer

2-1 The Definition of the Self-Assembly Behavior

Self-assembly is the spontaneous association of molecules under equilibrium conditions into stable, structurally well-defined aggregates joined by non-covalent bonding forces such as steric, hydrophobic, hydrogen-bonding, electrostatic interactions. Self-assembly is ubiquitous in biological systems. Using nature as a blueprint, a well-known example is the formation of collagen, the most abundant protein in mammals, in which three polypeptide chains fold into triple-stranded helices, which then, in a subsequent process, self-assemble into collagen fibers (Figure 2-1)¹. Besides biological architectures, self-assembly is also emerging as a new strategy in chemical synthesis, with the potential generating non-biological structures having dimensions of 1 to 10^2 nanometers (with molecular weights of 104 to 1010). Creating nanoscale architectures by using chemical synthesis has been, and still is the essential goals of many researchers in the fields of chemistry and physics.

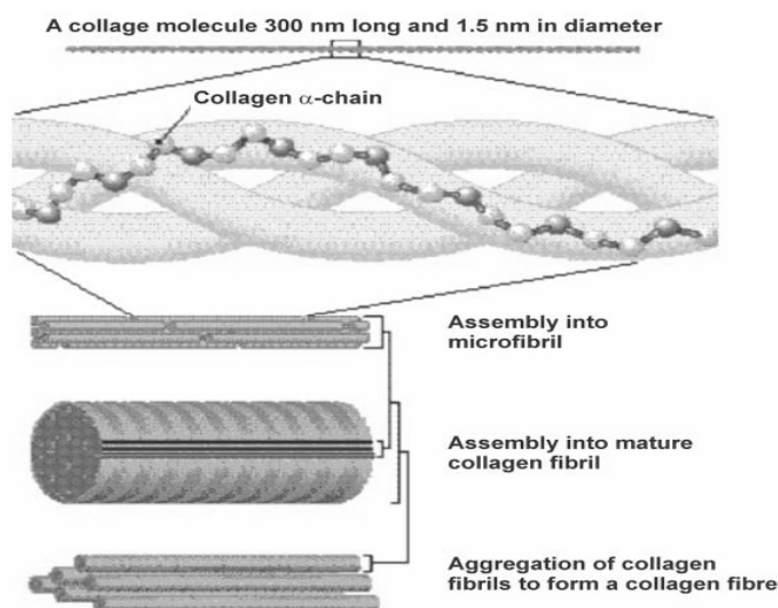


Figure 2-1. Hierarchical self-assembly of collagen.

In 2002, as commented by Whitesides, Self-assembly is the autonomous organization of components into patterns or structures without human intervention²⁻⁶. Self-assembling processes are common throughout nature and technology. They involve components from the molecular (crystals) to the planetary (weather systems) scale and many different kinds of interactions. There are two types of self-assembly: static and dynamic. Static self-assembly (Figure 2-2) involves systems that are at global or local equilibrium and do not dissipate energy. In static self-assembly, formation of the ordered structure may require energy (for example in the form of stirring), but once it is formed, it is stable. In dynamic self-assembly (Figure 2-3), the interactions responsible for the formation of structures or patterns between components only occur if the system is dissipating energy. The patterns formed by competition between reaction and diffusion in oscillating chemical reaction are simple examples; biological cells are much more complex ones. Most researches in self-assembly have focused in this static type.

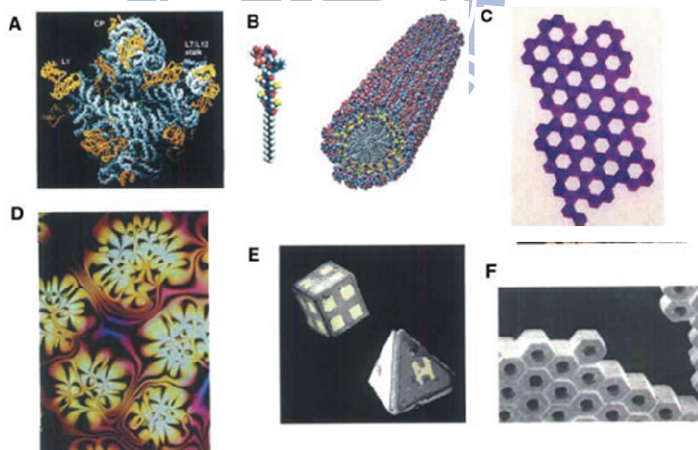


Figure 2-2. Examples of static self-assembly. (a) Crystal structure of a ribosome. (b) Self-assembled peptide amphiphile nanofibers. (c) An array of millimeter sized polymeric plates assembled at a water/perfluorodecalin interface by capillary interactions. (d) Thin film of a nematic liquid crystal on an isotropic substrate. (e) Micrometer sized metallic polyhedra folded from planar substrates. (f) A three-dimensional aggregate of micrometer plates assembled by capillary forces.

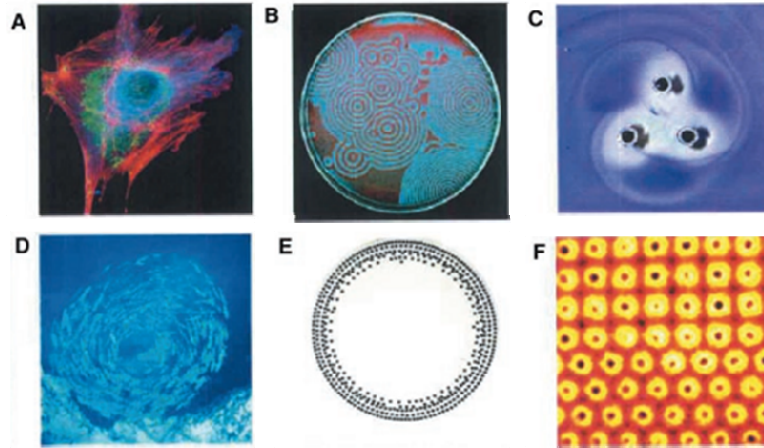


Figure 2-3. Examples of dynamic self-assembly. (a) An optical micrograph of a cell with fluorescently labeled cytoskeleton and nucleus; microtubules (~ 24 nm in diameter) are colored red. (b) Reaction-diffusion waves in a Belousov-Zhabotinski reaction in a 3.5-inch Petri dish. (c) A simple aggregate of three millimeter-sized, rotating, magnetized disks interacting with one another via vortex-vortex interactions. (d) A school of fish. (e) Concentric rings formed by charged metallic beads 1 mm in diameter rolling in circular paths on a dielectric support. (f) Convection cells formed above a micropatterned metallic support. The distance between the centers of the cells is ~ 2 mm.

2-2 Self-Assembly Behavior of Block Copolymer

Block copolymer are macromolecules composed of the two or more polymer blocks of chemically different monomer that are linked together by chemical bonds to form a single molecule. Owing to their mutual repulsion, dissimilar blocks tend to segregate into different domains so that the spatial extent of the domains is limited by the constraint imposed by the chemical connectivity of the blocks. As a result, the microphase-separated behavior occur in block copolymer system as shown in Figure 2-4.⁷ In the following section the self-assembly of block copolymers will be described with the help of some examples. They are divided into bulk phase and dilute solutions, each of them being well-suited for the preparation of interesting material.

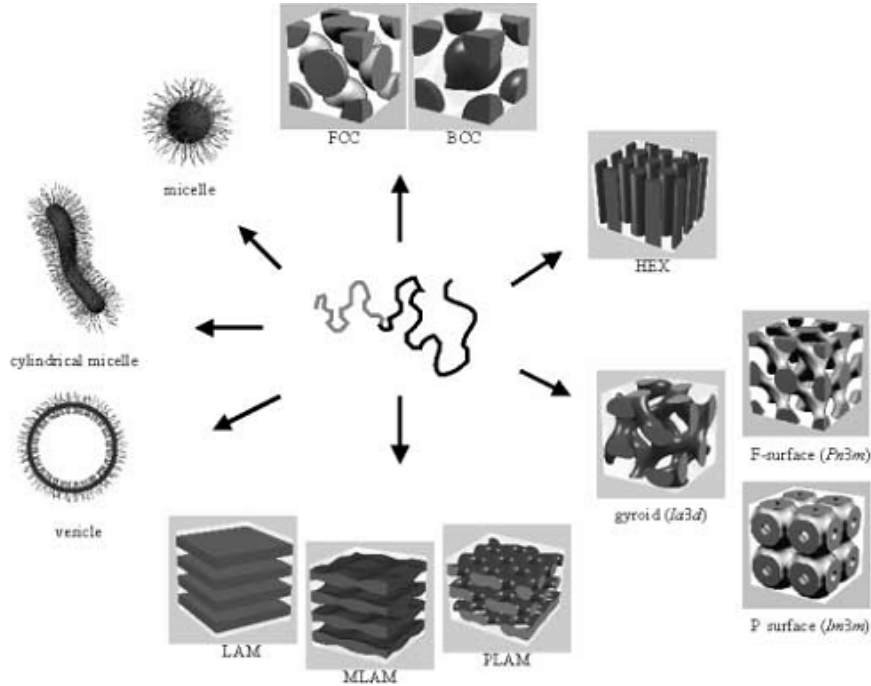


Figure 2-4. Self-organization structures of block copolymers and surfactants: spherical micelles, cylindrical micelles, vesicles, fcc- and bcc-packed spheres (FCC, BCC), hexagonally packed cylinders (HEX), various minimal surfaces (gyroid, F surface, P surface), simple lamellae (LAM), as well as modulated and perforated lamellae (MLAM, PLAM).

2-3 Self-Assembly Behavior of Block Copolymer in Bulk State

The phase behavior of diblock copolymers in bulk state has been the subject of numerous theoretical and experimental studies over the past decades, and is relatively well understood.⁸⁻¹⁰ This self-assembly process is driven by an unfavorable mixing enthalpy and a small mixing entropy, while the covalent bond connecting the blocks prevents macroscopic phase separation. This enthalpy is proportional to the Flory-Huggins segmental interaction parameter (χ), which is found to be inversely proportional to temperature and is usually parameterized as $\chi = A/T + B$, at which A and B are constants. Microphase separation gives rise to ordered nanostructures with periods of several R_g due to the chain stretching, where R_g is the copolymer radius of gyration. The entropic penalty associated with the chain stretching is proportional to the degree of polymerization (N). The product χN that expresses the

enthalpic-entropic balance is then used to parameterize BCP phase behavior along with the composition of BCP. For a diblock copolymer, the volume fraction of one component (f), controls which ordered nanostructures are accessed beneath the order-disorder transition (ODT).¹¹ Figure 2-5a shows the schematic illustration of the nanostructured phase. The volume fraction of BCP determines the shape of equilibrium morphology because the constituted block with different volume fraction would change the curvature of microphase separated interface to keep total uniform density and thermodynamic equilibrium so that different morphologies, such as sphere, cylinder, double gyroid and lamellae (Figure 2-5b), can be obtained.¹² Furthermore, the segregation product χN determines the degree of microphase separation. Depending on χN , three different regimes are distinguished; (a) the weak-segregation limit (WSL) for $\chi N \leq 10$; (b) the intermediate segregation region (ISR) for $10 < \chi N \leq 50$; (c) the strong segregation limit (SSL) for $\chi N \rightarrow \infty$.

Most of the experimental work on the phase behavior of coil-coil diblock copolymers has been performed in the SSL. In this regime, the phase boundaries are vertical lines and the microphase separated morphology can be varied from spheres via lamellae to inverse spheres by changing the volume fractions of the blocks (f). Well known are the results on the morphology of polystyrene-*b*-polyisoprene diblock copolymers by means of transmission electron microscopy (TEM) as a function of composition (Figure 2-6). (bcc = microspheres of the minority component ordered on a body-centered cubic lattice in a matrix of the second block; hex = hexagonally packed cylindrical microdomains of the minority component embedded in a matrix formed by the second block; obdd = ordered bicontinuous double diamond microstructure formed by the minority component embedded in a matrix of the second block; lam = microstructure consisting of alternating lamellae of the constituent blocks; ODT = order-disorder transition). Early theoretical work by Leibler, however, suggested that close to the ODT the phase boundaries are no longer vertical lines but acquire more and more curvature as they approach the ODT.⁸ This is shown in the phase diagram depicted in Figure

2-7. As an implication of the curved phase boundaries, thermally induced order-order transitions should become possible near the ODT.

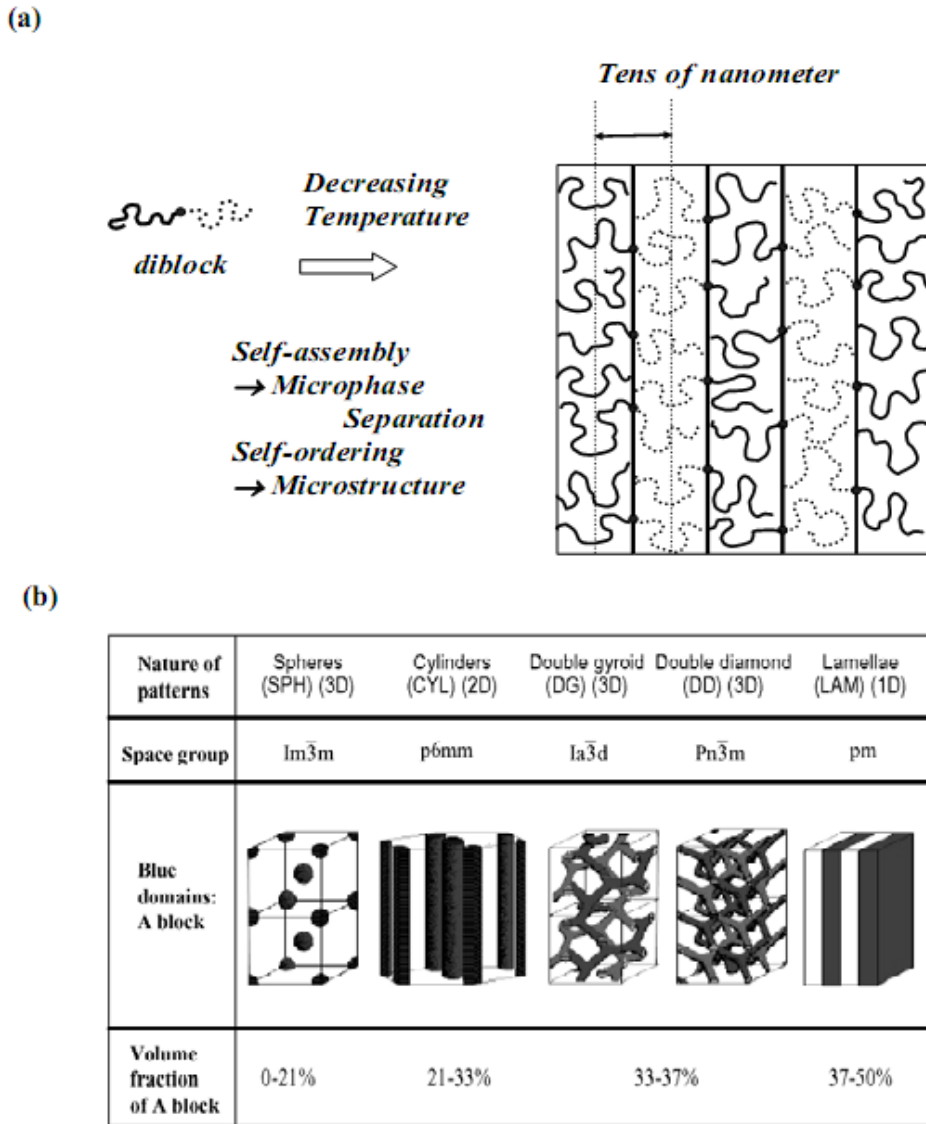


Figure 2-5. (a) Schematic illustration of the self-assembly and self ordering behavior of BCPs at which the scale of microphase separation is about tens of nanometer. (b) Schematic phase diagram showing the various “classical” BCP morphologies adopted by non-crystalline linear diblock copolymer.

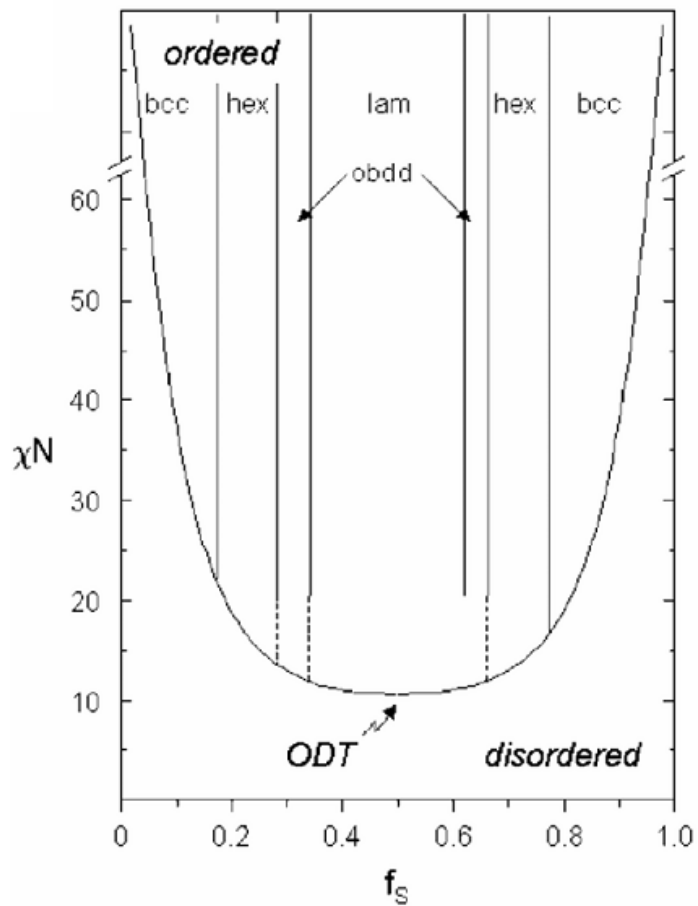


Figure 2-6. Experimental phase diagram for polystyrene-*b*-polyisoprene diblock copolymers.

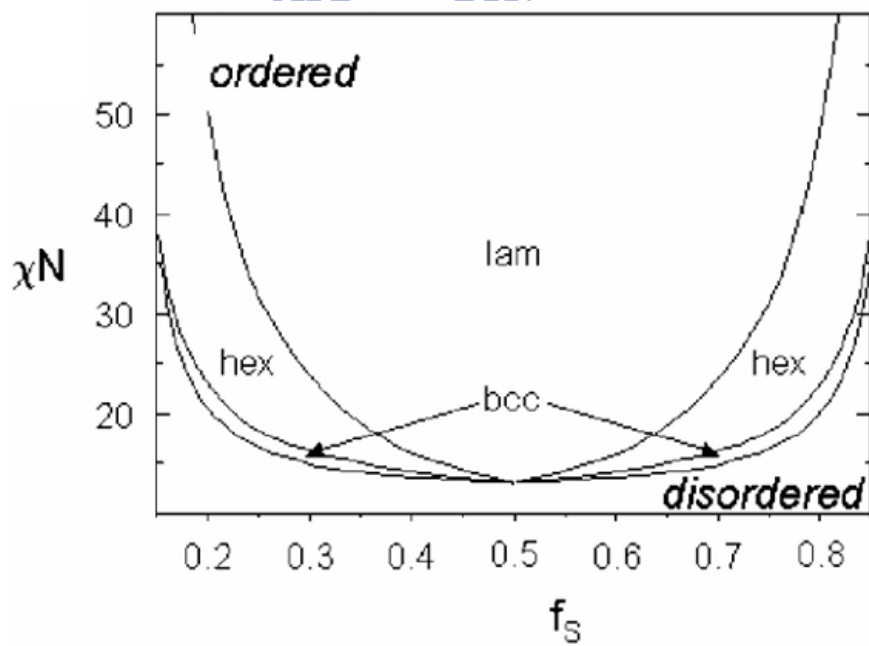


Figure 2-7. Theoretical phase diagram for a diblock copolymer near the ODT.

2-4 Self-Assembly Behavior of Block Copolymer/Homopolymer Blends in Bulk State

It is interesting to control the morphology of the microphase-separated block copolymer by adding a homopolymer. Most studies have concentrated on mixing immiscible A-*b*-B diblock copolymers with A homopolymer such as homopolymer PS and styrenic block copolymers. Hashimoto and co-workers demonstrated the phase behavior of homopolymer/BCP blends by using poly(styrene-*block*-isoprene) (PS-PI) and PS homopolymers.¹³ Low-molecular-weight PS homopolymers (HS) were found to be uniformly solubilized into the corresponding microdomain space. As illustrated in Figure 2-8a, low-molecular-weight HS is solubilized into the PS microdomains of the PS-PI BCPs. It generally causes the changes of the molecular conformations of HS chains and PS block chains, both tending to the stretched normal to the lamellar interface. The swelling causes the expansion of the average nearest-neighbor distance between the chemical junctions from a_{j0} for the pure block polymer to a_j , which would then cause the contraction of the conformation of PI block chains and hence the contraction of the thickness of PI microdomains from D_{B0} to D_B in order to maintain the bulk density of PI microdomains equal to that of pure PI homopolymers at which D_{B0} and D_B represent the domain size of PI microdomain before and after blending with the PS homopolymers, respectively. The decrease of D_B by the swelling is outweighed by the increase of D_A , resulting in the increase of the identity period from D_0 to D upon swelling by HS. Upon an increase in the content of the HS (ψ_H), the conformational entropy loss due to the chain perturbation increases. This penalty of the conformational entropy loss is reduced by producing the curvature in the interface in such a way that the minority phase B forms the discrete microdomains of cylinders or spheres. This reduction of the penalty associated with the conformational entropy is accompanied by an increase of the penalty due to the curvature free energy. As ψ_H increases, the free-energy penalty due to the conformational entropy becomes larger than that due to the curvature free energy, which would then cause the morphological transitions from lamellae to sphere (Figures 2-8b~2-8f).

Corresponding small-angle x-ray scattering (SAXS) profiles further confirmed the occurrence of phase transformation as shown in Figure 2-8g.

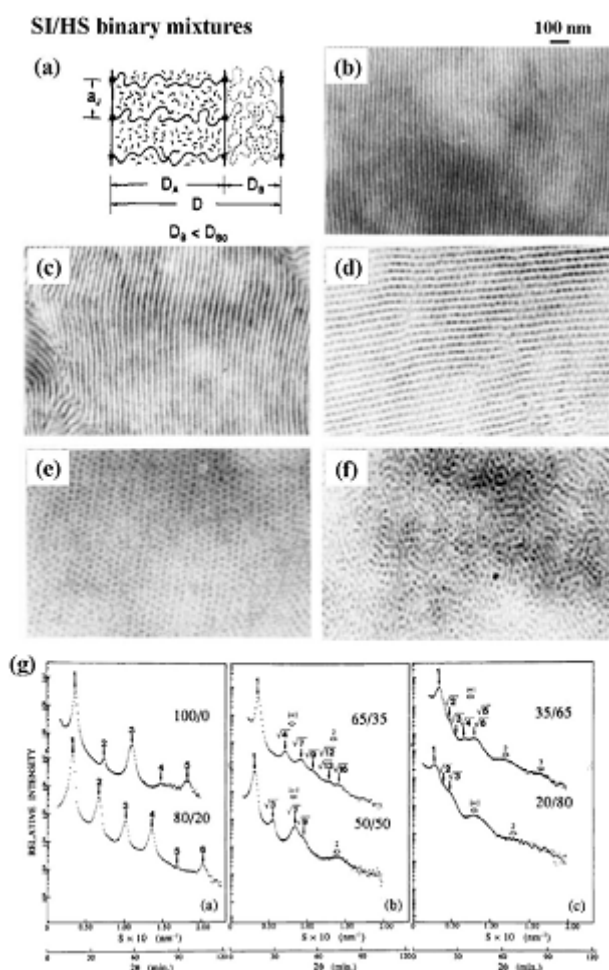


Figure 2-8. (a) Schematic illustration of the location of the HS within the HS/PS-PI blend. TEM images of the HS/PS-PI blends with different HS/SI ratio: (b) 0/100; (c) 20/80; (d) 50/50; (e) 65/35; (f) 80/20. The dark and white regions represent the PI and PS microdomains due to the OsO₄ staining. (g) Corresponding SAXS profiles for the samples (b)-(f).

By contrast, large-molecular-weight HS does not significantly change the average distance a_j between the chemical junctions of PS-PI along the interface, and hence does not swell the PS brush of the copolymer, especially in the region near the PS-PI interfaces.¹⁴ The large-molecular-weight HS is expected to be localized in the center of the PS phase, implying the dry brush formation as schematically shown in Figure 2-9a. With the increase the content

of HS, the solubilized HS expands the long period D of PS-PI. At the same time, it screens the interaction between the PS block chains which are emanating from the two SI interfaces facing each other, interfaces 1 and 1' or 2 and 2'. The screening causes the fluctuations of HS accommodated between the PS brushes of the copolymer, which, in turn, results in the observed broadening of the distribution of the interlamellar spacing D around the mean value D as shown in Figure 2-9b. Figures 2-9c~2-9f shows the transmission electron microscopy (TEM) images of HS/PS-PI blends with different HS contents, indicating that the localization of HS within HS/PS-PI blends increases with the increase of HS content (white region represents the localization of HS). In summary, original phase behavior of BCP blends can be modified by adding the homopolymers with different contents and sizes.

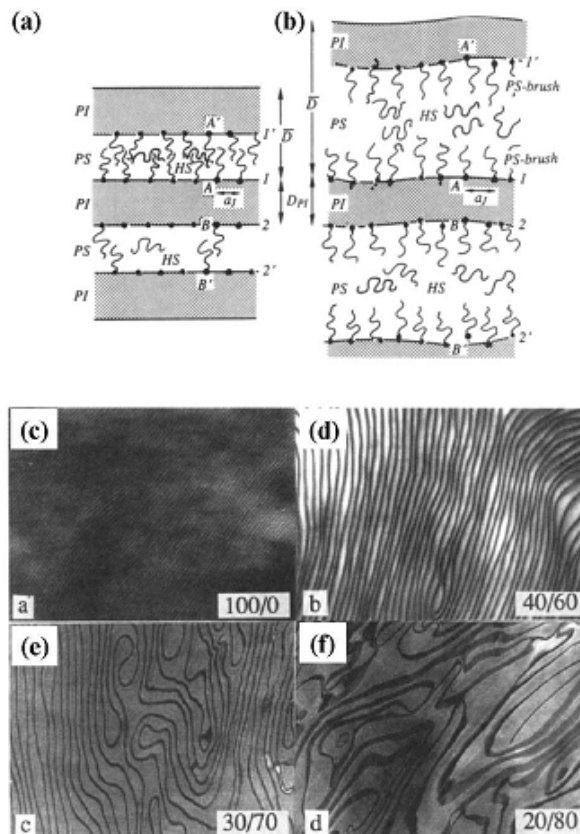


Figure 2-9. Schematic illustration of the dry brush systems formed in HS/PS-PI blends with (a) small amounts of HS and (b) large amounts of HS. TEM images of HS/PS-PI blends with different HS/SI ratio: (c) 0/100; (d) 60/40; (d) 70/30; (e) 80/20. The dark and white regions represent the PI and PS microdomains due to the OsO4 staining.

Blends of A-*b*-B copolymer with A homopolymer can undergo morphological transitions or macro-phase separation (i.e., at the solubility limit), processes that are strongly dependent upon (i) the ratio of the molar weight of the A homopolymer ($M_{A,\text{homo}}$) to that of the A block of copolymer ($M_{A,\text{block}}$) and (ii) the amount of the homopolymer added. Systematic studies of the phase behavior of A-*b*-B/A blend systems have been well explored.¹⁴⁻²⁵ Depending on the molecular weight ratio of the homopolymer A to the block copolymer A ($a = M_{h-A} / M_{b-A}$), A-*b*-B block copolymer/B homopolymer blend systems can be divided into three categories: completely phase-separated system ($a \gg 1$), “dry brush” blend system ($a = \text{ca. } 1$), and “wet brush” blend system ($a < 1$). In the wet brush system, the added homopolymer A dissolves uniformly in the microdomains of block copolymer A, resulting in changes of the micro-domain size or even the morphology.

Furthermore, the phase behavior of A-*b*-B/C blends is more interesting than that of A-*b*-B/A blends. For an A-*b*-B/C blend system, there are four different outcomes when C is miscible with A and/or B.²⁵ In the first case, A and B are immiscible and C is miscible with B but immiscible with A. Ikkala et al. prepared blends of the immiscible polyisoprene-*b*-poly(2-vinyl pyridine) (PI-*b*-P2VP) diblock copolymer with novolac resin, which is miscible with P2VP through hydrogen bonding but immiscible with PI as shown in Figure 2-10.²⁷ Matsushita et al. studied the various micro-phase separation structures of the poly(vinyl phenol) (PVPh)/poly(styrene-*b*-2-vinylpyridine) (PS-*b*-P2VP) blend system, where PVPh and P2VP are miscible through strong hydrogen bonding as shown in Figure 2-11.²⁴⁻²⁵ Interaction energy between the P α MS and PS blocks were responsible for the irregular swelling of the lamellar domain of the PB block.²⁸ Zhao et al. investigated blends of poly(styrene-*b*-vinyl phenol) (PS-*b*-PVPh) diblock copolymers with various hydrogen bond-acceptor polymers, such as poly(ethylene oxide) (PEO), poly(4-vinyl pyridine) (P4VP), and poly(butyl methacrylate) (PBMA), which can form hydrogen bonds with the PVPh block, while being immiscible with the PS block; micro-phase separation is expected in such

systems, but self-assembled nanostructures were not reported.²⁹

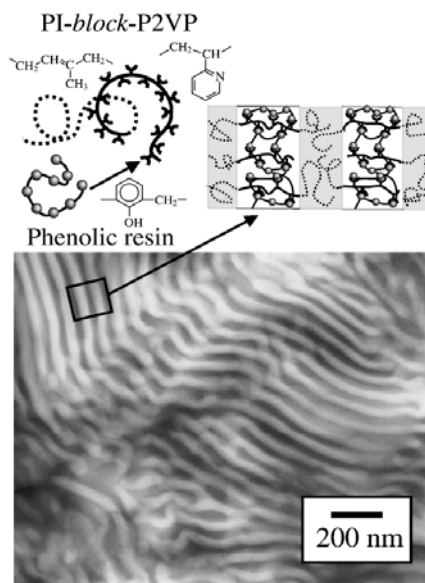


Figure 2-10. Schematic of the cross-linked lamellar structure of blends of novolac and P2VP-*b*-PI. The hydrogen bonding between novolac and P2VP is also indicated. TEM images of the HMTA cured lamellar structure is also shown.

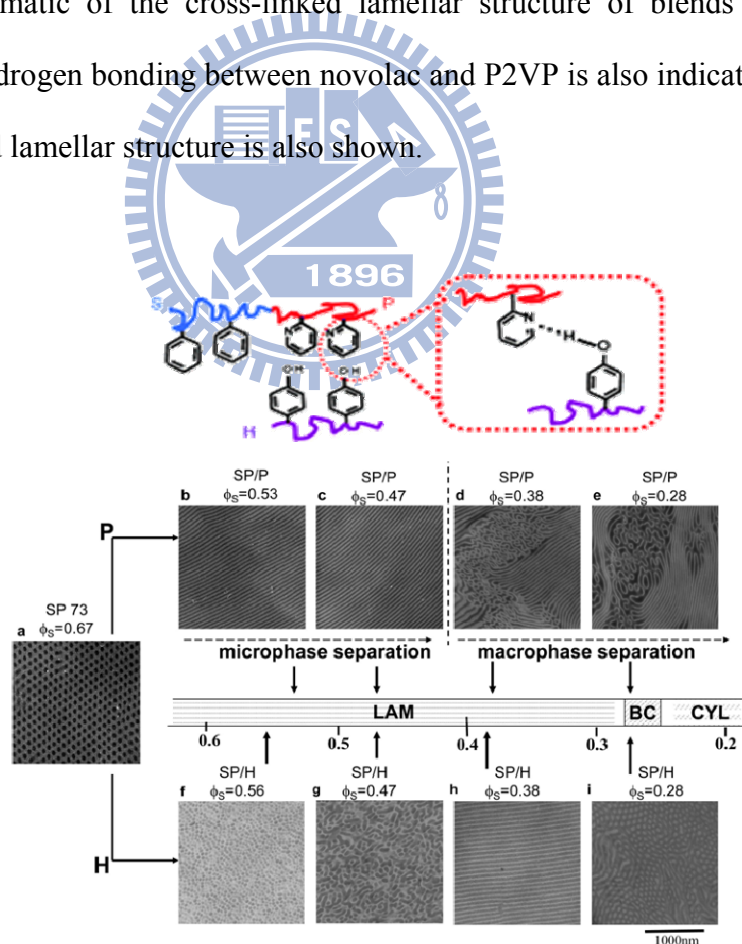


Figure 2-11. TEM micrographs showing different structures arising from mixing block copolymer SP 73 with homopolymers P and H.

Investigating the effect of repulsive interactions in the P α MS/SBS binary blend system, Hashimoto et al. found that the loss of combinatorial entropy of P α MS and a reduction in the interaction energy between the P α MS and PS blocks were responsible for the irregular swelling of the lamellar domain of the PB block.²⁸ Zhao et al. investigated blends of poly(styrene-*b*-vinyl phenol) (PS-*b*-PVPh) diblock copolymers with various hydrogen bond-acceptor polymers, such as poly(ethylene oxide) (PEO), poly(4-vinyl pyridine) (P4VP), and poly(butyl methacrylate) (PBMA), which can form hydrogen bonds with the PVPh block, while being immiscible with the PS block; micro-phase separation is expected in such systems, but self-assembled nanostructures were not reported.²⁹ In the second case, A and B are immiscible, but C is miscible with A and B. For example, Kwei et al. investigated blends of poly(styrene-*b*-vinyl phenol)/poly(vinyl methyl ether) (PS-*b*-PVPh/PVME), where PVME is miscible with both the PS and PVPh blocks and serves as a common solvent.²⁹ Guo et al. and Chen et al. reported blends of an immiscible A-*b*-B diblock copolymer with C, where C is miscible with both blocks A and B, but the hydrogen bonding interactions between the B and C segments is stronger than that between the A and C segments ($\chi_{BC} \gg \chi_{AC}$). They found that both blocks of poly(ϵ -caprolactone)-*b*-poly(vinyl pyridine) interacted with PVPh, poly(acrylic acid) (PAA), and phenoxy resin through hydrogen bonding, where both χ_{AC} and χ_{BC} were negative but χ_{BC} was more negative than χ_{AC} .³⁰⁻³³ Different hydrogen bonding interaction strengths lead to the formation of a variety of composition-dependent microphase separations. In the third case, A and B are miscible and C is miscible with both the A and B blocks. For example, we reported that the miscible PMMA-*b*-PVP copolymer blended with PVPh and the miscible PVPh-*b*-PMMA copolymer blended with PVP, where PVPh is miscible with both the PVP and PMMA blocks, but its interaction strength with the former (PVP) is significantly stronger than that with the latter (PMMA), resulting in unusual self-assembled morphologies.^{34,35} In the fourth case, A and B are miscible and C is miscible with B but immiscible with A. For example, Lin et al. reported that blending miscible PCL-*b*-PVPh with

PVP homopolymer resulted in self-assembly morphologies through competitive hydrogen bonding interactions, where χ_{BC} is more negative than χ_{AC} .³⁶

2-5 Self-Assembly Behavior of Block Copolymer in Solution State

Block copolymer self-organization occur not only in pure bulk material but also in dilute solution, particularly when the solvent is a good solvent for only one of the blocks. This property enables the creation of discrete object such as hollow spheres and cylinders. Similarly structures are formed by small lipid, but the block copolymer versions are large and more robust. Indeed, when a block copolymer is dissolved in a selective solvent, the insoluble (or less soluble) segments aggregate into dense micellar cores which are surrounded by coronas formed by the soluble blocks. The vast majority of block copolymer micelles has been constructed from AB diblock copolymers.³⁷⁻³⁸

In a solvent, block copolymer phase behavior is controlled by the interaction between the segments of the polymers and the solvent molecules as well as the interaction between the segments of the two blocks. If the solvent is unfavorable for one block this can lead to micelle formation in dilute solution. Thus, the micellization of block copolymers in a selective solvent of one of the blocks is a typical aspect of their colloid properties. In fact, when a block copolymer is dissolved in a liquid that is a thermodynamical good solvent for one block and a precipitant for the other, the copolymer chains may associate reversibly to form micellar aggregates which resemble in most of their aspects to those obtained with classical low molecular weight surfactants.

Micellization occurs when the block copolymer is dissolved in a large amount of a selective solvent for one block of the blocks. Under these circumstances, the polymer chains tend to organize themselves in a variety of structures from micelles or vesicle and cylinders. The soluble block will be oriented toward the continuous solvent medium and become the “corona” of the micelle formed, whereas the insoluble part will be shielded from the solvent

in the “core” of the structure. Two extreme of micellar structures can be distinguished for diblock copolymers, depending on the relative length of the blocks. If the soluble block is larger than the insoluble one, the micelles (see Figure 2-10) formed consist of a small core and a very large corona, and are called “hairy micelles” or “star micelles”. In contrast, micelles having a large insoluble segment with a short soluble corona are referred to as “crew-cut micelles”.³⁹

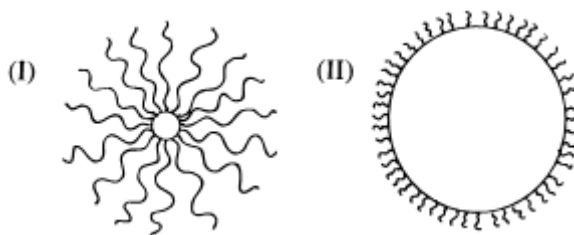


Figure 2-12. Schematic illustration of (I) a star and (II) a crew-cut micelle.

2-5.1 Theories of Self-Assembly Behavior of Block Copolymer in Solution State

Quite a number of theories were developed over the years in order to predict the structural parameter of a micelle (CMC, association number Z ; core radius R_C ; shell thickness L ; hydrodynamic radius R_h) as a function of the copolymer characteristics, e.g. its molecular weight and composition. The shape and size of the aggregates are controlled by a variety of parameters that affect the balance between three major forces acting over the system. These forces reflect: the extent of constraint between the blocks forming the core (the block will be more or less stretched depending on the solvent), the interaction between chains forming the corona, and the surface energy between the solvent and the core of the micelle. From the theoretical point of view, the description of the aggregate structure requires that the thermodynamic parameters of self-assembly be account for as well as the forces generated between the macromolecules inside the aggregates. These two factors (thermodynamics and intra-aggregate forces) combined with the interactions between different aggregates (inter-aggregate forces) determine the type of self-assembled structure formed at equilibrium.

It is then essential to understand the fundamental that govern the interdependence between morphology and size of the aggregates obtained by self-assembly, including decisive factors such as concentration, temperature, composition, block length, copolymer architecture, and the solvents used.

Theories at different levels of refinement have been developed to describe the behavior of block copolymers in solution and its dependence on parameters described above. The theories can be classified into two main groups. The first group belongs to the ‘scaling theory’ of de Gennes.⁴⁰ The second one is based on the ‘self-consistent mean field theory’ developed by Noolandi and Hong.⁴¹ In his theoretical approach, deGennes predicted parameters like the aggregation number or the radius for crew-cut type micelles from the block length and interfacial tension data.⁴² Daoud and Cotton⁴³ extended the range of applicability of this approach to the case of star-like micelles. More detailed studies have been carried out along these lines by Zhulina and Birshtein⁴⁴, who proposed a classification of micelles in four main categories based on the nature of the diblock copolymers. Other authors⁴⁵⁻⁴⁷, including Halperin for star-like micelles, or more recently Wu and Gao and Shusharina, have made theoretical contributions to this field, but a description of such studies is beyond the scope of this section.

2-5.2 Block Copolymer Micelle Free Energies

We consider a dilute solution of block copolymers, each comprising a hydrophobic block with the degree of polymerization N_B and a hydrophilic block with the degree of polymerization N_A . Both blocks are assumed to be intrinsically flexible. In the case of strongly asymmetric block copolymers (N_A, N_B) the size of the micellar core, R_{core} , is much smaller than the radius, R_{corona} , of the micellar corona, so that the micelle is reminiscent of the starlike polymer (see Figure 2-12I). In the framework of the scaling theory, the corona of the starlike micelle can be envisioned^{48,49} as an array of concentric spherical shells of

close-packed blobs. The condition of close packing imposes the blob size, $\xi(r) = rp^{-1/2}$, equal to the average distance between the coronal blocks (here r is the distance from the center of the micelle and p is the aggregation number). Each blob corresponds to the $\sim k_B T$ contribution to the free energy of steric repulsion between the coronal chains. After calculating the total number of blobs in the micellar corona, one finds the free energy of steric repulsion (per chain) as

$$\frac{F_{corona}(P)}{k_B T} \cong p^2 \ln \frac{R_{corona}}{R_{core}} \quad (2-1)$$

where $R_{corona} = N_A^{3/5} v_A^{1/5} p^{1/5}$ and $R_{core} = N_A^{1/2} p^{1/4}$ under good or θ -solvent conditions for coronal chains, respectively (here v_A is the second virial coefficients). The excess free energy of the core-water interface is given by

$$\frac{F_{surface}(P)}{k_B T} \cong \gamma A_C \cong (N_B \tau_B^2)^{2/3} p^{-1/3} \quad (2-2)$$

where $k_B T \gamma \approx k_B T \tau_B^2$ is the surface tension at the core-solvent interface and

$$A_C \cong \frac{R_{core}^2}{p} \cong (N_B \tau_B^2)^{2/3} p^{-1/3} \quad (2-3)$$

is the area of the core-solvent interface per chain. For strongly asymmetric copolymers the third contribution, F_{core} , is negligible, and the minimization of $F_{corona}(p) + F_{surface}(p)$ with respect to p results in an equilibrium aggregation number

$$P_{eq} \cong (N_B \tau_B^2)^{4/5} \left(\ln \frac{R_{corona}}{R_{core}} \right)^{6/5} \quad (2-4)$$

An important feature of eq 2-4 is an absence of the power-law dependence of the aggregation number p_{eq} on the length N_A of the coronal block. In the opposite limit of short polyelectrolyte blocks, N_A, N_B , the size of the micellar core, $R_{core}(p)$, exceeds by far the thickness of the corona. The coronae of these so-called crew-cut micelles can be viewed as quasiplanar polymer brushes^{50,51} (Figure 2-12II). The thickness of the corona $H_{corona} = R_{corona} - R_{core}$ scales as $H_{corona} \approx N_A v_A^{1/3} A_c^{-1/3}$ or $H_{corona} = N_A A_c^{-1/2}$ while the number of the coronal blobs per chain $\sim H_{corona}/\xi$ is proportional to the free energy of the interchain repulsion and

equals $F_{\text{corona}}/k_B T = N_A v_A^{1/3} A_c^{-5/6}$ or $F_{\text{corona}}/k_B T = N_A A_c^{-1}$ under good and θ -solvent conditions for the coronal chains, respectively. Taking into account eq 2-4 and minimizing the free energy with respect to p , we obtain the equilibrium aggregation number for the crew-cut micelles: $p_{\text{eq}} = N_B^2 \tau_B^{14/11} N_A^{-18/11} v_A^{-6/11}$ (good solvent) and $p_{\text{eq}} = N_B^2 \tau_B N_A^{-3/2}$ (θ solvent). In contrast to the case of starlike micelles, the equilibrium aggregation number in the crew-cut micelles strongly decreases upon an increase in the degree of polymerization of the soluble blocks because of their stronger interaction.

2-5.3 Estimation of Micelle Free Energy of Different Morphologies

To further understand the reasons for the appearance of micelle morphological changes from spheres to cylinders, to vesicles, free energies in each of these micelle morphologies must be estimated. The first parameter which needs to be calculated is the degree of stretching of core chains (S_c) based on the equation⁵²

$$S_c = R/R_0 \quad (2-5)$$

where R is the radius of the core chain in the spheres or in the cylinders. In the case of vesicles, R is half of the wall thickness. The quantity R_0 is the unperturbed end-to-end distance of a core chain.

The second parameter is the interfacial area per corona chain (A_c). Consider a spherical micelle with a core radius of R_{core} formed by a copolymer in which the degree of polymerization of core-forming block is N_{core} , the surface area per corona chain, A_c , is given by

$$A_c = 4\pi R^2 / p \quad (2-6)$$

where p is the aggregation number, which can be calculated from

$$p \cong \frac{f\left(\frac{4}{3}\right)\pi R_{\text{core}}^3}{V_c N_c} \quad (2-7)$$

where V_c is the volume per core chain repeat unit and f is the volume fraction of core chain blocks, considering that the micelle core is still swollen by the common solvent when the micelle structure becomes frozen, A combination of eqs [2-6] and [2-7] yields the relationship between A_c and the core radius as

$$A_c = 3V_c N_c / fR_{core} \quad (2-8)$$

Similarly, for cylindrical micelles and lamellar bilayer, respectively, one can obtain the relationships

$$A_c = 2V_c N_c / fR_{core} \quad (2-9)$$

$$A_c = V_c N_c / fR_{lamelle} \quad (2-10)$$

$R_{lamella}$ (half the wall thickness) is used to approximate the calculation in the case of vesicles.

By using above equations in the system of polystyrene-*block*-poly(ethylene oxide) in DMF/acetonitrile, the micelle free energies have been quantitatively estimated by Stephen and coworkers.⁵³ It has been shown that the energies decrease from spheres to cylinders and then to vesicles (Figure 2-13). Among three free energy components, the $F_{interface}$ dominates as compared to the terms of F_{core} and F_{corona} .

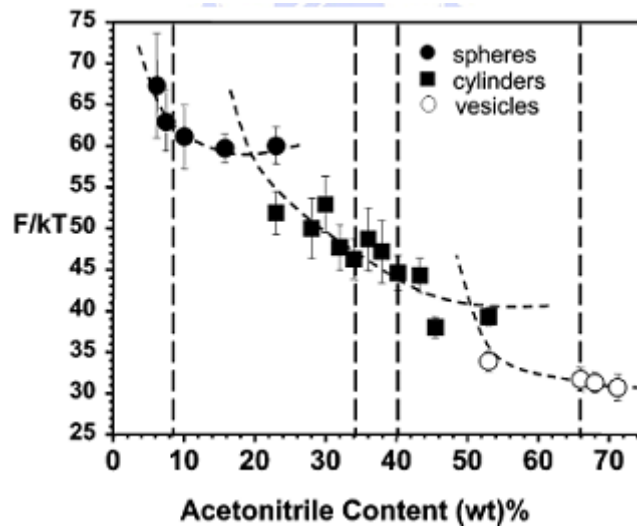


Figure 2-13. Free energy changes with acetonitrile content for various morphologies in the PS-*b*-PEO copolymer-DMF/acetonitrile system.

2-5.4 Geometrical Theories of Self-Assembly Behavior of Block Copolymer in Solution State

In the classical description, the factor determining the shape of self-assembled amphiphilic structures is the size of the hydrophobic moiety or tecton relative to the hydrophilic part. Israelachvili and coworkers⁵⁴ developed a very accessible approach using geometrical considerations that predicts the micellization phenomenon and the resultant morphologies. Initially developed to address the situation of amphiphilic molecules of low molar mass, this theory can also be applied to block copolymers. If we take the particular case of amphiphilic molecules in aqueous solution (Figure 2-14), the major forces governing the assembly into well defined structures are, on the one hand, the hydrophobic attraction between insoluble hydrophobic moieties, and on the other, the repulsion between the hydrophilic head groups due to electrostatic or steric interactions that both force amphiphilic molecules to be in contact with the aqueous solution.

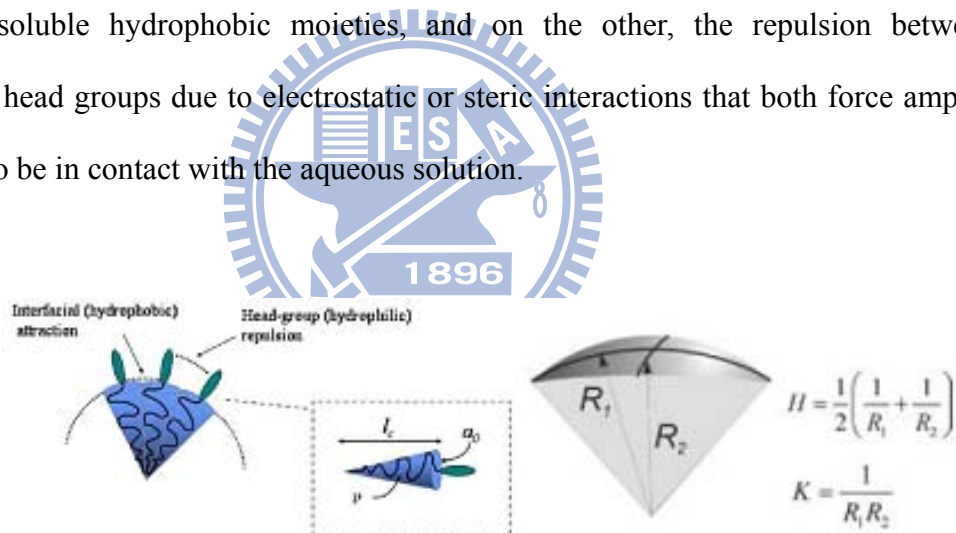


Figure 2-14. Description of amphiphile shape in terms of the surfactant parameter ($v/a_0 l_c$) and its relation to the interfacial mean curvature (H) and Gaussian curvature (K).

It determines the curvature of the hydrophobic-hydrophilic interface as described by its mean curvature H and its Gaussian curvature K , which are given by the two radii of curvature R_1 and R_2 , as shown in Figure 2-14. For the aggregation of phospholipids, a simple model has been developed by Israelachvili based on the geometry of the molecules. This model defines a packing parameter $p = v/a_0 l_c$, in which a_0 is the polar head surface area at the critical micellar

concentration (cmc) and v and l_c are the volume and chain length of the hydrophobic chains, respectively. Additionally, a_0 can also be applied as interfacial area of block copolymer micelles. The curvature is related to the surfactant packing parameter by^{54,55}

$$\frac{v}{a_0 l_c} = 1 + H l_c + \frac{K l_c^2}{3} \quad (2-11)$$

The simplest shapes are spheres, cylinder, and bilayer, which are characterized by certain values of the packing parameter and curvature as shown in Figure 2-15.

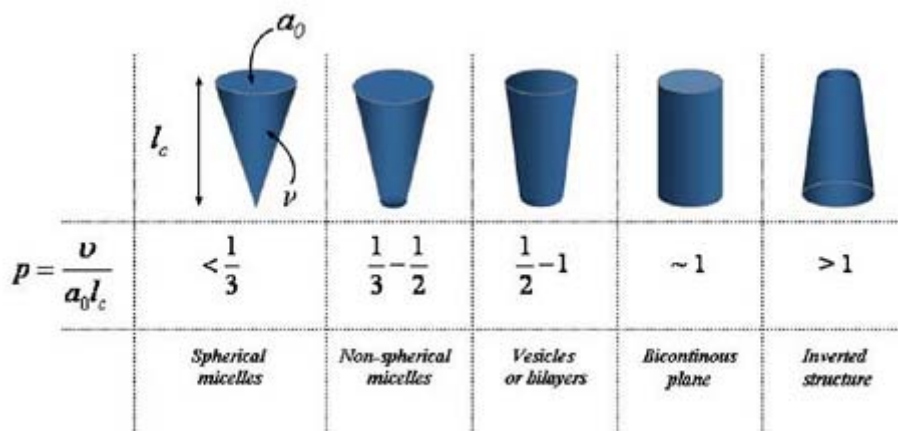


Figure 2-15. Dependence of final micelle structure on intrinsic molecular parameters: volume v of the hydrophobic group, and area a_0 and length l_c of the hydrophobic block.

If the attractive forces predominate, the interfacial area a_0 per molecule will decrease; and if repulsive forces predominate, a_0 will increase. The competition between these two opposing forces, which strongly depends on the geometry of both blocks, is mirrored in a variety of known morphologies. The hypothesis of Israelachvili assumes geometric properties to depend on three parameters (see Figure 2-13): the optimal interface a , the volume v occupied by the hydrophobic chains, and the maximum length l_c of these chains. These parameters are interrelated by $p = v/a_0 l_c$, where p is the packing parameter (also called the shape factor) that determines the final structure, varying from small values (less than unity) for spherical micelles to approximately unity for bicontinuous bilayers to greater

than unity for inverted structures (Figure 2-15). If $p < 1/3$, the amphiphile has a tendency to form spherical micelles; if $1/3 < p < 1/2$, cylindrical micelles will be favored; if $1/2 < p < 1$, bilayers with a spontaneous curvature (vesicles) are produced; if $p = 1$, planar bilayers will be favored; and if $p > 1$, micellar aggregates with a reverse curvature will be formed (Figure 2-16).

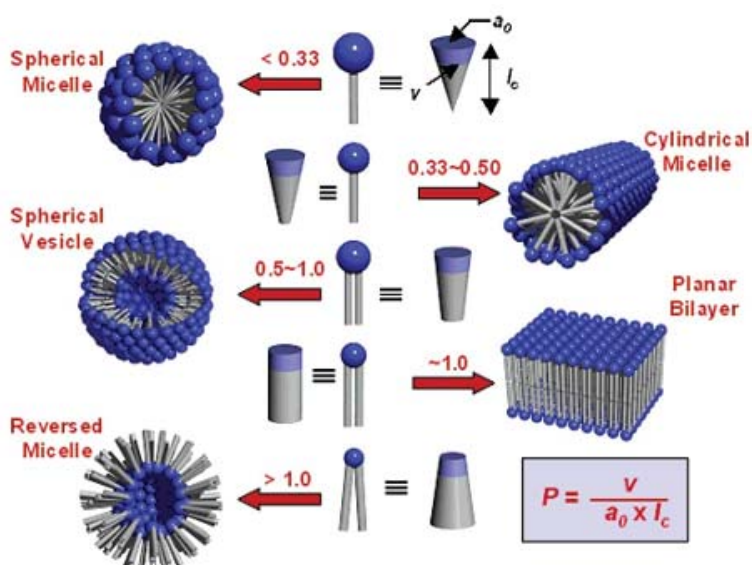


Figure 2-16. Different aggregate morphologies predicted by the packing parameter (p).

In order to obtain bilayers for a given tecton of volume v and length l_c , one needs to adjust the interfacial area a_0 until the packing parameter approaches unity. An example is shown in Figure 2-17 for a series of poly(butadiene)-*block*-poly(ethyleneoxide), PB-*b*-PEO, block copolymers, where a decrease of the hydrophilic/hydrophobic block copolymer ratio (as the interfacial area increase in proportion to the hydrophilic block length⁵⁶) lead to shape changes from spherical to cylindrical micelles and finally to vesicles.

More recently, and by analogy with Israelachvili's approach, Disher and Eisenberg¹⁸ tried to unify the experimental results obtained from different amphiphilic block copolymers. Reasoning from a series of examples drawn from the literature, they proposed a unifying rule for the formation of polymersomes (polymer-based vesicles) in water: i.e. a ratio f of the mass of the hydrophilic part to the total mass $35 \pm 10\%$, as in the case of phospholipids.⁵⁷ An

asymmetric molecule with a cylindrical shape and $f < 50\%$ presumably reflects a certain balance between its hydrated part and a disproportionately large hydrophobic fraction. Finally, molecules with $f > 45\%$ are expected to form micelles and those with $f < 25\%$ are expected to self-assemble into inverted structures.

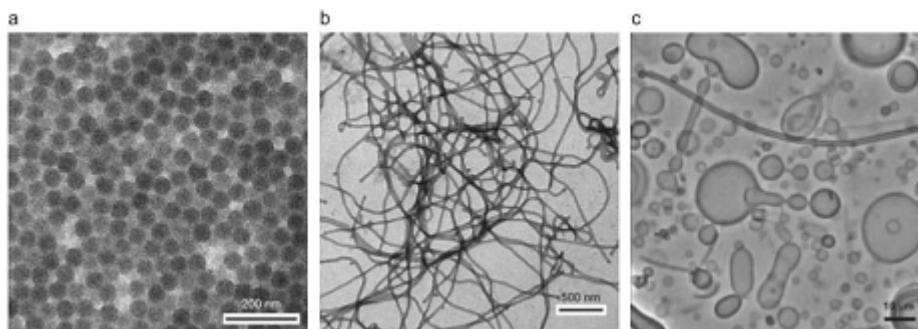


Figure 2-17. TEM images (a, b) and optical micrograph (c) of different shapes of aggregate structures for a series of PB-PEO block copolymers ranging from spherical micelles (PB₂₀₂-PEO₃₆₀) via cylindrical micelles (PB₁₂₅-PEO₁₅₅) to vesicles (PB₃₇-PEO₄₀). This figure illustrated the influence of the packing parameter on the self-assembly structure.

2-6 Self-Assembly Behavior of Polymer Blends in Solution State

Recent advancement has demonstrated that the interpolymer complexation can also lead to micellization through electrostatic interaction⁵⁸ or hydrogen bonding⁵⁹. An interpolymer complexation can change significantly in terms of the polymers solubility and conformation, which facilitates the intercomplex aggregates. Meanwhile, nanostructures can also be obtained involving copolymer and low-molecular-mass compound (LMC, surfactant or organic molecules with a polar head and a nonpolar tail) that have recently been investigated extensively and offer many possibilities to change the microstructure.⁵⁹ The micellization behavior of a block copolymer/LMC complex can be controlled by the amount of adding LMC, and a variation in the environment which affect the interaction between block copolymer and LMC.⁶⁰ Hydrogen bonds play an important role in the construction of supramolecular polymers by self-assembly due to their moderate bonding energy offering the

flexibility for association and dissociation processes. It is well-known that the strength and extent of hydrogen bonding in copolymers or polymer blends depends on their respective affinities between the hydrogen bond donors and acceptors.⁶¹⁻⁶⁵ In addition, the solvent medium plays other important role to affect or control the type of complex formation. In our previous studies,^{64,65} different morphologies used formed from the mixtures of PVPh-*b*-PS and PMMA-*b*-P4VP due to the different chain behaviors of PVPh/P4VP block mixtures in different common solvents as shown in Figure 2-18. The hydrogen bonding interaction between PS-*b*-PVPh and PMMA-*b*-P4VP in DMF solution is relatively weaker than that in THF solution. As a result, the interpolymer hydrogen-bonded complexation core of PVPh and P4VP chains more stretching, and thus vesicular complexes were formed surrounded by PMMA and PS chains in THF solution. In contrast to the THF solution, DMF solution had relatively lower degree of stretching of the core chains (PVPh/P4VP) and stronger repulsion of the coronal chains (PS and PMMA), consequently, spherical micelles were formed with PVPh/P4VP as the core and PS/PMMA as the corona.

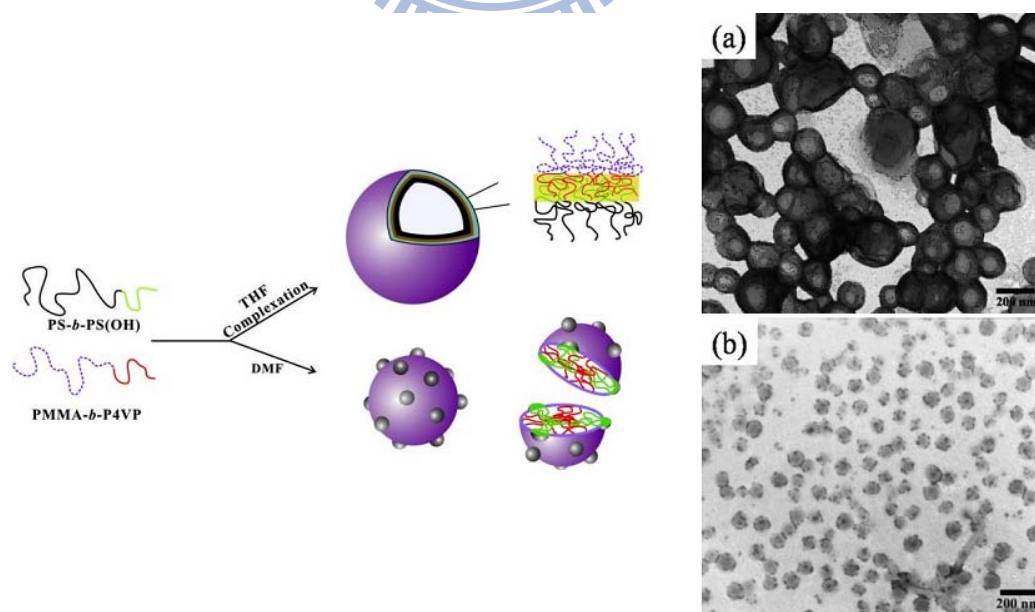


Figure 2-18. Models of micelle formation through mediated by hydrogen-bonding interaction of diblock copolymers mixtures and TEM images in THF (a) and DMF (b).

References

- [1] Prockop, D. J.; Fertala, A. *J. Struct. Biol.* **1998**, *122*, 111.
- [2] Whitesides, G. M.; Grzybowski, B. *Science* **2002**, *295*, 2418.
- [3] Philip, D.; Stoddart, J. F. *Angew. Chem. Int. Ed.* **1996**, *35*, 1155.
- [4] Jakubith, S.; Rotermund, H. H.; Engel, W.; von Oertzen, A.; Ertl, G. *Phys. Rev. Lett.* **1990**, *65*, 3013.
- [5] Whitesides, G. M.; Ismagilov, R. F. *Science* **1999**, *284*, 89.
- [6] Clark, T. D.; Tien, J.; Duffy, D. C.; Paul, K. E.; Whitesides, G. M. *J. Am. Chem. Soc.* **2001**, *123*, 7677.
- [7] Förster, S.; Plantenberg, T. *Angew. Chem. Int. Ed.* **2002**, *41*, 688.
- [8] Leibler, L. *Macromolecules* **1980**, *13*, 1602.
- [9] Bates, F. S. *Science* **1991**, *251*, 898.
- [10] Fredrickson, G. H.; Bates, F. S. *Annu. Rev. Mater. Sci.* **1996**, *26*, 501.
- [11] Hamly, I. W. “*The Physics of Block Copolymer*”, Oxford University Press, Inc., New York, **1998**.
- [12] Bates, F. S.; Fredrickson, G. H. *Phys. Today* **1999**, *52*, 32.
- [13] Tanaka, H.; Hasegawa, H.; Hashimoto, T. *Macromolecules* **1991**, *24*, 240.
- [14] Koizumi, S.; Hasegawa, H.; Hashimoto, T. *Macromolecules* **1994**, *27*, 7893.
- [15] Jeon, K. J.; Roe, R. J. *Macromolecules* **1994**, *27*, 2439.
- [16] Shull, K. R.; Winey, K. I. *Macromolecules* **1992**, *25*, 2637.
- [17] Bodycomb, J.; Yamaguchi, D.; Hashimoto, T. *Macromolecules* **2000**, *33*, 5187.
- [18] Winey, K. I.; Thomas, E. L.; Fetters, L. J. *Macromolecules* **1992**, *25*, 2645.
- [19] Xie, R.; Li, G.; Liu, C.; Jiang, B. *Macromolecules* **1996**, *29*, 4895..
- [20] Lee, S.-H.; Char, K.; Kim, G. *Macromolecules* **2000**, *33*, 7072.
- [21] Winey, K. I.; Thomas, E. L.; Fetters, L. J. *Macromolecules* **1992**, *25*, 422.
- [22] Yamaguchi, D.; Shiratake, S.; Hashimoto, T. *Macromolecules* **2000**, *33*, 8258.

- [23] Mayes, A. M.; Russell, T. P.; Satijia, S. K.; Majkrzak, C. F. *Macromolecules* **1992**, *25*, 6523.
- [24] Dobrosielska, K.; Wakao, S.; Takano, A.; Matsushita, Y. *Macromolecules*, **2008**, *41*, 7695.
- [25] Dobrosielska, K.; Wakao, S.; Suzuki, J.; Noda, K.; Takano, A.; Matsushita, Y. *Macromolecules* **2009**, *42*, 7098.
- [26] Kuo, S. W. *Polym. Inter.* **2009**, *58*, 455.
- [27] Kosonen, H.; Ruokolainen, J.; Nyholm, P.; Ikkala, O. *Polymer* **2001**, *42*, 9481.
- [28] Kimishima, K.; Hashimoto, T.; Han, C. D. *Macromolecules* **1995**, *28*, 3842.
- [29] Zhao, J. Q.; Pearce, E. M.; Kwei, T. K. *Macromolecules* **1997**, *30*, 7119.
- [30] Hameed, N.; Guo, Q. *Polymer* **2008**, *49*, 922.
- [31] Hameed, N.; Guo, Q. *Macromolecules* **2008**, *41*, 7596.
- [32] Hameed, N.; Guo, Q. *Polymer* **2008**, *49*, 5268.
- [33] Chen, W. C.; Kuo, S. W.; Lu, C. H.; Jeng, U. S. Chang, F. C. *Macromolecules* **2009**, *42*, 3580.
- [34] Lee, H. F.; Kuo, S. W.; Huang, C. F.; Lu, J. S.; Chan, S. C. Chang, F. C. *Macromolecules* **2006**, *39*, 5458.
- [35] Chen, W. C.; Kuo, S. W.; Jeng, U. S. Chang, F. C. *Macromolecules* **2008**, *41*, 1401.
- [36] Lin, I. H.; Kuo, S. W.; Chang, F. C. *Polymer* **2009**, *50*, 5276.
- [37] Riess, G. *Prog. Polym. Sci.* **2003**, *28*, 1107.
- [38] Mori, H.; Müller, A. E. H. *Prog. Polym. Sci.* **2003**, *28*, 1403.
- [39] Moffitt, M.; Khougaz, K.; Eisenberg, A. *Acc. Chem. Res.* **1996**, *29*, 95.
- [40] Hu, J.; Liu, G. *Macromolecules* **2005**, *38*, 8058.
- [41] Noolandi, J.; Hong, K. M. *Macromolecules* **1983**, *16*, 1443.
- [42] (a) De Gennes, P. G. *J. Phys.* **1976**, *37*, 1445. (b) De Gennes, P. G. *Macromolecules* **1980**, *13*, 1069.

- [43] Daoud, M.; Cotton, J. P. *J. Phys.* **1982**, *43*, 531.
- [44] Zhulina, E. B.; Birshtein, T. M. “*Conformation of molecules of block copolymers in selective solvents (micellar structure)*” *Vysokomolekulyarnye Soedineniya, Seriya A* **1985**, *27*, 511.
- [45] Halperin, A. *Macromolecules* **1987**, *20*, 2943.
- [46] Wu, C.; Gao, J. *Macromolecules* **2000**, *33*, 645.
- [47] (a) Shusharina, N. P.; Nyrkova, I. A.; Khoklov, A. R. *Macromolecules* **1996**, *29*, 3167.
(b) Shusharina, N. P.; Alexandridis, P.; Linse, P.; Balijepalli, S.; Gruenbauer, H. J. M. *Eur. Phys. J.* **2003**, *10*, 45.
- [48] Daoud, M.; Cotton, J. P. *J. Phys. (Paris)* **1982**, *43*, 531.
- [49] Zhulina, E. B. *Polym. Sci. USSR* **1984**, *26*, 794.
- [50] Alexander, S. *J. Phys. (Paris)* **1977**, *38*, 983.
- [51] De Gennes, P. G. *Macromolecules* **1980**, *13*, 1069.
- [52] Israelachvili, J. N. *Intermolecular and surface forces*. London: Harcourt Brace and Company; **1992**.
- [53] Hyde, S. T. *J. Phys.* **1990**, *51*, 7209.
- [54] Förster, S.; Zisenis, M.; Wenz, E.; Antonietti, J. *Chem. Phys.* **1996**, *104*, 9956.
- [55] Disher, D. E.; Eisenberg, A. *Science* **2002**, *297*, 967.
- [56] Aranda-Espinoza, H.; Bermúdez, H.; Bates, F. S.; Disher, D. E. *Phys. Rev. Lett.* **2001**, *87*, 208301.
- [57] Bhargava, P.; Zheng, J. X.; Li, P.; Quirk, R. P.; Harris, F. W.; Cheng, S. Z. D. *Macromolecules* **2006**, *39*, 4880.
- [58] Ruokolainen, J.; Saariaho, M.; Ikkala, O.; ten Brinke, G.; Thomas, E. L.; Torkkeli, M.; Serimaa, R. *Macromolecules* **1999**, *32*, 1152.
- [59] (a) Ruokolainen, J.; Mäkinen, R.; Torkkeli, M.; Makela, T.; Serimaa, R.; ten Brinke, G.; Ikkala, O. *Science* **1998**, *280*, 557. (b) Ruokolainen, J.; ten Brinke, G. Ikkala, O. *Adv.*

- Mater.* **1999**, *11*, 777. (c) Ruokolainen, J.; Torkkeli, M.; Serimaa, R.; Komanschek, E.; ten Brinke, G.; Ikkala, O. *Macromolecules* **1997**, *30*, 2002. (d) de Moel, K.; Alberda van Ekenstein, G. O. R.; Nijland, H.; Polushkin, E.; ten Brinke, G.; Maki-Ontto, R.; Ikkala, O. *Chem. Mater.* **2001**, *13*, 4580.
- [60] (a) Wang, M.; Jiang, M.; Ning, F.; Chen, D.; Liu, S.; Duan H. *Macromolecules* **2002**, *35*, 5980. (b) Liu, S.; Zhu, H.; Zhao, H.; Jiang, M.; and Wu, C. *Langmuir* **2000**, *16*, 3712.
- [61] Chen, S. C.; Kuo, S. W.; Jeng, U S.; Su, C. J.; Chang, F. C. *Macromolecules* **2010**, *43*, 1083.
- [62] Kuo, S. W.; Chang, F. C. *Macromolecules* **2001**, *34*, 5224.
- [63] He, Y.; Zhu, B.; Inoue, Y. *Prog. Polym. Sci.* **2004**, *29*, 1021.
- [64] Kuo, S. W.; Tung, P. H.; Lai, C. L.; Jeong, K. U.; Chang, F. C. *Macromol. Rapid Commun.* **2008**, *29*, 229.
- [65] Hsu, C. H.; Kuo, S. W.; Chen, J. K.; Ko, F. H.; Liao, C. S.; Chang, F. C. *Langmuir* **2008**, *24*, 7727.



Chapter 3

Syntheses, Specific Interactions, and pH-Sensitive Micellization Behavior of Poly[vinyl phenol-*b*-2-(dimethylamino)ethyl methacrylate] Diblock Copolymers

Abstract

We have used anionic polymerization to prepare a series of poly[vinyl phenol-*b*-2-(dimethylamino)ethyl methacrylate] (PVPh-*b*-PDMAEMA) block copolymers. These block copolymers are miscible, with strong specific interactions occurring between the OH groups of the PVPh segments and the tertiary ammonium groups of the PDMAEMA segments. These PVPh-*b*-PDMAEMA diblock copolymers exhibit higher glass transition temperatures than do the corresponding PVPh/partially protonated PDMAEMA blends obtained from DMSO solution, which we suspect exist in the form of separate coils. The blocks of the PVPh-*b*-PDMAEMA diblock copolymers interact strongly, resulting in polymer complex aggregation similar to the behavior of PVPh/partially protonated PDMAEMA blend complexes obtained in methanol. In addition, these PVPh-*b*-PDMAEMA diblock copolymers exhibit a novel type of pH-sensitivity: at low pH, compact spherical micelles are formed possessing PDMAEMA coronas and PVPh cores; at medium pH, vesicles are observed, consisting of partially protonated hydrophilic PDMAEMA shells and hydrophobic PVPh cores; at high pH, the spherical micelles that formed comprised ionized PVPh coronas and deprotonated hydrated-PDMAEMA cores, i.e., phase inversion of the micelles formed at pH 2.

3-1 Introduction

A vast majority of the studies aimed at enhancing the miscibility of polymer blends have involved incorporating local centers capable of participating in strong noncovalent interactions (e.g., ion–ion, ion–dipole, and hydrogen bonding interactions) into the blend components.^{1–3} It is well-known that the strength and extent of hydrogen bonding in copolymers or polymer blends depend on the respective affinities between the hydrogen bond donors and acceptors.^{4–6} Because poly(vinyl phenol) (PVPh) possesses strong proton-donor groups, it is miscible with proton-acceptor polymers such as poly(methacrylate), polyether, and polyester.^{7–12} Poly[(dimethylamino)ethyl methacrylate] (PDMAMEA) possesses three possible proton-accepting sites: the C=O oxygen, ether oxygen, and nitrogen atoms. Goh et al. studied the miscibility and thermal behavior of PVPh/PDMAEMA blends in low-polarity solvents (e.g., methanol, ethanol, and MEK).¹³ The nature of the solvent plays an important role affecting the formation of polymer complexes.¹⁴ For example, PVPh/poly(*N,N*-dimethylacrylamide) (PDMA) blends form a complex precipitate in dioxane, but do not precipitate from DMF. Because solvent molecules can also participate in hydrogen bonding interactions, they compete with PDMA for coordination to the OH groups of PVPh. Consequently, when the polymer–polymer interactions are sufficiently strong to overcome the polymer–solvent interactions, the two polymer chains can co-precipitate in the form of highly associated materials (complexes). If the solvent interacts so strongly with the polymers that it prevents precipitation, the resulting materials obtained upon evaporation of the solvent are considered to be merely blends. In general, a single glass transition temperature (T_g) is obtained for both miscible blends and complexes, indicating that they are single-phase materials. Nevertheless, the values of T_g of complexes are usually higher than those of miscible blends having similar compositions because of the more compact nature of the complexes.^{15–19} In a previous study, we observed the interesting result that PVPh-*b*-poly(4-vinylpyridine) (P4VP) diblock copolymers possess higher values of T_g

relative to those of their corresponding PVPh/P4VP blends. These diblock copolymers may form inter- and intrapolymer complex aggregates similar to the PVPh/P4VP complexes obtained from methanol solution.²⁰ Although the polymer chain behavior of these diblock copolymers is similar to that of its corresponding blend complexes, it is not clear whether the same conclusion is applicable to all diblock copolymers experiencing strong interactions.

Multiple-stimulus-responsive copolymers that are soluble in water are attracting increasing attention because of their diverse self-assembly behavior in response to such stimuli as pH, temperature, and ionic strength.²¹⁻³² These copolymers can form two or more types of aggregates, including inverted structures, upon judicious adjustment of the environmental conditions. Therefore, depending upon the response to an applied stimulus, a number of applications can be contemplated for the same precursor copolymer, e.g., cosmetics, detergents, encapsulation, drug delivery, and enhanced recognition of a predetermined target. The first findings in this field, dealing with poly[2-(diethylamino)ethyl methacrylate-*b*-2-(*N*-morpholino)ethyl methacrylate] (PDEA-*b*-PMEMA), were reported by Armes in 1998.^{21,22} The diblock copolymer was dissolved in aqueous media at pH 4 and then PDEA-core micelles were formed merely by adjusting the solution pH. The formation of inverted PMEMA-core micelles occurred upon the addition of an electrolyte through selective “salting out” of the PMEMA block. The second known example was that of poly[propylene oxide-*b*-2-(diethylamino)ethyl methacrylate] (PPO-*b*-PDEA), which possesses a thermally sensitive PPO block and a pH-sensitive PDEA block.²³ This diblock copolymer dissolved in cold water at pH 6.5, but formed PPO-core micelles upon increasing the temperature; the PDEA-core micelles were obtained by increasing the pH to 8.5 at 5 °C. Several other sensitive copolymers have been investigated since then, including the block copolymers poly[succinyl ethyl methacrylate-*b*-2-(diethylamino)ethyl methacrylate] (PSEMA-*b*-PDEAEMA),²⁴ poly[4-vinylbenzoic acid-*b*-2-(*N*-morpholino)ethyl methacrylate] (PVBA-*b*-PMEMA),²⁵ and poly(hydroxystyrene-*b*-methacrylic acid) (PSOH-*b*-PMAA).²⁶

In this paper, we report the preparation of a series of novel pH-sensitive PVPh-*b*-PDMAEMA diblock copolymers by combining protected group chemistry with anionic polymerization. Using ^1H NMR spectroscopy, DSC, FTIR spectroscopy, 2D correlation-IR spectroscopy, and ^{13}C solid state NMR spectroscopy, we characterized the chemical structures, glass transition behavior, specific interactions, and polymer chain behavior of these diblock copolymers. Additionally, we investigated the pH-sensitive reversible micellization behavior of these PVPh-*b*-PDMAEMA diblock copolymers using ^1H NMR spectroscopy and TEM analyses.



3-2 Experimental Section

3-2.1 Materials

4-*tert*-Butoxystyrene (*t*BOS, Aldrich, 99%) and 2-(dimethylamino)ethyl methacrylate (DMAEMA, Aldrich, 99%) were distilled from finely ground CaH₂ prior to use. Tetrahydrofuran (THF), the polymerization solvent for anionic polymerization, was purified through distillation under argon from a red solution of diphenylhexyllithium [produced through the reaction of 1,1-diphenylethylene and *n*-butyllithium (*n*-BuLi)]. *sec*-BuLi (Acros, 1.3 M in cyclohexane) was used as the initiator for anionic polymerization.

3-2.2 Poly[vinyl phenol-*b*-2-(dimethylamino)ethyl methacrylate] Diblock Copolymer

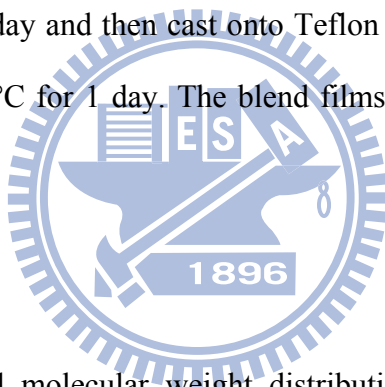
Poly[4-*tert*-butoxystyrene-*b*-2-(dimethylamino)ethyl methacrylate] (*Pt*BOS-*b*-PDMAEMA) diblock copolymer was synthesized through sequential living anionic polymerization of *t*BOS and DMAEMA in THF, using *sec*-BuLi as initiator (Scheme 3-1). Lithium chloride (LiCl) was added to prevent side reactions.³³⁻³⁷ Polymerizations were performed in THF at -78 °C under an inert atmosphere. The *t*BOS monomer was polymerized first for 2 h; an aliquot of the poly(*t*BOS) was isolated for analysis after termination with degassed methanol. DMAEMA was then introduced into the reactor; the reaction was terminated after 2 h through the addition of degassed methanol.

The *Pt*BOS-*b*-PDMAEMA copolymer was converted into PVPh-*b*-PDMAEMA through hydrolysis. The *Pt*BOS-*b*-PDMAEMA diblock copolymer product was dissolved in dioxane, and then a 10-fold excess of 37 wt% hydrochloric acid was added to the solution. The hydrolysis was continued for 2 days at 85 °C under an atmosphere of argon and then the product was neutralized to pH 8 with 10 wt% aqueous NaOH. The resulting solution was purified for 2 weeks through dialysis against regularly distilled water; the product was then precipitated in cold ethyl ether. Before drying under vacuum, the final copolymer was subjected to two dissolve (DMF)/precipitate (ethyl ether) cycles.

Using a living anionic polymerization procedure similar to the one described above, the homopolymer of PVPh was synthesized to compare its thermal properties with those of the copolymers. In addition, the homopolymer of PDMAEMA was synthesized through atom transfer radical polymerization using ethyl α -bromoisobutyrate as initiator; the degree of protonation was adjusted to ca. 15% using HCl (partially protonated PDMAEMA).

3-2.3 Blend Preparation

Blends of PVPh/partially protonated PDMAEMA (15% protonation) were prepared through solution-casting. Separate DMSO solutions of pure PVPh and pure partially protonated PDMAEMA were stirred together in various molar ratios. The resulting polymer mixtures were stirred for 1 day and then cast onto Teflon dishes. The samples were then left to evaporate slowly at 100 °C for 1 day. The blend films were then dried for 1 week under vacuum at 100 °C.



3-2.4 Characterization

Molecular weights and molecular weight distributions were determined through gel permeation chromatography (GPC) using a Waters 510 HPLC equipped with a 410 differential refractometer, a RI detector, a UV detector, and three Ultrastyrigel columns (100, 500, and 10^3 Å) connected in series; THF was the eluent; the flow rate was 0.6 mL/min at 35 °C. The molecular weight calibration curve was obtained using polystyrene standards. ^1H and ^{13}C NMR spectra were obtained using an INOVA 500 instrument; CDCl_3 and dimethylsulfoxide- d_6 were used as the solvents. The molecular weights and PtBOS/PDMAEMA ratios of the various copolymers were evaluated from ^1H NMR spectra and compared with the corresponding values obtained from GPC analysis. All infrared (IR) spectra were recorded under nitrogen using a Nicolet Avatar 320 FTIR spectrometer; 32 scans were collected at resolution of 1 cm^{-1} . Each sample was dissolved in DMSO and then cast

directly onto a KBr pellet. All of the vacuum-dried films were sufficiently thin within the absorbance range such that the Beer–Lambert law was obeyed. 2D Correlation analysis was performed using the 2D Shige software programmed by Shigeaki Morita (Kwansei-Gakuin University, Japan). All of the spectra applied to the 2D-IR correlation analyses were normalized; the negative intensities of the auto- or cross-peaks in 2D-IR correlation spectra were indicated by blue-colored regions; positive intensities were indicated by red-colored regions. Thermal analyses were performed using a DuPont 910 controller operated at a scan rate of 20 °C/min over the temperature range from –60 to +250 °C under a nitrogen atmosphere. The sample (ca. 5–10 mg) was weighted and sealed in an aluminum pan, quickly quenched to –60 °C from the first scan, and then rescanned between –60 and +250 °C at a scan rate of 20 °C/min. The glass transition temperature was obtained as the inflection point of the heat capacity jump. High-resolution solid state ^{13}C NMR spectra were recorded at 25 °C using a Bruker DSX-400 spectrometer operating at resonance frequencies of 399.53 and 100.47 MHz for ^1H and ^{13}C , respectively. The ^{13}C CP/MAS spectra were measured using a 3.9- μs 90° pulse, a 3-s pulse delay time, a 30-ms acquisition time, and 2048 scans. All NMR spectra were recorded at 300 K using broad-band proton decoupling and a normal cross-polarization pulse sequence. A magic-angle sample spinning (MAS) rate of 5.4 kHz was used to avoid absorption overlapping. The proton spin-lattice relaxation time in the rotating frame ($T_{1\rho}^H$) was determined indirectly via carbon observation using a 90°- τ - spin lock pulse sequence prior to cross-polarization. The data acquisition was performed via ^1H decoupling with delay times ranging from 0.1 to 20 ms and a contact time of 1.0 ms. For transmission electron microscopy (TEM) studies, a drop of the micelle solution was sprayed onto a Cu TEM grid covered with a Formvar support film that had been precoated with a thin film of carbon. After 1 min, the excess of the solution was blotted away using a strip of filter paper. All samples were left to dry at room temperature for 1 day prior to observation. After drying,

the samples were stained with RuO₄ and viewed under a Hitachi H-7500 TEM instrument operated with an accelerating voltage of 100 kV.



3-3 Results and Discussion

3-3.1 Syntheses of Poly[vinyl phenol-*block*-2-(dimethylamino)ethyl methacrylate]

Diblock Copolymers

The PVPh-*b*-PDMAEMA diblock copolymers were prepared through anionic living polymerization of *Pt*BOS-*b*-PDMEMA and subsequent hydrolytic deprotection. The hydrolysis of the *Pt*BOS-*b*-PDMAEMA copolymers, performed at 85 °C in dioxane in the presence of conc. HCl, gave the PVPh-*b*-PDMAEMA diblock copolymers quantitatively (Scheme 3-1). The molecular weights and polydispersities of the pure *Pt*BOS and *Pt*BOS-*b*-PDMAEMA diblock copolymers were analyzed using GPC.

¹H and ¹³C NMR spectra were recorded from *Pt*BOS-*b*-PDMAEMA and PVPh-*b*-PDMAEMA to confirm their chemical compositions and structures. Figure 3-1 displays typical ¹H NMR spectra of the diblock copolymers recorded before and after deprotection, together with assignments of their characteristic peaks. The signal at 1.29 ppm, corresponding to the *tert*-butyl groups of the *Pt*BOS-*b*-PDMAEMA copolymer (in CDCl₃), disappeared in the spectrum of the hydrolyzed block copolymer, and only the signals of the polymer backbone protons appear in the region 1–2 ppm. In addition, a peak (8.9 ppm), corresponding to the protons of the OH groups, appears after hydrolysis. Figure 3-2a reveals that the signal of the quaternary carbon atom of the *tert*-butyl group in the *Pt*BOS segment appeared at 78.0 ppm.³⁸ After hydrolysis, this signal disappeared (Figure 3-2b), indicating that the hydrolysis reaction was complete. The FTIR spectrum (Figure 3-3) of the block copolymer after hydrolysis still clearly exhibits the C=O stretching vibration band of the PDMEMA segment in the region from 1690 to 1750 cm⁻¹. The broad peak at 3350 cm⁻¹ in Figure 3-3c indicates the presence of OH groups after deprotection. The compositions of the PVPh-*b*-PDMAEMA block copolymers were essentially identical to those of the corresponding *Pt*BOS-*b*-PDMAEMA block copolymers, as determined from the relative intensities of the peaks of the aromatic rings and the ethyl protons, located at 6.1–6.9 and

4.1–4.2 ppm, respectively. Table 3-1 lists the molecular parameters of the polymers and summarizes the characterization data for each PVPh-*b*-PDMAEMA copolymer.

3-3.2 FTIR Spectroscopic Analyses

FTIR spectroscopy has been successfully applied to the analysis of numerous diblock copolymers and blends featuring intermolecular hydrogen bonding interactions. The OH stretching region in the IR spectra of PVPh-*b*-PDMAEMA diblock copolymers is sensitive to the degree and type of hydrogen bonding. Figure 3-4 displays the OH stretching region (2700–4000 cm⁻¹) of the FTIR spectra of the pure PVPh and various PVPh-*b*-PDMAEMA diblock copolymers cast from DMSO solution at room temperature. The spectrum of pure PVPh reveals two unresolved bands in the OH-stretching region, corresponding to the free OH groups at 3525 cm⁻¹ and a broad band centered at 3350 cm⁻¹ arising from the absorption of hydrogen-bonded OH groups (self-association).²⁰ Figure 3-4 indicates that the intensity of the signal of the free OH groups decreased gradually upon increasing the PDMAEMA content in the diblock copolymer, i.e., a greater fraction of OH groups interacted with PDMAEMA upon increasing the PDMAEM content. In the meantime, the intensity of the OH stretching band shifted to lower wavenumber upon increasing the DMAEMA content, indicating that a new distribution of the OH stretching region was formed from competition between the multiply hydrogen-bonded OH groups within the pure PVPh and the specific interactions between PVPh and PDMAEMA. Surprisingly, the trend is different from that observed by Goh et al.,⁷ who found that the signal for OH–OH hydrogen bonding (3350 cm⁻¹) shifted to higher wavenumber (3430 cm⁻¹) upon increasing the PDMAEMA content in the PVPh/PDMAEMA blend system because of the formation of hydrogen bonds between the OH groups of PVPh and the C=O oxygen atoms and N atoms of PDMAEMA.

We suspected that the differences observed between the FTIR spectra of the block copolymer system and the blend system may have arisen from different types of noncovalent

interactions in these systems. According to the procedure employed for the synthesis of the block copolymer, tertiary ammonium groups are formed from the hydrolysis reaction. Although our block copolymer was neutralized with 10 wt% NaOH solution to pH 8 after hydrolysis, a small fraction of tertiary ammonium groups would still be present in the block copolymer. Therefore, we speculated that the difference in the IR spectra resulted from the formation of stronger specific interactions between the OH groups of PVPh and the tertiary ammonium groups of PDMAEMA. Thus, we prepared a model blend corresponding to our block copolymer, i.e., a PVPh/fully protonated PDMAEMA blend. Figure 3-5 displays the OH stretching region of the FTIR spectra of the pure PVPh and the PVPh/fully protonated PDMAEMA blend. The PVPh/fully protonated PDMAEMA blend and our block copolymer system exhibit a similar trend: the broad hydrogen-bonded OH band shifted to lower wavenumber for the PVPh/fully protonated PDMAEMA blend, thereby confirming the presence of a specific interaction between the OH groups of PVPh and the tertiary ammonium groups of PDMAEMA. According to Pullman's study of the interactions between the tetramethylammonium (TMA) ion and phenol, the phenol leans toward one hydrogen atom of TMA while the O-H bond rotates out of the molecular plane to orient the oxygen atom's lone pair optimally (O...H distance: 2.35 Å; OH rotation: 32°); the formation of the "hydrogen bond-like" interaction clearly gives rise to the increment in stability observed with respect to benzene-TMA.³⁹ Our spectroscopic investigation confirmed that the specific (hydrogen bond-like) interaction was formed via the oxygen atom's lone pair of electrons of the OH groups interacting with the charge of the tertiary ammonium groups. It is reasonable to assign the band at 3220 cm⁻¹ to the signal of OH groups of PVPh hydrogen bonding to the tertiary ammonium groups of PDMAEMA. In addition, we used titration analysis to determine that the degree of protonation of the diblock copolymers was ca. 15%.

Taking into account the effect of the composition, the tertiary ammonium groups of

PDMAEMA compete with self-associated OH groups, the C=O oxygen atoms, and the nitrogen atoms of PDMAEMA for hydrogen bonding opportunities, causing the shift of the signal for the OH band toward lower wavenumbers gradually upon decreasing the vinylphenol content. Coleman and co-workers used the frequency difference ($\Delta\nu$) between the hydrogen-bonded and free OH absorptions to roughly estimate the average hydrogen bond strength.⁴⁰ In this respect, on the basis of the reference of the free OH stretching band at 3525 cm^{-1} , the frequency differences resulting from OH \cdots C=O ($\Delta\nu = 95 \text{ cm}^{-1}$), OH \cdots N ($\Delta\nu = 95 \text{ cm}^{-1}$), and OH \cdots OH ($\Delta\nu = 175 \text{ cm}^{-1}$) interactions are all weaker than the OH \cdots tertiary ammonium interactions ($\Delta\nu = 305 \text{ cm}^{-1}$). In this situation, only the latter type of interaction is predominant and, thus, the OH stretching band is relatively narrow.

Next, we turned our attention to compare the chain behavior of the blend systems with that of the block copolymer system. To compare the chain behavior, we blended PVPh with partially protonated PDMAEMA. Figure 3-6 displays the OH stretching region of the FTIR spectra of the pure PVPh and various PVPh/partially protonated PDMAEMA blends. The spectra are similar to those of the block copolymer system: the peak for the broad OH stretching band shifts to lower wavenumber upon increasing the content of partially protonated PDMAEMA because of the specific interactions between the OH groups of PVPh and the tertiary ammonium groups of PDMAEMA. Thus, specific interactions are indeed formed between the OH groups of PVPh and the tertiary ammonium groups of PDMAEMA.

Figure 3-7 presents the scale-expanded FTIR spectra (C=O stretching range; 1660–1800 cm^{-1}) of pure PVPh, pure PDMAEMA, the PVPh-*b*-PDMAEMA block copolymers, and their blends. The peaks at 1730 and 1705 cm^{-1} correspond to the free and hydrogen-bonded C=O groups, respectively. As expected, a higher number of hydrogen-bonded C=O groups results at a higher content of vinylphenol units. To obtain the fraction of hydrogen-bonded C=O group, it is necessary to know the absorptivity ratio for the contributions of hydrogen-bonded

and free C=O groups; we employed the value of $\alpha_{\text{HB}}/\alpha_{\text{F}}$ of 1.5 that had previously been calculated by Moskala et al.⁴¹ Table 3-2 summarizes the fraction of hydrogen-bonded C=O groups, as determined through curve fitting of the data from the copolymers and binary blends. The fraction of hydrogen-bonded C=O groups increased upon increasing the PVPh content for both the PVPh-*b*-PDMAEMA and PVPh/partially protonated PDMAEMA blend systems. Moreover, the fraction of hydrogen-bonded C=O groups of the copolymers was always higher than that of the blend system at similar PVPh contents. This observation can be explained in terms to the difference in the degrees of rotational freedom of the polymer blend and block copolymer.⁴² The polymer chain architecture of a homopolymer blend is significantly different from that of a copolymer because of intramolecular screening.^{43–47} The PVPh segment in a copolymer system has more contacts with PDMAEMA segments than it does in blend systems because of both chain connectivity and intramolecular screening effects. Intramolecular screening results from an increase in the number of same-chain contacts due to polymer chains bending back upon themselves. This “screening” process reduces the number of intermolecular hydrogen bonds formed in a polymer blend. Thus, the inter-association hydrogen bonding density of a copolymer system is relatively higher than that of a corresponding blend system. As a result, the density of hydrogen-bonded C=O groups in the PVPh/partially protonated PDMAEMA blend was relatively lower than that in the corresponding PVPh-*b*-PDMAEMA copolymer having the same composition.

3-3.3 2D-IR Correlation Analyses

To further understand the chain behavior and the order of the interaction for block copolymer and its blend, we recorded 2D-IR correlation spectra for the PVPh-*b*-PDMAEMA copolymer and the PVPh/partially protonated PDMAEMA blends. Throughout this paper, the blue- and red-colored regions of the 2D-IR correlation counter maps indicate negative and positive correlation intensities, respectively. We obtained two types of spectra: 2D

synchronous and asynchronous spectra. The intensity of a signal in a synchronous 2D-IR correlation spectrum $\Phi(\nu_1, \nu_2)$ represents the simultaneous or coincidental change of the spectral intensity variations measured at ν_1 and ν_2 ; the intensity of a signal in an asynchronous spectrum $\Psi(\nu_1, \nu_2)$ represents sequential or successive changes of spectral intensities observed at ν_1 and ν_2 . The sign of a synchronous cross-peak [$\Phi(\nu_1, \nu_2)$] becomes positive if the intensity variations of the two peaks ν_1 and ν_2 follow the same trend (both increase or both decrease) under the environmental perturbation. On the other hand, the sign of an asynchronous cross-peak [$\Psi(\nu_1, \nu_2)$] becomes negative and the intensities of the two peaks at ν_1 and ν_2 vary in opposite directions (one increases, the other decreases) under perturbation. Based on analysis of the cross-peaks in synchronous and asynchronous maps, we can obtain the specific order of the spectral intensity changes occurring when a sample is subjected to environmental perturbation. According to Noda's rule,⁴⁸⁻⁵⁰ when $\Phi(\nu_1, \nu_2)$ is zero and $\Psi(\nu_1, \nu_2)$ is positive (red-colored region), the intensity change of ν_1 occurs prior to that of ν_2 . If $\Psi(\nu_1, \nu_2)$ is negative (blue-colored region), the intensity change of ν_1 will occur after that of ν_2 . This rule is reversed, however, when $\Phi(\nu_1, \nu_2)$ is zero. On the basis of this unique feature of asynchronous spectra, we obtained additional information concerning the specific interactions in the PVPh-*b*-PDMAEMA copolymer and the PVPh/partially protonated PDMAEMA blends.

Figures 3-8 and 3-9 display the synchronous and asynchronous maps of the block copolymers and blend systems in the range 1490–1780 cm^{-1} . Figure 3-8a (synchronous map) reveals bands at 1730 cm^{-1} for the free C=O groups of PDMAEMA and 1510 or 1612 cm^{-1} for the phenyl–OH bonds of PVPh. Two auto- and cross-peaks at 1730 and 1510 cm^{-1} indicate the specific interactions occurring between these two groups. According to the sign of the cross-peaks at (1730, 1510) cm^{-1} in Figure 3-8, the intensity of the band at 1510 cm^{-1} increases, while the band at 1730 cm^{-1} decreases (i.e., changes in opposite directions).

Obviously, the intensity of the signal for the free C=O groups of PDMAEMA decreased upon increasing the PVPh content because more OH groups were available to interact with them. In contrast, the signs of the weak cross-peaks appearing at (1705, 1510) cm^{-1} in the block copolymer were both positive, implying that increasing the PVPh content induced intensity variations for the two peaks at 1705 and 1510 cm^{-1} in the same direction; i.e., the number of hydrogen-bonded C=O groups increased upon increasing the PVPh content. Note, however, that the intensities of the auto- and cross-peaks at 1510 and 1730 cm^{-1} for the blend system in Figure 3-8b were relatively weaker than those for the block copolymer in Figure 3-8a. This result can be explained in terms of the difference between the inter-association equilibrium constants (K_A), which describe the extent of inter-association of PDMAEMA with PVPh, of the PVPh-*b*-PDMAEMA copolymers and the PVPh/partial protonated PDMAEMA blends. As mentioned above in the discussion of the difference in the degrees of rotation freedom between blend and block copolymer, the polymer chain architecture of a homopolymer is significantly different from that of a block copolymer because of intramolecular screening and functional group accessibility caused by the covalent bond connectivity of the latter. This phenomenon implies that the effective inter-association equilibrium constant of the block copolymer is greater than that of the blend system. As a result of the greater inter-association equilibrium constant, the auto- and cross-peaks of the block copolymer are stronger than those of the blend system. This result also infers that the polymer chains in the blends and copolymers display different chain behavior.

The asynchronous 2D-IR correlation spectra in Figure 3-9 are asymmetric with respect to the diagonal line. The positive cross-peaks at (1730, 1510) cm^{-1} reveal that the out-of-phase spectral changes occur at two wavenumbers.⁴⁸ As explained by Noda,⁴⁸⁻⁵⁰ the cross-peaks of the block copolymer and blend have opposite signs in the synchronous and asynchronous maps, implying that when the content of PVPh is increased, the intensity of the band at 1510 cm^{-1} varies before the band at 1730 cm^{-1} does. This result can be explained in terms of the

difference in compatibility between PVPh and PVPh and between PVPh and PDMAEMA. Because self-association OH \cdots OH hydrogen bonding is stronger than inter-association OH \cdots O=C hydrogen bonding, the compatibility between OH groups is higher than that between OH and C=O groups. Therefore, OH groups tend to interact with other OH groups preferentially, rather than with C=O groups, upon increasing the PVPh content. Another reason for the intensity changing in the order OH groups > C=O groups for PVPh-*b*-PDMAEMA is due to the architecture of the polymer chains. Upon increasing the PVPh content, these OH groups are closer to other OH groups in the block copolymer and, thus, make more contacts with neighboring OH groups than with C=O groups. Another positive cross-peak centered at (1730, 1705) cm⁻¹ can be identified in Figure 3-9; it exhibits the same sign in the synchronous maps, implying that the intensity of the peak at 1730 cm⁻¹ changes prior to that of the one at 1705 cm⁻¹. Thus, the C=O groups do indeed interact with the OH groups first to form hydrogen-bonded C=O groups. The observed cross-peaks at (1730, 1510) and (1730, 1705) cm⁻¹ in the 2D maps provide clear evidence that the sequence changes of these three bands occur in the order 1510 > 1730 > 1705 cm⁻¹ (where “>” means “changes prior to”).

3-3.4 Thermal Analyses

Generally, only a single glass transition temperature can be observed when the components of blends and block polymers are thermodynamically miscible. Figure 3-10 presents the DSC thermograms of PVPh-*b*-PDMAEMA block copolymers and blends containing various PVPh contents, revealing that essentially all of the DSC traces possess only a single glass transition temperature, strongly suggesting that these systems are fully miscible and possess a homogeneous amorphous phase. Meanwhile, these single values of T_g were all higher than that of the pure PDMAEMA, even when the composition of PVPh in the block copolymer was low. The high positive deviation in the value of T_g of the copolymer

indicates that a strong interaction exists between its two blocks. This result is similar to the T_g behavior of the PVPh/partially protonated PDMAEMA miscible blend obtained from a DMSO solution. Over the years, a number of empirical equations have been offered to predict the variations in glass transition temperatures of miscible blends and diblock copolymers as a function of composition. The Kwei equation⁵¹ is usually employed for systems displaying specific interactions:

$$T_g = \frac{W_1 T_{g1} + kW_2 T_{g2}}{W_1 + kW_2} + qW_1W_2 \quad (3-1)$$

where w_1 and w_2 are the weight fractions of the components, T_{g1} and T_{g2} are the corresponding glass transition temperatures, and k and q are fitting constants. The parameter q corresponds to the strength of specific interactions in the system, reflecting a balance between the breaking of the self-association interactions and the forming of the inter-association interactions. Using a nonlinear least-squares “best fit” method, we obtained (Figure 3-11) values for k and q of 1 and 390, respectively, for the block copolymers and 1 and 240, respectively, for the blends. A greater positive value of q corresponds to stronger interactions between the OH groups of the PVPh segment and the tertiary ammonium groups of the PDMAEMA segment in addition to the self-association of the OH groups of PVPh. The dependence of T_g on the composition not only obeys the thermodynamics of interaction enthalpy but also must take into account the chain conformation entropy of the polymer chain. Additionally, the high positive values of q (390 and 240) obtained for these systems indicate that the inter-association hydrogen-bonding interactions existing between the OH groups of PVPh and the C=O oxygen atoms, nitrogen atoms, and the tertiary ammonium groups of PDMAEMA in the block copolymers were stronger than those corresponding interactions in the blends; this finding is similar to those of our previous studies.^{20,42,52}

The PVPh₅₅-*b*-PDAMEMA₄₅ displays a single glass transition at 184 °C, close to the value of T_g of the PVPh/partially protonated PDMAEMA = 55:45 complex (179 °C) obtained

from methanol solution (Table 3-3). This result can be explained in terms of the polymer chain behavior. Jiang et al.^{53,54} reported that an ordinary miscible blend formed an inter-polymer complex upon increasing the density of intermolecular hydrogen bonds and that the transition from separated polymer coils to complex aggregates took place in solution where intermolecular hydrogen bonding is strong. They also found that, in the solid state, further strengthening of hydrogen bonding can transform a miscible blend into a complex state. In a previous study,⁷ we found that the polymer chain behavior in PVPh-*b*-P4VP diblock copolymers is similar to that in inter-polymer complexes because of strong hydrogen bonding between the OH groups of PVPh and the pyridine groups of P4VP. Therefore, we speculate that our PVPh-*b*-PDMAEMA diblock copolymers may display the same polymer chain behavior because of strong interactions between the OH groups of PVPh and the tertiary ammonium groups of PDMAEMA. Thus, we used solid state NMR spectroscopic analyses to determine the spin lattice relaxation time in the rotating frame and, thereby, investigate the homogeneity of the polymer blends and diblock copolymers.

3-3.5 Solid State NMR Spectroscopic Analyses

Evidence for specific interactions within polymer blends and copolymers can be determined from changes in chemical shifts or line shapes of solid state NMR spectra. Moreover, the molecular mobility of a polymer blend or copolymer can be estimated from the proton spin-lattice relaxation time in the rotating frame ($T_{1\rho}^H$), measured using solid state NMR spectroscopy. Figure 3-12 presents the ¹³C CP/MAS spectra (with peak assignments) of pure PVPh, pure PDMAEMA, and various PVPh-*b*-PDMAEMA copolymers. Table 3-4 summarizes the chemical shifts observed in the ¹³C CP/MAS spectra of PVPh-*b*-PDMAEMA copolymers. The signal of the phenolic carbon atom of PVPh at 153.3 ppm underwent a gradual downfield shift upon increasing the PVPh content. A shift of ca. 3 ppm occurred for the diblock copolymer containing 84 mol% PDMAEMA, indicating that specific interactions

were indeed present between the PVPh and PDMAEMA blocks, consistent with the results of our earlier FTIR spectroscopic analyses.

Solid state NMR spectroscopy can be used to understand the phase behavior and miscibility of diblock copolymers and blends. A single value of T_g determined through DSC analysis reveals that the mixing of two blending components occurs on a scale of ca. 20–40 nm.⁴ Dimensions of mixing less than 20 nm can be obtained through measurement of the spin-lattice relaxation time in the rotating frame ($T_{1\rho}^H$).⁴ We estimated the values of $T_{1\rho}^H$ of the diblock copolymers and blend complexes through delayed-contact ¹³C CP/MAS experiments, using the equation

$$M_\tau = M_o \exp[-\tau / T_{1\rho}(H)] \quad (3-2)$$

where τ is the spin-lock time used in the experiment and M_0 and M_τ are the intensities of the peaks initially and at time τ , respectively. Figures 3-13a and 3-13b display typical plots of $\ln(M_\tau/M_0)$ vs. τ for the PDMAEMA resonance at 45 ppm and the PVPh resonance at 115 ppm of the diblock copolymer. The experimental data obtained are in good agreement with Eq. (2). We determined the value of $T_{1\rho}^H$ from the slope of the fitting line. All of the copolymers, blends, and blend complexes exhibited only a single composition-dependent value of $T_{1\rho}^H$; Table 3-5 reveals the high miscibility and dynamic homogeneity of both the PVPh and PDMAEMA phases. These results are also consistent with our earlier DSC analyses. The single values of $T_{1\rho}^H$ for the PVPh-*b*-PDMAEMA and blend complexes are lower than that for the corresponding PVPh/partially protonated PDMAEMA blend. This observation suggests that the domain size of the diblock copolymer is smaller relative to that of the corresponding polymer blend, i.e., the degree of homogeneity of the diblock copolymer is relatively higher than that of the blend. The shorter $T_{1\rho}^H$ relaxation time of the block copolymer suggests a more rigid nature of the polymer chain and a higher value of T_g . A

similar trend has been observed previously: the values of $T_{1\rho}^H$ of polymer blends of poly(acrylic acid) (PAA)/polyvinylpyrrolidone (PVP) are greater than those of blend complexes of PAA/PVP.⁵⁵ We have reported previously that the polymer chain behavior of the strongly hydrogen-bonded PVPh-*b*-P4VP diblock copolymer occurs in the form of complex aggregates, similar to the inter-polymer PVPh/P4VP complex obtained from methanol solution.⁷ Therefore, we conclude that the different behavior in the values of T_g between PVPh-*b*-PDMAEMA diblock copolymers and their corresponding blends resulted from their different chain conformations.

To confirm this behavior, we compared the FTIR spectra and ¹³C solid state NMR spectra of the PVPh-*b*-PDMAEMA copolymers with those of their corresponding blends and blend complexes. Figure 3-14 presents the FTIR spectra (OH stretching region) and ¹³C solid state NMR spectra of the blend, blend complex, and diblock copolymer having a PVPh-to-PDMAEMA ratio of 55:45. We observe that the signal of the phenolic carbon atom (C-6) at 153 ppm for both the diblock copolymer and blend complex shifted downfield by the same amount. Moreover, the OH stretching signal for the specific interaction was also shifted by the same amount in the FTIR spectra of the blend, blend complex, and block copolymer, indicating that the specific interaction had identical strength in all systems. We observed, however, that the relative intensity ratio of the OH···OH (3350 cm⁻¹) and OH···tertiary ammonium (3220 cm⁻¹) hydrogen bonded signals was greater for the copolymer. As a result, we speculate that intra-chain contacts play an important role in the block copolymer system. On the basis of our DSC, solid state NMR spectroscopic, and FTIR spectroscopic analyses, we deduce that the polymer chain behavior of the PVPh-*b*-PDMAEMA copolymers occurs through strong specific interactions in the form of a complex, similar to that in the inter-polymer complex formed from PVPh and the partially protonated PDMAEMA obtained from methanol solution. The polymer chains of a miscible polymer blend are well separated in

a highly polar solvent (e.g., DMF or DMSO) prior to solvent evaporation when, for example, the inter-association hydrogen bonding between PVPh/DMSO is stronger than that in the PVPh/partial protonated PDMAEMA blend. Nevertheless, copolymer complex aggregation can occur because of the higher strength of intra-chain interactions in diblock copolymer chains. Two possible mechanisms may be involved in the formation of inter-polymer complexes: (i) two individual diblock copolymer chains interact through inter-chain hydrogen bonding or (ii) an intra-polymer complex forms through folding of the same diblock copolymer chain through intra-chain hydrogen bonding. For a polymer blend, the inter-chain interaction is the only route available to form a complex. This result is consistent with our FTIR spectral observation that the relative intensities of the signals for the OH \cdots OH, OH \cdots O=C, OH \cdots N, and OH \cdots tertiary ammonium interactions in the blend complex system were low, indicating that most interactions resulted from inter-chain contact. As a result, both the inter- and intra-polymer complexes in the diblock copolymer have smaller domain sizes than the relatively more separated coils in the miscible blend, consistent with the values of $T_{1\rho}^H$. Again, we employed 2D-IR correlation spectroscopy to confirm the existence of intra-chain interactions for PVPh-*b*-PDMAEMA. Figure 3-15a presents the synchronous 2D correlation maps in the range from 2700 to 3800 cm $^{-1}$. Clearly, positive cross-peaks exist in this range from 3200 to 3500 cm $^{-1}$, corresponding to the OH stretching signals of the PVPh block, implying that the hydrogen bonding interactions did indeed occur between the OH groups. In contrast, the corresponding asynchronous 2D correlation map for PVPh-*b*-PDMAEMA [Figure 3-15b] does not reveal any auto or cross peaks within the same wavenumber range, implying that the OH groups of the PVPh block undergo intramolecular hydrogen bonding interactions.

3-3.6 pH-Induced Micellization of PVPh-*block*-PDMAEMA Copolymers

PDMAEMA is a weak polybase that is soluble in neutral and acidic media because of its protonated tertiary amino groups; PVPh is soluble in basic media as a result of the ionization of its OH groups. Therefore, we anticipated that the PVPh-*b*-PDMAEMA diblock copolymer might display pH-reversible micellization behavior, forming micelles with hydrophobic PVPh cores and hydrophilic PDMAEMA shells at low pH and hydrophilic PDMAEMA cores and hydrophobic PVPh shells at high pH. To confirm the pH-sensitive behavior of the PVPh-*b*-PDMAEMA diblock copolymer, we analyzed NMR spectra and TEM images of PVPh₃₂-*b*-PDMAEMA₆₈ at various values of pH.

Figure 3-16 displays the ¹H NMR spectra of PVPh₃₂-*b*-PDMAEMA₆₈ in D₂O under acidic (pH 2), neutral (pH 7), and basic (pH 13) conditions, with reference to the spectrum of the copolymer in DMSO-*d*₆ as a standard. The signals due to the aromatic protons of PVPh at 6.1–6.9 ppm disappeared at both neutral and acidic pH, while the signals due to the ethyl protons of PDMAEMA at 4.2–4.4 ppm remained prominent. In contrast, the signal due to the aromatic protons of PVPh at 6.1–6.9 ppm was present at pH 13, whereas the signal due to the ethyl protons of PDMAEMA at 4.2–4.4 ppm was suppressed and broadened, indicating the lower mobility and decreasing solvation of these blocks. These NMR spectral data revealed subtle variations in the hydrophilic/hydrophobic balance of the diblock copolymer, providing a unique opportunity to prepare either PVPh-core micelles or PDMAEMA-core micelles from the same copolymer merely by changing the pH of the solution; i.e., pH-induced micellar self-assembly of PVPh-*b*-PDMAEA.

Figure 3-17 displays TEM images of the morphologies formed from PVPh₃₂-*b*-PDMAEMA₆₈ at various values of pH. Nano-spherical micelles of PVPh₃₂-*b*-PDMAEMA₆₈ formed at pH 2 (Figure 3-17a). To our surprise, these spherical micelles transformed into vesicles when we increased the pH to 7 (Figure 3-17b). Meanwhile, we have been carried out the dynamic light scattering and static light scattering measurements

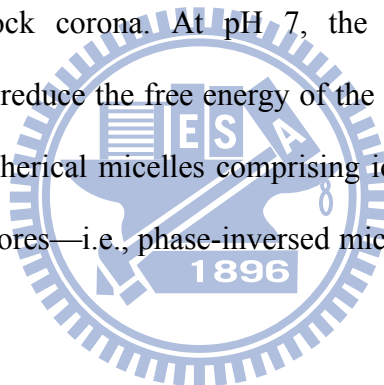
for confirming the structure of the PVPh₃₂-*b*-PDMAEMA₆₈ block copolymer in aqueous media at pH 7. The ratio R_g/R_h provides an indication of the shape of the scattering particle, for example, the ratio of hard sphere is 0.775, the ratio of random coil is near 1.5, and the ratio of vesicle is approximately 1.⁵⁹ Figure 3-18 presents the static light scattering and dynamic light scattering analyses of the PVPh₃₂-*b*-PDMAEMA₆₈ block copolymer in aqueous media at pH 7. The values of R_g and R_h which are 186.46 nm and 175.25 nm, respectively, can be obtained from the DLS and SLS analyses of the PVPh₃₂-*b*-PDMAEMA₆₈ block copolymer in aqueous media at pH 7. Therefore, the ratio R_g/R_h which is 1.06 can be obtained. Base on the value of R_g/R_h which is approximated 1, we can further confirm that the structure of the aggregates of the PVPh₃₂-*b*-PDMAEMA₆₈ block copolymer in aqueous media at pH 7 is vesicle. When we increased the pH further (to pH 13), these aggregates return to the form of nano-spherical micelles (Figure 3-17c). Several factors influence the morphologies of block copolymer aggregates in a solution;^{56,57} the free energies of aggregation are affected by the inter-coronal chain interaction, the core-coronal interfacial energy, and the degree of core-chain stretching. At pH 2, the spherical micelles formed as result of the hydrophobic interactions of the uncharged PVPh blocks in water. Only small fraction of the protonated PDAMEAM interacted with the OH groups of PVPh, while the remaining protonated PDMAEMA units formed the corona of the micelle, thereby stabilizing its structure. Thus, at low pH, we suspect that each spherical micelle comprised (i) a core of hydrophobic PVPh blocks and some PVPh/protonated PDMAEMA complexes and (ii) a cationic PDMAEMA corona. Upon increasing the pH to 7, the PDMAEMA blocks began to lose some of their cationic character as a result of deprotonation of the ammonium units, resulting in a decrease in the strength of the electrostatic repulsive interactions among the corona chains. Consequently, the size of the aggregates increased to reduce the interfacial energy between the core and the solvent. The degree of stretching of the PVPh chains increased because the interactions between the PVPh and PDMAEMA segments became weaker, indicating that the

entropic penalty increased. To reduce the total free energy in the system, the aggregates transformed their morphology from spherical micelles to vesicles.⁵⁸ At pH 13, the tertiary amino groups of PDMAEMA were almost completely deprotonated and, thus, these blocks became particularly hydrophobic;³² in contrast, the PVPh blocks were completely ionized in their anionic form. Nevertheless, a few signals at 4.2–4.4 ppm due to the ethyl protons of PDMAEMA were still evident in the NMR spectrum, indicating that the PDMAEMA blocks remained partially solvated, i.e., the micellar core retained some degree of hydration; similar observations have been reported by Lowe et al. for the micellization of PDMAEMA-*b*-PMAA diblock copolymers.³¹ Therefore, at high pH, the spherical micelles comprised PDMAEMA hydrated cores and PVPh anionic coronas.

Figure 3-19 displays our proposed microstructures for the PVPh₃₂-*b*-PDMAEMA₆₈ diblock copolymer at various values of pH. At pH 2, compact spherical micelles formed from the hydrophobic association of the PVPh segments and a few PVPh/protonated PDMAEMA complexes, driven by entropic considerations—i.e., a gain in entropy occurred when water molecules were released from the disrupted solvent cage surrounding the hydrophobic PVPh segments. At pH 7, the electrostatic repulsive forces among protonated PDMAEMA segments weakened and the stretching of PVPh segments increased. As a result, the morphology of the diblock copolymer transformed from spherical micelles to vesicles to reduce the free energy of the system. At pH 13, the aggregates change shape from vesicles to spherical micelles comprising ionized PVPh-coronas and deprotonated PDMAEMA-hydrated cores—i.e., a phase inversion of the structure of the micelles formed at pH 2.

3-4 Conclusions

We have synthesized novel pH-sensitive PVPh-*b*-PDMAEMA diblock copolymers through anionic polymerization. FTIR and solid state NMR spectroscopic analyses provided evidence for strong interactions existing between the OH groups of PVPh and the tertiary ammonium groups of PDMAEMA. From DSC analyses, we observed that the glass transition temperatures of the diblock copolymers increased significantly as a result of strong interactions between the OH groups of PVPh and the tertiary ammonium groups of PDMAEMA. ¹H NMR spectroscopic and TEM analyses revealed the pH-sensitive self-assembly behavior of PVPh-*b*-PDMAEMA diblock copolymer in aqueous media. At pH 2, spherical micelles formed comprising a neutral PVPh block surrounded by a protonated-PDMAEMA block corona. At pH 7, the diblock copolymer's morphology transformed into vesicles to reduce the free energy of the system. At pH 13, these aggregates changed from vesicles to spherical micelles comprising ionized-PVPh coronas and hydrated deprotonated-PDMAEMA cores—i.e., phase-inversed micelles relative to those formed at pH 2.



References

- [1] Utracki, L. A. *Polymer Alloys and Blends: Thermodynamics and Rheology*, Carl Hanser Verlag: Munich, **1989**.
- [2] Coleman, M. M.; Graf, J. F.; Painter, P. C. “*Specific Interactions and the Miscibility of Polymer Blends. Technomic Publishing*”, Lancaster, PA, **1991**.
- [3] Coleman, M. M.; Painter, P. C. *Prog. Polym. Sci.* **1995**, *20*, 1.
- [4] Kuo, S. W.; Chang, F. C. *Macromolecules*, **2001**, *34*, 4089.
- [5] Kuo, S. W.; Chang, F. C. *Macromolecules*, **2001**, *34*, 5224.
- [6] He, Y.; Zhu, B.; Inoue, Y. *Prog. Polym. Sci.* **2004**, *29*, 1021.
- [7] Serman, C. J.; Painter, P. C.; Coleman, M. M., *Polymer* **1991**, *32*, 1049.
- [8] Zhang, X.; Takegoshi, K.; Hikichi, K., *Macromolecules* **1991**, *24*, 5756.
- [9] Li, D.; Brisson, J., *Macromolecules* **1996**, *29*, 868.
- [10] Dong, J.; Ozaki, Y., *Macromolecules* **1997**, *30*, 286.
- [11] Kuo, S. W.; Liu, W. P.; Chang, F. C. *Macromolecules* **2003**, *36*, 5165.
- [12] Kuo, S. W.; Liu, W. P.; Chang, F. C. *Macromol. Chem. Phys.* **2005**, *206*, 2307.
- [13] Huang, X. D.; Goh, S. H.; Lee, S. Y.; Zhao, Z. D.; Wong, M. W.; Huan, C. H. A. *Macromolecules* **1999**, *32*, 4327.
- [14] Kuo, S. W.; Tung, P. H.; Lai, C. L.; Jeong, K. U.; Chang, F. C. *Macromol. Rapid Commun.* **2008**, *29*, 229.
- [15] Wang, L. F.; Pearce, E. M.; Kwei, T. K. *J. Polym. Sci., Polym. Phys. Ed.* **1991**, *29*, 619.
- [16] Dai, J.; Goh, S. H.; Lee, S. Y.; Siow, K. S. *Polym. J.* **1994**, *26*, 905.
- [17] Luo, X. F.; Goh, S. H.; Lee, S. Y. *Macromolecules* **1997**, *30*, 4934.
- [18] Liu, Y.; Goh, S. H.; Lee, S. Y.; Huan, C. H. A. *Macromolecules* **1999**, *32*, 1967.
- [19] Zhong, Z.; Guo, Q. *Polym. Int.* **1996**, *41*, 315.
- [20] Kuo, S. W.; Tung, P. H.; Chang, F. C. *Macromolecules* **2006**, *39*, 9388
- [21] Butun, V.; Billingham, N. C.; Armes, S. P. *J. Am. Chem. Soc.* **1998**, *120*, 11818

- [22] Butun, V.; Billingham, N. C.; Armes, S. P.; et al. *Macromolecules* **2001**, *34*, 1503
- [23] Liu, S. Y.; Billingham, N. C.; Armes, S. P. *Angew. Chem. Int. Ed.* **2001**, *40*, 2328
- [24] Bories-Azeau, X.; Armes S. P.; Van den Haak, H. J. W. *Macromolecules* **2004**, *37*, 2348.
- [25] Liu, S.; Armes, S. P. *Langmuir* **2003**, *19*, 4432.
- [26] Mountrichas, G.; Pispas, S. *Macromolecules* **2006**, *39*, 4767.
- [27] Butun, V.; Billingham, N. C.; Armes, S. P. *J. Am. Chem. Soc.* **1998**, *120*, 12135
- [28] Dou, H. J.; Jiang, M. *Angew. Chem. Int. Ed.* **2003**, *42*, 1516.
- [29] Butun, V.; Top, R. B.; Ufuklar, S. *Macromolecules* **2006**, *39*, 1216.
- [30] Wan, S.; Jiang, M.; Zhang, G. *Macromolecules* **2007**, *40*, 5552.
- [31] Lowe, A. B., Billingham, N. C.; Armes, S. P. *Macromolecules* **1998**, *31*, 5991.
- [32] Gohy, J. F.; Creutz, S.; Garcia, M.; Mahltig, B.; Stamm, M.; Jerome, R. *Macromolecules* **2001**, *33*, 6378.
- [33] Varshney, S. K.; Zhong, X. F.; Eisenberg, A. *Macromolecules* **1993**, *26*, 701.
- [34] Quirk, R. P.; Corona-Galvan, S. *Macromolecules* **2001**, *34*, 1192.
- [35] Biggs, S.; Vincent, B. *Colloid Polym. Sci.* **1992**, *270*, 505.
- [36] Hubert, P.; Soum, A.; Fontanille, M. *Macromol. Chem. Phys.* **1995**, *196*, 1023.
- [37] Quirk, R. P.; Lee, Y. *J. Polym. Sci., Part A: Polym. Chem.* **2000**, *38*, 145.
- [38] Jiang, X.; Tanaka, K.; Takahara, A.; Kajiyama, T. *Polymer* **1998**, *39*, 2615.
- [39] Pullman, A.; Berthier, G.; Savinelli, R. *J. Am. Chem. Soc.* **1998**, *120*, 8553.
- [40] Moskala, E. J.; Varnell, D. F.; Coleman, M. M. *Polymer* **1985**, *26*, 228.
- [41] Moritani, T.; Fujiwara, Y. *Macromolecules* **1977**, *10*, 532.
- [42] Lin, C. L.; Chen, W. C.; Liao, C. S.; Su, Y. C.; Huang, C. F.; Kuo, S. W.; Chang, F. C. *Macromolecules* **2005**, *38*, 6435.
- [43] Painter, P. C.; Veytsman, B.; Kumar, S.; Shenoy, S.; Graf, J. F.; Xu, Y.; Coleman, M. M. *Macromolecules* **1997**, *30*, 932.
- [44] Coleman, M. M.; Pehlert, G. J.; Painter, P. C. *Macromolecules* **1996**, *29*, 6820.

- [45] Pehlert, G. J.; Painter, P. C.; Veytsman, B.; Coleman, M. M. *Macromolecules* **1997**, *30*, 3671.
- [46] Pehlert, G. J.; Painter, P. C.; Coleman, M. M. *Macromolecules* **1998**, *31*, 8423.
- [47] Coleman, M. M.; Guigley, K. S.; Painter, P. C. *Macromol. Chem. Phys.* **1999**, *200*, 1167.
- [48] Noda, I. *Appl. Spectrosc.* **1993**, *47*, 1329.
- [49] Noda, I. *Appl. Spectrosc.* **2000**, *54*, 994.
- [50] Noda, I.; Story, G. M.; Marcott, C. *Vibr. Spectrosc.* **1999**, *19*, 461.
- [51] Kwei, T. K. *J. Polym. Sci., Polym. Lett. Ed.* **1984**, *22*, 307.
- [52] Kuo, S. W.; Huang, C. F.; Tung, P. H.; Huang, W. J.; Huang, J. M.; Chang, F. C. *Polymer* **2005**, *46*, 9348.
- [53] Jiang, M.; Li, M.; Xiang, M.; Zhou, H. *Adv. Polym. Sci.* **1999**, *146*, 121.
- [54] Wang, M.; Jiang, M.; Ning, F. L.; Chen, D. Y.; Liu, S. Y.; Duan, H. W. *Macromolecules* **2002**, *35*, 5980.
- [55] Lau, C.; Mi, Y. *Polymer* **2002**, *43*, 823.
- [56] Zhang, L.; Eisenberg, A. *Polym. Adv. Technol.* **1998**, *9*, 677.
- [57] Zhang, L.; Eisenberg, A. *J. Am. Chem. Soc.* **1996**, *118*, 3168.
- [58] Zhang, L.; Eisenberg, A. *Macromolecules* **1996**, *29*, 8805.
- [59] Anders, H.; Mats, J.; Eva, M. *Adv. Polym. Sci.*, **1999**, *143*, 113.

Table 3-1. Molecular Characterization of Poly[vinylphenol-*b*-2-(dimethylamino)ethyl methacrylate] Diblock Copolymers Prepared Using Anionic Polymerization

precursor copolymer	copolymer	$M_{n,PtBOS}^a$	Total M_n^a	PVPh (mol %) ^b	M_w/M_n^a	T_g (°C)
PtBOS	PVPh	14600	10000	100	1.05	172
PtBOS ₁₆ - <i>b</i> -PDMAEM ₈₄	PVPh ₁₆ - <i>b</i> -PDMAEMA ₈₄	2900	17300	14	1.11	113
PtBOS ₃₂ - <i>b</i> -PDMAEM ₆₈	PVPh ₃₂ - <i>b</i> -PDMAEMA ₆₈	5280	13650	32	1.11	136
PtBOS ₅₅ - <i>b</i> -PDMAEM ₄₅	PVPh ₅₅ - <i>b</i> -PDMAEMA ₄₅	11100	15400	55	1.15	184
PtBOS ₇₀ - <i>b</i> -PDMAEM ₃₀	PVPh ₇₀ - <i>b</i> -PDMAEMA ₃₀	16100	16300	70	1.10	177
	PDMAEMA	-	14130	0	1.10	14

^a Polydispersity index and molecular weight, measured by GPC, of the whole diblock copolymer in the form of PtBOS-*b*-P4VP.

^b Obtained from ¹H NMR measurement.

Table 3-2. Fraction of Hydrogen Bonding Groups of PVPh-*b*-PDMAEMA:

Block Copolymer	H-bonded C=O			Free C=O			f _b (%)
	ν , cm ⁻¹	W _{1/2}	A _f %	ν , cm ⁻¹	W _{1/2}	A _b %	
PVPh ₁₄ - <i>b</i> - PDMAEMA ₈₆	1712	27	17	1731	25	83	12
PVPh ₃₂ - <i>b</i> - PDMAEMA ₆₈	1712	28	22	1730	24	78	16
PVPh ₅₅ - <i>b</i> - PDMAEMA ₄₅	1711	28	30	1731	25	70	22
PVPh ₇₀ - <i>b</i> - PDMAEMA ₃₀	1711	28	40	1731	25	60	31

Polymer Blend	H-bonded C=O			Free C=O			f _b (%)
	ν , cm ⁻¹	W _{1/2}	A _f %	ν , cm ⁻¹	W _{1/2}	A _b %	
PVPh ₁₄ /PDMAEMA ₈₆	1708	28	16	1730	28	84	12
PVPh ₃₂ /PDMAEMA ₆₈	1709	28	19	1730	28	81	14
PVPh ₅₅ /PDMAEMA ₄₅	1709	28	25	1731	27	75	18
PVPh ₇₀ /PDMAEMA ₃₀	1708	28	30	1730	28	70	22

Table 3-3. Values of T_g Obtained From PVPh/Partially Protonated PDMAEMA Blends and PVPh/Partially Protonated PDMAEMA Blend Complex Systems

	T_g (°C)
PVPh/partial protonated PDMAEMA	
16/84	77
32/68	128
55/45	156
70/30	164
PVPh/partial protonated PDMAEMA complex	
55/45	179

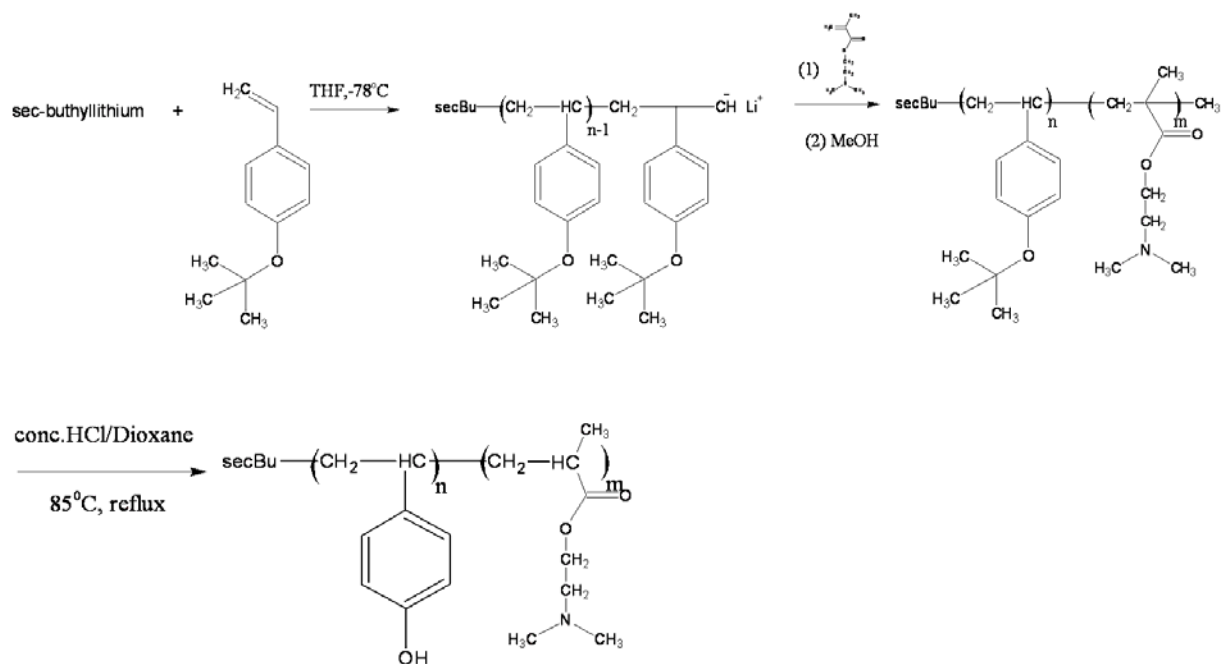
Table 3-4. Relaxation Times, $T_{1\rho}^H$, for Blends, Blend Complexes, and Diblock Copolymers

at Magnetization Intensities of 45 and 115 ppm

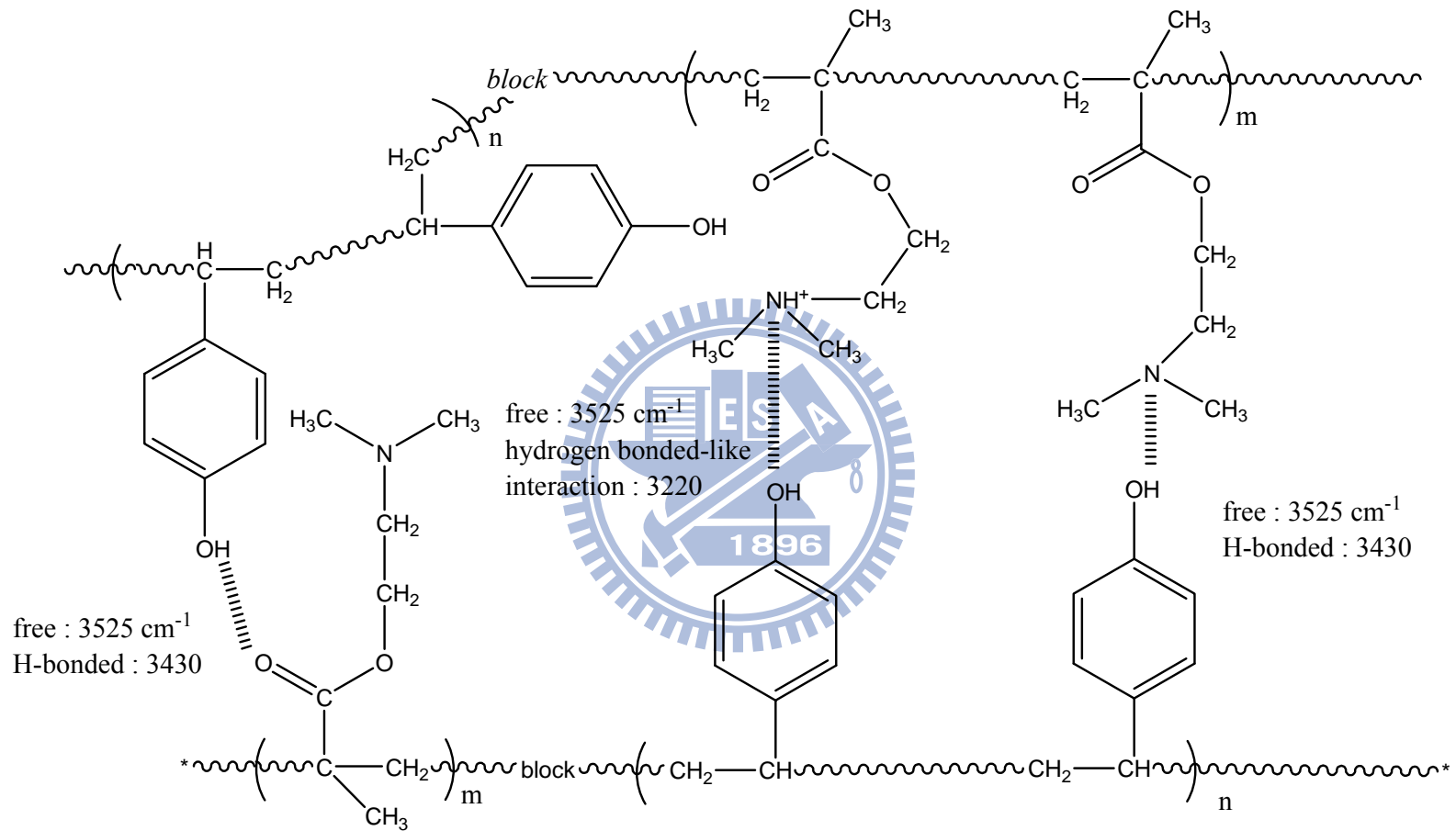
45 ppm		115 ppm	
Sample	$T_{1\rho}^H$ (ms)	Sample	$T_{1\rho}^H$ (ms)
Pure PDMAEMA	5.82	Pure PDMAEMA	
14- <i>b</i> -86	3.17	14- <i>b</i> -86	2.89
32- <i>b</i> -68	2.85	32- <i>b</i> -68	3.26
55- <i>b</i> -45	4.19	55- <i>b</i> -45	3.69
70- <i>b</i> -30	4.04	70- <i>b</i> -30	3.77
55/45 complex	5.3	55/45 complex	5.6
55/45 blend	5.6	55/45 blend	6.52
Pure PVPh		Pure PVPh	6.78



Scheme 3-1. Synthesis of Poly[vinylphenol-*b*-2-(dimethylamino)ethyl methacrylate] Diblock Copolymers Using Anionic Polymerization



Scheme 3-2. Schematic Representation of the Types of Interactions that Exist Between PVPh-*b*-PDMAEMA Diblock Copolymer Units



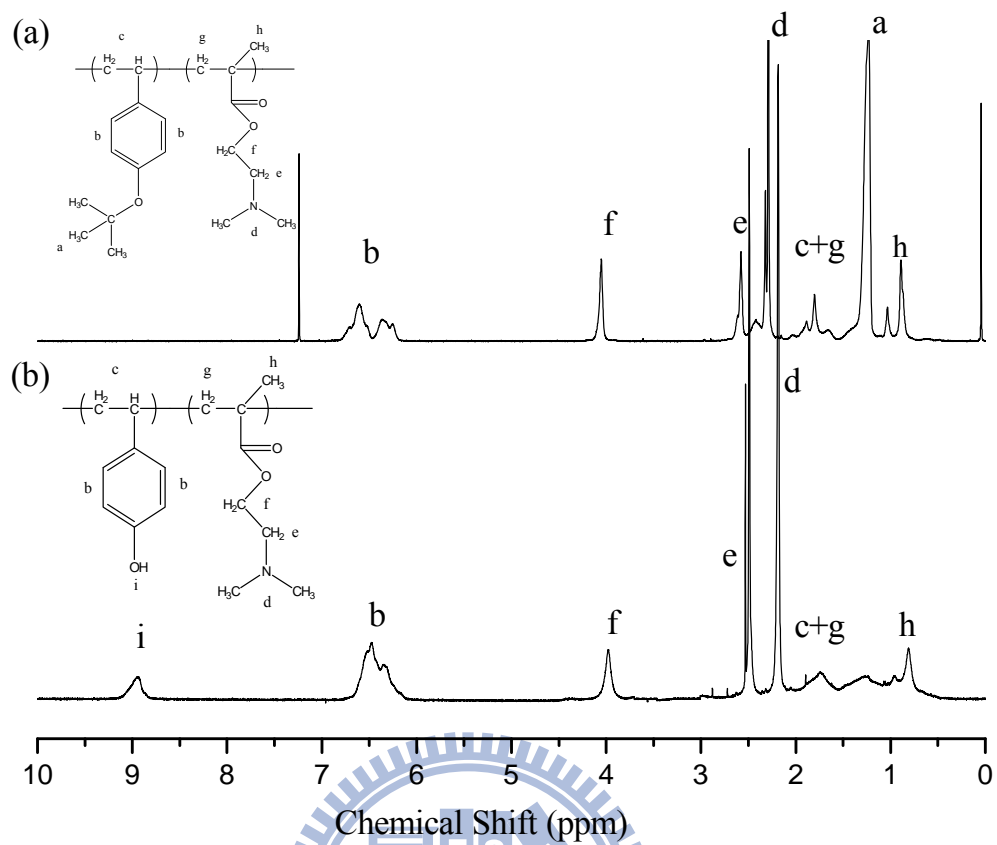


Figure 3-1. ^1H NMR spectra: (a) before hydrolysis, PtBOS-*b*-PDMAEMA; (b) after hydrolysis, PVPh-*b*-PDMAEMA.

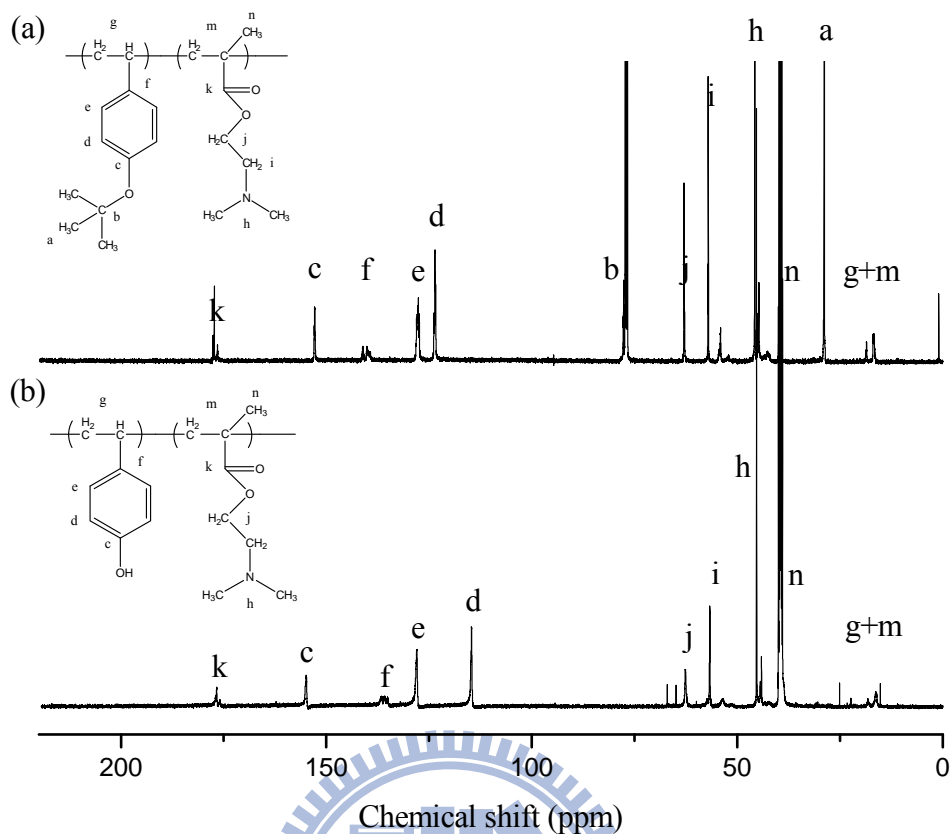


Figure 3-2. ^{13}C NMR spectra: (a) before hydrolysis, PtBOS-*b*-PDMAEMA; (b) after hydrolysis, PVPh-*b*-PDMAEMA.

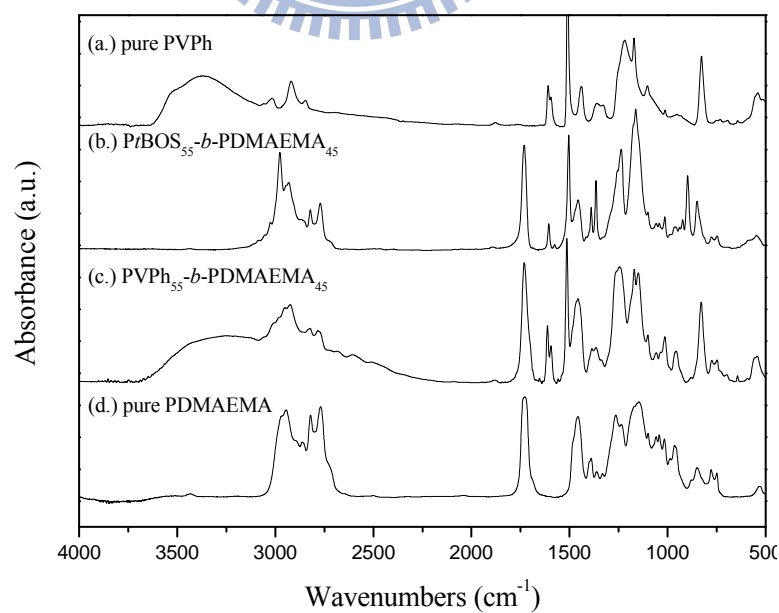


Figure 3-3. FTIR spectra (room temperature, 400–4000 cm^{-1}) of (a) pure PVPh, (b) PtBOS-*b*-PDMAEMA, (c) PVPh-*b*-PDMAEMA, and (d) pure PDMAEMA

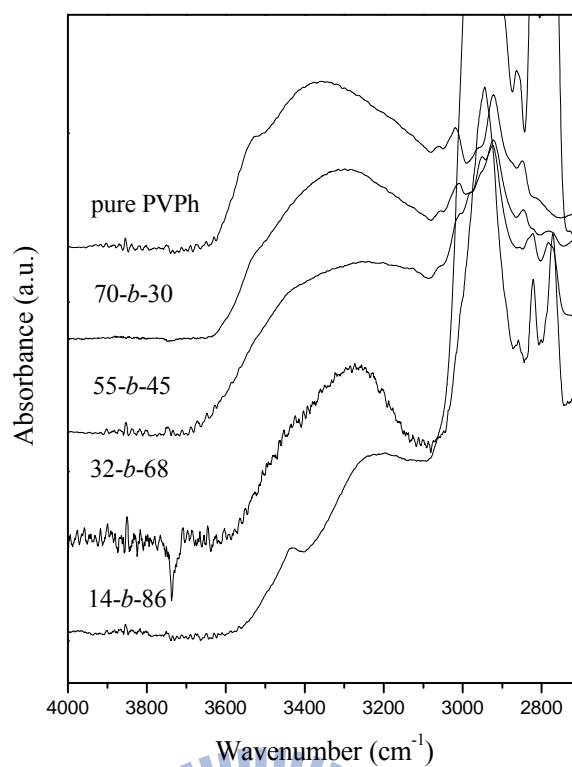


Figure 3-4. FTIR spectra (room temperature, OH stretching region) of PVPh-*b*-PDMAEMA diblock copolymers cast from DMSO solutions.

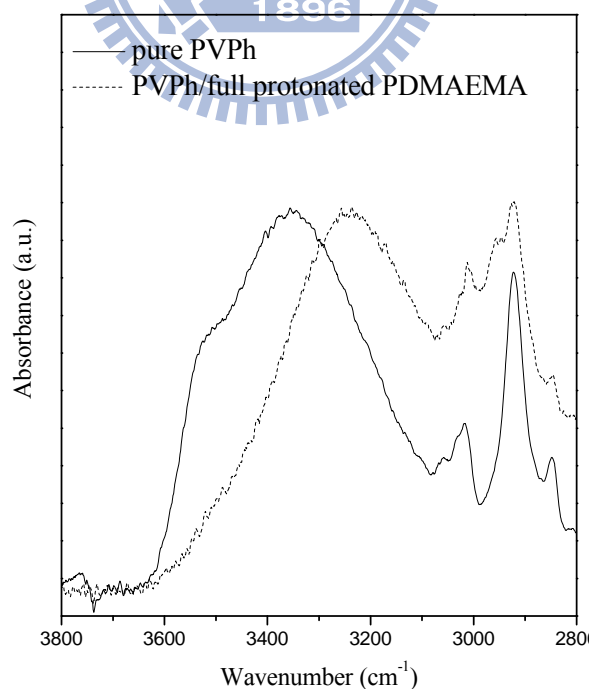


Figure 3-5. FTIR spectra (room temperature, OH stretching region) of a PVPh/fully protonated PDMAEMA blend cast from DMSO solution.

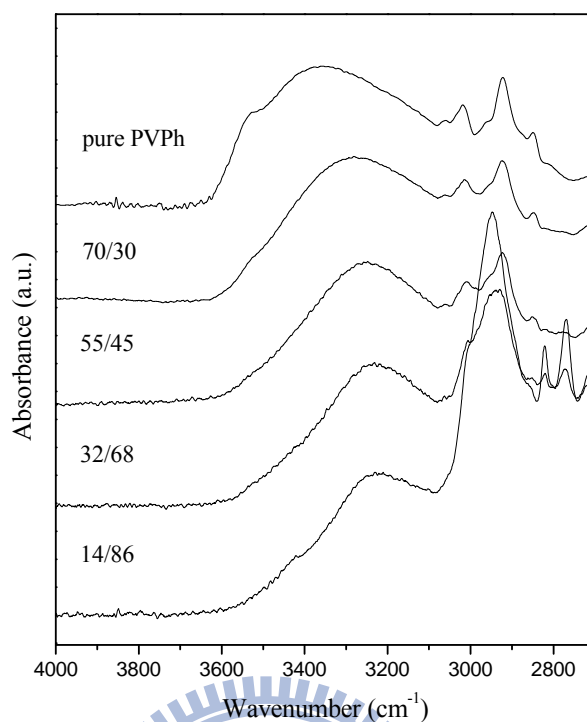


Figure 3-6. FTIR spectra (room temperature, OH stretching region) of PVPh/partially protonated PDMAEMA blends cast from DMSO solutions

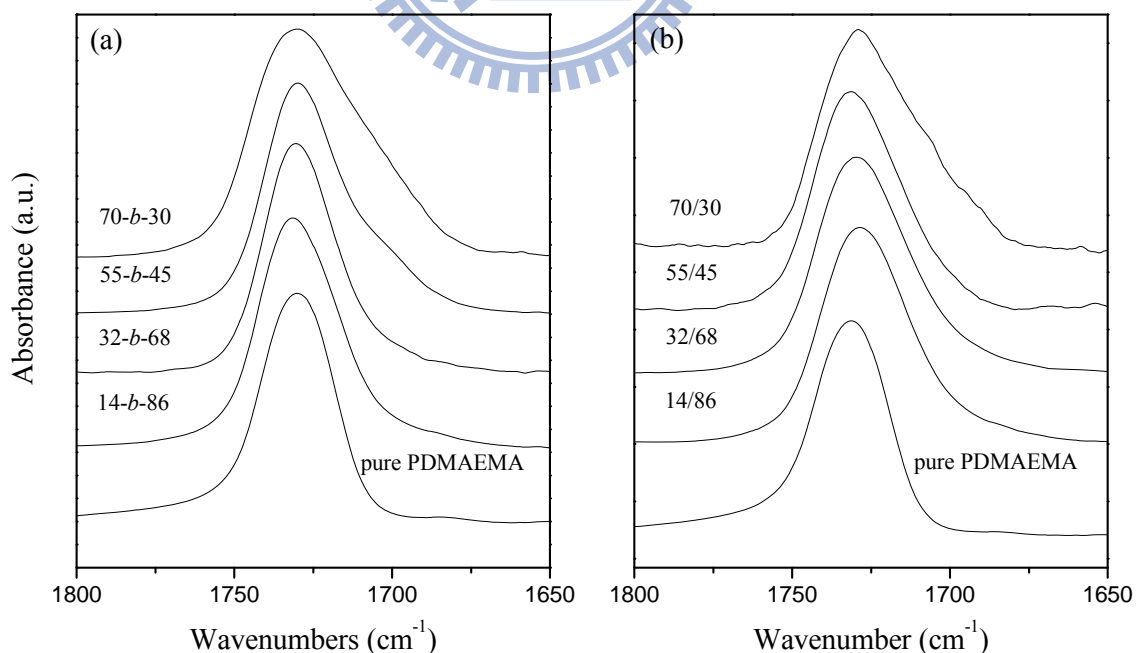


Figure 3-7. FTIR spectra of (a) PVPh-*b*-PDMAEMA diblock copolymers and (b) PVPh/partially protonated PDMAEMA blends cast from DMSO solutions.

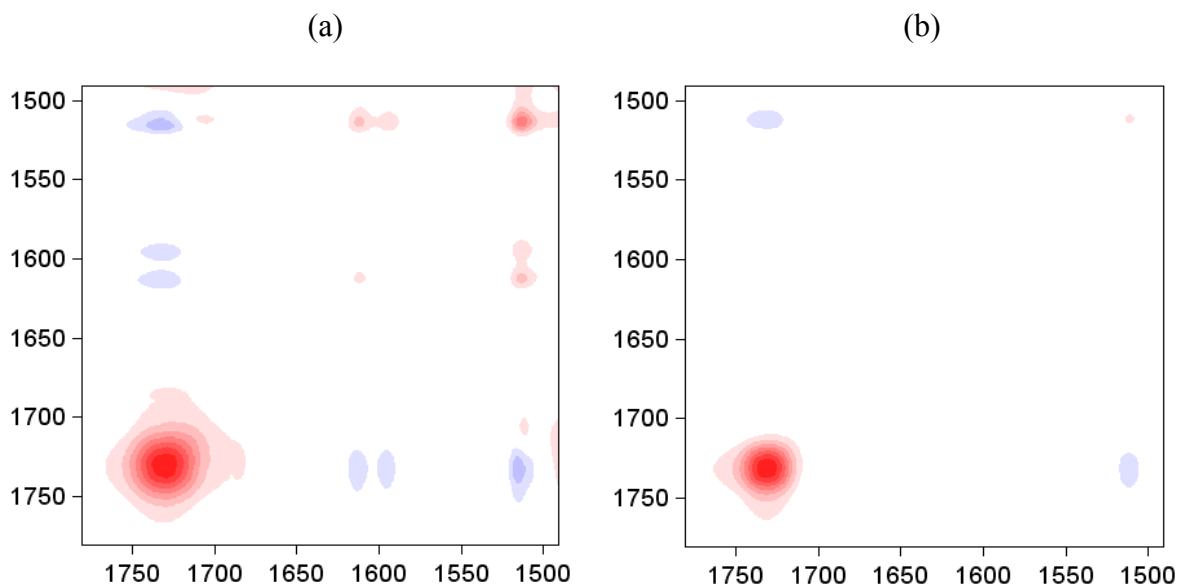


Figure 3-8. Synchronous 2D correlation map ($1490\text{--}1780\text{ cm}^{-1}$) for (a) PVPh-*b*-PDMAEMA diblock copolymers and (b) PVPh/partially protonated PDMAEMA blends.

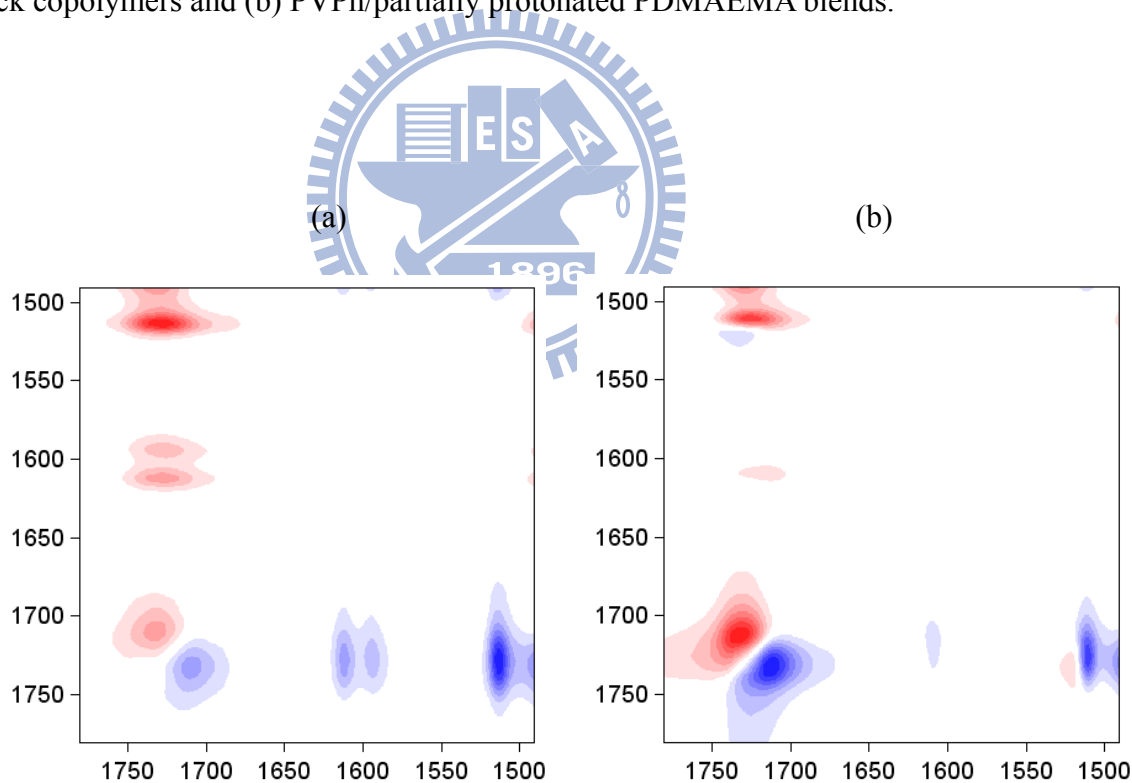


Figure 3-9. Asynchronous 2D correlation map ($1490\text{--}1780\text{ cm}^{-1}$) for (a) PVPh-*b*-PDMAEMA diblock copolymers and (b) PVPh/partially protonated PDMAEMA blends.

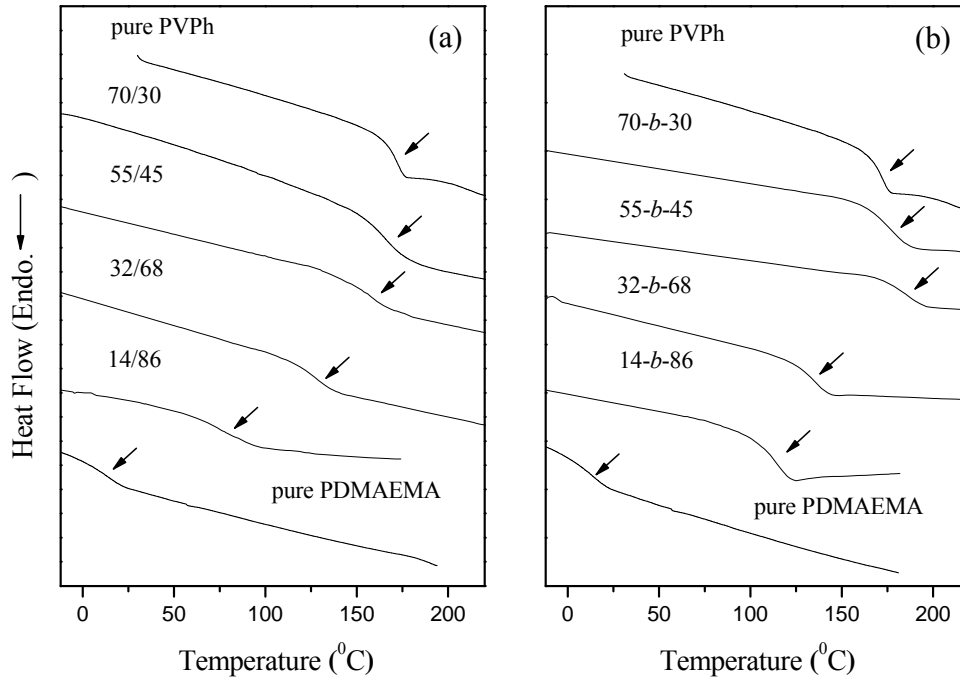


Figure 3-10. DSC curves of (a) PVPh/partially protonated PDMAEMA blends and (b) PVPh-*b*-PDMAEMA diblock copolymers.

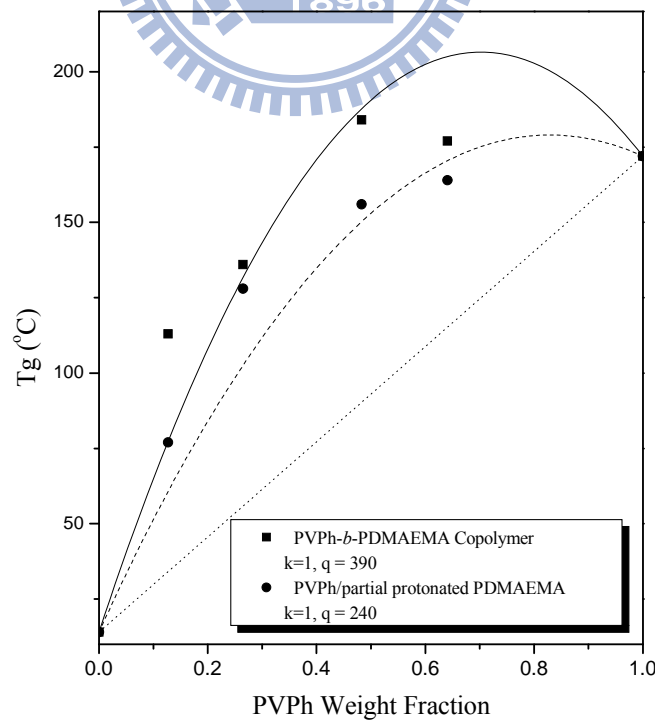


Figure 3-11. Plots of T_g with respect to composition, based on the Kwei equation, for blends and diblock copolymers.

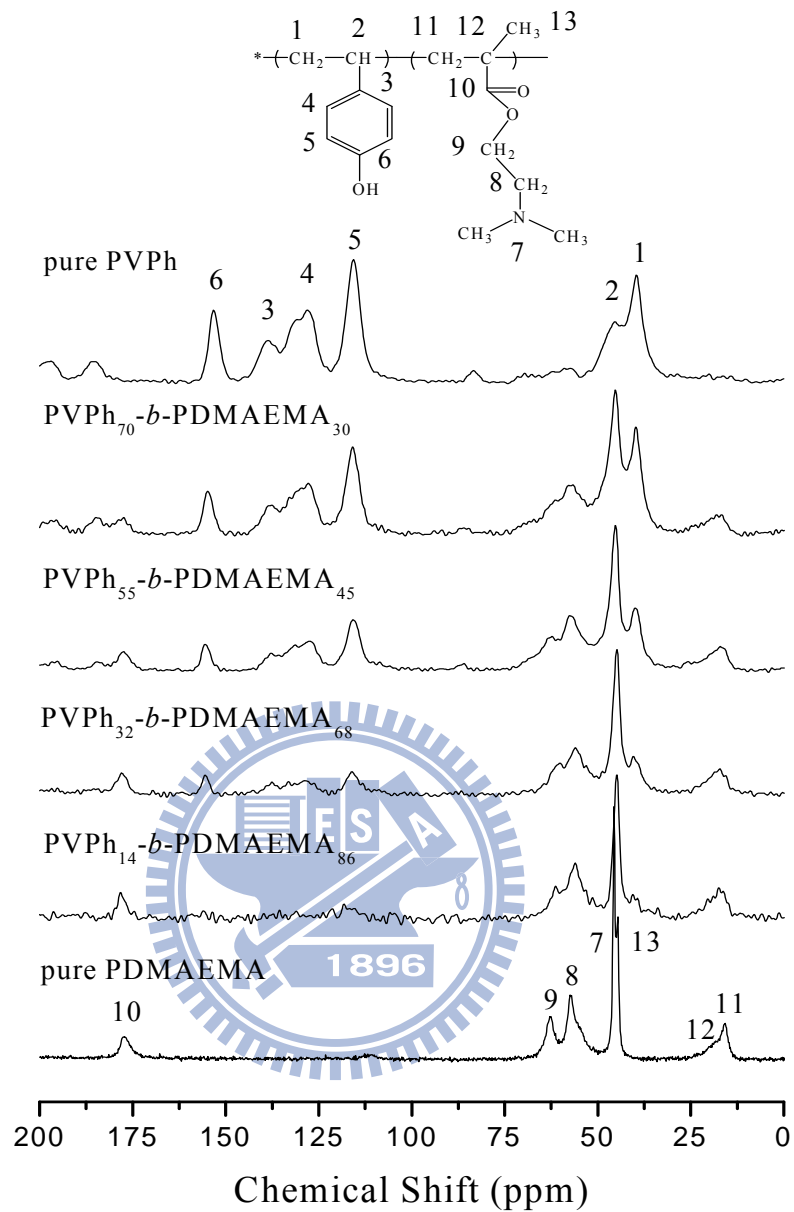


Figure 3-12. ^{13}C CP/MAS NMR spectra of PVPh-*b*-PDMAEMA diblock copolymers containing various PVPh compositions.

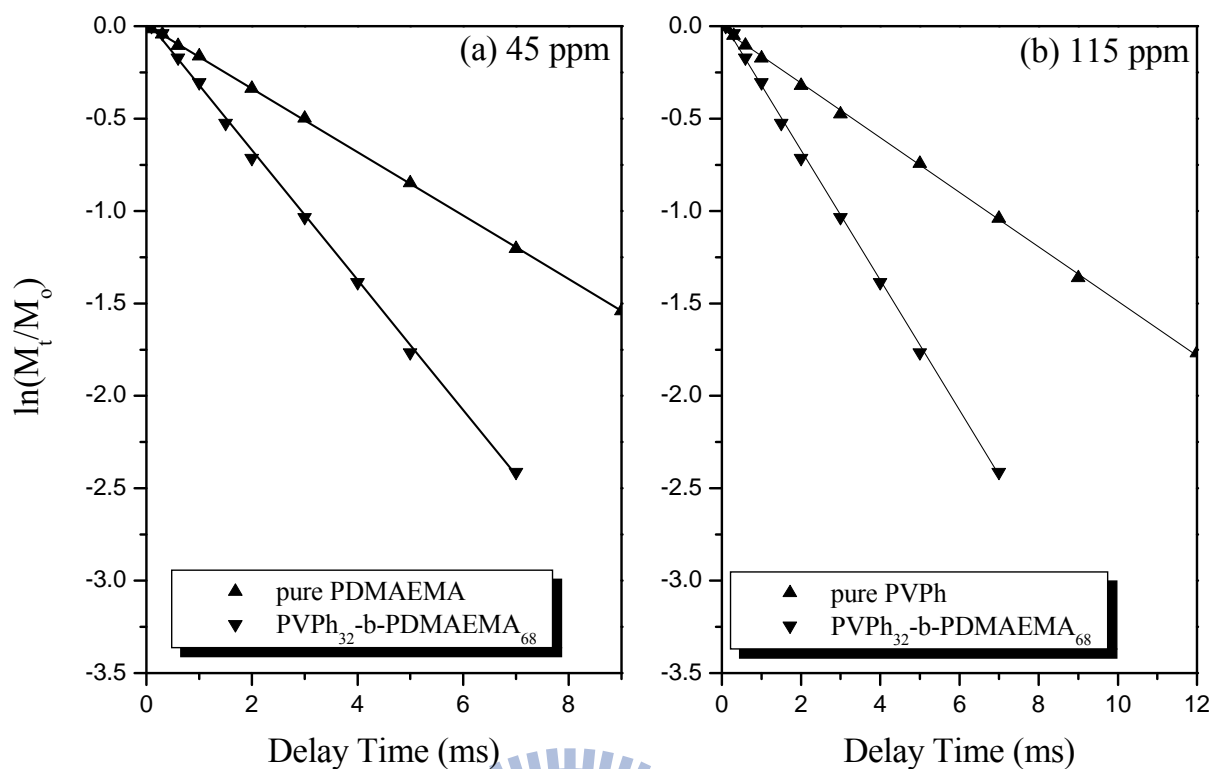


Figure 3-13. Logarithmic plots of the intensities of the signals at (a) 45 and (b) 115 ppm with respect to the delay time from the ^{13}C CP/MAS NMR spectra of PVPh-*b*-PDMAEMA diblock copolymers.

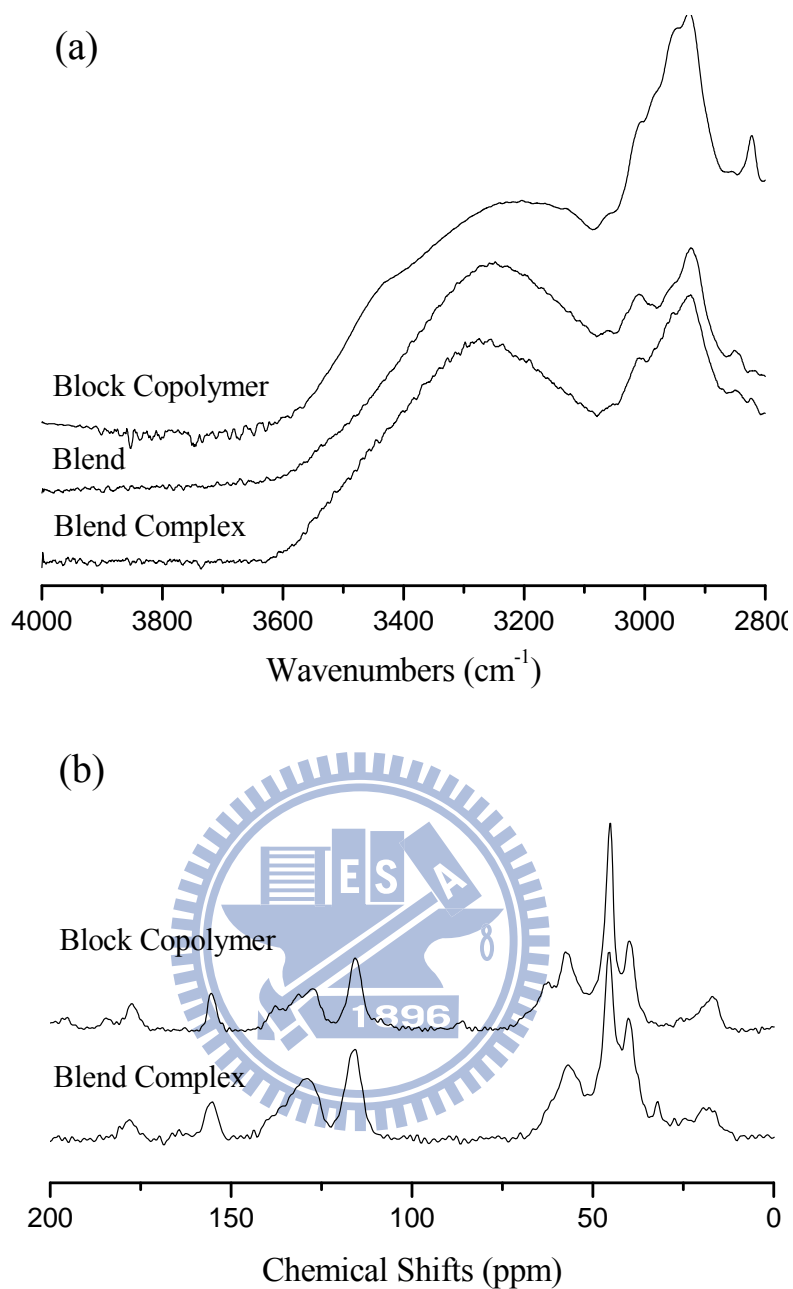


Figure 3-14. (a) FTIR and (b) ¹³C solid state NMR spectra of the diblock copolymer, blend complex, and blend having a PVPh:PDMAEMA ratio of 55:45.

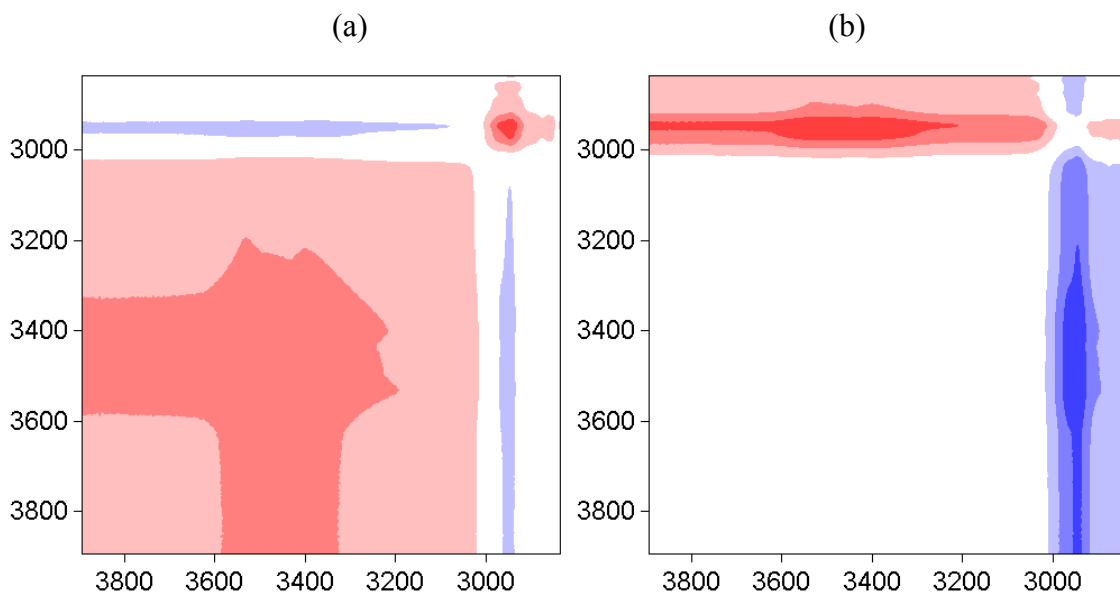
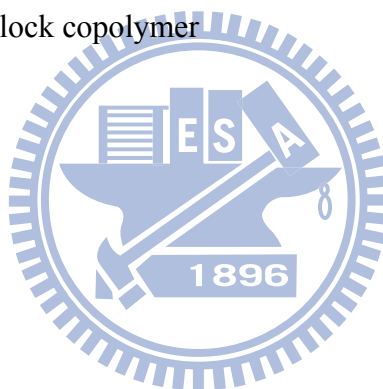


Figure 3-15. (a) Synchronous and (b) asynchronous 2D correlation maps ($2700\text{--}3800\text{ cm}^{-1}$) for PVPh-*b*-PDMAEMA diblock copolymer



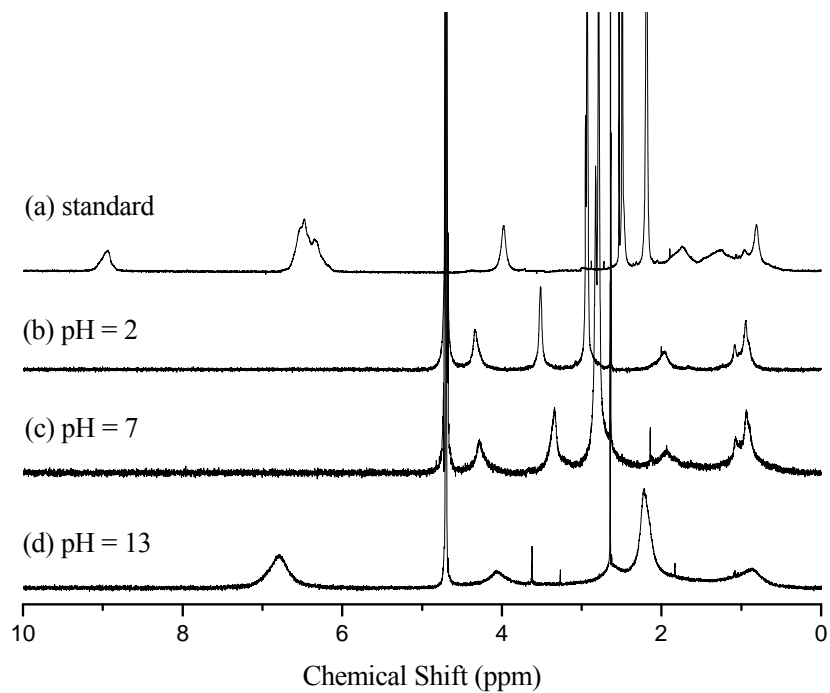


Figure 3-16. ^1H NMR spectra of the $\text{PVPh}_{32}\text{-}b\text{-PDMAEMA}_{68}$ diblock copolymer in (a) $\text{DMSO-}d_6$, (b) D_2O at pH 2, (c) D_2O at pH 7, and (d) D_2O at pH 13.

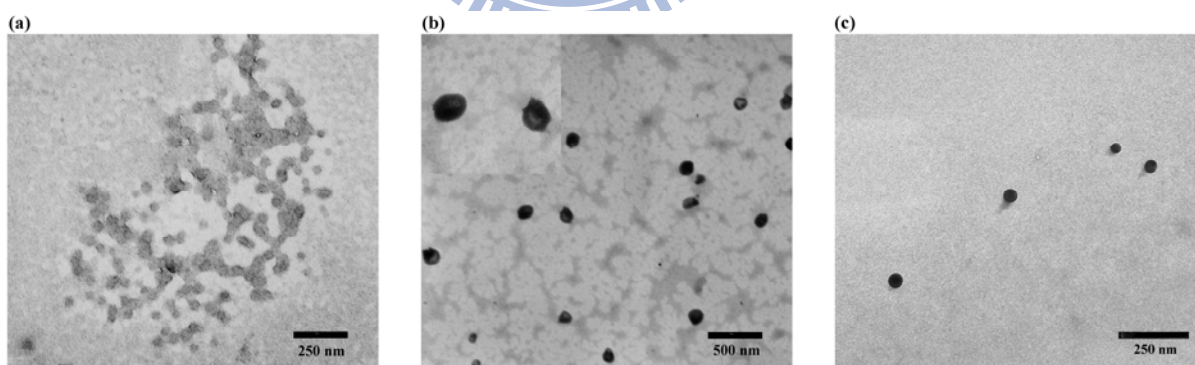


Figure 3-17. TEM images of the morphologies of the $\text{PVPh}_{32}\text{-}b\text{-PDMAEMA}_{68}$ diblock copolymer prepared in aqueous media at (a) pH 2, (b) pH 7, and (c) pH 13.

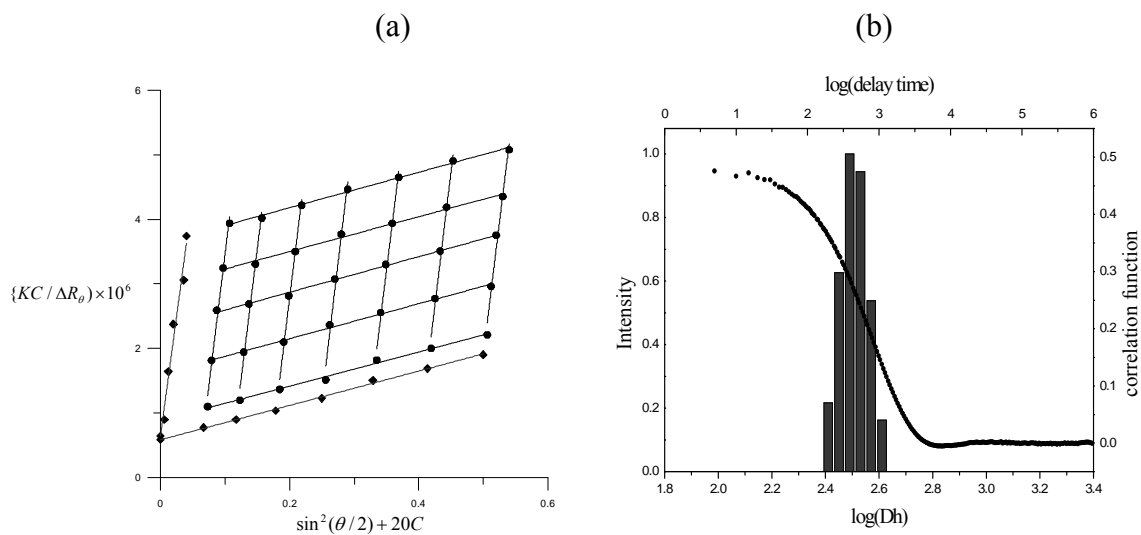


Figure 3-18. (a) The Zimm plot analysis and (b) the hydrodynamic radius distribution of the PVPh₃₂-*b*-PDMAEMA₆₈ block copolymer in aqueous media at pH 7.



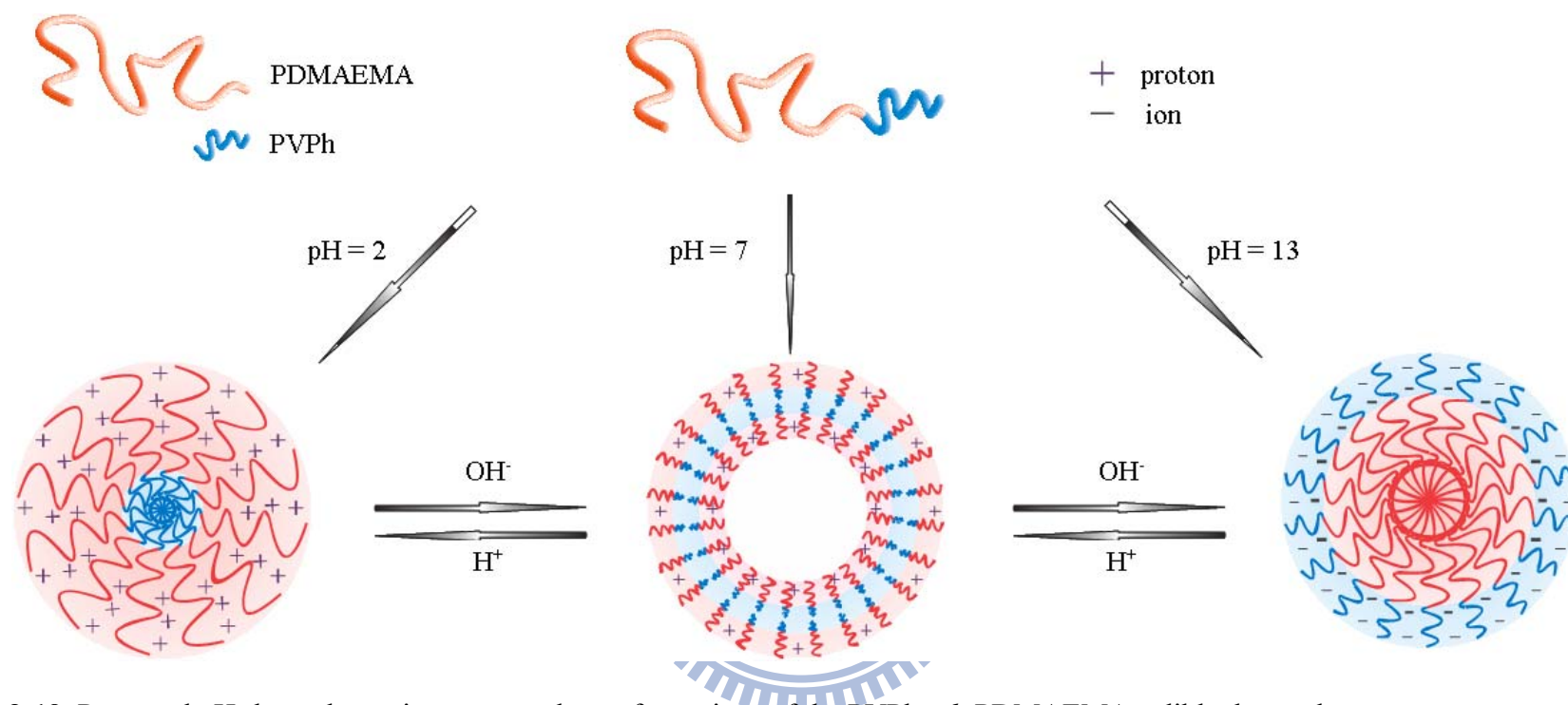


Figure 3-19. Proposed pH-dependent microstructural transformations of the $\text{PVPh}_{32}\text{-}b\text{-PDMAEMA}_{68}$ diblock copolymer

Chapter 4

On Modulating the Phase Behavior of Block Copolymer/Homopolymer Blends via Hydrogen Bonding

Abstract

We have investigated the phase behavior of poly(4-vinylphenol-*b*-styrene) (PVPh-*b*-PS) when respectively blended with poly(4-vinylpyridine) (P4VP), poly(methyl methacrylate) (PMMA), and PVPh homopolymers, of systematically decreased hydrogen-bonding strengths with the PVPh block of the copolymer. The PVPh-*b*-PS/P4VP blend has a much higher fraction (f_H) of hydrogen bonded PVPh blocks for a significantly higher miscibility, compared to the blends with PMMA and PVPh homopolymers. Consequently, the PVPh-*b*-PS/P4VP blend, behaving as a neat diblock copolymer, exhibited a series of order-order phase transitions from the lamellar, gyroid, hexagonally packed cylinder, to body-centered cubic structures. In contrast, both the PVPh-*b*-PS/PMMA and PVPh-*b*-PS/PVPh blends maintained essentially the lamellar structure; the lamellar structure, however, was distorted to different extends at higher volume fractions of the additives, depending on the hydrogen bonding strength. The ratio of inter-association equilibrium constant (K_A) over self-association equilibrium constant (K_B), K_A/K_B , is introduced as a convenient guide in estimating the phase behavior of similar polymer blends, featuring hydrogen bonding interactions between the homopolymer additive and copolymer: with a K_A/K_B ratio much larger than unity, the blend system tends to behave as a neat copolymer; with a K_A/K_B ratio significantly smaller than unity, phase separation instead of order-order phase transitions can be expected for the blend above certain volume fraction of homopolymer additive.

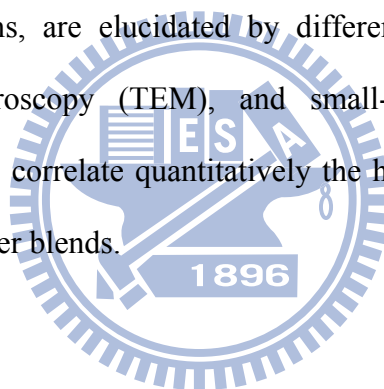
4-1 Introduction

Self-assembly of block copolymers plays a key role in the design of new functional supramolecular materials for a wide range of applications such as pollution control and drug delivery.^{1,2} Blending homopolymers into diblock copolymers for enriched phase behaviors furthermore broadens the applications.³⁻²⁸ An efficient blend of such kind, however, critically depends on (1) the ratio of the molar weight of the additive homopolymer to that of the associated block of the copolymer, and (2) the volume fraction and miscibility of the additive homopolymer in the blend.²⁹⁻⁴⁰

In blends based on a diblock copolymer (A - b - B) and a homopolymer (C), where C is different from A and B , the phase behavior is particularly rich, due to more parameters available on controlling the miscibility between the homopolymer and the two blocks of the copolymer, as demonstrated by a significant number of studies.⁴⁰ Depending on the miscibility between C/A , and C/B , and A/B , there can be several interesting combinations for the blending; here, we are interested in one of them where A and B are immiscible and C is miscible with B but immiscible with A . Along this line of study, Ikkala et al. prepared blends from a polyisoprene- b -poly(2-vinyl pyridine) (PI- b -P2VP) copolymer added with a homopolymer P2VP which is immiscible with the PI block.⁴¹ Dobrosielska *et al.* studied various microphase-separated structures of the poly(vinyl phenol) (PVPh)/poly(styrene- b -2-vinylpyridine) (PS- b -P2VP) blend system, in which PVPh and P2VP are miscible through strong hydrogen bonding but PVPh and PS are immiscible.³⁸⁻³⁹ Zhao et al. investigated blends of poly(styrene- b -vinyl phenol) (PS- b -PVPh) diblock copolymers with several homopolymers having hydrogen bonding acceptors with the PVPh block, such as poly(ethylene oxide) (PEO), poly(4-vinyl pyridine) (P4VP), and poly(butyl methacrylate) (PBMA); these homopolymers are immiscible with the PS block.⁴³ In all these studies mentioned, hydrogen bonding plays a critical role in modulating the miscibility between the additives and the copolymers, resulting in enriched morphology transitions for

the polymer blends.

Inspired by the studies mentioned, we intend to quantify the influence of hydrogen bonding on the phase behavior of homopolymer-copolymer blends of the *A-b-B/C* type, basing on a model system of PVPh-*b*-PS diblock copolymer respectively blended with homopolymers of different hydrogen bonding strengths (therefore different miscibilities) with the PVPh blocks, including poly(4-vinylpyridine) (P4VP), poly(methyl methacrylate) (PMMA), and PVPh. The three additives are immiscible with the PS blocks. With Fourier transform infrared (FTIR) spectroscopy, we map out the fraction of hydrogen bonded groups as a function of the additive volume fraction for the polymer blends; the corresponding thermal properties and phase behavior, including microphase-separated structures and order-order phase transitions, are elucidated by differential scanning calorimetry (DSC), transmission electron microscopy (TEM), and small-angle X-ray scattering (SAXS). Integrating these results, we correlate quantitatively the hydrogen bonding strength with the phase behavior of the polymer blends.



4-2 Experimental Section

4-2.1 Block Copolymer and Homopolymer Syntheses

The precursor to polystyrene-*block*-poly(4-vinylphenol) (PS-*b*-PVPh) was polystyrene-*block*-poly(4-*tert*-butoxystyrene) (PS-*b*-PtBOS), which was synthesized through sequential anionic polymerization of styrene and 4-*tert*-butoxystyrene using *sec*-butyllithium as the initiator. After the polymerization was complete and quenched with degassed MeOH, the polymer was precipitated in MeOH and dried under vacuum. This precursor block copolymer was hydrolyzed to PS-*b*-PVPh under reflux in 1,4-dioxane, using concentrated HCl acid as the catalyst, at 85 °C for 24 h. The final product was neutralized and purified through Soxhlet extraction with water for 72 h before being dried under vacuum at 80 °C. A detailed description of the procedure can be found elsewhere.⁶⁴ The block copolymers were designated as PVPh₆₃-*b*-PS₁₀₉ (denoted HS), where the number in parentheses indicates the molecular molar fraction (mol%). Using living anionic polymerization procedures similar to the one described above, the homopolymers of PVPh₄₂ (denoted H), PMMA₅₃ (denoted M), and P4VP₅₂ (denoted V) were also synthesized. The molecular weights of PVPh-*b*-PS diblock copolymer and the PVPh, P4VP, and PMMA homopolymers are summarized in Table 4-1.

4-2.2 Sample Preparation

Blends of PVPh-*b*-PS/P4VP, PVPh-*b*-PS/PMMA, and PVPh-*b*-PS/PVPh (denoted as HS/V, HS/M, and HS/H, respectively), with a series of volume fractions of homopolymer up to 70 %, were prepared through solution casting. After stirring for 6–8 h, thin films specimens were cast on Teflon dishes from dimethylformamide (DMF) solutions containing 5 wt% polymer mixture, followed by a slow evaporation at 100 °C for 7 days and a subsequent thermal annealing at 120 °C under vacuum for another 7 days. Samples thus prepared could be reproduced for the same thermal properties and same structures.

4-2.3 Characterization Methodology

DSC traces were measured using a DuPont TA Instrument Q-20 controller at a scan rate of 20 °C/min, over the temperature range from 30 to 250 °C under N₂. Infrared spectra were recorded with a resolution of 1 cm⁻¹ using a Nicolet Avatar 320 FTIR spectrometer under N₂; the vacuum-dried sample thin films, satisfying the Beer-Lambert law within the absorbance range, were cast directly onto KBr pellets from the DMF sample solutions.

TEM images were taken for the samples with either the PS block stained with RuO₄ or the P4VP block with I₂, using a Hitachi H-7500 transmission electron microscope operated at an accelerating voltage of 100 kV. Ultrathin sections of the TEM samples (ca. 70 nm thickness) were prepared using a Leica Ultracut UCT microtome equipped with a diamond knife. SAXS experiments were performed using the BL23A SWAXS instrument at the National Synchrotron Radiation Research Center (NSRRC), Taiwan,^{48,49,65} using a 10 keV (wavelength $\lambda = 1.24 \text{ \AA}$) beam with a 0.5 mm diameter. The scattering wavevector transfer $q = 4\pi\lambda^{-1}\sin\theta$ is defined by λ and the scattering angle 2θ of X-rays. Samples for SAXS (thickness $\sim 1\text{mm}$) were sealed between two thin Kapton windows (80 μm thickness each), and measured at an ambient temperature $\sim 26 \text{ }^\circ\text{C}$.

4-2.4 IR Data Analysis

The fractions of hydrogen-bonded pyridine rings of the PVPh block in the polymer blends were estimated using⁶³

$$f_b = \frac{A_b / a}{A_b / a + A_f}, \quad (4-1)$$

where A_f and A_b are integrated areas over two characteristic absorption bands of the free and the hydrogen-bonded functional groups; the conversion coefficient a is the specific absorption ratio between the two absorption bands. For the HS/M system, absorptions of the free and hydrogen-bonded C=O groups of PMMA at 1730 and 1705 cm⁻¹, respectively, were selected

to calculate A_f and A_b , therefore f_b values, with $a = 1.5$ suggested by Moskala et al.⁴ For the HS/V blends, f_b values were calculated based on the two characteristic absorptions bands at 993 and 1005 cm^{-1} related to the free and hydrogen-bonded pyridine rings of P4VP, together with $a = 1$ suggested by Moskala et al. Table 4-2 and 4-3 summarizes the fraction of hydrogen-bonded C=O groups and hydrogen-bonded pyridine groups determined through curve fitting of the data from the blends.⁷³

4-2.5 SAXS Data Analysis

SAXS data with lamellar peaks were analyzed using the one-dimensional correlation function,

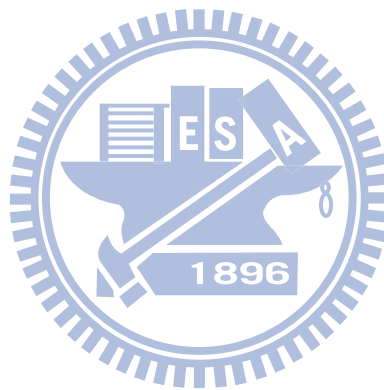
$$\gamma(x) = \frac{1}{Q} \int_0^{\infty} I(q) q^2 \cos(qx) dq, \quad (4-2)$$

obtained from the Fourier-transform of the corresponding one-dimensional SAXS intensity profile $I(q)$, with the scattering invariant $Q = \int_0^{\infty} I(q) q^2 dq$.³⁷ For an ideal two-phase lamellar structure, the first maximum of $\gamma(x)$ corresponds to the long period D of the lamellae; the thickness of the thinner phase l_c of the lamellar stacks can be estimated from the intersection of the two lines passing respectively the first minimum and the first inflection point of the correlation function, as illustrated in Figure 4-1d.²² As the $\gamma(x)$ function cannot account for the interfacial zone width D_{tr} of the studied blends of a non-ideal two-phase structure, the layer thicknesses for the PS-block layer and the PVPh-homopolymer layer thus extracted are smeared over the interfacial zone thickness.

To extract D_{tr} for the blends with a lamellar morphology, direct Fourier transform with phase factors taken into account was applied to the SAXS data for a relative electron density profile⁷¹

$$\rho_e(z) \sim \sum_{k=1}^n \sqrt{I(q_k) q_k^2} \varphi_k \cos(q_k z). \quad (4-3)$$

Here, n is the total number of diffraction orders observed ($n > 3$ for a more reliable electron density profile), and q_k , $I(q_k)$, and φ_k are respectively the scattering vector, integrated intensity, and phase factor, of the k^{th} reflection. For a centrosymmetrical system φ_k is either +1 or -1. It was found that for the polymer blend studied, the most reasonable combination for the phase factors of the first four lamellar peaks are (-1, +1, +1, -1); with the phase factors, the extracted electron densities for the mixed PVPh-P4VP, PVPh-PMMA, and PVPh-PVPh layers are, as expected, higher than that of the PS layer.



4-3 Results and Discussion

4-3.1 FTIR Result

Scheme 4-1 summarizes the signals observed for the free OH and hydrogen-bonded OH \cdots pyridine and OH \cdots O=C vibrations in the FTIR spectra of PMMA and P4VP mixed with PVPh-*b*-PS. Figure 4-2 displays the FTIR spectra, recorded at 120 °C in the region 2700–4000 cm⁻¹ (OH stretching), for pure PVPh-*b*-PS and various HS/V and HS/M blends. The spectrum of pure PVPh-*b*-PS reveals two unresolved bands in the OH stretching region, corresponding to the free OH at 3525 cm⁻¹ and a broad band centered at 3350 cm⁻¹ arising from the absorption of hydrogen-bonded OH (self-association). Figure 4-2a indicates that the intensity of the free OH decreased gradually upon increasing the P4VP content in the HS/V blends, because a greater fraction of OH groups interacted with P4VP. Therefore, it is reasonable to assign band at 3125 cm⁻¹ to the OH groups bonded to pyridine units. For the HS/M blends in Figure 4-2b, the broad band representing the self-associated OH \cdots OH interaction shifted to higher wavenumber when PMMA was the dominant component in the blend, implying that the signal for the OH groups interacting with C=O groups appeared at 3440 cm⁻¹. Coleman and co-workers used the frequency difference ($\Delta\nu$) between the hydrogen-bonded and free OH absorptions to roughly estimate the average hydrogen bond strength.⁴ Based on the reference of the free OH stretching at 3525 cm⁻¹, the OH \cdots O=C (PMMA) inter-association ($\Delta\nu = 85$ cm⁻¹) and OH \cdots OH self-association ($\Delta\nu = 175$ cm⁻¹) were both weaker than the OH \cdots pyridine (P4VP) inter-association ($\Delta\nu = 400$ cm⁻¹).

Shown in Figure 4-3a,b are the two IR spectra for the HS/V and HS/M blends. Figure 4-3c displays the corresponding f_b profiles deduced from the IR spectra, based mainly on the two characteristic absorptions at 993 and 1005 cm⁻¹ for the HS/V blends and 1730 and 1705 cm⁻¹ for the HS/M blends, as detailed previously. The f_b values for the HS/V system are systematically much higher than that of the HS/M system, reflecting a substantially better hydrogen bonding efficiency. This result is consistent with the much higher K_A/K_B value (~ 9

(for the ratio between inter- and self-association equilibrium constants derived based on the PCAM model⁶³) of the HS/V blend system than that ($K_A/K_B \sim 0.6$) for the HS/M blend. The deduced f_b values (and their multiplies with the volume fractions for hydrogen-bounded volume fractions) serve as a guide for the order-order morphology transitions of the polymer blends, as detailed below.

4-3.2 Thermal Properties

Figure 4-4 presents the DSC traces of PVPh-*b*-PS, PVPh, PMMA, P4VP, and the blends with systematically increased volume fractions of the homopolymers. The pure PS-*b*-PVPh diblock copolymer exhibits two glass transitions at 108 and 167 °C, corresponding to the PS and PVPh phases, respectively. The increases in both the T_g values of the PS and PVPh blocks (relative to the homopolymers) are attributed to the microphase separation effect of the block copolymer and the much higher molecular weight of the PVPh block (\sim fourfold) than the homopolymer, as revealed by FTIR and X-ray diffraction. Corresponding DSC measurement indicates an increase of 18 °C for the T_g of the PS block, compared to that of the PS homopolymer of $M_n=10800$ g/mole and $PDI=1.05$ (Figure 4-5a). Furthermore, the FTIR spectra reveal an enhanced absorption in the range of $2800-3200\text{ cm}^{-1}$, indicating that a stronger self-interaction of the PVPh blocks in the copolymer than that of the homopolymer (Figure 4-5b). The X-ray diffraction result (Figure 4-5c) also shows a slightly smaller peak width for the amorphous halo of the PVPh blocks at $2\theta = 20^\circ$, implying a slightly better chain packing than that of the homopolymer. These results support that the increase of T_g of the PVPh block may be attributed to the microphase separation of the block copolymer and the much higher molecular weight of the PVPh block (\sim fourfold) than the additive homopolymer. (cf. Figure 4-5). For homopolymers, T_g values of 152, 105, and 133 °C were observed for P4VP, PMMA, and PVPh, respectively. For all the HS/V blends, two distinct T_g values could be observed, corresponding to the PS phase and the mixed phase of PVPh/P4VP, respectively;

this result indicates that the blend can form a stable mixed phase with a wide range of homopolymer volume fraction, which is essential for order-order phase transitions (detailed below). In contrast, the T_g for the mixed phase of PVPh-PMMA is, in general, less clear-cut and decreased systematically in value upon increase of the PMMA content, implying a less stable mix phase with respect to the addition of homopolymer, presumably, owing to a smaller hydrogen bonding strength. The even faster drop in the T_g value of the mixed phase of the HS/H blend upon increasing the content of the PVPh homopolymer up to 20 vol. %, indicates a venerable stability of the mixed phase. Upon further addition of PVPh homopolymer, T_g of the mixed phase was replaced by T_g of the PVPh homopolymer; this implies a solubility limit of $\sim 20\%$ of PVPh homopolymer in the PVPh blocks of the copolymer.

4-3.3 Order-Order Structural Transitions for the HS/V Blends

The TEM images shown in Figure 4-6 for the HS/V blends exhibited a series of order-order phase transitions from the lamellar, gyroid, hexagonally packed cylinder (HCP), to body-centered cubic (BCC) structures, as the volume fraction of P4VP increases from 6-13, 15-22, 29, to 71 %. Such phase transition behavior of the blend follows closely that for a neat diblock copolymer, implying a collective behavior of PVPh and P4VP chains in the mixed phase.

Complementarily, SAXS profiles for the HS/V system in Figure 4-7 display scattering patterns that match nearly ideally to the structures observed by TEM (Figure 4-6). Specifically, the SAXS profiles for the neat diblock copolymer PVPh-*b*-PS and HS/V blends with compositions of 94/6, 90/10, and 87/13, all demonstrate lamellar peaks that are consistent with the TEM images in Figure 4-6a-d. Similar SAXS profiles were observed for the blends with compositions 85/15, HS/V = 78/22, and HS/V = 76/24; the first four scattering peaks can be associated with the (211), (220), (321), and (332) reflection planes, of

a gyroid structure, which has been evidenced by the TEM images shown in Figure 4-6e-f. With the P4VP content increased to 29 %, the SAXS profile clearly exhibits organized peaks with peak ratios $1:\sqrt{3}:2:\sqrt{7}:3:\sqrt{12}$, indicating hexagonally packed cylinders, as also imaged in Figure 4-6g. With further increased P4VP contents to 52 and 71 %, the corresponding SAXS profiles both show scattering peaks with the ratios of $1:\sqrt{2}:\sqrt{5}$, indicating micro-separated domains with BCC-packed spheres, as visualized in Figure 4-6h.

4-3.4 Order-Disorder Structural Transitions for the HS/M and HS/H Blends

The HS/M and HS/H blending systems show respectively modest and low hydrogen bonding between homopolymer and copolymer, as compared to the HS/V blends. Consequently, TEM images (Figure 4-8 and 4-9) taken for the two systems show mainly the order-to-disorder (lamellar to distorted lamellar) structural change, when the volume fraction of the additive increased in the same range (6-70%) as that in HS/V system. At high volume fractions of additives, phase separation of the additive homopolymers was observed in especially the HS/H blends with weak hydrogen bonding. Before phase separation, an intermediate structure of swollen lamellae coexisting with the unswollen ones could be observed (Figure 4-8e and 4-9c,d) for both systems, as also evidenced from the broad double peaks in the corresponding SAXS profiles (indicated by the thick arrows in Figure 4-10a and 4-10b). Especially for in the HS/H blends, TEM image (Figure 4-9e) indicates that the large amount of homopolymer finally discrete the lamellae of the diblock copolymer into single slabs (single bilayers); previously, the DSC result has also suggested a dissociation of the mixed phase based on the diminishing T_g (Figure 4-4c). Likely, upon losing the steric interactions between the lamellar slabs, the dangling slabs bent and curve in the excess homopolymer phase; the formation of hollow tubes with single-bilayer wall as shown in Figure 4-9e, however, is a surprising.

Shown in Figure 4-10a,b are a series of SAXS profiles for the HS/M and HS/H systems.

Unlike that for the order-order phase transition in the HS/V system, these SAXS profiles essentially reflect that the lamellar structure in either system is gradually distorted upon the increase of homopolymer, as that shown in the corresponding TEM images (Figure 4-8,4-9). Up to 70 vol. % of the additive, the three residual lamellar peaks in the SAXS profile (Figure 4-10a) indicates that the HS/M system of intermediate hydrogen bonding strength can essentially hold the lamellar structure. Whereas in the HS/M system, the first lamellar peak melts in the SAXS profile (Figure 4-10b) at this high volume fraction of additive (70%), implying that the lamellar structure is completely destroyed; this is consistently observed in the DSC and TEM results shown previously. Note that the three broad scattering maxima in the SAXS profile (indicated by the thick arrows marked with circled numbers in Figure 4-10b) are not the lamellar peaks; rather, they are contributed by the form factor scattering of isolated PS layers (cf. the TEM image in Figure 4-9e), as calculated using a slab geometry with a slab thickness of 24 nm.

To illustrate the reliability of the prescribed volume fractions for the mixed phase in these blends, we note that in the SAXS profile of the neat HS containing ~40 vol. % PVPh, the 5th reflection (Figure 4-10a) nearly diminishes as it should be, owing to a destructive interference under this volume fraction; upon the addition of 21% PMMA into the blend for equal volume fractions of the PS and PVPh-PMMA phases (i.e. the 79:21 case in Figure 4-10a), lamellar peaks of even orders of destructive phase factors disappear accordingly. Interestingly, the two sets of SAXS profiles of the HS/M and HS/H blends illustrate opposite shifting of the first peak position; namely, the first peak in the HS/M blend shifts systematically towards higher- q region as the PMMA content increases, corresponding a shrinkage of the lamellar spacing. In the case of HS/H blends, the first lamellar peak shifts toward lower q upon increasing the PVPh content, corresponding to an increase of the lamellar spacing. The origin of this dissimilarity is discussed below based on the hydrogen bonding (attractive interactions) of the additive homopolymers with the copolymer.

4-3.5 Correlation between the Hydrogen Strength and Phase Transition

The DSC, TEM, and SAXS results collectively show that the HS/V blends follow a phase transition behavior similar to that of a neat copolymer of PS-*b*-PVPh. The HS/M and HS/H blends, on the other hand, are subject to phase separation to different extents at high volume fractions of homopolymer additives. Integrating the FTIR result in Figure 4-3c, we further correlate the hydrogen bonding strength to the phase behaviors of the polymer blends. We shown in Figure 4-11 that lamellar-to-gyroid phase transition in similar polymer blends may require a fraction of hydrogen-bonded groups in the range of $0.3 \lesssim f_b \lesssim 0.8$ at a mixed phase volume fraction $V_{\text{mix}} \sim 46\%$; transition from gyroid to HCP may occur with $0.20 \lesssim f_b \lesssim 0.65$ at $V_{\text{mix}} \sim 56\%$, whereas $0.15 \lesssim f_b \lesssim 0.38$ at $V_{\text{mix}} \sim 70\%$ for HCP-to-BCC transition.

Figure 4-11 provides a quantitative correlation between the phase behavior and the hydrogen bonding strength (efficiency) for the PS-*b*-PVPh-based, *A-b-B/C* type of polymer blends. Furthermore, based on the Painter–Coleman association model (PCAM) and the inter-association equilibrium constant K_A and self-association equilibrium constants K_B , we suggest the simple ratio K_A/K_B can also be used as a convenient guide in estimating the phase behavior of similar polymer blends. The K_A and K_B values for the hydrogen-bonded PVPh/P4VP ($K_A = 598$) and PVPh/PMMA ($K_A = 37.4$) and the self-association equilibrium constant for PVPh ($K_B = 66.8$) have been determined previously.⁵¹⁻⁶² Based on these values, the phase behavior the HS/V blends with $K_A/K_B \sim 9$ ($\gg 1$) of strong hydrogen bonding strength follows closely that of a typical diblock copolymer; with $K_A/K_B \sim 0.6$ for the HS/M blends, phase separation instead of order-order transition is observed above certain volume fraction of homopolymer, as that illustrated in Figure 4-12.

4-3.6 Distribution/Chain Conformation of the Additive Homopolymers in the Blends

As we have clarified the hydrogen bonding effect on the phase behavior of the A-*b*-B/C type of polymer blends based on PS-*b*-PVPh, with P4VP, PMMA, and PVPh additives, we are now in a good position to examine how additive homopolymers conform and distribute their chains in the blends to fulfill the different structural characteristics required for the different ordered phases observed.

Summarizes in Table 4-4 are the thicknesses of the PS layer, D_{PS} , the mixed layer (of PVPh-homopolymer), D_{mix} , and the long period D , of all the blends of lamellar morphology, obtained from the 1-D correlation function (cf. Figure 4-1); the relative changes in D upon the addition of homopolymers, i.e. D/D_0 where $D_0 = 39$ nm is the D value for the neat copolymer, are presented in Figure 4-13a. Furthermore, the correlated changes in the average distance a_J of the chemical junctions along the interface, thus the relative changes a_J/a_{J0} (where a_{J0} is for the neat copolymer), can be derived for the blends. Simple volumetric conservation leads to $D/D_0 = (\rho_J/\rho_{J0})\Phi^{-1}$ for a lamellar structure, where ρ_J is the number of block chains per unit interfacial area ($\sim a_J^2$), thus $a_J/a_{J0} \approx (\rho_J/\rho_{J0})^{-1/2}$, and Φ is the volume fraction of the block copolymer in the blend. Similarly, $D/D_0 = (\rho_J/\rho_{J0})[(2/\sqrt{3})\pi f \Phi_{block}^{-1}]^{1/2}$ for hexagonally packed cylinders, and $D/D_0 = (\rho_J/\rho_{J0})[(27\sqrt{3}/8)\pi f^2 \Phi_{block}^{-1}]^{1/2}$ for BCC spheres, as suggested by Hashimoto et al. (ref). Based on these relations, we have derived the values of ρ_J/ρ_{J0} and a_J/a_{J0} for the blends, which are summarized in Table 4-5 and Figure 4-13b.

For the HS/H blends with low volume fractions of the additive homopolymer (below 20%), Figure 4-13a exhibits a nearly linear growth of D/D_0 with the homopolymer volume fraction, accompanied by a constant a_J/a_{J0} (=1) (Figure 4-12b). Such a result suggests that the homopolymer additive prefers to stay in-between the P4Ph blocks, and does not intervene in the interface of the PS and PVPh blocks. With such a behavior, continuous swelling of the mixed phase with higher and higher volume fractions of PVPh homopolymer inevitably

discretizes the lamellae of the diblock copolymer into single bilayers, as evidenced in the TEM and SAXS results. In contrast, both the HS/M and HS/V blends characterized with hydrogen bonding display a contraction in the lamellar spacing, i.e. $D/D_0 < 1$ (Figure 4-13a) accompanied by an expansion in a_I , ($a_I/a_{I0} > 1$ in Figure 4-13b). Presumably, the additive homopolymers can intervene in (and *wet*) the PVPh chains of the block copolymer at the interfaces, resulting in the observed expansion in a_I . The PS blocks, being chemically linked to the PVPh blocks, cannot but contract to accommodate the expanded interface zone. Consequently, the PS layer thickness, therefore, the lamellar spacing, decreases with the addition of either of the two homopolymers. Correspondingly, the PVPh chains of the block copolymer stretch only slightly for more hydrogen-bonding interfaces with the P4VP chains (cf. the slightly larger D_{mix} in Table 4-4); whereas these chains remain about the same conformation when associated with PMMA of intermediate hydrogen bonding affinity, as suggested by a nearly constant layer thickness of the mixed phase (cf. D_{mix} in Table 4-4).

Upon increase of the additive volume fraction, a_I/a_{I0} of the HS/V blend grows continuously for an increasingly larger surface area per chemical junction, leading to interfaces with increasingly higher curvatures that are needed for the successive phases of gyroid, HPC, and BBC spheres (TEM and SAXS results), as elucidated in Figure 4-13b. With a significantly smaller hydrogen bonding efficiency (cf. Figure 4-3), the HS/M blend, however, fails to expand a_I large enough for the curvature needed in a lamellar-to-gyroid phase transition (as that occurred in the HS/V system). Likely, PMMA homopolymer can only intervene into the PVPh chains at the interface with a limited fraction, and then partially phase-separates out from the interfacial zone; in terms of the free energy consideration, the modest hydrogen bonding strength between PVPh and PMMA may not be able to compensate, like that of PVPh-P4VP does, the free energy added by the interfaces of increased curvatures for an order-order phase transition.

4-3.7 Interfacial Zone of the Polymer Blends

As mentioned above, the distributions of the three homopolymer additives in the respective polymer blends are characteristically different: the stronger the hydrogen bonding strength is, the higher tendency for the additive to stay at the interface. It is interesting to see how the interfacial zone of the respective blends copes with these chain distributions. For this, we have obtained the relative electron density profiles for the blends having a lamellar morphology (Figure 4-14b), using direct Fourier transform as described previously. In general, the respective layer thicknesses of the PS and PVPh-homopolymer phases extracted from the relative electron density profiles of the three types of blends are consistent with those obtained using 1-D correlation function (Table 4-4); in addition, the transition zone thickness D_{tr} can be defined from the electron density profile as illustrated in Figure 4-14a.

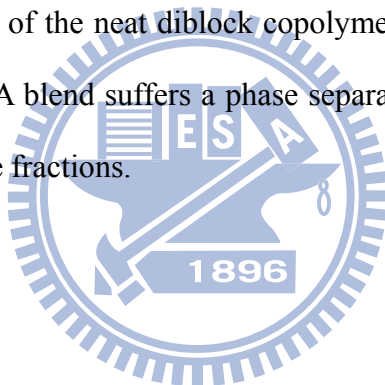
Shown in Figure 4-14c are the D_{tr} values obtained for the three kinds of blends. The obvious increase of D_{tr} from 5.0 to 6.3 nm with the increase of the additive volume fraction up to 10 % for the HS/H blends, implies significantly disturbed interfaces by the homopolymer. Rather than interdiffusion of PS and PVPh chains at the interface, we attribute the increased D_{tr} to the undulation of lamellar thickness induced by an irregular distribution the PVPh homopolymer in-between the PVPh layers of the copolymer. Consequently, coexistence of swollen and unswollen lamellae can be observed from TEM (cf. Figure 4-9c) at higher volume fractions of PVPh homopolymer. On the other hand, the D_{tr} changes only marginally (from 5.0 to 5.3 nm) in both the HS/V and HS/M blends, in a similar range of homopolymer volume fraction (0 -15 %); presumably, the added P4VP and PMMA homopolymers selectively reside at the interface areas with the PVPh blocks via hydrogen bonding; and the mixed PVPh and homopolymer chains act as a collective phase, resulting in a similar transition zone thickness. As the electron densities of the PVPh, PMMA, and P4VP, are all similar, it is difficult to differentiate the distribution of the homopolymer additive of PVPh, PMMA, or P4VP, in the PVPh blocks of the copolymer from the SAXS data; small

angle neutron scattering with selected contrast variation will be more direct in addressing the issue of chain conformation of the additive homopolymers in a copolymers-homopolymer blend, as demonstrated by Hashimoto et al. (ref).



4-4 Conclusions

We have used FTIR spectroscopy, DSC, TEM, and SAXS techniques to investigate the phase behavior of the HS/V, HS/M, and HS/H blend systems of different hydrogen bonding strengths between the homopolymers and diblock copolymers. Integrated results show clearly that the phase behavior for the *A-b-B/C* type of polymer blends based on PS-*b*-PVPh, can be modulated via the hydrogen bonding strength between the homopolymer and copolymer. Fraction of hydrogen bonded groups may be used in quantitatively correlating the hydrogen bonding strength to the phase behavior of the polymer blends. With the inter-association equilibrium constant (K_A) over self-association equilibrium constant (K_B), K_A/K_B , much larger than unity, the phase behavior of the PS-*b*-PVPh/P4VP blend of strong hydrogen bonding strength follows closely that of the neat diblock copolymer; with a K_A/K_B value smaller than unity, the PS-*b*-PVPh/PMMA blend suffers a phase separation, instead of phase transition, at higher homopolymer volume fractions.



References

- [1] Muthukumar, M.; Ober, C. K.; Thomas, E. L. *Science* **1997**, *277*, 1225.
- [2] Stupp, S. I.; Braun, P. V. *Science* **1997**, *277*, 1242.
- [3] Hashimoto, T.; Tanaka, H.; Hasegawa, H. *Macromolecules* **1990**, *23*, 4378. Tanaka, T.; Hasegawa, H.; Hashimoto, T. *Macromolecules* **1991**, *24*, 240.
- [4] Moskala, E. J.; Varnell, D. F.; Coleman, M. M. *Polymer* **1985**, *26*, 228.
- [5] Bendejacq, D.; Ponsinet, V.; Joanicot, M. *Macromolecules* **2002**, *35*, 6645.
- [6] Holoubek, J.; Baldrian, J.; Lednický, F.; Malkova, S.; Lal, J. *Macromol. Chem. Phys.* **2006**, *207*, 1834.
- [7] Tucker, P. S.; Barlow, J. W.; Paul, D. R. *Macromolecules* **1988**, *21*, 2794.
- [8] Tucker, P. S.; Paul, D. R. *Macromolecules* **1988**, *21*, 2801.
- [9] Lowenhaupt, B.; Steurer, A.; Hellmann, G. P. *Polymer* **1991**, *32*, 1065.
- [10] Lowenhaupt, B.; Steurer, A.; Hellmann, G. P.; Gallot, Y. *Macromolecules* **1994**, *27*, 908.
- [11] Han, Y. K.; Pearce, E. M.; Kwei, T. K. *Macromolecules* **2000**, *33*, 1321.
- [12] Jiang, M.; Xie, H. K. *Prog. Polym. Sci.* **1991**, *16*, 977.
- [13] Jiang, M.; Huang, T.; Xie, J. *Macromol. Chem. Phys.* **1995**, *196*, 787.
- [14] Jiang, M.; Huang, T.; Xie, J. *Macromol. Chem. Phys.* **1995**, *196*, 803.
- [15] Zoelen, W. V.; Ekenstein, G. A. V.; Ikkala, O.; Brinke, G. T. *Macromolecules* **2006**, *39*, 6574.
- [16] Akaba, M.; Nojima, S. *Polym. J.* **2006**, *38*, 559.
- [17] Huang, Y. M.; Liu, H. L.; Hu, Y. *Macromol. Theory Simul.* **2006**, *15*, 321.
- [18] Huang, Y. Y.; Chen, H. L.; Hashimoto, T. *Macromolecules* **2003**, *36*, 764.
- [19] Likhman, A. E.; Semenov, A. N. *Macromolecules* **1997**, *30*, 7273.
- [20] Huang, Y. Y.; Hsu, J. Y.; Chen, H. L.; Hashimoto, T. *Macromolecules* **2007**, *40*, 3700.
- [21] Matsushita, Y. *Macromolecules* **2007**, *40*, 771.
- [22] Stoykovich, M. P.; Edwards, E. W.; Solak, H. H. *Phys. Rev. Lett.* **2006**, *97*, 147802.

- [23] Jinnai, H.; Hasegawa, H.; Nishikawa, Y.; Sevink, G. J. A.; Braunfeld, M. B.; Agard, D. A.; Spontak, R. J. *Macromol. Rapid Commun.* **2006**, *27*, 1424.
- [24] Lee, J. H.; Balsara, N. P.; Chakraborty, A. K.; Krishnamoorti, R.; Hammouda, B. *Macromolecules* **2002**, *35*, 7748.
- [25] Vaidya, N. Y.; Han, C. D. *Polymer* **2002**, *43*, 3047.
- [26] Huang, P.; Zhu, L.; Cheng, S. Z. D.; Ge, Q.; Quirk, R. P.; Thomas, E. L.; Lotz, B.; Hsiao, B. S.; Liu, L. Z.; Yeh, F. J. *Macromolecules* **2001**, *34*, 6649.
- [27] Vavasour, J. D.; Whitmore, M. D. *Macromolecules* **2001**, *34*, 3471.
- [28] Maurer, W. W.; Bates, F. S.; Lodge, T. P. *J. Chem. Phys.* **1998**, *108*, 2989.
- [29] Jeon, K. J.; Roe, R. J. *Macromolecules* **1994**, *27*, 2439.
- [30] Shull, K. R.; Winey, K. I. *Macromolecules* **1992**, *25*, 2637.
- [31] Bodycomb, J.; Yamaguchi, D.; Hashimoto, T. *Macromolecules* **2000**, *33*, 5187.
- [32] Winey, K. I.; Thomas, E. L.; Fetters, L. J. *Macromolecules* **1992**, *25*, 2645.
- [33] Xie, R.; Li, G.; Liu, C.; Jiang, B. *Macromolecules* **1996**, *29*, 4895..
- [34] Lee, S.-H.; Char, K.; Kim, G. *Macromolecules* **2000**, *33*, 7072.
- [35] Winey, K. I.; Thomas, E. L.; Fetters, L. J. *Macromolecules* **1992**, *25*, 422.
- [36] Koizumi, S.; Hasegawa, H.; Hashimoto, T. *Macromolecules* **1994**, *27*, 7893.
- [37] Yamaguchi, D.; Shiratake, S.; Hashimoto, T. *Macromolecules* **2000**, *33*, 8258.
- [38] Mayes, A. M.; Russell, T. P.; Satijia, S. K.; Majkrzak, C. F. *Macromolecules* **1992**, *25*, 6523.
- [39] Dobrosielska, K.; Wakao, S.; Takano, A.; Matsushita, Y. *Macromolecules*, **2008**, *41*, 7695.
- [40] Dobrosielska, K.; Wakao, S.; Suzuki, J.; Noda, K.; Takano, A.; Matsushita, Y. *Macromolecules* **2009**, *42*, 7098.
- [41] Kuo, S. W. *Polym. Inter.* **2009**, *58*, 455.
- [42] Kosonen, H.; Ruokolainen, J.; Nyholm, P.; Ikkala, O. *Polymer* **2001**, *42*, 9481.

- [43] Kimishima, K.; Hashimoto, T.; Han, C. D. *Macromolecules* **1995**, *28*, 3842.
- [44] Zhao, J. Q.; Pearce, E. M.; Kwei, T. K. *Macromolecules* **1997**, *30*, 7119.
- [45] Hameed, N.; Guo, Q. *Polymer* **2008**, *49*, 922.
- [46] Hameed, N.; Guo, Q. *Macromolecules* **2008**, *41*, 7596.
- [47] Hameed, N.; Guo, Q. *Polymer* **2008**, *49*, 5268.
- [48] Chen, W. C.; Kuo, S. W.; Lu, C. H.; Jeng, U. S. Chang, F. C. *Macromolecules* **2009**, *42*, 3580.
- [49] Lee, H. F.; Kuo, S. W.; Huang, C. F.; Lu, J. S.; Chan, S. C. Chang, F. C. *Macromolecules* **2006**, *39*, 5458.
- [50] Chen, W. C.; Kuo, S. W.; Jeng, U. S. Chang, F. C. *Macromolecules* **2008**, *41*, 1401.
- [51] Lin, I. H.; Kuo, S. W.; Chang, F. C. *Polymer* **2009**, *50*, 5276.
- [52] Lin, C.-L.; Chen, W.-C.; Liao, C.-S.; Su, Y.-C.; Huang, C.-F.; Kuo, S.-W.; Chang, F.-C. *Macromolecules* **2005**, *38*, 6435.
- [53] Kuo, S. W.; Tung, P. H.; Chang, F. C. *Macromolecules* **2006**, *39*, 9388.
- [54] de Mefathi, M. V.; Frechet, J. M. J. *Polymer* **1988**, *29*, 477.
- [55] Dai, J.; Goh, S. H.; Lee, S. Y.; Siow, K. S. *Polym. J.* **1994**, *26*, 905.
- [56] Wang, J.; Cheung, M. K.; Mi, Y. *Polymer* **2001**, *42*, 3087.
- [57] Xiang, M.; Jiang, M.; Zhang, Y.; Wu, C. *Macromolecules* **1997**, *30*, 2313.
- [58] Zhang, Y.; Xiang, M.; Jiang, M.; Wu, C. *Macromolecules* **1997**, *30*, 6084.
- [59] Serman, C. J.; Painter, P. C.; Coleman, M. M. *Polymer* **1991**, *32*, 1049.
- [60] Zhang, X.; Takegoshi, K.; Hikichi, K. *Macromolecules* **1991**, *24*, 5756.
- [61] Li, D.; Brisson, J. *Macromolecules* **1996**, *29*, 868.
- [62] Dong, J.; Ozaki, Y. *Macromolecules* **1997**, *30*, 286.
- [63] Coleman, M. M.; Graf, J. F.; Painter, P. C. *Specific Interactions and the Miscibility of Polymer Blends*, Technomic Publishing: Lancaster, PA, **1991**.
- [64] Tung, P. S.; Kuo, S. W.; Chen, S. C.; Lin, C. L.; Chang, F. C. *Polymer* **2007**, *48*, 3192.

- [65] Li, M.; Douki, K.; Goto, K.; Li, X.; Coenjarts, C.; Smilgies, D. M.; Ober, C. K. *Chem. Mater.* **2004**, *16*, 3800.
- [66] Lai, Y. H.; Sun, Y. S.; Jeng, U.; Lin, J. M.; Lin, T. L.; Sheu, H. S.; Chuang, W. T.; Huang, Y. S.; Hsu, C. H.; Lee, M. T.; Lee, H. Y.; Liang, K. S.; Gabriel, A.; Koch, M. H. J. *J. Appl. Crystallogr.* **2006**, *39*, 871.
- [67] Kwei, T. K. *J. Polym. Sci., Polym. Lett. Ed.* **1984**, *22*, 307.
- [68] Tanaka, H.; Hashimoto, T. *Macromolecules* **1991**, *24*, 5713.
- [69] Winey, K. I.; Thomas, E. L.; Fetters, L. J. *J. Chem. Phys.* **1991**, *95*, 9367.
- [70] Yang, Z.; Han, C. D. *Macromolecules* **2008**, *41*, 2104.
- [71] Iriarte, M.; Alberdi, M.; Shenoy, S. L.; Irwin, J. J. *Macromolecules* **1999**, *32*, 2661.
- [72] Wu, C. M.; Liou, W.; Chen, H. L.; Lin, T. L.; Jeng, U. S. *Macromolecules* **2004**, *37*, 4974.
- [73] Moskala, E. J.; Howe, S. E.; Painter, P. C.; Coleman, M. M.; *Macromolecules* **1984**, *17*, 1671.

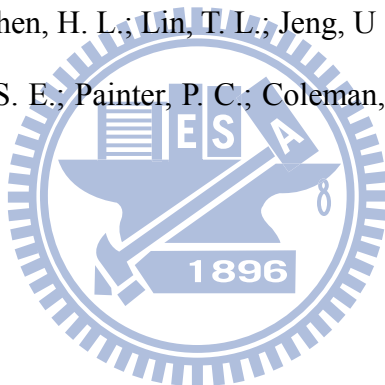


Table 4-1. Molecular weights of PVPh-*b*-PS, PVPh, PMMA, and P4VP used in preparing the polymer blends. The volume fractions of PVPh and PS blocks in the neat block copolymer are respectively 37.6 and 62.4%.

Polymer	M_n
PVPh ₆₃ - <i>b</i> -PS ₁₀₉ (HS)	18900
PVPh ₄₂ (H)	5040
PMMA ₅₃ (M)	5300
P4VP ₅₂ (V)	5460

Table 4-2. Curve Fitting of the Fraction of Hydrogen-Bonded Carbonyl Groups of PVPh-*b*-PS/ PMMA Blend System

PVPh- <i>b</i> -PS/PMMA	H-bonded C=O			free C=O			f_b %
	ν , cm ⁻¹	$W_{1/2}$, cm ⁻¹	A_b , %	ν , cm ⁻¹	$W_{1/2}$, cm ⁻¹	A_b , %	
HS/M = 30/70	1706	25	16	1732	25	84	11
HS/M = 49/51	1707	25	21	1732	25	79	15
HS/M = 62/38	1706	25	22	1732	25	78	16
HS/M = 72/28	1706	24	30	1732	25	70	22
HS/M = 79/21	1706	24	35	1732	24	65	26
HS/M = 85/15	1706	24	38	1732	24	62	29
HS/M = 90/10	1706	24	39	1732	24	61	30
HS/M = 94/6	1706	24	40	1732	24	60	31
HS/M = 97/3	1707	24	46	1732	24	54	36

Table 4-3. Curve Fitting of the Fraction of Hydrogen-Bonded Pyridine Groups of PVPh-*b*-PS/P4VP Blend System

PVPh- <i>b</i> -PS/P4VP	H-bonded pyridine			Free pyridine			f_b %
	ν , cm^{-1}	$W_{1/2}$, cm^{-1}	A_b , %	ν , cm^{-1}	$W_{1/2}$, cm^{-1}	A_b , %	
HS/V = 29/71	1005	10	14	993	8	86	14
HS/V = 48/52	1005	10	38	993	8	62	38
HS/V = 61/39	1005	10	49	993	8	44	53
HS/V = 76/24	1005	11	66	993	7	23	74
HS/V = 78/22	1005	11	65	993	8	22	75
HS/V = 90/10	1005	11	73	993	7	5	93
HS/V = 94/6	1005	11	65	994	8	4	94

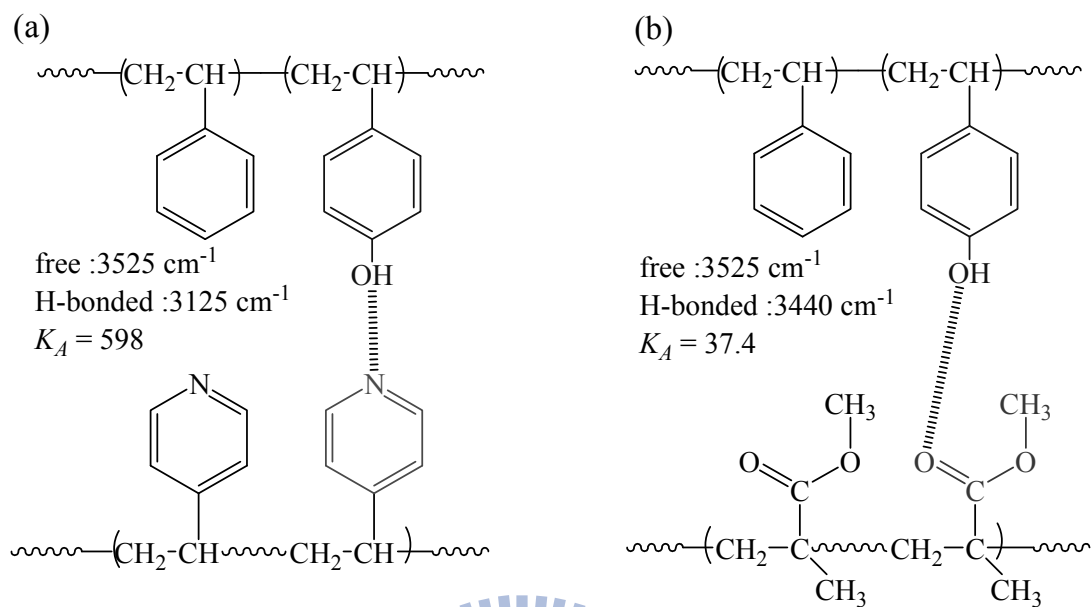
Table 4-4. Thicknesses of the PS (D_{PS}) and PVPh-homopolymer layers (D_{mix}) determined from 1-D correlation function.

Sample	D_{PS} (nm)	D_{Mix} (nm)	D (nm)
HS	23.6	15.4	39
HS/H = 94/6	23.7	18.2	41.9
HS/H = 90/10	24.1	19.8	43.9
HS/H = 80/20	25.9	21.4	47.3
HS/M = 94/6	21.4	15.6	37
HS/M = 90/10	20.3	16.1	36.4
HS/M = 79/21	18.9	15.6	34.5
HS/M = 62/38	18.3	15.1	33.4
HS/M = 31/69	18.1	13.1	30.2
HS/V = 94/6	21.2	16.5	37.7
HS/V = 90/10	20.7	17.2	37.9
HS/V = 87/13	19.3	17	36.3

Table 4-5. The relative changes (with respect to the neat copolymer) in D , ρ_j , and a_j for the HS/H, HS/M, and HS/V blends; the interdomain spacing for the HS/V blends 71/29 (HPC), 48/52 (BCC spheres), and 29/71 (BCC spheres), are 45.6, 37.4, and 35.7 nm, respectively.

Sample	Morphology	D/D_0	ρ_{j0}/ρ_j	a_j/a_{j0}
HS	Lamellar	1	1	1
HS/H = 94/6	Lamellar	1.07	1.01	1
HS/H = 90/10	Lamellar	1.12	1.01	1
HS/H = 80/20	Lamellar	1.21	0.97	1.01
HS/M = 94/6	Lamellar	0.95	0.89	1.06
HS/M = 90/10	Lamellar	0.93	0.84	1.09
HS/M = 79/21	Lamellar	0.88	0.71	1.19
HS/M = 62/38	Lamellar	0.86		
HS/M = 30/70	Lamellar	0.78		
HS/V = 94/6	Lamellar	0.97	0.9	1.05
HS/V = 90/10	Lamellar	0.97	0.87	1.07
HS/V = 87/13	Lamellar	0.93	0.81	1.11
HS/V = 85/15	Gyroid			
HS/V = 78/22	Gyroid			
HS/V = 76/24	Gyroid			
HS/V = 71/29	HP cylinder		0.66	1.23
HS/V = 48/52	BCC sphere		0.39	1.6
HS/V = 29/71	BCC sphere		0.31	1.8

Scheme 4-1. Schematic Representation of the Types of Hydrogen Bonding Interactions Existing in the (a) PVPh-*b*-PS/P4VP and (b) PVPh-*b*-PS/PMMA Blend Systems.



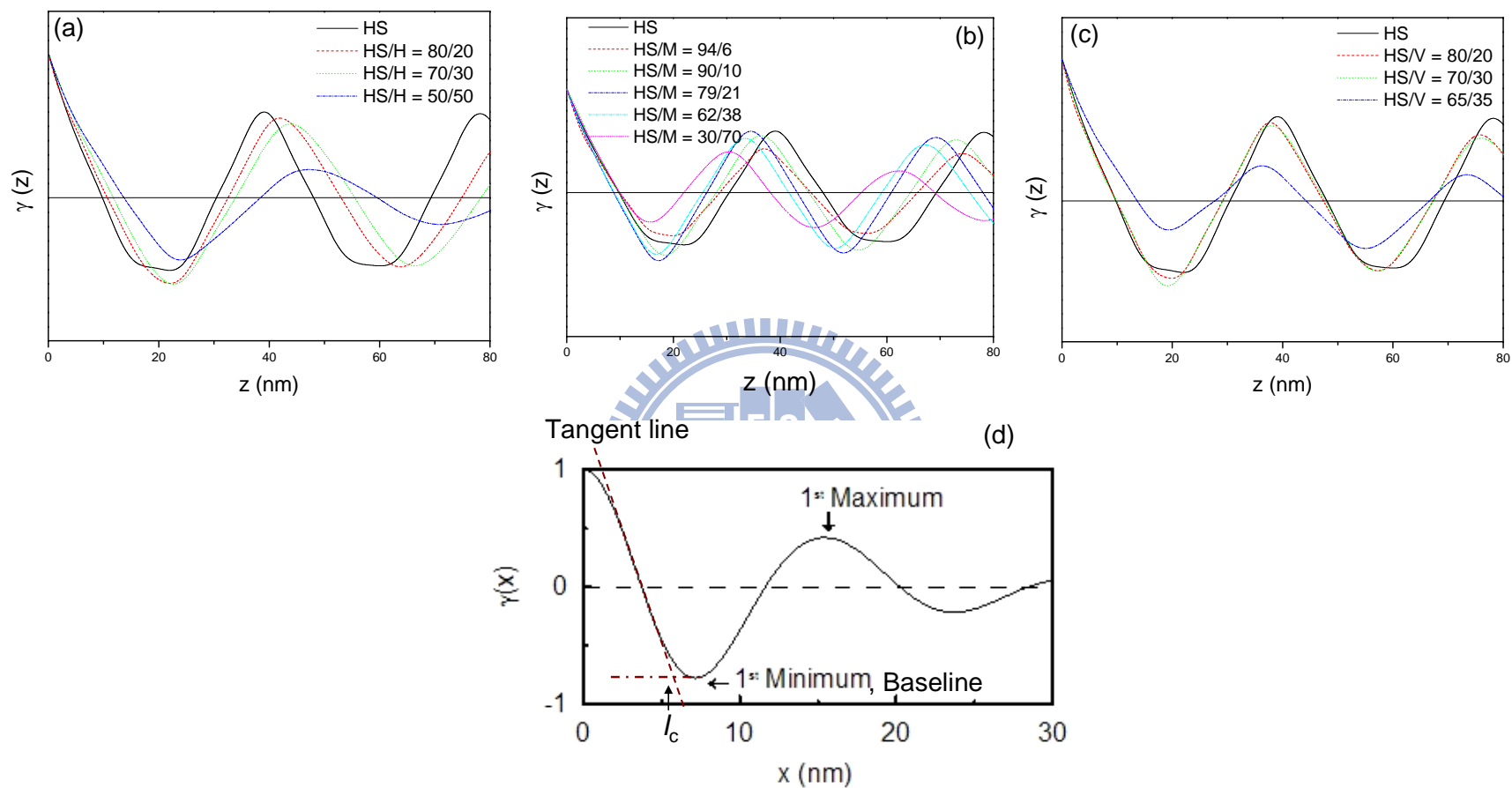


Figure 4-1. One-dimensional correlation functions of the (a) HS/H, (b) HS/M, and (c) HS/V blend systems. The thickness of the lamellar long period was calculated from the position of the first peak; the average thickness of the thinner phase is determined from the intersection of the tangent line and baseline, as illustrated in (d) for an ideal two-phase lamellar structure.

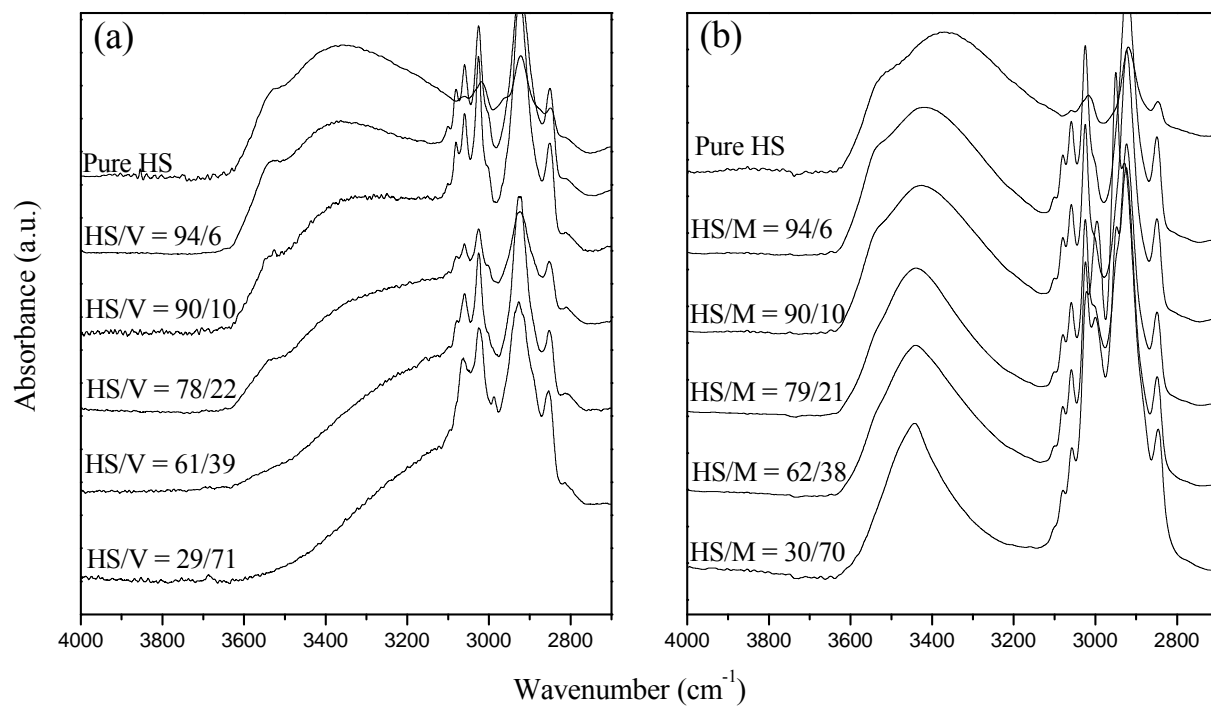


Figure 4-2. FTIR spectra, recorded at 120 °C, of the OH stretching region of the (a) HS/V and (b) HS/M blend systems cast from DMF solutions.



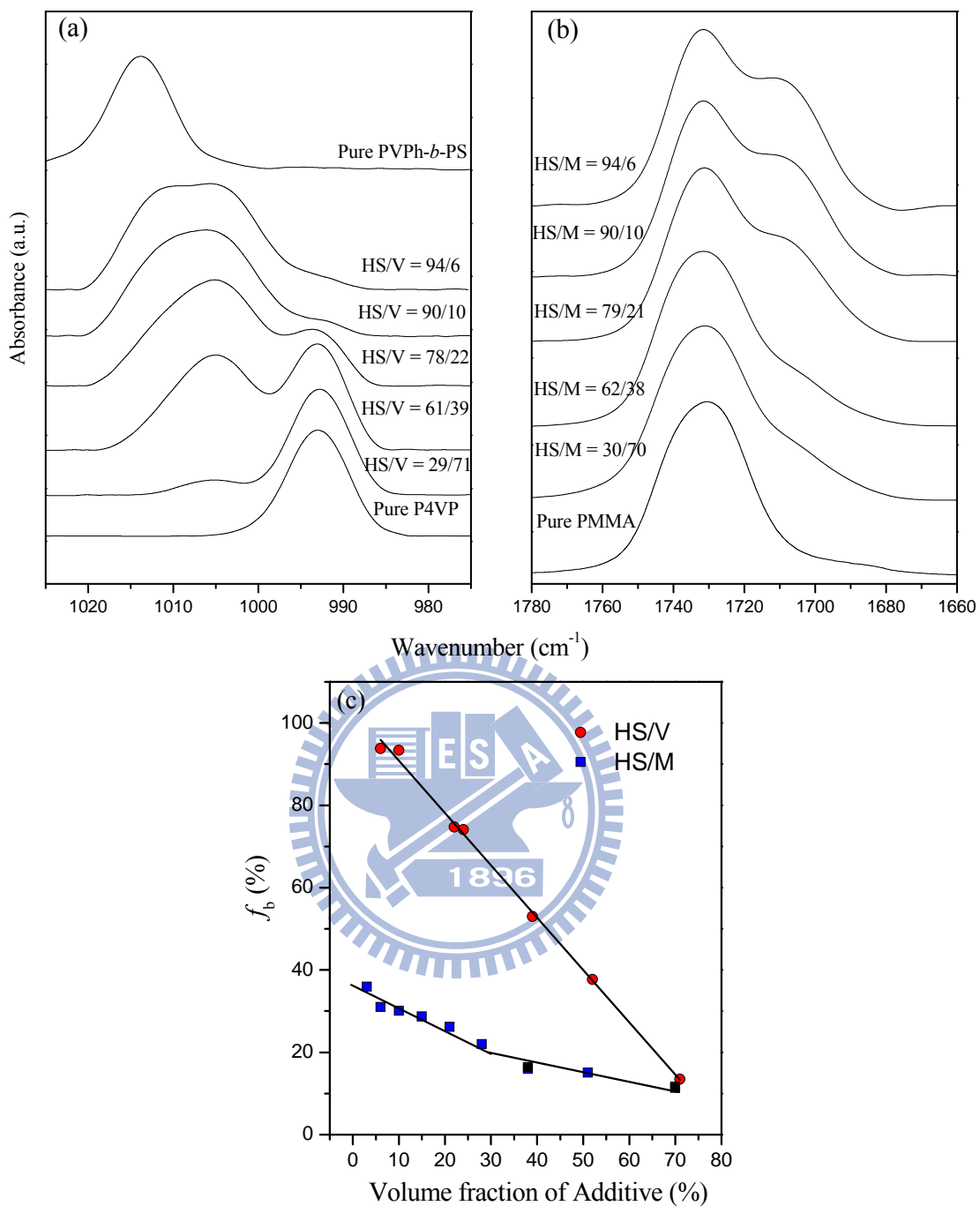


Figure 4-3. FTIR spectra recorded at 120 °C in (a) the pyridine absorption region for the HS/V blends and (b) the C=O absorption region for the HS/M blends. The compositions are indicated above the respective profiles. (c) The corresponding f_b values for the fraction of hydrogen-bonded groups. Lines drawn over the data points are only for eye-guiding. The decrease of f_b (i.e. reduction of hydrogen bonding efficiency) with increase of the homopolymer volume fraction reveals a systematically decreased miscibility in both blends.

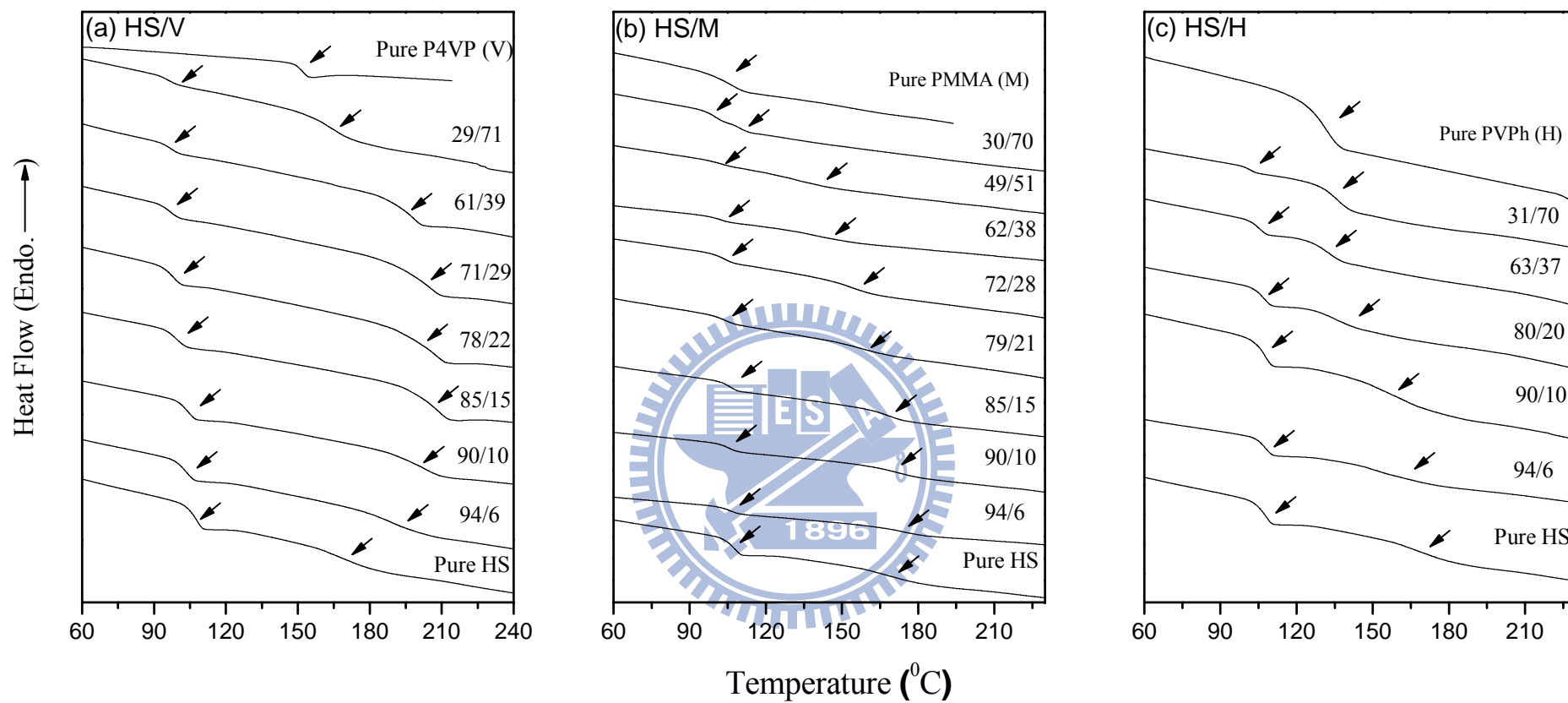


Figure 4-4. DSC traces of the (a) HS/V, (b) HS/M, and (c) HS/H blends, with the respective compositions indicated. Arrows indicate the respective T_g values.

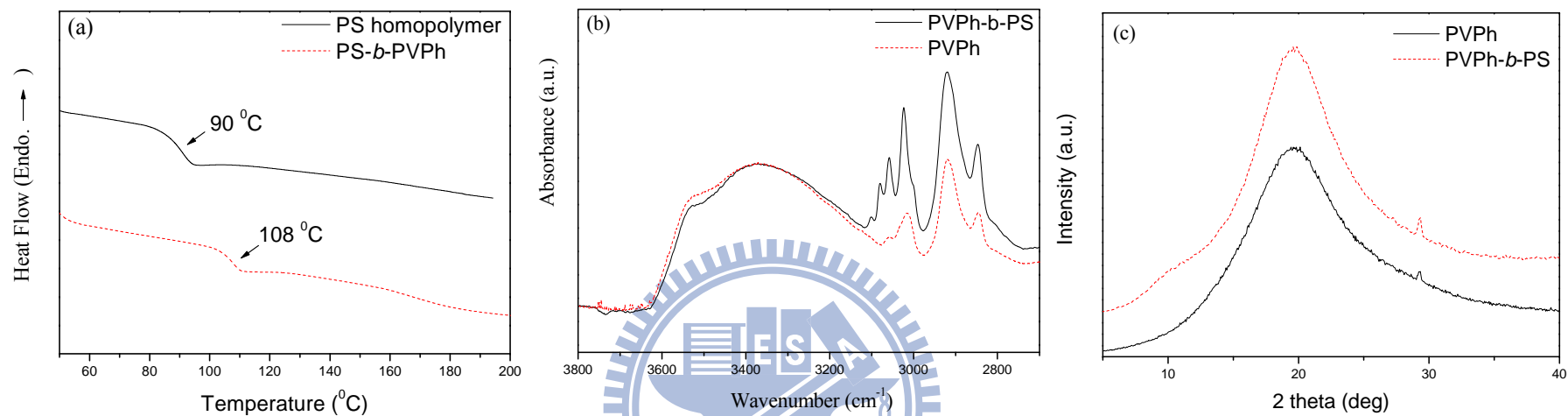


Figure 4-5: From left to right are the DSC, FTIR, and XRD results for the PVPh-*b*-PS copolymer and the PVPh homopolymer.

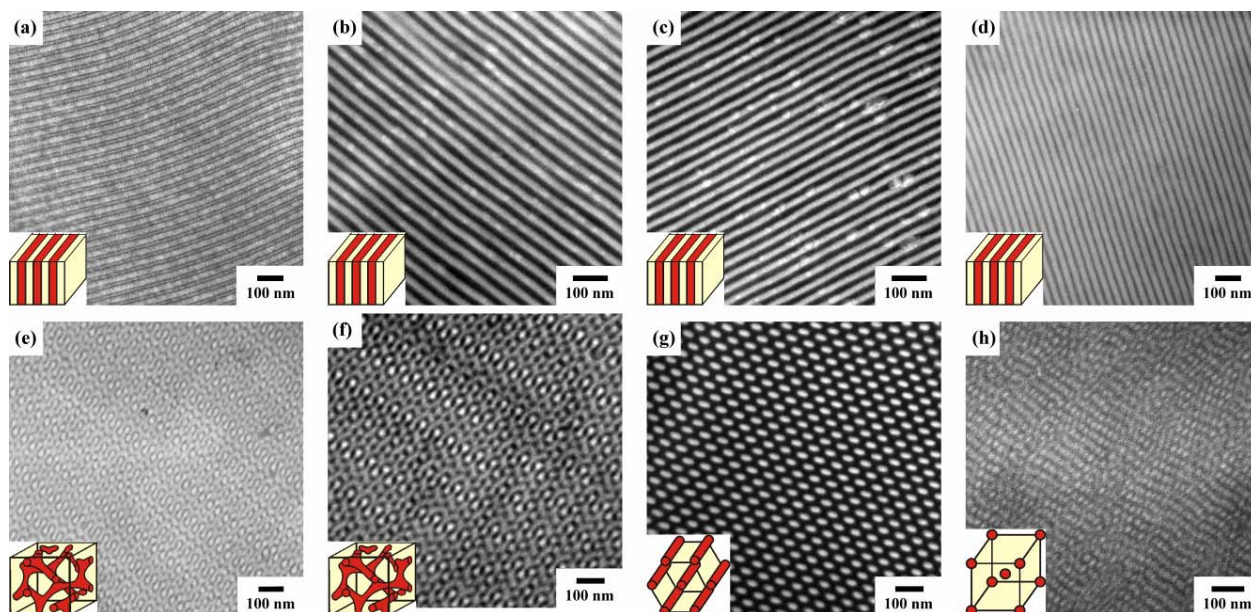


Figure 4-6. TEM images for the HS/V blends, after staining with I_2 for 24 h (the dark regions correspond to the PVPh-P4VP phase): (a) pure HS, (b) HS/V = 94/6, (c) HS/V = 90/10, (d) HS/V = 87/13, (e) HS/V = 85/15, (f) HS/V = 78/22, (g) HS/V = 71/29, and (h) HS/V = 29/71. Shown in the insets are the corresponding structures proposed.

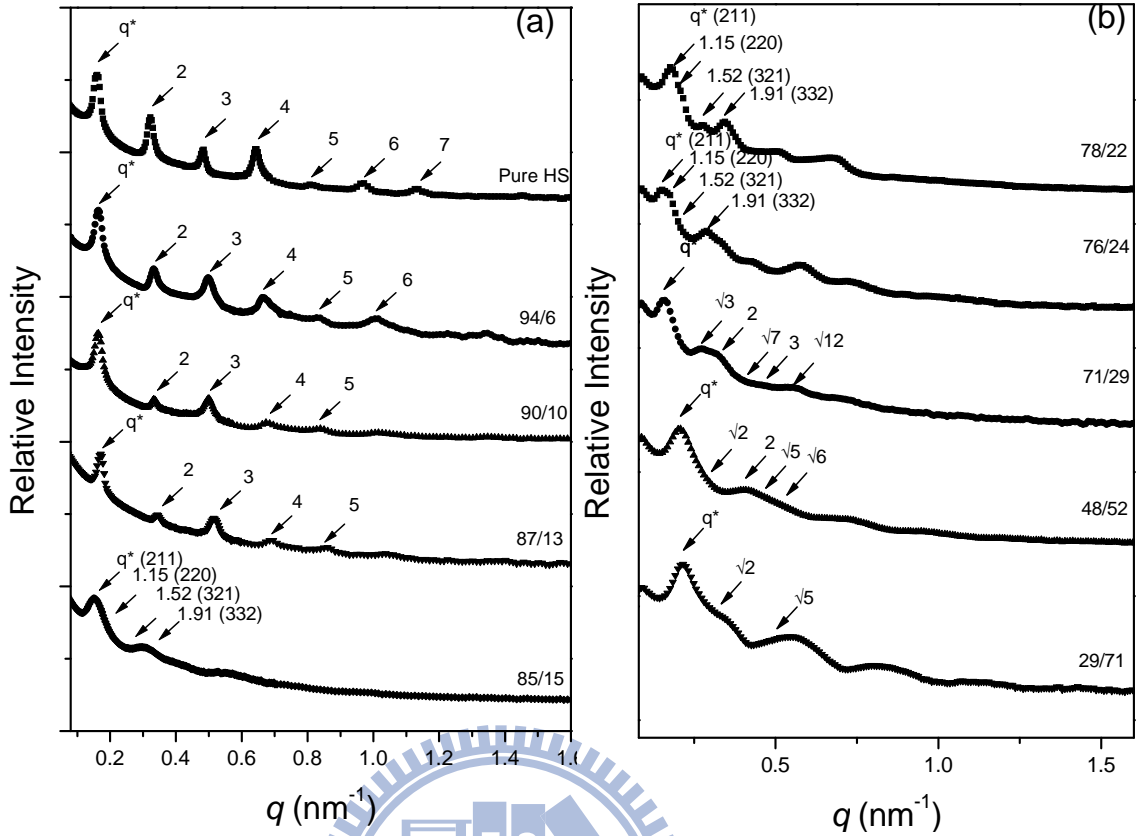


Figure 4-7. SAXS data for the pure HS and the blends HS/V = 94/6, HS/V = 90/10, HS/V = 87/13, and HS/V = 85/15 in (a), and HS/V = 78/22, HS/V = 76/24, HS/V = 71/29, HS/V = 48/52, and HS/V = 29/71 in (b). The peak ratios (relative to the first peak position marked as q^*) or reflections planes for the corresponding ordered structures are indicated by arrows.

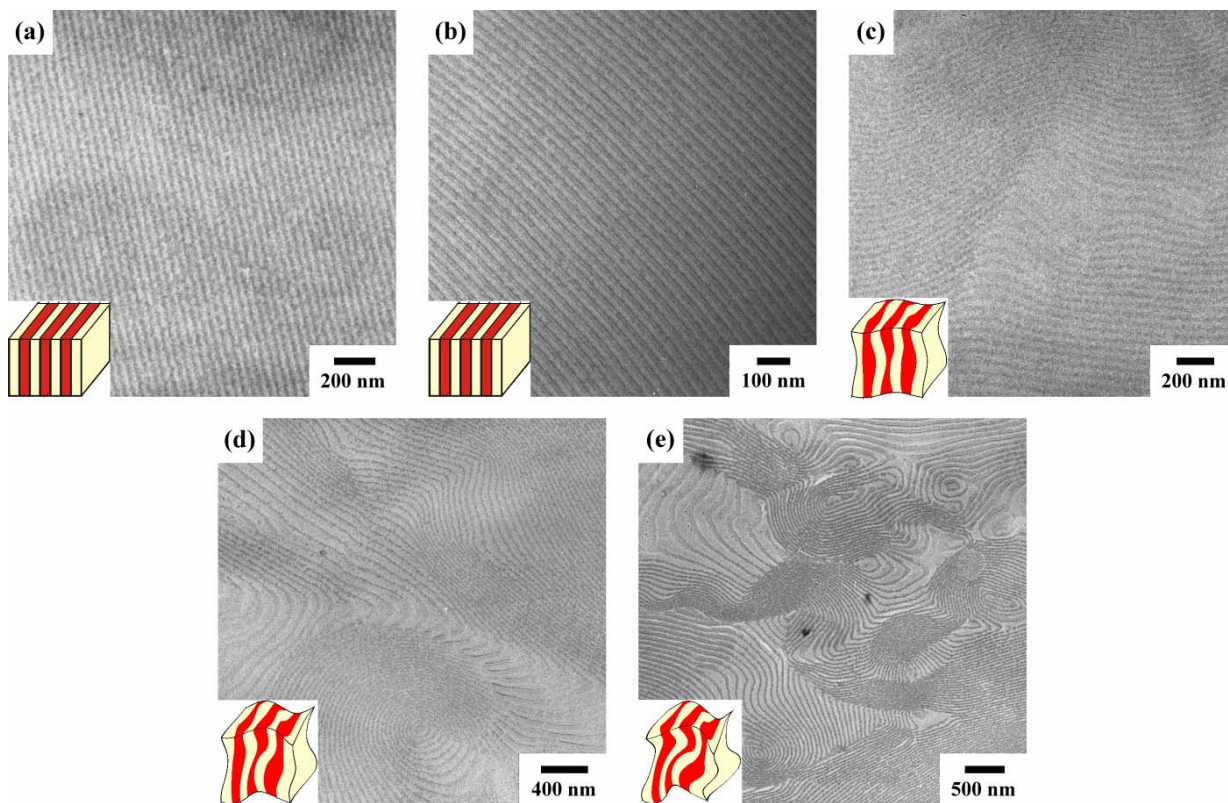


Figure 4-8. TEM images of the solution-cast films of the HS/M blends (dark regions correspond to the PS domains): (a) HS/M = 94/6, (b) HS/M = 90/10, (c) HS/M = 79/21, (d) HS/M = 62/38, and (e) HS/M = 30/70. Cartoons in the insets present the corresponding structures proposed.

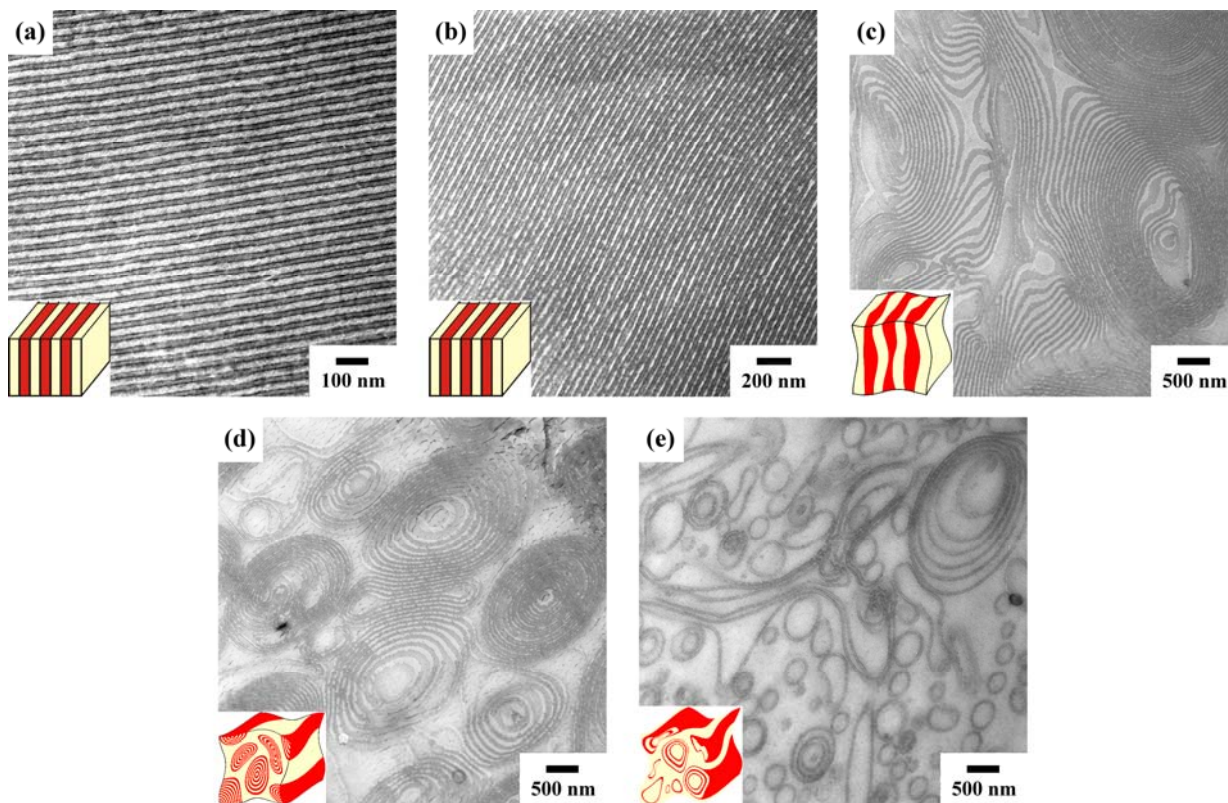


Figure 4-9. TEM images of the solution-cast films of the blends (dark regions correspond to the PS domains): (a) HS/H = 94/6, (b) HS/H = 90/10, (c) HS/H = 80/20, (d) HS/H = 63/37, and (e) HS/H = 31/69. Proposed 3-D structures are shown in the insets. Cartoons in (d) and (e) illustrate concentric tubes and hollow tubes (of a single-bilayer wall) rolled from the distorted lamellar slabs.

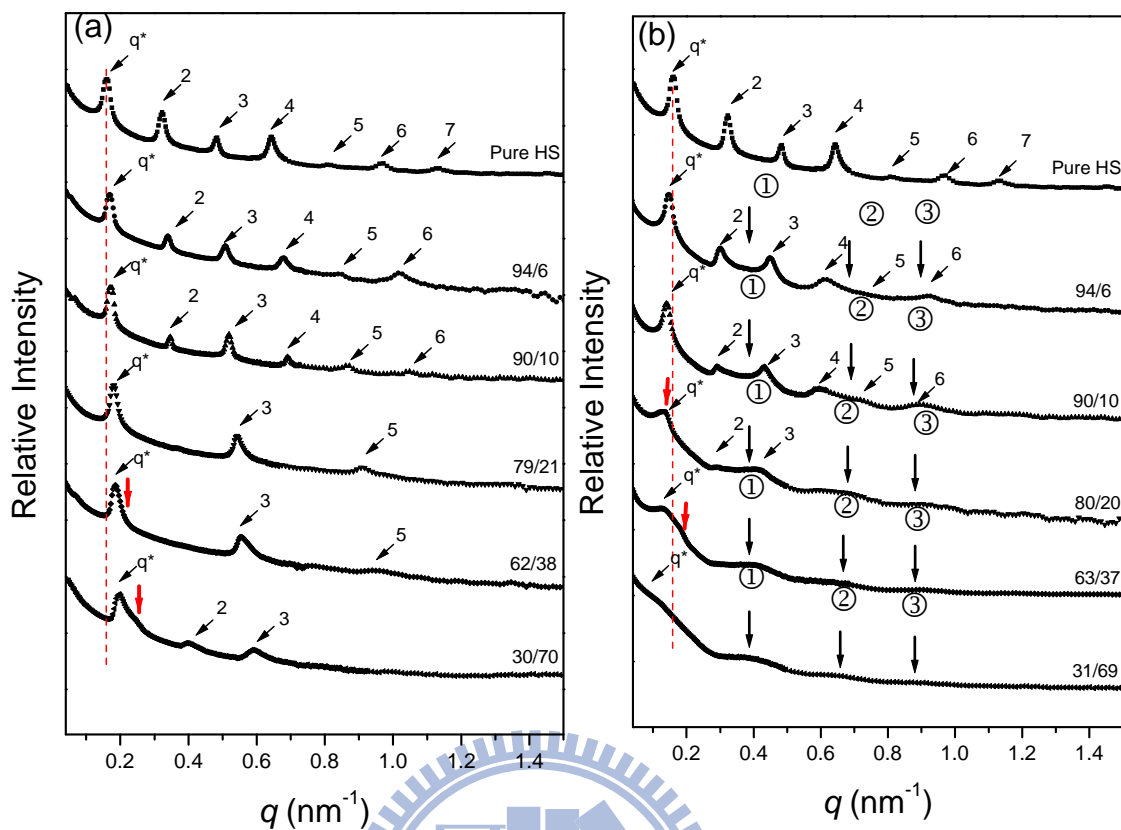


Figure 4-10. SAXS intensity profiles measured for the (a) HS/M and (b) HS/H blends, with the respective compositions indicated. The lamellar reflections are marked by the thin arrows, whereas the scattering humps from the form factor of slabs are marked with circled numbers in (b). The thick arrows nearby the first lamellar peaks indicate the coexisting of two types of lamellae. In (a) and (b) the two dotted lines across all the SAXS profiles for the HS/V and HS/M blends illustrate the opposite shifting directions of the first peak position.

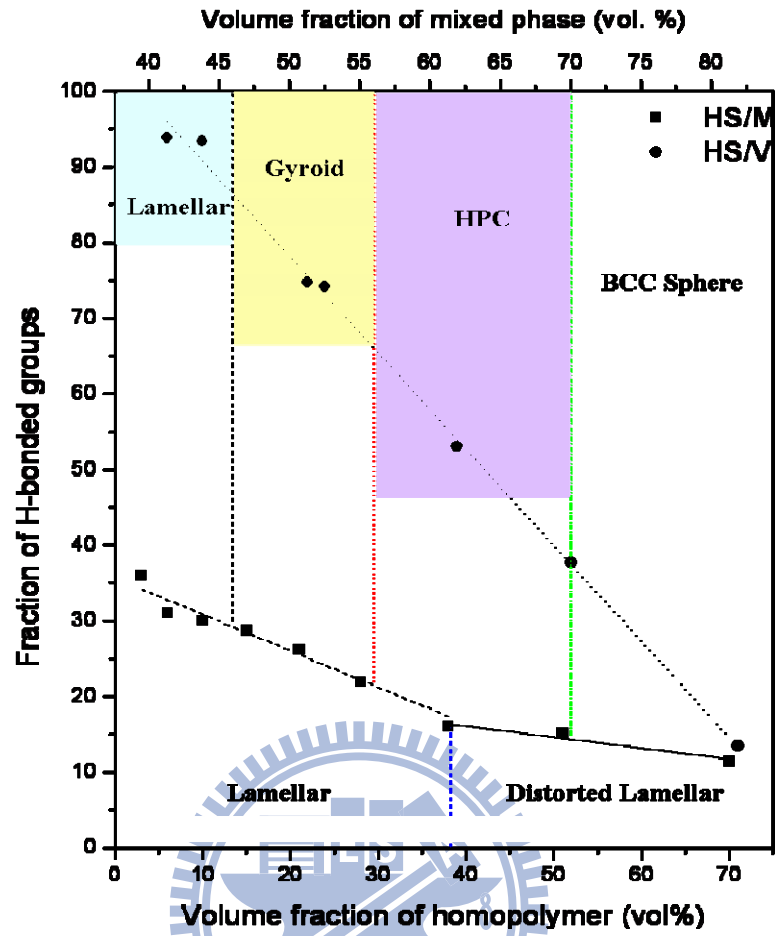


Figure 4-11. Correlation between the fraction of hydrogen bonded groups f_b deduced from FTIR and the phase behavior observed via TEM and SAXS, for the PS-*b*-PVPh-based, *A-b-B/C* type of polymer blends.

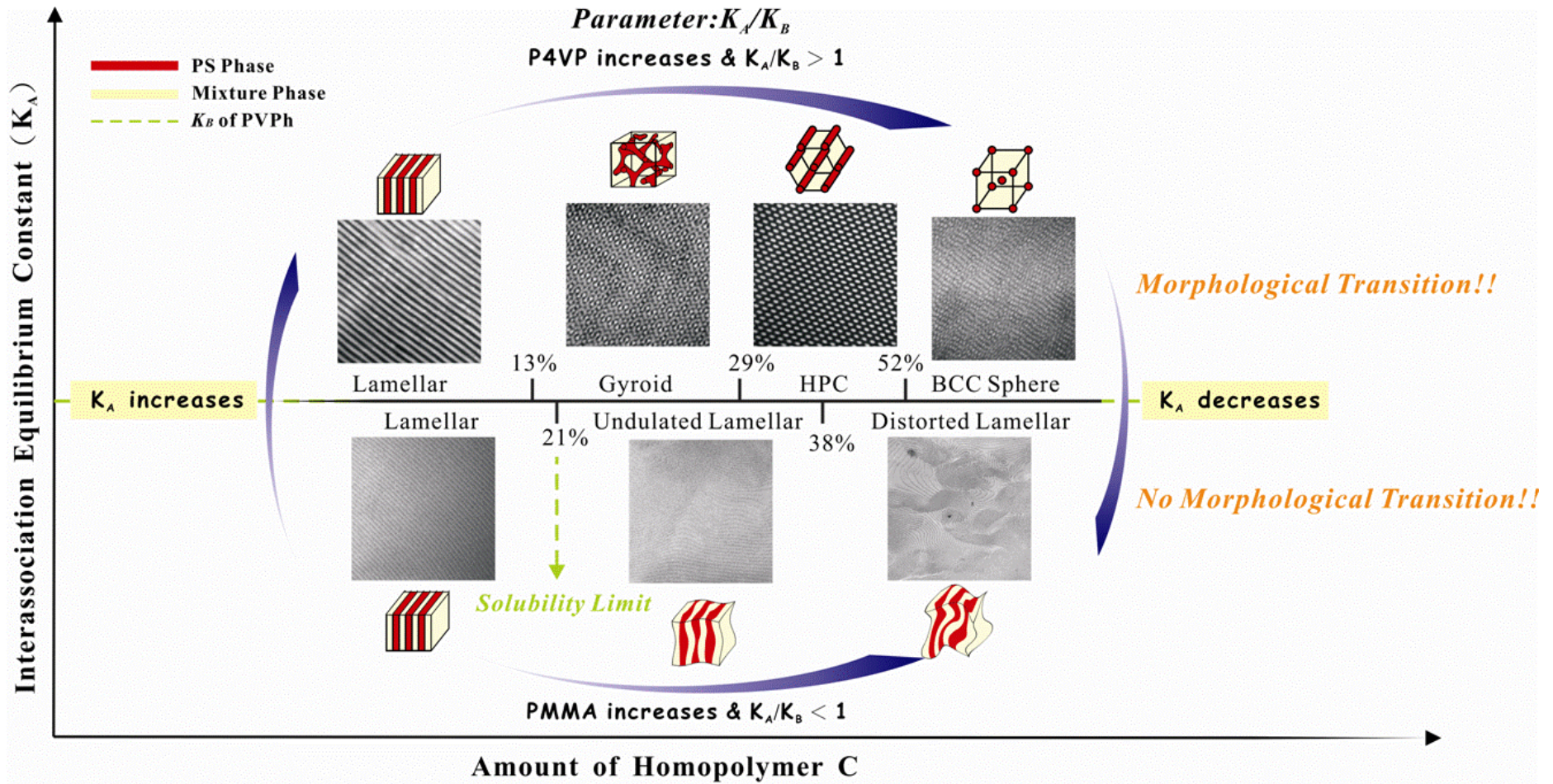


Figure 4-12. Schematic representation of an A-b-B/C blend system featuring in hydrogen bonding interactions. Note that the molar weight of the homopolymer should be comparable or smaller than that of the hydrogen-bonding associated block of the copolymer.

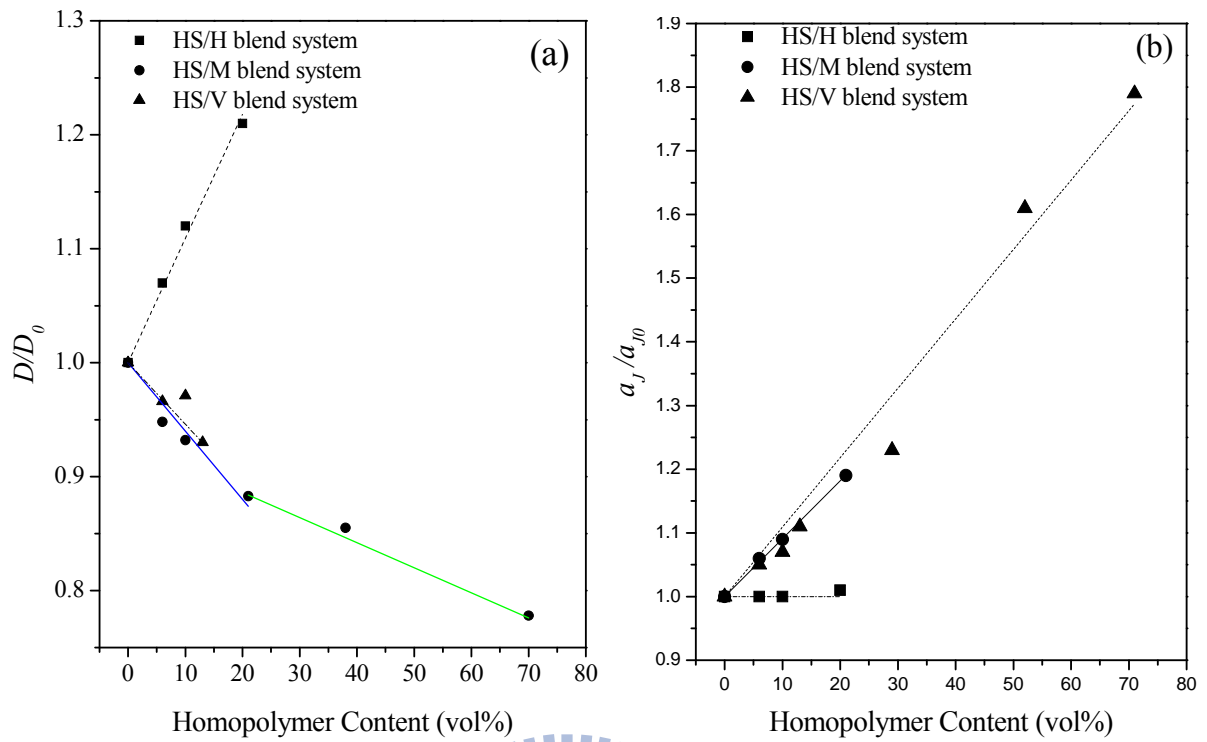


Figure 4-13. Relative changes in (a) the lamellar long period D/D_0 and (b) the average distance of the chemical junctions along the interface a_j/a_{j0} , for the HS/H, HS/M, and HS/V blends, upon addition of the homopolymer. The lines over the data points are only for eye-guiding.

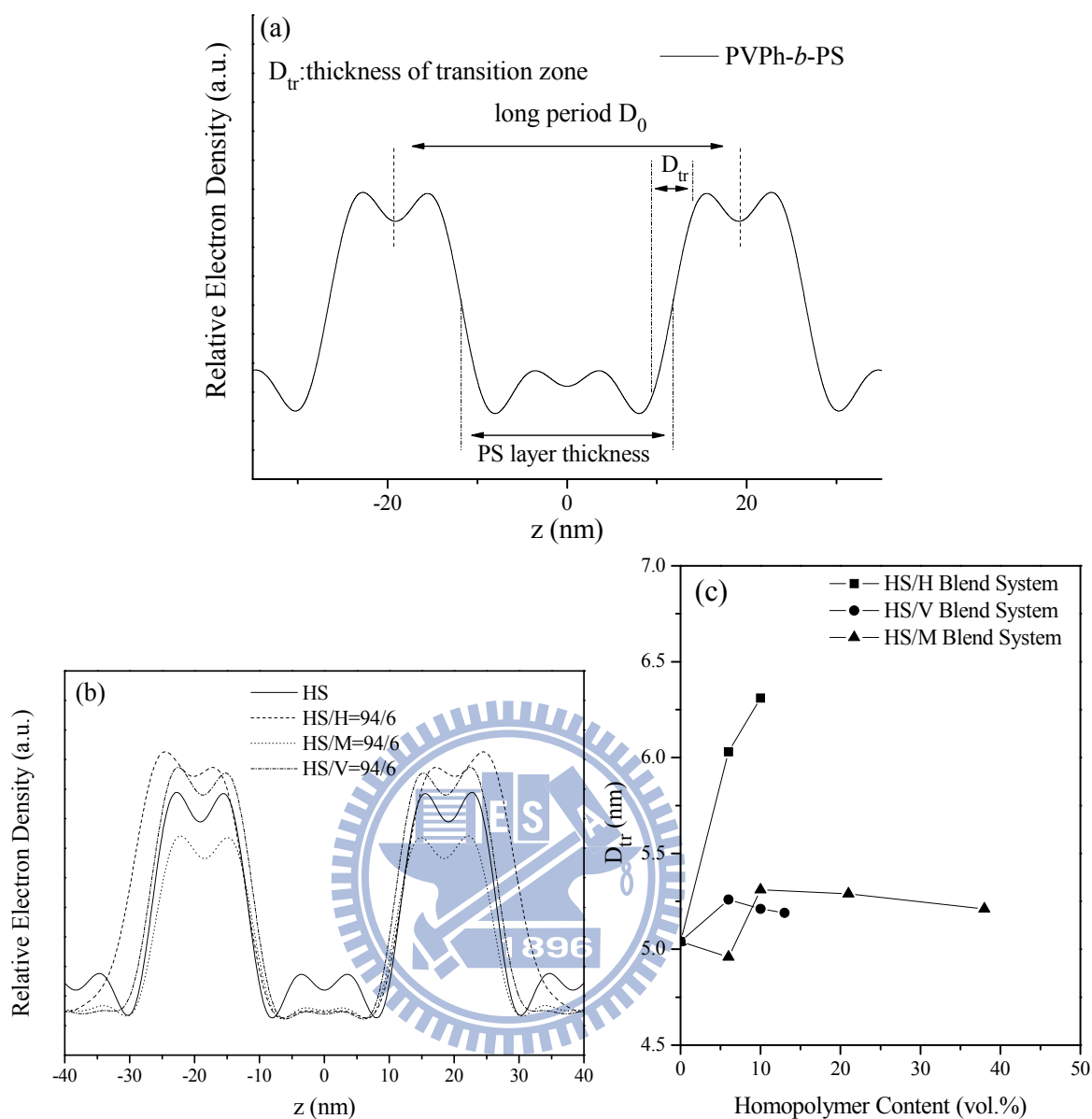


Figure 4-14. Representative relative electron density profiles of (a) the neat PVPh-*b*-PS and (b) the three blends of (b) HS/H=94/6, HS/M=94/6, and HS/V=94/6. (c) The transition zone thickness D_{tr} extracted for all the blends with a lamellar phase at lower volume fractions of homopolymers. In (a), the D_0 and D_{ps} values thus defined are consistent with the values obtained from the 1-D correlation function. The D_{tr} is defined by the zone where the electron density grows from 10% to 90% of the peak value, as illustrated.

Chapter 5

On Modulating the Self-Assembly Behaviors of Poly(styrene-*b*-4-vinylpyridine)/Octyl Gallate Blends in Solution State via Hydrogen Bonding from Different Common Solvents

Abstract

We have investigated the complexation-induced phase behavior of the mixtures of poly(styrene-*b*-4-vinylpyridine) (PS-*b*-P4VP) and octyl gallate (OG) due to hydrogen bonding in different solvents. The Fourier transform infrared spectroscopic result indicates that the hydrogen-bonding was formed between the P4VP blocks and OG in both THF and chloroform, implying the P4VP blocks can bind to OG. For PS-*b*-P4VP/OG mixture in chloroform, the morphological transitions were induced from the unimer configuration to swollen aggregate and complex-micelles by adding OG. Interestingly, the complex-micelles can lead the formation of the honeycomb structure from chloroform solution. The PS-*b*-P4VP/OG mixture in THF, behaving an amphiphilic diblock copolymer in solution state, exhibited a series of morphological transitions from sphere, pearl-necklace-like rod, worm-like rod, vesicle, to core-shell-corona aggregates by increasing the OG content. In contrast, the PS-*b*-P4VP/OG mixture in DMF maintained the unimer configuration upon adding OG. Therefore, the complexation-induced morphology of the mixtures of PS-*b*-P4VP and OG can be mediated by adopting different common solvents to affect the self-assembly behavior.

5-1 Introduction

Block copolymers are the focus of the intense research due to their ability to self-assemble into nanostructures with well-defined morphology and size. Many types of block copolymers have been synthesized and their characteristic nano- and micro-phase separation structures have been investigated in solid state and in solution state.¹⁻¹¹ Micelles are formed that consist of a core containing the insoluble blocks surrounded by a corona of the solvated blocks which exhibit fascinating structures, such as spherical, cylindrical, lamellar and vesicular micelles, etc.^{12, 13} In particular, polymeric micelles have received significant attention in drug delivery, templates for the preparation of inorganic nanoparticles including metals, metal oxides or semiconductors, and traps for environmental pollutants or metabolites due to their small size and high stability.¹⁴⁻¹⁹

It is well-known that the equilibrium aggregate morphologies in solution can be determined by the free-energy balance among three main effects: stretching of the core-forming blocks, inter-coronal interactions, and the interfacial energy between the solvent and the micelle core.²⁰ Many factors affect the above three terms, and by tuning one of these three factors, the forces balancing the micelles can be upset, leading to a transformation from one morphology into another. Examples of such factors have been investigated previously including the initial copolymer concentration in solution, common solvent used, the amount of selective solvent, block length of the copolymer, the type and amount of the adding ions (such as salt, acid, or base), etc.²¹

Recent advancement has demonstrated that the interpolymer complexation can also lead to micellization through electrostatic interaction²⁴ or hydrogen bonding²⁵. An interpolymer complexation can change significantly in terms of the polymers solubility and conformation, which facilitates the intercomplex aggregates. Meanwhile, nanostructures can also be obtained involving copolymer and low-molecular-mass compound (LMC, surfactant or organic molecules with a polar head and a nonpolar tail) that have recently been investigated

extensively and offer many possibilities to change the microstructure.²⁵ The micellization behavior of a block copolymer/LMC complex can be controlled by the amount of adding LMC, and a variation in the environment which affect the interaction between block copolymer and LMC.²⁶ Hydrogen bonds play an important role in the construction of supramolecular polymers by self-assembly due to their moderate bonding energy offering the flexibility for association and dissociation processes.²⁶ It is well-known that the strength and extent of hydrogen bonding in copolymers or polymer blends depends on their respective affinities between the hydrogen bond donors and acceptors.^{11, 28-31} In addition, the solvent medium plays other important role to affect or control the type of complex formation. In our previous studies,^{30, 31} different morphologies used formed from the mixtures of PVPh-*b*-PS and PMMA-*b*-P4VP due to the different chain behaviors of PVPh/P4VP block mixtures in different common solvents. The hydrogen bonding interaction between PS-*b*-PVPh and PMMA-*b*-P4VP in DMF solution is relatively weaker than that in THF solution. As a result, the interpolymer hydrogen-bonded complexation core of PVPh and P4VP chains more stretching, and thus vesicular complexes were formed surrounded by PMMA and PS chains in THF solution. In contrast to the THF solution, DMF solution had relatively lower degree of stretching of the core chains (PVPh/P4VP) and stronger repulsion of the coronal chains (PS and PMMA), consequently, spherical micelles were formed with PVPh/P4VP as the core and PS/PMMA as the corona.

In the present study, we will report that the diverse micellization behaviors can be controlled via introducing octyl gallate (OG) into PS-*b*-P4VP solution in different common solvents (chloroform, DMF, and THF). The solubility of the different common solvents for PS-*b*-P4VP and OG will affect the strength of hydrogen bonding between the P4VP block and OG and the self-assembly behaviors in solution state. As a result, the various micellization behavior can be obtained through using different common solvents.

5-2 Experimental Section

5-2.1 Material and Synthesis of Block Copolymer

The styrene monomers (Aldrich, 99%) and 4-vinylpyridine (Aldrich, 99%) were distilled from the finely ground CaH_2 before use. Tetrahydrofuran (THF) as the polymerization solvent for anionic polymerization was purified by distillation under argon from the red solution obtained by diphenylhexyllithium (produced by the reaction of 1,1-diphenylethylene and *n*-BuLi). *sec*-Butyllithium (Acros, 1.3 M in cyclohexane) was used as the initiator for anionic polymerization. Octyl gallate (OG, 99%) was purchased from Fluka, was recrystallized from an ethanol/chloroform (9:1 volume ratio) azeotropic mixture prior to use. Poly(styrene-*block*-4-vinylpyridine) diblock copolymer was synthesized through sequential anionic polymerization of 4-vinylpyridine followed by styrene using *sec*-butyllithium as the initiator. After the polymerization was complete and quenched with degassed methanol, the polymerization was precipitated in methanol and dried in a vacuum.³² The sample was characterized by gel permeation chromatography (GPC) using a Waters 510 HPLC equipped with a 410 differential refractometer, a refractive index (RI) detector, and, an UV detector. Three Ultrastyrigel columns (100, 500, and 103 Å) connected in series in order of increasing pore sizes using THF as an eluent at a flow rate of 0.6 mL/min, and polystyrene standards were employed for column calibration. And the molecular molar fraction was determined from the relative intensity of ^1H peaks of the aromatic ring and the hydrogen of the vinylpyridine units which was recorded on the INOVA 500 in chloroform-*d* at room temperature.

5-2.2 Preparation of the PS-*b*-P4VP Aggregates by Adding OG

PS₆₁-*b*-P4VP₉₁ and OG with different molar ratio *R* of 4VP/OG (the ratio of OG/PVP is named *R*) ranging from 1/100 to 1 and were dissolved together in chloroform (THF or DMF), and the solutions were stirred for more than 2 days at room temperature. These P4VP blocks

are expected to interact with the OG through complementally hydrogen bonding interaction. Scheme 1 presents the hydrogen bonding interaction between P4VP block and OG. All initial copolymer concentrations were maintained at 1mg/2ml.

5-2.3 Characterization Methodology

^1H and ^{13}C NMR spectra were obtained using an INOVA 500 instrument. The molecular weights and PS/P4VP ratios of the various copolymers were evaluated from ^1H NMR spectra and compared with the corresponding values obtained from GPC analysis. Infrared spectra were recorded at 25 °C at a resolution of 1cm^{-1} on a Nicolet AVATAR 320 FTIR spectrometer using polymer films cast onto KBr pellets from solutions. All FTIR spectra were obtained within the range $4000\text{-}400\text{ cm}^{-1}$; 32 scans were collected at a resolution of 1 cm^{-1} purged with nitrogen to maintain the film's dryness. The hydrodynamic diameters of the assemblies were measured by DLS using a Brookhaven 90 plus model equipment (Brookhaven Instruments Corporation, USA) with a He-Ne laser with a power of 35 mW at 632.8 nm. All DLS measurements were carried out with a wavelength of 632.8 nm at 25°C with 90° angle of detection. All samples were measured five times. In transmission electron microscopy (TEM) studies, a drop of the micelle solution was sprayed onto a Cu TEM grid covered with a Formvar support film that had been precoated with a thin film of carbon. After 1 min, the excess of the solution was blotted away using a strip of filter paper. All samples were left to dry at room temperature for 1 day prior to observation. After drying, the samples were stained with RuO_4 and viewed under a Hitachi H-7500 TEM instrument operated with an accelerating voltage of 100 kV. The contact angle of the polymer sample was measured at 25 °C using a Krüss GH-100 goniometry interfaced with image-capture software by injecting a 5 μL liquid drop.

5-3 Results and Discussion

5-3.1 Synthesis of Poly(styrene-*block*-4-vinyl pyridine) Diblock Copolymer

The PS-*b*-P4VP diblock copolymer with molecular weight of 15900 g.mol⁻¹ and narrow molecular weight distribution (PDI = 1.12) was prepared through anionic living polymerization. ¹H and ¹³C NMR spectra were recorded for PS-*b*-P4VP sample to confirm its chemical composition and structure. Figure 5-1a displays typical ¹H NMR spectrum of the diblock copolymer with assignments of its characteristic peaks. The signals due to the aromatic protons and the pyridine ring were observed at 6.1–6.9 ppm and 8.2-8.5 ppm, respectively. Figure 5-1b displays the ¹³C NMR spectra of the PS-*b*-P4VP copolymer where the signals corresponding to the aromatic carbons and the pyridine ring were observed at 120–130 ppm and 150 ppm, respectively. Thus, we confirmed that the PS-*b*-P4VP diblock copolymer was successfully synthesized through the anionic living

5-3.2 FTIR Analyses

Figures 5-2a and 5-2b present the stretching band of the pyridine groups (1580-1640 cm⁻¹) of the pure P4VP and the mixtures of PS-*b*-P4VP and OG with various molar ratios cast from THF and chloroform solutions at room temperature. The pyridine band at 1597 cm⁻¹ shifted to higher wavenumbers upon adding the OG, indicating that the hydrogen bonding between the pyridine groups of the P4VP blocks and the OH groups of the OG was formed.³³ Furthermore, Figures 5-2c and 5-2d show the IR spectra of the pyridine ring absorption region (980-1020 cm⁻¹) of the pure P4VP and the mixtures of PS-*b*-P4VP and OG with various molar ratios cast from THF and chloroform solutions at room temperature. Pure P4VP has a characteristic band at 993 cm⁻¹, corresponding to the uncomplexed pyridine ring absorption. The new band at 1005-1010 cm⁻¹ is assigned to hydrogen-bonded pyridine units, and its intensity increases upon the increase OG content in comparison to the PS-*b*-P4VP copolymer.³³ As a result, we can confirm that the complex of the OG and P4VP segment are

indeed formed due to the stronger hydrogen-bonding interaction between the hydroxyl groups of the OG and pyridine groups of P4VP.

5-3.3 Characterization of the PS-*b*-P4VP / OG Aggregates in Chloroform.

The copolymer mixtures were analyzed by dynamic light scattering (DLS). The experimental correlation function was analyzed by the method of the Cumulant and by the CONTIN algorithm, as reported elsewhere.² The Stokes–Einstein approximation was used to convert the diffusion coefficient into the hydrodynamic diameter (D_h). Figures 5-3 and 5-4 present the hydrodynamic diameters and light scattering intensities of the pure PS-*b*-P4VP and mixtures of the PS-*b*-P4VP and the OG with various molar ratios (R) at a given constant concentration in chloroform. The copolymer without containing OG (Figure 5-3a) was dissolved in chloroform molecularly as unimer, with D_h of around 8-12 nm and very low scattering intensity. The addition of the OG resulted in D_h increase at $R < 1/10$ due to binding between polymer and OG which has also been observed for various other blend systems.³⁴ Figures 5-3b and 5-3c show that the hydrodynamic diameter distributions for mixtures of PS-*b*-P4VP and OG at $R < 1/10$ in chloroform are bimodal at 8-12 nm and 120-265 nm. As the R is less than 1/10, the content of the OG is lower in system, the free unbound polymer chains and those bound with OG in solution are coexisted. The interaction between PS-*b*-P4VP and OG leads to the formation of aggregates composing of the P4VP/OG-complex core and PS-corona in the system because the solubility of the bound polymer chains becomes relatively lower. As a result, the bimodal distributions corresponding to free unbound polymer chains (8-12 nm) and aggregates of the OG bound polymers are formed. However, the scattering intensity was low even though the aggregates were formed in the system at $R < 1/10$, implying that the structure of these aggregates were loose and unstable because the amount of the pyridine groups of P4VP blocks was too low to form dense and stable micelles. With further increasing the OG content, the D_h decreased

remarkably to 40 nm. While the scattering intensity sharply increased, and the aggregates showed a remarkably narrow size distribution. This result indicates that these aggregates became denser with a well-defined structure, as a result of the formation of micellization. The insolubility of the bound pyridine units due to enough bound pyridine groups drives the aggregation of the P4VP/OG complex to form the micellization with further increase in OG content. ^1H spectra data provided further evidence to demonstrate the formation of complexation between the P4VP blocks and OG.

Figure 5-5 presents the ^1H NMR spectra of the pure PS-*b*-P4VP and mixtures of the PS-*b*-P4VP and OG with the different R in CDCl_3 . The intensity of the signals due to H_d of P4VP at 8.2-8.5 ppm was depressed at $R = 1/20$, finally, it totally disappeared at $R = 1$. Additionally, at $R = 1$, the intensity ratio of H_e to H_c comes close to 3/2, corresponding to the number ratio of the H_e to H_c in the benzene rings. These ^1H spectra data indicate that the formation of aggregates between the bound P4VP blocks caused depression or even disappearance of P4VP signals because the mobility was restricted.

The morphologies of these non-covalent complex aggregates were investigated by transmission electron microscopy (TEM). Figure 5-6 presents the TEM images for mixtures of the PS-*b*-P4VP and OG with different molar ratios R from chloroform solutions. At $R = 1/50$, the aggregates possess diameter about 300 nm and weak contrast, indicating that the structure of these aggregates were loose and polydisperse. As the R was increased to 1/10, the aggregates showed dual size distribution, one has a diameter about 200 nm, and another possesses a diameter about 50 nm. The former aggregates correspond to the loose structure, whereas the latter arose from the dense micelles due to enough bound pyridine units. When the R was increased to 1/3 and 1, these structures showed uniform size and well-defined shape spheres. These TEM images are consistent with the DLS results, implying that the complexation-induced micellization by hydrogen-bonding indeed occurred.

Figure 5-7 shows various SEM images of cast films for mixtures of PS-*b*-P4VP and OG

with different molar R in chloroform solution after solvent evaporation. No morphology was observed from the PS-*b*-P4VP without containing OG from chloroform solution as shown in Figure 5-7a. Most interestingly, the honeycomb-structured porous films were obtained by adding the OG. At $R = 1/100$, the broken and imperfect porous film was obtained. With increasing the OG content to $R=1/50$, only irregular pores were formed. Further increasing the molar ratio R from 1/50 to 1/10, 1/3, and 1, the degree of the regularity of the porous film increased remarkably, and the pore size decreased. Additionally, Fast Fourier transfer (FFT) pattern (Figure 7, inset images) also indicated a hexagonal arrangement of the pores formed on the surface, while the regularity of the porous film increased upon increasing the OG content.

By casting onto solid substrates, these aggregates spontaneously converted into honeycomb structure. The spherical shape of the porous structure reflected the shape of template water droplets and the observed honeycomb architecture was formed by the “breath figures” method. According to the “breath figures” mechanism, the water droplets act as the template to form the honeycomb structure, and the stabilization of the water droplets is the crucial point for preparing a regular honeycomb structure. The interfacial activity of the various aggregates of different mixtures provided different degrees of the stabilization of the water droplets and resulted in the different structures. It is well-known that the ability of adsorbed aggregates to stabilize the water-solution interface is relative to the aggregates wettability. The wettability of the aggregates at the solvent-water interface can be quantified by the corresponding interfacial contact angle θ_{ws} , which can be calculated according to the modified Young’s equation:^{41, 47}

$$\theta_{ws} = \cos^{-1} \left[\left(\gamma_w \cos \theta_w - \gamma_s \cos \theta_s \right) / \gamma_{w/s} \right] \quad (5-1)$$

where γ_w and γ_s are the surface tensions of water and solution, respectively, $\gamma_{w/s}$ is the interfacial tension between water and solution, and the static contact angles of water and

chloroform (θ_w and θ_s) can be measured on the flat film of nanoparticles, respectively. If the particles are either too hydrophilic or too hydrophobic, they tend to remain dispersed in either the aqueous ($\theta_{ws} < 90^\circ$) or the oil phase ($\theta_{ws} > 90^\circ$) and cannot sufficiently stabilize the water droplets. The wettability of the aggregates is believed to play an important role for forming a honeycomb structure.

The wettability of the aggregate with the different molar ratio R at the water-solvent interface could be quantified by the corresponding contact angles, and the θ_{ws} can be calculated according to eq. 1 by measuring the contact angles on the flat films.^{42, 48} We measured the θ_w and estimated $\theta_s \doteq 0$ for chloroform entirely wets all film surfaces of these aggregates. The θ_w and the corresponding calculated contact angles θ_{ws} at the interface between water and chloroform are summarized in Table 5-1. The θ_w gradually decreased from 105 to 70° upon increasing R from 1/100 to 1. The θ_{ws} values cannot be obtained at $R = 1/100$ and 1/50, implying that the loose aggregates tended to disperse in the chloroform phase due to the high hydrophobicity and cannot stay at the water/chloroform interface for stabilizing the water droplets. As expected, the irregular porous films with a relatively broad distribution of the pore size were induced because of the fusion of the water droplets. With further increasing R to 1/10, 1/3, and 1, the θ_{ws} progressively decreased to close 90°, reflecting that the hydrophobicity of the aggregates decreased as the loose aggregates became the dense micelles, and these micelles effectively stabilized the water droplets and preserved the structure of the porous film during drying. Then, an order honeycomb was obtained as shown in Figure 5-7f. As a result, the dense and mono-disperse micelles have a suitable wettability to stabilize the water droplets to prevent the condensation of water droplets; however, the loose structure contained a lot of solvent and became too hydrophobic to stabilize the water droplets. In summary, the mixtures with the different R can self-assemble the different aggregates which possess the different wettability and provide the porous films with the various regularity.

5-3.4 Characterization of the PS-*b*-P4VP / OG Aggregates in THF and DMF.

Now, we turn our attention to the behaviors of the mixtures of the PS-*b*-P4VP and OG with the different R in THF solutions. Figure 5-8 presents the ^1H NMR spectra of the pure PS-*b*-P4VP and mixtures of the PS-*b*-P4VP and OG with the different R in THF-*d*. The unusual phenomenon was obtained that the intensity of signals due to H_d of P4VP at 8.2-8.5 ppm increased with increasing the OG content, and the intensities of the signals due to H_c and H_e were depressed. These results indicated that the P4VP blocks had the reverse behavior and became more mobile by adding OG. Thus, the core-domains composed of P4VP and bound P4VP blocks were swollen and increased the mobility.

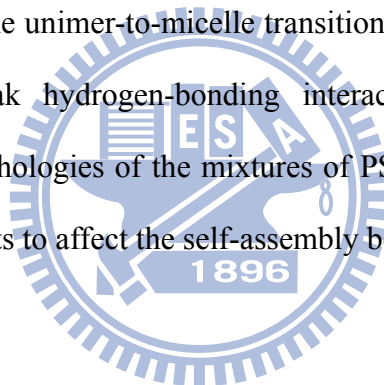
Figure 5-9 shows the TEM images for various morphologies formed from the mixtures of the PS-*b*-P4VP and OG with different R in THF. Nano-spherical micelles of the PS-*b*-P4VP without OG were formed as shown in Figure 5-9a, implying that the THF has the different selectivity for the PS and P4VP block (i.e. the THF has a better solubility for the PS blocks) resulting in the formation of the micelles. At $R = 1/50$, the morphology of the mixture maintained the spherical micelle. At $R = 1/20$, the aggregates transformed into coexisting pearl-necklace-liked rod micelles and spherical micelles as shown in Figure 5-9c. On further increasing the OG content, the morphology of the aggregates changed to the worm-like micelles at $R = 1/10$, then to the vesicular aggregates at $R = 1/5$. Most interestingly, at $R = 1$, the morphology of the aggregates transferred to an unusual structure which was similar to core-shell-corona structure as shown in Figure 5-9f.

It is well-known that several factors influence the morphologies of block copolymer aggregates in a solution;^{21, 32, 50} the free energies of aggregation are affected by the inter-coronal chain interaction, the core-coronal interfacial energy, and the degree of core-chain stretching. Here, the OG moieties were capable of forming strong hydrogen-bonding interaction with P4VP blocks. Based on the NMR analysis, the OG could increase the size of the core and promote the architectural changes. In addition, it is believed

that the long tail of OG could reduce the inter-coronal chain interaction by providing the more space between the corona chains due to their hydrophobic character. The degree of P4VP stretching increases in response to the increase in the core diameter. This increased chain stretching is subject to an entropic penalty, and in the present system the aggregates undergo morphological change in order to relieve this entropy strain. For core-shell-corona aggregates at $R = 1$, we speculated that the excess of OG would fill the core (i.e. P4VP phase) of the vesicles and remarkably swell the core domain, thus, core, shell, and corona are composing of PS/P4VP/OG, P4VP/OG, and PS/P4VP/OG, respectively, shown in Figure 5-11. Consequently, the addition of OG can induce a series of morphological transition from sphere, pearl-necklace-liked rod, worm-liked rod, vesicle, to core-shell-corona aggregates, indicating that the morphologies can be controlled by changing the OG content. Meanwhile, the mixtures of the PS-*b*-P4VP and OG with the different R in DMF solutions were studied. Figure 5-10 displays the hydrodynamic diameter and light scattering intensities of the mixtures of the PS-*b*-P4VP and OG with the different R in DMF. The D_h maintained the similar value upon adding the OG and even at $R = 1$, and the intensity was weak, indicating that the addition of the OG cannot lead any self-assembled aggregates in DMF. Taft et al. demonstrated that the solvatochromic comparison method was used to unravel, quantify, correlate and rationalize multiple solvent effects on many types of physicochemical properties and presented reactivity parameters, and comprehensive collection of π^* , α , and β values.⁵¹⁻⁵² The π^* scale is an index of solvent dipolarity/polarizability, which was measured the ability of the solvent to stabilize a charge or a dipole by virtue of its dielectric effect. The α scale of solvent HBD (hydrogen-bond donor) acidities describes the ability of the solvent to donate a proton in a solvent-to-solute hydrogen bond. The β scale of HBA (hydrogen-bond acceptor) basicities provides a measure of the solvent's ability to accept a proton (donate an electron pair) in a solute-to-solvent hydrogen bond. Due to Taft's reports,⁵¹⁻⁵² the values of β of chloroform, THF, and DMF are 0.00, 0.55, and 0.69, respectively, and the values of π^* of

chloroform, THF, and DMF are 0.58, 0.58, and 0.88. The values of β and π^* indicate that chloroform and THF is less polar than DMF, and DMF has higher hydrogen-bond-acceptor ability than chloroform and THF. Thus, we speculated that the hydrogen-bonding between the P4VP blocks and OG were less efficiently formed due to the polarity of DMF, thus, the relatively weak interaction between the P4VP blocks and OG cannot form aggregates.

In summary, Figure 5-11 displays our proposed mechanism for the morphologies of the mixtures of the PS-*b*-P4VP and OG from the different solvent. For chloroform system, the self-assembled nano-objects were formed by adding OG, and the honeycomb structures were obtained through these aggregates acting as the stabilizer for the water droplets. For THF system, a series of morphological transition was induced to reduce the free energy of the system. For DMF system, the unimer-to-micelle transition cannot be lead through adding OG due to the relatively weak hydrogen-bonding interaction in DMF. As a result, the complexation-induced morphologies of the mixtures of PS-*b*-P4VP and OG can be mediated by adopting different solvents to affect the self-assembly behavior.



5-4 Conclusions

Hydrogen bonding between P4VP blocks of PS-*b*-P4VP diblock copolymer and OG in different solvents results in various complexation-induced micellization. Both FTIR and NMR analyses provided evidence for the formation of the P4VP binding to OG due to hydrogen bonding between the P4VP blocks and OG. Integrated results of TEM images and DLS data clearly show that the self-assembly behaviors of the mixtures of the PS-*b*-P4VP and OG can be modulated via adopting the different solvents. For PS-*b*-P4VP/OG mixture in chloroform, the morphological transitions were induced from the unimer configuration to swollen aggregate and complex-micelles by adding OG. Interestingly, the complex-micelles can lead the formation of the honeycomb structure from chloroform solution. The PS-*b*-P4VP/OG mixture in THF, behaving an amphiphilic diblock copolymer in solution state, exhibited a series of morphological transitions from sphere, pearl-necklace-like rod, worm-like rod, vesicle, to core-shell-corona aggregates by increasing the OG content. In contrast, the PS-*b*-P4VP/OG mixture in DMF maintained the unimer configuration upon adding OG due to relatively weak hydrogen-bonding.

References:

- [1] Patten, T. E.; Matyjaszewski, K. *Adv. Mater.* **1998**, *10*, 901.
- [2] Sakurai, S.; Kawada, H.; Hashimoto, T. Fetter, L. J. *Macromolecules* **1993**, *26*, 5796.
- [3] Hamley, I. W. *The Physics of Block Copolymers* (Oxford University Press, New York, 1998).
- [4] Kreutzer, G.; Ternat, C.; Nguyen, T. Q.; Plummer, C. J. G.; Manson, J.-A. E.; Castelletto, V.; Hamley, I. W.; Sun, F.; Sheiko, S. S.; Herrmann, A.; Ouali, L.; Sommer, H.; Fieber, W.; Velazco, M. I.; Klok, H.-A. *Macromolecules* **2006**, *39*, 4507.
- [5] Cong, Y.; Li, B.; Han, Y.; Li, Y.; Pan, C. *Macromolecules* **2005**, *38*, 9836.
- [6] He, H.; Huang, L.; Liang, H.; Pan, C. *J. Chem. Phys.* **2003**, *118*, 9861.
- [7] Hadjichristidis, N.; Iatrou, H.; Pitsikalis, M.; Pispas, S.; Avgeropoulos, A. *Prog. Polym. Sci.* **2005**, *30*, 725.
- [8] Khelfallah, N.; Gunari, N.; Fischer, K.; Gkogkas, G.; Hadjichristidis, N.; Schmidt, M.; *Macromol. Rapid Commun.* **2005**, *26*, 1693.
- [9] Asari, T.; Matsuo, S.; Takano, A.; Matsushita, Y. *Macromolecules*, **2005**, *38*, 8811.
- [10] Zheng, R.; Liu, G.; Yan, X. *J. Am. Chem. Soc.* **2005**, *127*, 15358.
- [11] Chen, S. C.; Kuo, S. W.; Jeng, U S.; Su, C. J.; Chang, F. C. *Macromolecules* **2010**, *43*, 1083.
- [12] Rodríguez-Hernández, J.; Chécot, F.; Gnanou, Y.; Lecommandoux, S. *Prog. Polym. Sci.* **2005**, *30*, 691.
- [13] Kataoka, K.; Kwon, G. S.; Yokoyama, Y.; Okano, T.; Sakurai, Y. J. *Controlled Release* **1993**, *24*, 119.
- [14] Kitazawa, Y.; Miyata, Furukawa, S.; K.; Kataoka, *Adv. Mater.* **2004**, *16*, 699.
- [15] Yan, X.; Liu, G.; Haeussler, M.; Tang, B. Z. *Chem. Mater.* **2005**, *17*, 6053.
- [16] Aizawa, M.; Buriak, J. M. *J. Am. Chem. Soc.* **2005**, *127*, 8932.
- [17] Djalali, R.; Li, S.-Y.; Schmidt, M. *Macromolecules* **2002**; *35*, 4282.

- [18] Selvan, S. T.; Hayakawa, T.; Nogami, M.; Moller, M. *J. Phys. Chem. B.* **1999**, *103*, 7441.
- [19] Wang, X. S.; Wang, H.; Coombs, N.; Winnik, M. A.; Manners, I. *J. Am. Chem. Soc.* **2005**, *127*, 8924.
- [20] Zhang, L.; Eisenberg, A. *J. Am. Chem. Soc.* **1996**, *118*, 3168.
- [21] Zhang, L.; Shen, H.; Eisenberg A. *Macromolecules* **1997**, *30*, 1001.
- [22] (a) Harada, A.; Kataoka, K. *Macromolecules* **1995**, *28*, 5294. (b) Alexander V. Kabanov, A. V.; Bronich, T. K.; Kabanov, V. A.; Yu, K.; Eisenberg, A. *Macromolecules* **1996**, *29*, 6797.
- [23] (a) Duan, H.; Chen, D.; Jiang, M.; Gan, W.; Li, S.; Wang, M.; Gong, J. *J. Am. Chem. Soc.* **2001**, *123*, 12097. (b) Yao, X.; Chen, D.; Jiang, M. *Macromolecules* **2004**, *37*, 4211. (c) Zhu, J.; Yu, H.; Jiang, W. *Macromolecules* **2005**, *38*, 7492.
- [24] Ruokolainen, J.; Saariaho, M.; Ikkala, O.; ten Brinke, G.; Thomas, E. L.; Torkkeli, M.; Serimaa, R. *Macromolecules* **1999**, *32*, 1152.
- [25] (a) Ruokolainen, J.; Mäkinen, R.; Torkkeli, M.; Makela, T.; Serimaa, R.; ten Brinke, G.; Ikkala, O. *Science* **1998**, *280*, 557. (b) Ruokolainen, J.; ten Brinke, G. Ikkala, O. *Adv. Mater.* **1999**, *11*, 777. (c) Ruokolainen, J.; Torkkeli, M.; Serimaa, R.; Komanschek, E.; ten Brinke, G.; Ikkala, O. *Macromolecules* **1997**, *30*, 2002. (d) de Moel, K.; Alberda van Ekenstein, G. O. R.; Nijland, H.; Polushkin, E.; ten Brinke, G.; Maki-Ontto, R.; Ikkala, O. *Chem. Mater.* **2001**, *13*, 4580.
- [26] (a) Wang, M.; Jiang, M.; Ning, F.; Chen, D.; Liu, S.; Duan H. *Macromolecules* **2002**, *35*, 5980. (b) Liu, S.; Zhu, H.; Zhao, H.; Jiang, M.; and Wu, C. *Langmuir* **2000**, *16*, 3712.
- [27] Kuo, S. W.; Chang, F. C. *Macromolecules* **2001**, *34*, 4089.
- [28] Kuo, S. W.; Chang, F. C. *Macromolecules* **2001**, *34*, 5224.
- [29] He, Y.; Zhu, B.; Inoue, Y. *Prog. Polym. Sci.* **2004**, *29*, 1021.
- [30] Kuo, S. W.; Tung, P. H.; Lai, C. L.; Jeong, K. U.; Chang, F. C. *Macromol. Rapid*

- Commun.* **2008**, *29*, 229.
- [31] Hsu, C. H.; Kuo, S. W.; Chen, J. K.; Ko, F. H.; Liao, C. S.; Chang, F. C. *Langmuir* **2008**, *24*, 7727.
- [32] Chen, S. C.; Kuo, S. W.; Liao, C. S.; Chang F. C. *Macromolecules* **2008**, *41*, 8865.
- [33] Ruokolainen, J.; Torkkeli, M.; Serimaa, R.; Vahvaselka, S.; Saariaho, M.; ten Brinke, G.; Ikkala, O. *Macromolecules* **1996**, *29*, 6621.
- [34] Tan, J. F.; Too, H. P.; Hatton, T. A.; Tam K. C. *Langmuir* **2006**, *22*, 3744.
- [35] Widawski, G.; Rawiso, M.; Francois, B. *Nature* **1994**, *369*, 387.
- [36] Limaye, A. V.; Narhe, R. D.; Dhote, A. M.; Ogale, S. B. *Phys. Rev. Lett.* **1996**, *76*, 3762.
- [37] Maruyama, N.; Koito, T.; Nishida, J.; Sawadaishi, T.; Cieren, X.; Ijiro, K.; Karthaus, O.; Shimomura, M. *Thin Solid Films* **1998**, *327-329*, 854.
- [38] Srinivasarao, M.; Collings, D.; Philips, A.; Patel, S. *Science* **2001**, *292*, 79.
- [39] Stowell, C.; Korgel, B. A. *Nano Lett.* **2001**, *1*, 595.
- [40] Nishikawa, T.; Ookura, R.; Nishida, J.; Arai, K.; Hayashi, J.; Kurono, N.; Sawadaishi, T.; Hara, M.; Shimomura, M. *Langmuir* **2002**, *18*, 5734.
- [41] Shah, P.S.; Sigman Jr., M.B.; Stowell, C.A. ; Lim, K.T.; Johnston, K.P.; Korgel, B.A. *Adv. Mater.* **2003**, *15*, 971.
- [42] Park, M. S.; Kim, J. K. *Langmuir* **2004**, *20*, 5347.
- [43] Cheng, C. X.; Tian, Y.; Shi, Y. Q.; Tang, R. P.; F. Xi, F. *Langmuir* **2005**, *21*, 6576.
- [44] Lin, C. L.; Tung, P. H.; Chang, F. C. *Polymer* **2005**, *46*, 9304.
- [45] Li, J.; Peng, J.; Huang, W.; Wu, Y.; Fu, J.; Cong, Y.; Xue, L.; Han, Y. *Langmuir* **2005**, *21*, 2017.
- [46] Park, M. S.; Joo, W.; Kim, J. K. *Langmuir* **2006**, *22*, 4594.
- [47] Sun, H.; Li, H.; Bu, W.; Xu, M.; Wu, L. *J. Phys. Chem. B* **2006**, *110*, 24847.
- [48] Tung, P. H.; Kuo, S. W.; Jeong, K. U.; Cheng, S. Z. D.; Huang, C. F.; Chang, F. C. *Macromol. Rapid Commun.* **2007**, *28*, 271.

- [49] Kadla, J. F.; Asfour, F. H.; Bar-Nir, B. *Biomacromolecules* **2007**, *8*, 161.
- [50] Tung, P. H.; Kuo, S. W.; Chen, S. C.; Lin, C. L.; Chang, F. C. *Polymer* **2007**, *48*, 3192.
- [51] Kamlet, M. J.; Taft, R. W. *J. Am. Chem. Soc.* **1976**, *98*, 377.
- [52] Kamlet, M. J.; Abboud, J. L. M.; Abraham, M. H.; Taft, R. W. *J. Org. Chem.* **1983**, *48*, 2877.

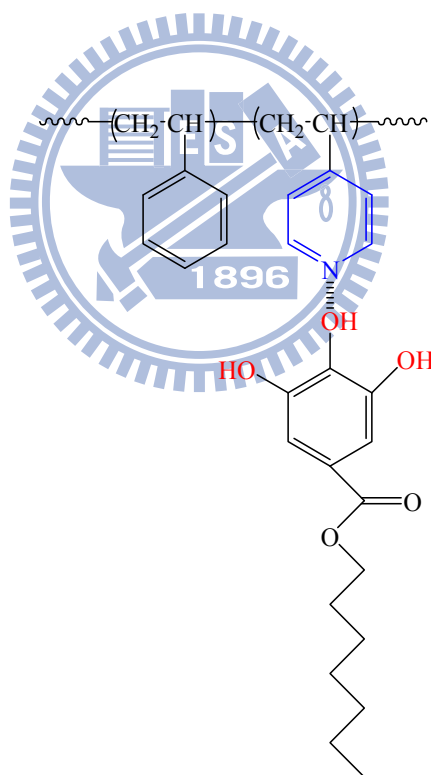


Table 5-1. Summary of the Structural Parameters and Corresponding θ_w and θ_{ws} of Aggregates Formed by PS-*b*-P4VP/OG Mixtures in Chloroform.

Molar Ratio, R	Morphology	θ_w (deg) $\pm 1^\circ$	θ_{ws} (deg) $\pm 1^\circ$
1/100	loose aggregate	105	N/A ^a
1/50	loose aggregate	102	N/A ^a
1/10	loose aggregate + spherical micelle	89	143
1/3	spherical micelle	73	100
1	spherical micelle	70	94

^a It cannot be calculated according to eq. 1

Scheme 5-1. Schematic Representation of the Interaction that Exist Between P4VP Blocks and Octyl Gallate.



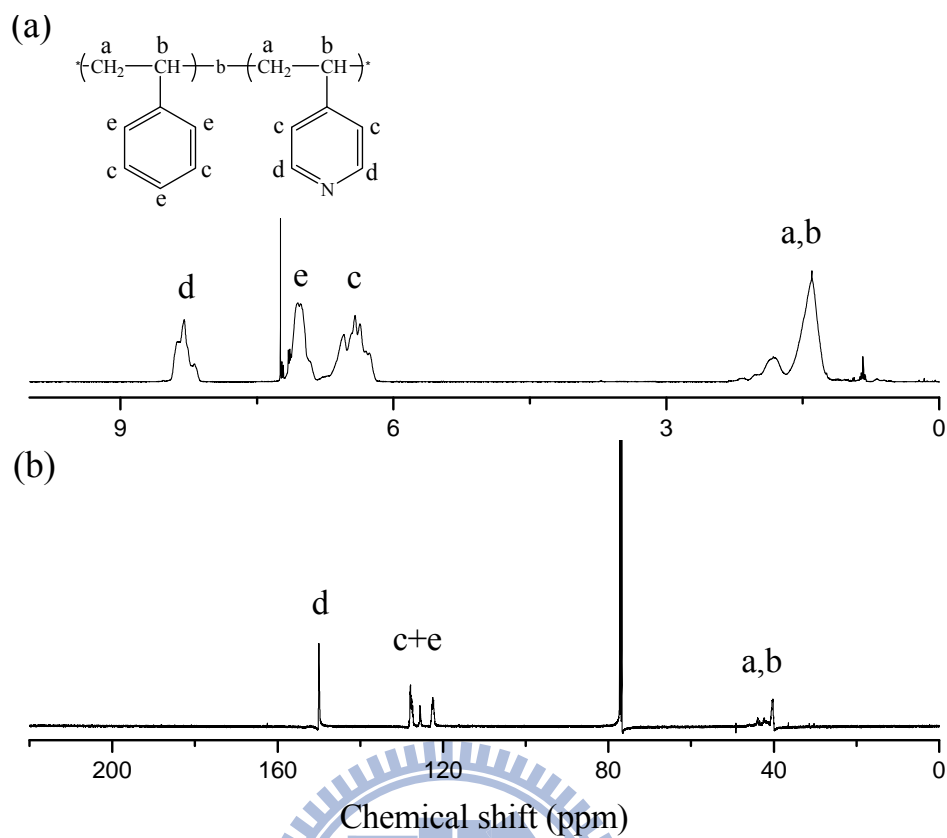


Figure 5-1. (a) ^1H and (b) ^{13}C NMR spectra of PS-*b*-P4VP.

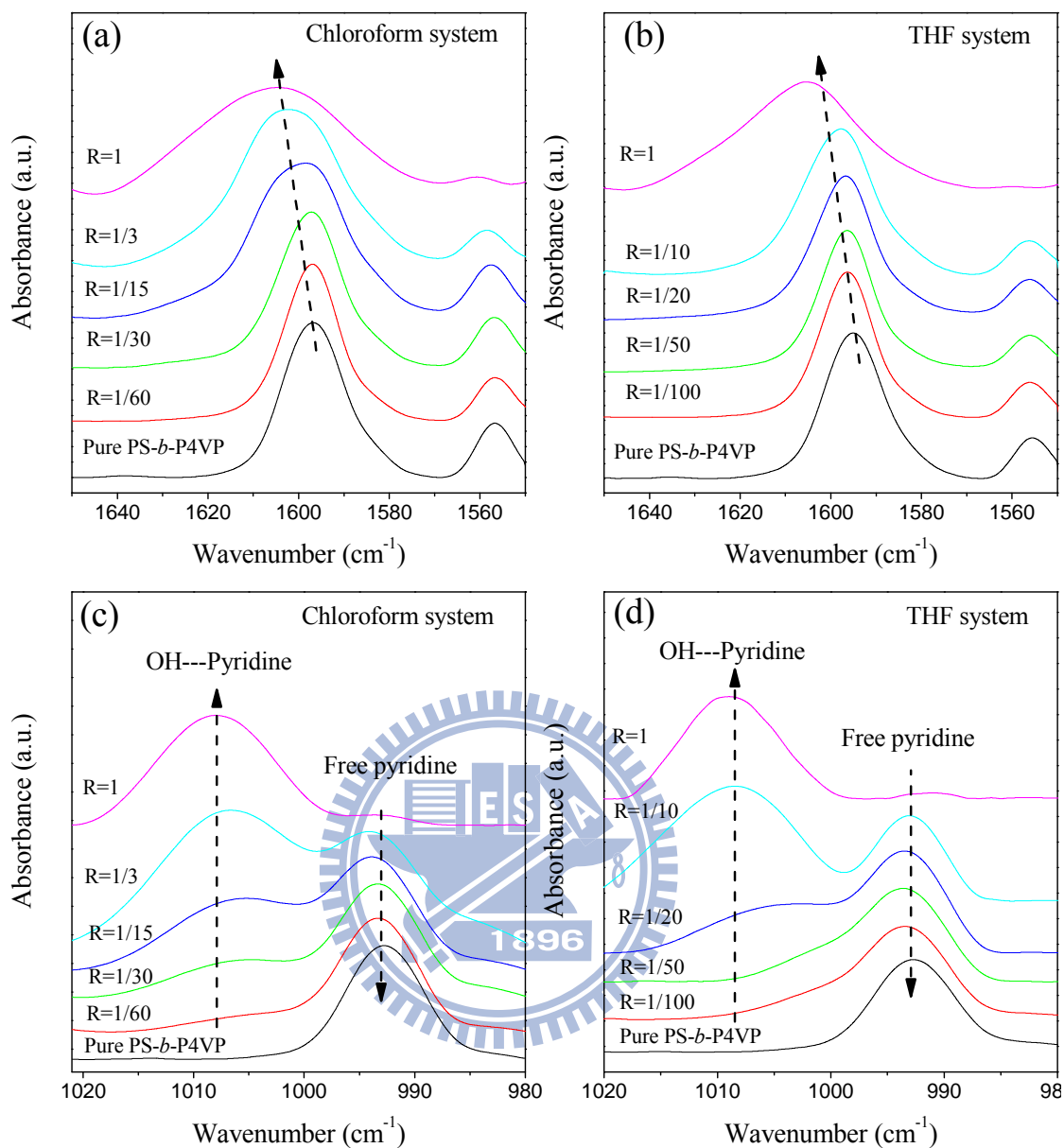


Figure 5-2. FTIR spectra of the pyridine band of the pure PS-*b*-P4VP and mixtures of OG and PS-*b*-P4VP in the range 1550-1650 cm⁻¹ in (a) chloroform and (b) THF and in the range 990-1020 cm⁻¹ in (c) chloroform and (d) THF with the different molar ratios, respectively.

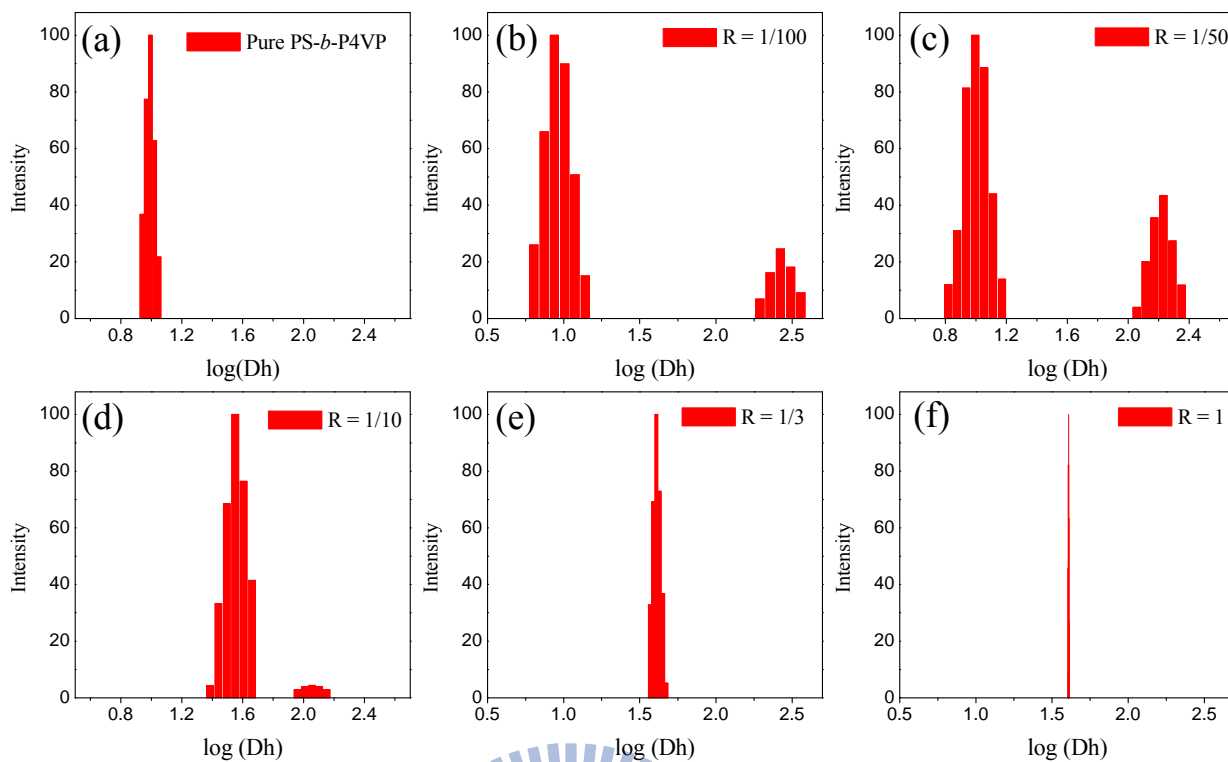


Figure 5-3. The hydrodynamic diameter distribution of the mixtures of OG and PS-*b*-P4VP with the different molar ratios in chloroform.

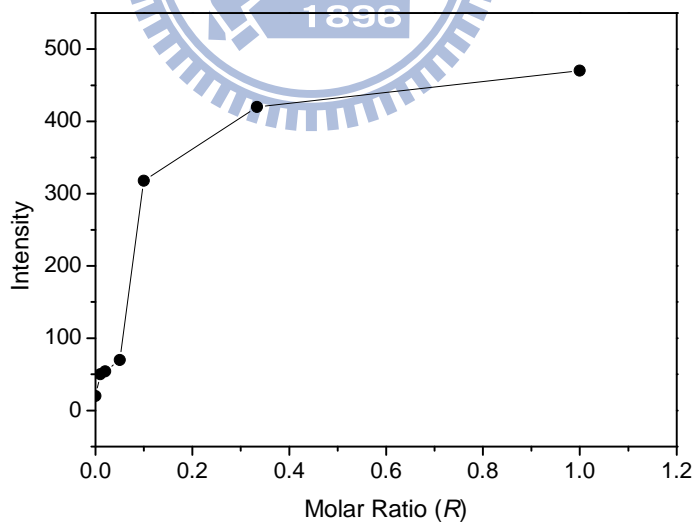


Figure 5-4. The intensity of the scattering of the mixtures of OG and PS-*b*-P4VP with the different molar ratios in chloroform.

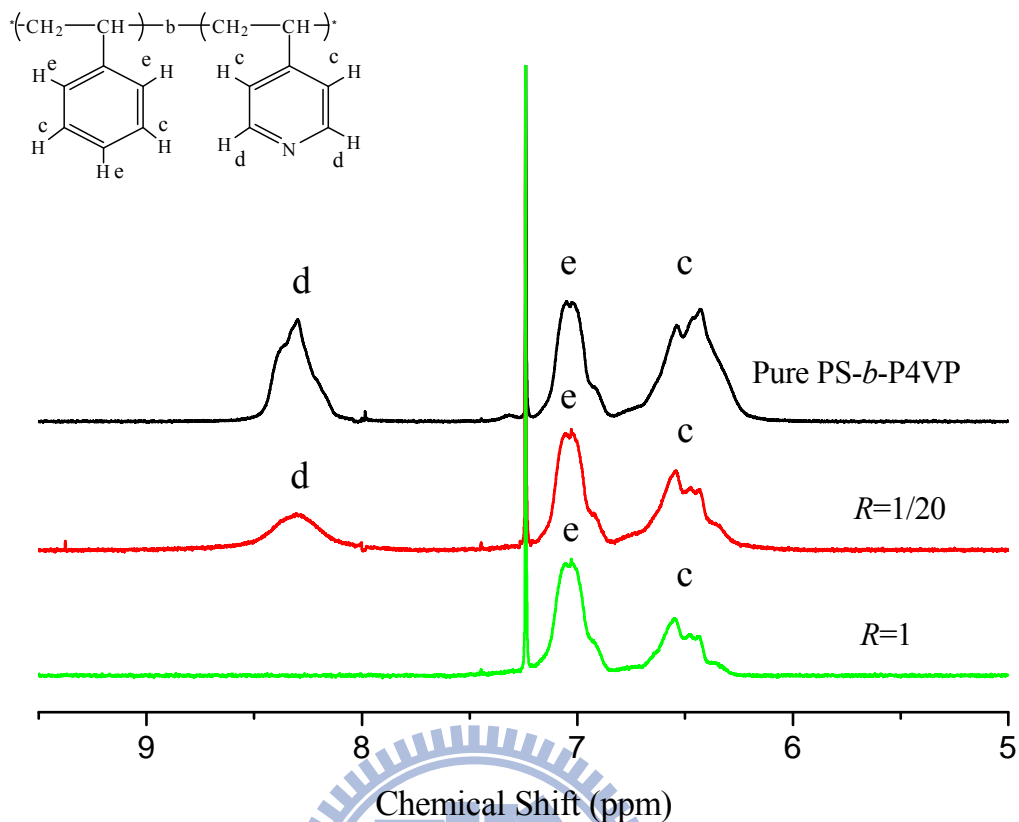


Figure 5-5. ^1H NMR spectra of the (a) pure PS-*b*-P4VP and the mixtures of OG and PS-*b*-P4VP (b) at $R = 1/20$ and (c) $R = 1$ in CDCl_3 .

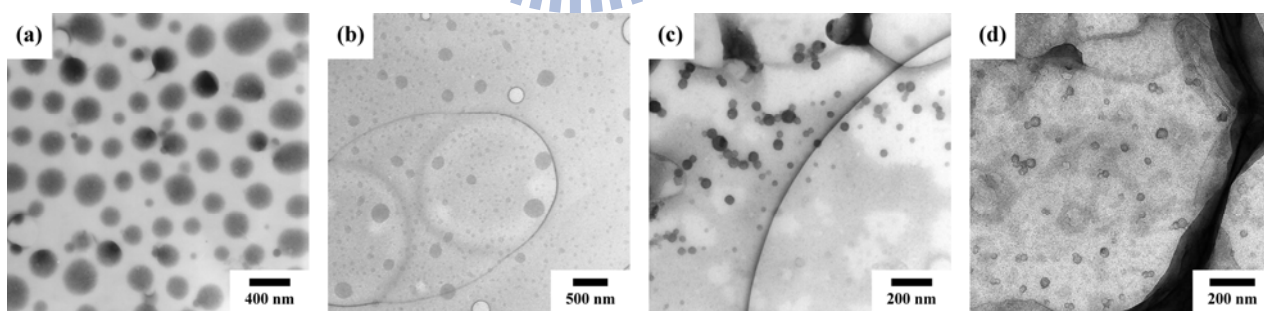


Figure 5-6. TEM images of the morphologies of the mixtures of OG and PS-*b*-P4VP (a) at $R = 1/50$, (b) at $R = 1/10$, (c) at $R = 1/3$, and (f) at $R = 1$.

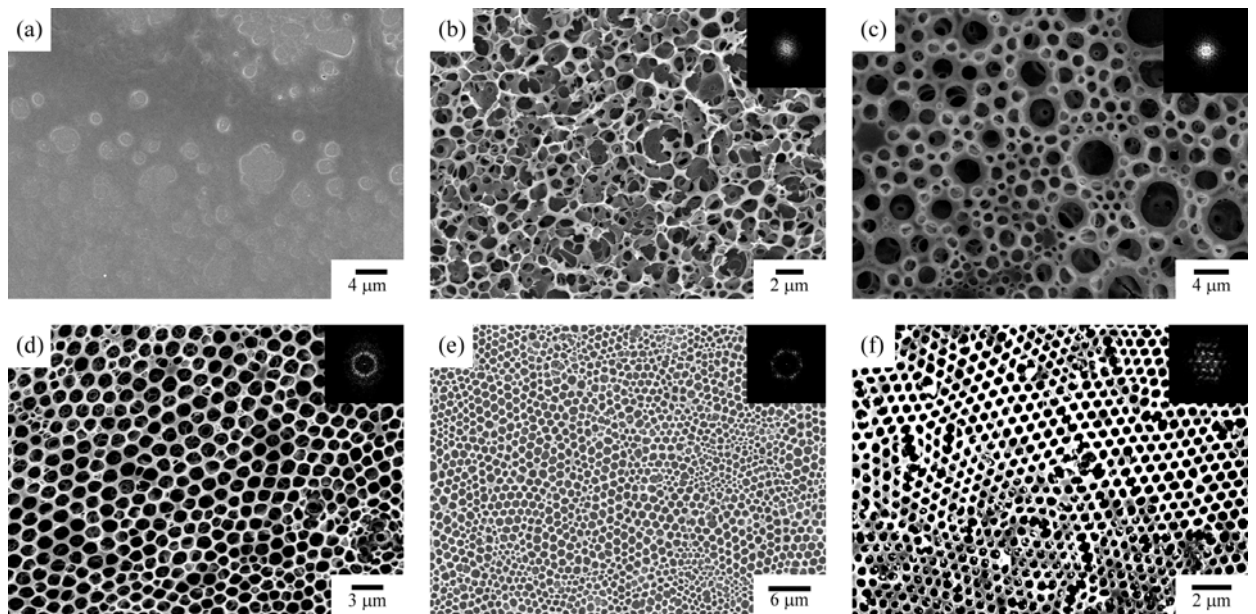
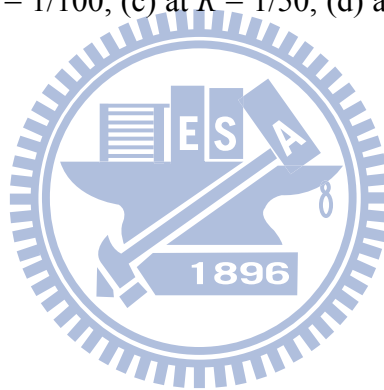


Figure 5-7. SEM images of the morphologies of the (a) pure PS-*b*-P4VP and the mixtures of OG and PS-*b*-P4VP (b) at $R = 1/100$, (c) at $R = 1/50$, (d) at $R = 1/10$, (e) at $R = 1/3$, and (f) at $R = 1$.



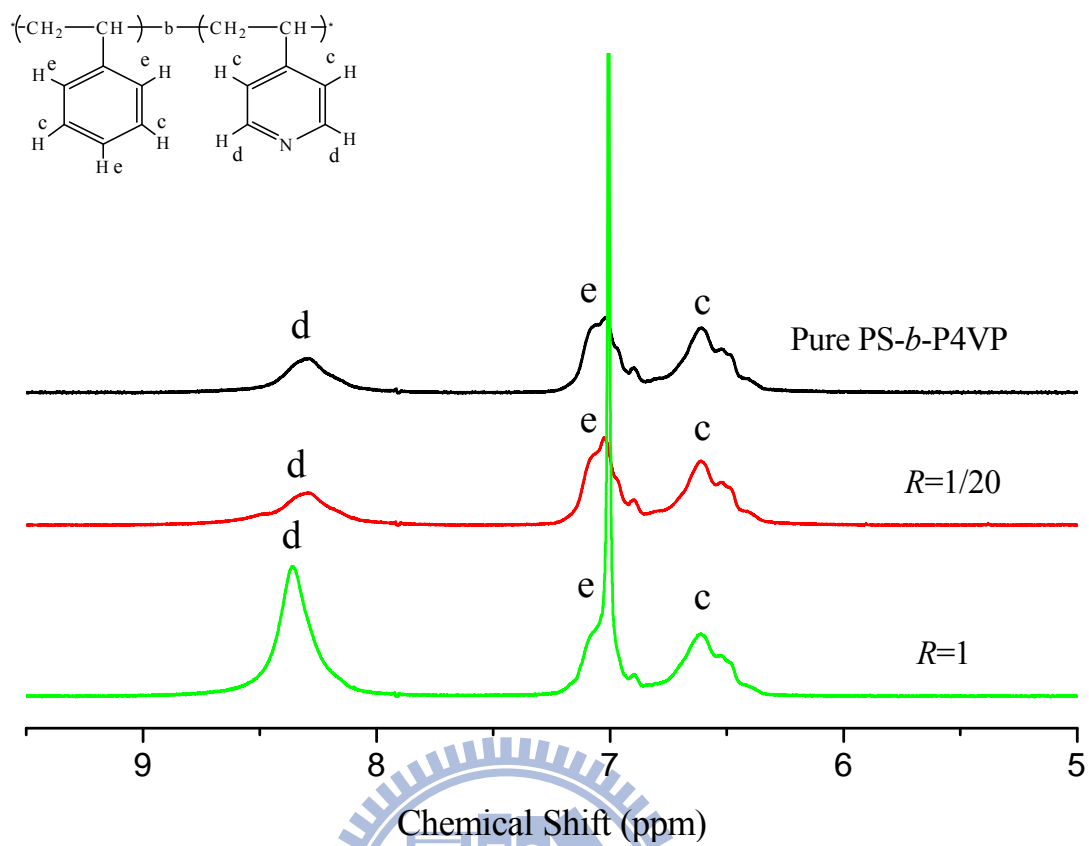


Figure 5-8. ^1H NMR spectra of the (a) pure PS-*b*-P4VP and the mixtures of OG and PS-*b*-P4VP (b) at $R = 1/20$ and (c) $R = 1$ in THF-*d*.

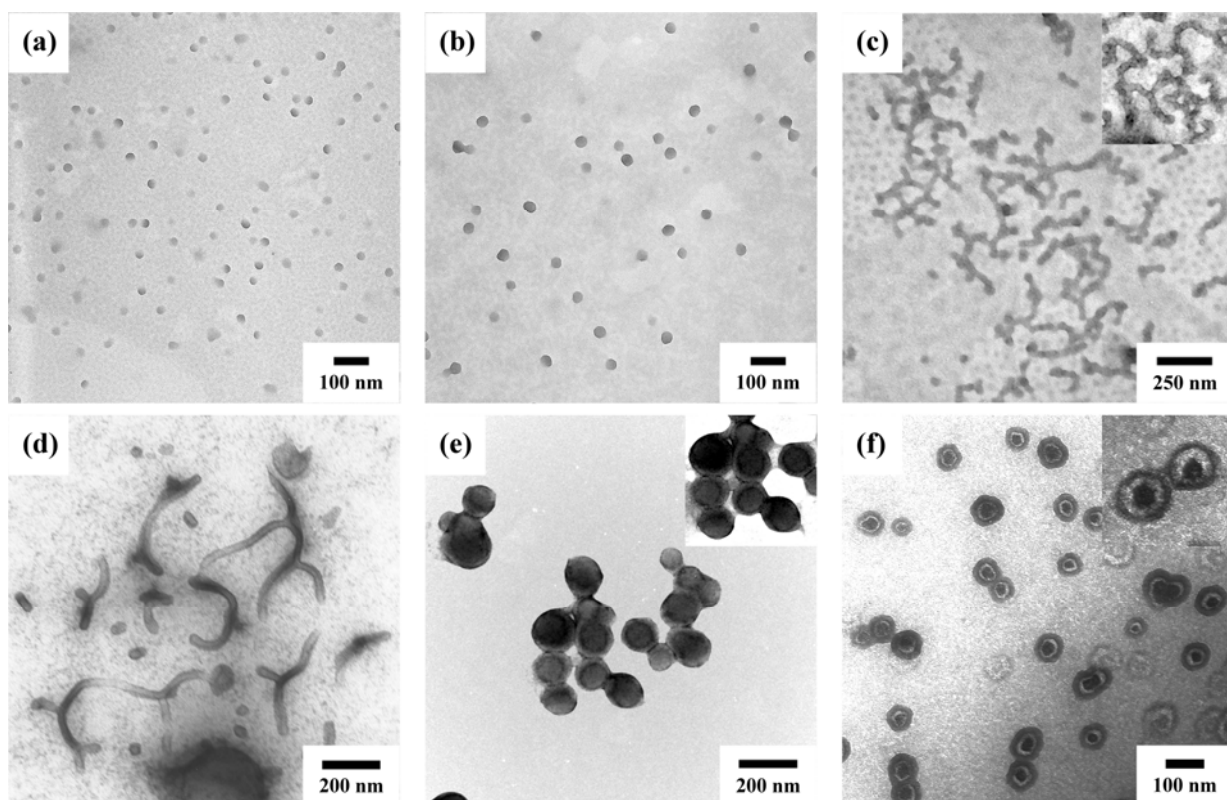


Figure 5-9. TEM images of the morphologies of the (a) pure PS-*b*-P4VP and the mixtures of OG and PS-*b*-P4VP (b) at $R = 1/50$, (c) at $R = 1/20$, (d) at $R = 1/10$, (e) at $R = 1/5$, and (f) at $R = 1$.

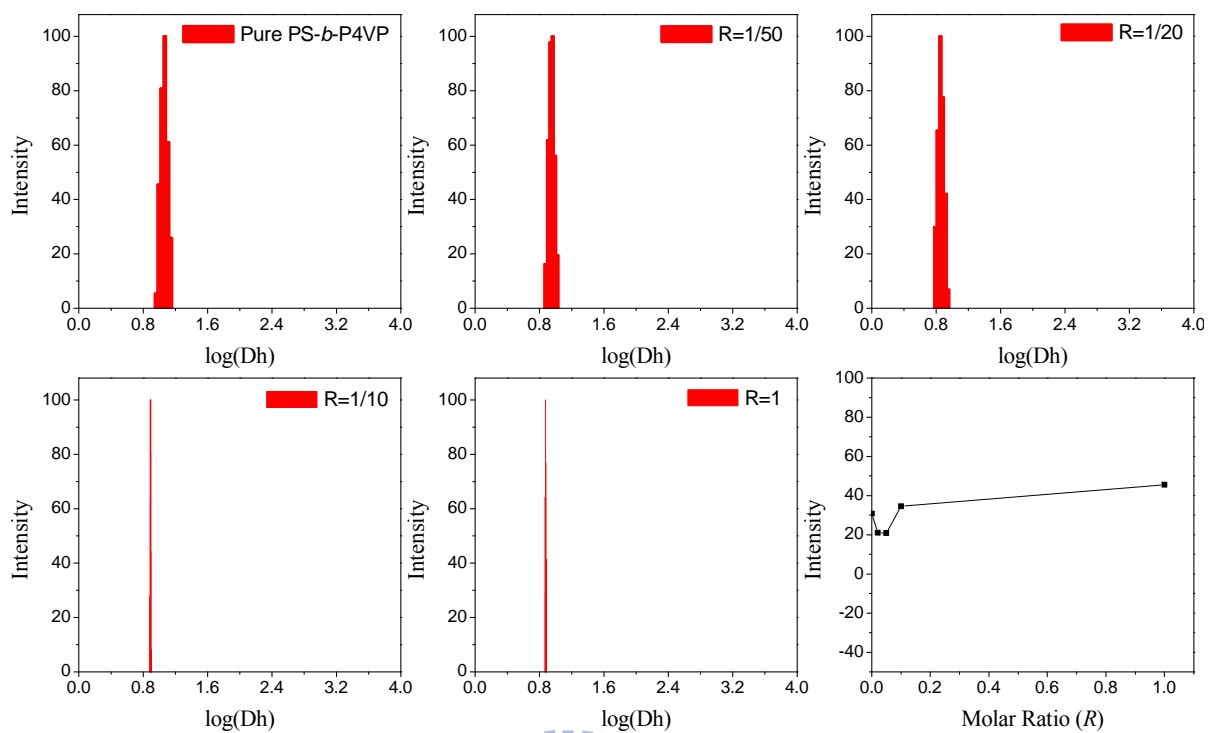
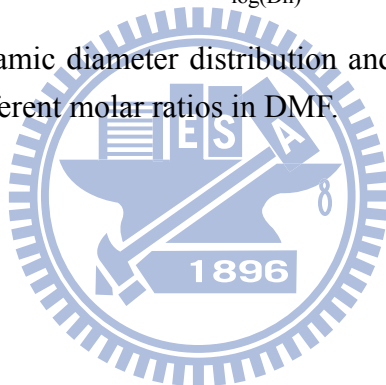


Figure 5-10. The hydrodynamic diameter distribution and intensities of the mixtures of OG and PS-*b*-P4VP with the different molar ratios in DMF.



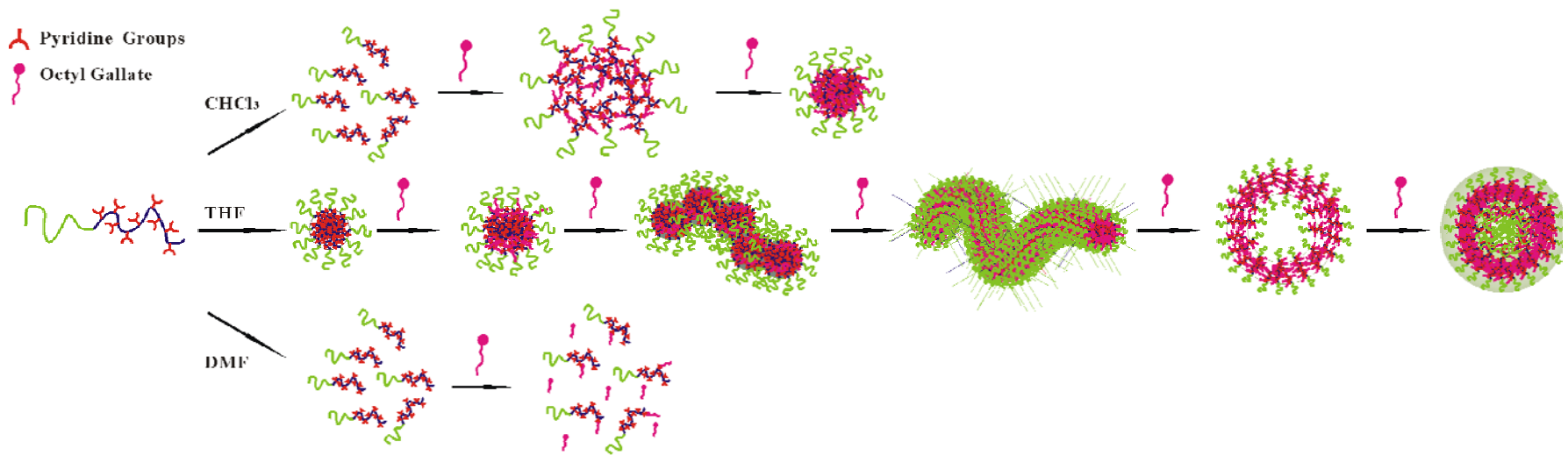


Figure 5-11. Proposed the aggregate behaviors of the mixtures of OG and PS-*b*-P4VP with the different molar ratios from the different common solvents



Chapter 6

Conclusions

We have synthesized novel pH-sensitive PVPh-*b*-PDMAEMA diblock copolymers through anionic polymerization. FTIR and solid state NMR spectroscopic analyses provided evidence for strong interactions existing between the OH groups of PVPh and the tertiary ammonium groups of PDMAEMA. From DSC analyses, we observed that the glass transition temperatures of the diblock copolymers increased significantly as a result of strong interactions between the OH groups of PVPh and the tertiary ammonium groups of PDMAEMA. ¹H NMR spectroscopic and TEM analyses revealed the pH-sensitive self-assembly behavior of PVPh-*b*-PDMAEMA diblock copolymer in aqueous media. At pH 2, spherical micelles formed comprising a neutral PVPh block surrounded by a protonated-PDMAEMA block corona. At pH 7, the diblock copolymer's morphology transformed into vesicles to reduce the free energy of the system. At pH 13, these aggregates changed from vesicles to spherical micelles comprising ionized-PVPh coronas and hydrated deprotonated-PDMAEMA cores—i.e., phase-inversed micelles relative to those formed at pH 2.

In the studies of phase behaviors of the A-*b*-B/C blends featuring the mediated hydrogen bonding, we have used FTIR spectroscopy, DSC, TEM, and SAXS techniques to investigate the phase behavior of the HS/V, HS/M, and HS/H blend systems of different hydrogen bonding strengths between the homopolymers and diblock copolymers. Integrated results show clearly that the phase behavior for the A-*b*-B/C type of polymer blends based on PS-*b*-PVPh, can be modulated via the hydrogen bonding strength between the homopolymer and copolymer. Fraction of hydrogen bonded groups may be used in quantitatively correlating the hydrogen bonding strength to the phase behavior of the polymer blends. With the inter-association equilibrium constant (K_A) over self-association equilibrium constant (K_B), K_A/K_B , much larger than unity, the phase behavior of the PS-*b*-PVPh/P4VP blend of strong

hydrogen bonding strength follows closely that of the neat diblock copolymer; with a K_A/K_B value smaller than unity, the PS-*b*-PVPh/PMMA blend suffers a phase separation, instead of phase transition, at higher homopolymer volume fractions.

For block copolymer/LMC blends with hydrogen bonding in different common solvent, PS-*b*-P4VP/octyl gallate system was studied. Hydrogen bonding between P4VP blocks of PS-*b*-P4VP diblock copolymer and OG in different solvents results in various complexation-induced micellization. Both FTIR and NMR analyses provided evidence for the formation of the P4VP binding to OG due to hydrogen bonding between the P4VP blocks and OG. Integrated results of TEM images and DLS data clearly show that the self-assembly behaviors of the mixtures of the PS-*b*-P4VP and OG can be modulated via adopting the different solvents. For PS-*b*-P4VP/OG mixture in chloroform, the morphological transitions were induced from the unimer configuration to swollen aggregate and complex-micelles by adding OG. Interestingly, the complex-micelles can lead the formation of the honeycomb structure from chloroform solution. The PS-*b*-P4VP/OG mixture in THF, behaving an amphiphilic diblock copolymer in solution state, exhibited a series of morphological transitions from sphere, pearl-necklace-liked rod, worm-liked rod, vesicle, to core-shell-corona aggregates by increasing the OG content. In contrast, the PS-*b*-P4VP/OG mixture in DMF maintained the unimer configuration upon adding OG due to relatively weak hydrogen-bonding.

List of Publications

(A) Journal

1. Pao-Hsaing Tung, Chih-Feng Huang, **Shih-Chien Chen**, Chih-Hao Hsu, and Feng-Chih Chang "Regular Honeycomb Porous Polymer Films based on Amphiphilic Block Copolymer" *Desalination* **2006**, *200*, 55.
2. Pao-Hsiang Tung, Shiao-Wei Kuo, **Shih-Chien Chen**, Chen-Lung Lin, Feng-Chih Chang "Micellar Morphologies of Self-Associated Diblock Copolymers in Acetone Solution" *Polymer* **2007**, *48*, 3192.
3. Pao-Hsaing Tung, Shiao-Wei Kuo, **Shih-Chien Chen**, Chih-Hao Hsu, Chih-Feng Wang, and Cheng-Chih Chang "Micellization and the Surface Hydrophobicity of Amphiphilic Poly(vinylphenol)-*block*-Polystyrene Block Copolymers" *Macromol. Chem. Phys.* **2007**, *208*, 1823.
4. **Shih-Chien Chen**, Shiao-Wei Kuo, Chun-Syong Liao, and Feng-Chih Chang "Syntheses, Specific Interactions, and pH-Sensitive Micellization Behavior of Poly[vinylphenol-*b*-2-(dimethylamino)ethyl methacrylate] Diblock Copolymers" *Macromolecules* **2008**, *42*, 8865.
5. **Shih-Chien Chen**, Shiao-Wei Kuo, U-Ser Jeng, Chun-Jen Su, and Feng-Chih Chang "On Modulating the Phase Behavior of Block Copolymer/Homopolymer Blends via Hydrogen Bonding" *Macromolecules* **2010**, *43*, 1083.

6. **Shih-Chien Chen**, Shiao-Wei Kuo, and Feng-Chih Chang "On Modulating the Self-Assembly Behaviors of Poly(styrene-*b*-4-vinylpyridine)/Octyl Gallate Blends in Solution State via Hydrogen Bonding from Different Common Solvents" in submitted.

(B) Conference

1. **Shih-Chien Chen**, Shiao-Wei Kuo, U-Ser Jeng, Chun-Jen Su, and Feng-Chih Chang "Mediating the Hydrogen Bonding Strength Modulates the Phase Behaviors of the Block Copolymer/Homopolymer Blends" 2010 *Material Research Society Spring Meeting* Oral presenter. (Oral)
2. **Shih-Chien Chen**, Shiao-Wei Kuo, U-Ser Jeng, Chun-Jen Su, and Feng-Chih Chang "Mediating the Hydrogen Bonding Strength Modulates the Phase Behaviors of the Block Copolymer/Homopolymer Blends" *The 15th NSRRC Users' Meeting & Workshops* 2009. (Post)
3. **Shih-Chien Chen**, Chun-Syong Liao, U-Ser Jeng, and Feng-Chih Chang "Microphase-Separated Structure of AB Block Copolymer/ C Homopolymer Blends with Various Strength of Hydrogen Bonding" *The 33rd POC Polymer Symposium* 2009. (Post)
4. **Shih-Chien Chen**, Pao-Hsaing Tung, Shiao-Wei Kuo, Chun-Syong Liao, and Feng-Chih Chang "Synthesis and the Study of Strongly Hydrogen-Bonded Poly(vinylphenol-*b*-2-(dimethylamino)ethyl methacrylate) Diblock Copolymer through Anionic Polymerization" *The 32nd POC Polymer Symposium* 2008. (Post)

Introduction to the Author

English name: Shih-Chien Chen

Chinese name: 陳世堅

Birthday: 1983, 05, 11

Address: 238 台北縣樹林市千歲街 92 巷 7 弄 20 號 1 樓



Education:

2001.09 ~ 2005.06 **B. S.**, Department of Chemical Engineering, National Chung Hsing University, Taichung, Taiwan

2005.09 ~ 2006.06 **M. S.**, Institute of Applied Chemistry, National Chiao Tung University, Hsin Chu, Taiwan

2006.09 ~ 2010.07 **Ph. D.**, Institute of Applied Chemistry, National Chiao Tung University, Hsin Chu, Taiwan

